Revisiting neuronal polarity in the context of PCP

Ana Dorrego Rivas

université de BORDEAUX

THÈSE PRÉSENTÉE POUR OBTENIR LE GRADE DE

DOCTEUR DE L'UNIVERSITÉ DE BORDEAUX

ÉCOLE DOCTORALE DES SCIENCES DE LA VIE ET DE LA SANTE
SPÉCIALITÉ BIOLOGIE CELLULAIRE ET PHYSIOPATHOLOGIE

Revisiting neuronal polarity in the context of PCP

Par **Ana DORREGO RIVAS**

Sous la direction de : Jérôme EZAN

Soutenue publiquement le 26 Mars 2021

Membres du jury :

Mme. SOUSA, Monica	Université de Porto	Rapportrice
M. GRUBB, Matthew	King's College London	Rapporteur
Mme. ENGELHARDT, Maren	Université de Heidelberg	Examinatrice
M. GEORGE, François	Université de Bordeaux	Président
Mme. MONTCOUQUIOL, Mireille	Université de Bordeaux	Invitée
M. EZAN, Jérôme	Université de Bordeaux	Directeur de thèse

université de BORDEAUX

THÈSE PRÉSENTÉE POUR OBTENIR LE GRADE DE

DOCTEUR DE L'UNIVERSITÉ DE BORDEAUX

ÉCOLE DOCTORALE DES SCIENCES DE LA VIE ET DE LA SANTE
SPÉCIALITÉ BIOLOGIE CELLULAIRE ET PHYSIOPATHOLOGIE

Revisiting neuronal polarity in the context of PCP

Par **Ana DORREGO RIVAS**

Sous la direction de : Jérôme EZAN

Soutenue publiquement le 26 Mars 2021

Membres du jury :

Mme. SOUSA, Monica	Université de Porto	Rapportrice
M. GRUBB, Matthew	King's College London	Rapporteur
Mme. ENGELHARDT, Maren	Université de Heidelberg	Examinatrice
M. GEORGE, François	Université de Bordeaux	Président
Mme. MONTCOUQUIOL, Mireille	Université de Bordeaux	Invitée
M. EZAN, Jérôme	Université de Bordeaux	Directeur de thèse

To my supportive and loving parents

To Mireille: mentor, daily inspiration and friend

Table of contents

Acknowledgements

I want to thank **Maren Engelhardt, Matthew Grubb, Monica Sousa and François George** for having accepted to be in this thesis jury and dedicated the time to read the manuscript. I want to thank the Ministère de l'Enseignement Supérieur, de la Recherche et de l'Innovation (MESRI) for the 3-year PhD fellowship that supported this work. I am thankful to the LABEX Brain initiative that funded first a 4th year and then 6 extra months for the pandemics-derived delays: without this funding my thesis would have never made it this far.

I want to thank **Jerome** for giving me the opportunity to carry this PhD thesis, the discussions around papers and for his availability.

I have no words to describe how thankful I am to **Mireille**. You are part of the special people I dedicate this thesis and it is not by chance. I have grown scientifically, professionally, personally, thanks to you. I have enjoyed all the evolution of the project, from top to bottom: the scientific conversations, the discussion of new ideas, the discovery of the latest papers and the rediscovery of the not so new ones. Thanks for standing my contradictions ("no I don't think trying that is a good idea" -*4 months later*- "you know, I was thinking maybe we should do that immuno you talked about"), or our "fights" to see who was right on that experiment in X paper. You are a true mentor because you made me better by listening, trusting and I did flourish upon that. You taught me to think critically when I read a paper or when I analyze data, both mine and from others. That is what science is about. It was great to be always on the same page, to think alike, and the times we disagreed, well…we know who was right the 99% of times (but I owe that 1%!). Discussing science with you is a joy, your passion for your work is contagious at all levels. Thanks for bringing me down to earth when I was overwhelmed, stressed or when I wanted to do way too many things. I surely hope you continue to train and motivate students the way you do, the dedication you put into it is difficult to find. On the personal side, you have been a crucial support in many aspects of my life, especially when I was going through very hard and dark times. You are more than a mentor to me, and I feel extremely lucky to have you in my life. Thanks for the shared birthdays, the conversations about life and the mutual support. I'll keep texting you (minimum) for the next 10 years!

Thank you very much to **Nathalie**, essential piece of this project despite the fact that her schedule is busier than that of the president of France. Thank you, Nath, for always making the time to discuss experiments, science, the progress of the project, for bringing the best input specially for all the biochemistry part. Thanks for always being there for the neuronal cultures, for having the patience to teach me how to properly dissect a rat hippocampus at E18.5 without my passionate need of destroying the whole brain. But, specially, thanks for always caring for the students, for mentoring, for training. You are an amazing scientist and leader and I truly admire you.

Thank you very much to my favorite duo **Nathalie Aubailly and Maïté**. You both are extraordinary lab mates. **Nath**, my partner in crime at the R+2 (and R+1 sometimes): thanks for teaching me how to do perfusions in mouse and rat (with our scientific jargon based on complicated terms such as “pinkish” or “whitish”), for making the 1 million gels for blots (approximative number), for helping with the never-ending quantifications in the mutants, for your dedication with the histology experiments, for helping with the electroporations when this manuscript was taking all of my time. Thanks for the homemade collar for our rat Pixar/Luxo Jr made with western blot films, tape and elastics from masks! I still think it deserves a spot at the European Patent Office. You are and have been indispensable for this work. I want to thank you as well for all the things you did for me out of the lab, including driving me home when it was late (though I know you love going through that Casino parking lot), helping me moving between apartments in less than 10 minutes, giving me full boxes of coffee capsules when my brain was begging for caffeine and all the conversations and support. Your presence at the lab is a bless. **Maïté**, I am beyond thankful for working with you, especially with the *in utero* electroporations. I learnt many things during those surgery sessions at the R+2, including how to properly do a surgical suture on a rat (thanks for the endless patience!) AND how to put 30% of cream on the scar of the rat and 70% elsewhere. Your expertise on this technique was essential to get our fantastic data. Thanks for all the work on the behavioral tests and for always having the time to discuss the results, thanks for the overall input you always give to the project and for solving my occasional doubts on the daily lab life. Thanks for your support and for celebrating all my successes, from extension grants to postdoc positions. You are a super woman and a core piece of the lab.

A very special thanks to **Noémie**. Since the moment you stepped in the lab (when we were both young and full of energy) we connected and became friends quickly. I knew you would be a good friend since the moment you brought me a piece of cake for my birthday without knowing me at all (you bring me food? You got me). We understand and support each other, we communicate via memes (“it ain’t much but it’s honest work”), we share our failed experiments while trying to laugh a bit about it (because what would life be without a bit of humor?) and we created the best list of the world, called “titles of your thesis”, which I hope we can use in the near future. You are definitely a true friend who has always been there for me, who has listened and supported me in the tough times. Thanks for each “you are valid”, for having the patience to hear me stressing about the writing (and stressing for everything in general, because that is my passion). Thanks for the *apéro clandestin*, for all the moments at Neurosocials, your apartment, the movie theater or just random places in Bordeaux. Thanks for trusting me everytime, I am so grateful we met.

Thanks to **Léonie** because only good friends of mine know what my favorite fruit is and you dared to fill my desk with bananas! Thanks for helping with my experiments, for making maxi preps when I could not (“you are going to ask me to put a bacteria culture to grow, right?” such a good intuition you have), for splitting HEK 2 million times, for your eternal fight with

the cloning, for making me laugh with the Frenglish (this is a blasphème!), for the "ah but you have a brain? Didn't notice". Thanks for listening and for the support. Thanks for the conversations around a coffee and around a drink when that was possible: the lockdown got right in the midst of our friendship, but I truly hope to keep sharing moments with you!

Thanks to **Shri**, my eternal yellow office partner 24/7! I think besides our PhD we are going to have a degree on memes and Harry Potter, because we know everything about them! We also know a bit about emergency rooms: your fantastic first days in France from ER to ER in company of a crazy Spanish woman who falls asleep at the waiting room, what could go wrong? Thanks for being my partner during the weekends and the late nights, for bringing me snacks when I was low on energy and for telling me about your daily adventures!

Thanks to the postdocs of the lab **Steven** and **Marie**. **Steven**, thank you for helping me to slice a brain like an electrophysiologist does and get difficult stainings working. Thank you for all the time you dedicated to the single cell electroporations in neurons (there will be more, not to worry) and the scientific discussions. **Marie**, it's been fewer time we met but thanks for your kindness, the daily conversations we hold at the lab answering my 1000 questions about electrophysiology and for having thoroughly read the introduction of this thesis!

Thanks to our newest members of the lab: **Sonia**, queen and master of the cell culture (and soon of neurons too!) Your enthusiasm is contagious and I hope to keep working together on plenty of experiments during the upcoming months. **Eloise,** thanks for your kindness but specially thanks for your brownies!

Thanks to **Yann** for all his help on the GST experiments and advice for the use of equipment at the biochemistry platform.

Thanks to **Fériel**, **Julie**, **Shobana** and **Charles**, the master students who contributed to this project with their hard work and motivation: you were key for its progress!

Thanks to the past members of the lab, specially to **Anne**, **Jennifer** and **Stéphanie** who made my first months here easier to handle. Thanks for the relaxing moments at Petit Quebec, the afternoons at the theater, the Saturday evenings playing Diablo on Play Station, the pizzas, the cola-cao in the terrace and the "calm" nights that would end up at 2 am at Café des Moines. Thanks to **Camille** for her valuable contribution to this project in molecular biology, but also support in the difficult times, conversations about the future, about science, politics or even Pokémon or videogames (because "nerds" is our second name). Thanks to **Isa** for literally having me in cheek pain for too much laughing, I really appreciated our jokes and terrible black humor to carry on when we were feeling tired. Thanks for being every Tuesday early at the lab to prepare the neuronal culture, for letting me teach you AIS quantifications (counting in Spanish!) and for being, with me, the craziest and noisiest guests a wedding can

have. Thanks for the “Gottingen palace” moment that made me die of laughter. Thanks to **Steve** and his sense of humor and all the times he gave a hand to this project whenever he could. Thanks for reminding me about the chores when my mind was on the moon and for the discussions about Tarantino movies, really weird videos on internet or books in Spanish. Thanks to **Sybille** for being such a good friend: in the few time we got to share together I already saw you are an extraordinary human being! I’ll see you soon in UK. Thanks to **Ronan**, **Chantal**, **Ben**, **Jean Michel**, **Audrey**, **Mehdi, Arnaldo** and all the other lab members that contributed to the project or were just being nice coworkers!

Thanks to **Arne** for his involvement in the project and for thorough reading and commenting the AIS part of the introduction. Thanks for the Na_v staining protocol (did it take time to work!), the preliminary recordings on the shPk2 neurons and scientific discussions.

Thank you very much to all the people at the Bordeaux Imaging Center (BIC), especially **Fabrice Cordelières** for the development of the AIS ImageJ macro for quantifications. Huge thanks to **Magali Mondin**, who had the patience to teach this girl to use STORM right from the beginning. I arrived not knowing how to close a ludin chamber and finished imaging actin rings at the AIS! Thank you very much for your kindness, for solving all my question, for saying “this will take max 5 minutes” and actually be true. You dedicated a lot of time to my training in super resolution microscopy and I am infinitely grateful for it.

Thanks to all the animal caretakers of the institute, specially **Melyssa**, for answering patiently and quickly to my demands, even if those were last minute! Your work is an essential piece for all of the team. Many thanks also to the people from the **genotyping facility** of Magendie and their efficient work.

A big thanks to all the people in the institute with which I enjoyed Neurosocials, afternoons at a bar, parties, or just spontaneous conversations at the corridors of the institute: **Mari, Christopher, Nuria, Roman, Mabel, Unai, Ashley, Georgina, Maria, Shaam, Eva and Valentine.**

Thanks to my flatmates **Victor** and **Andrea** and the relaxing moments we spent together after a hard day at work!

Thanks to **Naima** and **Maitane**, my favorite Basque girls who introduced me to life in Bordeaux when I arrived! Thanks for being such good friends and for keeping in touch despite the time and the distance.

I want to thank all my friends in Spain (but that in reality are a bit distributed all over the world): **David**, **Marina**, **Carlos Lopez**, **Carlos Leston**, **Aroa**, **Iris, Ana, Irene, Cristina, Alba Barrachina, Alba Gonzalez, Andrea, Roger, Andrés, Julia, Maria Peña, Maria Pereira and**

Nando. You are an amazing group of people and I feel the luckiest person in the world for having you. Thanks for the unconditional friendship, support, zoom calls during lockdown, vocal messages on whatsapp, trips, parties, afternoons and nights at bars in Barcelona and worldwide. Thanks for the big surprise in Paris (will never forget that) thanks for being at my PhD defense even if virtual (we will throw a big party as soon as we can!), thanks for being the way you are, meaning thanks for being the stupidest people (with me, of course) who laugh over a thing one million times (Kaixo – Apple Pay!, "sabes a quién te das un aire? A Javier", "Tú denúnciame", "Era una performance, vale?", "De la cárcel se sale", « I don't see the moment »). My life gets extra years after spending some time with all of you.

Last, but not least, I want to thank my family. Thanks to **Carmen** and **Jesus**, my supportive and loving parents, for having the patience of following her daughter wherever she goes. Thanks for your calls, for the trips to Barcelona, to Bordeaux (probably the future ones to London), for your unconditional love. Thanks for teaching me to work hard to get what I want in life, for never giving up. Thanks to my sister **Silvia**, my mirror, for, despite the fact of not understanding at all why would I choose such a life, she still supports me and is happy to see me back home. Thanks to her for giving me the two most important people in my life: my nieces **Vera** and **Martina**, who make this world a little bit brighter. Thanks to my grandparents **Charo** and **Manuel** for their unconditional love and support at all levels. I could never be where I am now without you.

Scientific productions

Scientific articles

- **Dorrego-Rivas A**, Ezan J, Depret N, De Neve J, Moreau M, Sankar S, Blanchard C, Chassac S, Aubailly N, Wu D, Battefeld A, Sans* N, Montcouquiol* M. *Planar cell polarity proteins regulate the assembly and function of the axon initial segment*. Manuscript in preparation. *Equal contribution.

- Lubiana T, Weber S, Andrade Paranhos B, Araujo D, **Dorrego-Rivas A,** Franzen D, Nogueira Vicosa G, Ghosh A and Hojas Garcia-Plaza, I. *ANN: a platform to annotate text with wikidata IDs* (2020, preprinted).

Oral communications

- *A new role for planar cell polarity signaling in neuronal polarity and axonal function.* "Hot topics", internal seminar of the Neurocentre Magendie (November 2020).

- *Prickle-2: a PCP protein regulating the psychiatric risk factor ANK3*. Datablitz of the Annual Symposium of the Neurocentre Magendie (September 2019).

- *How does planar cell polarity modulate axon initial segment morphofunctional plasticity?* "Hot topics", internal seminar of the Neurocentre Magendie (February 2018).

Posters

- **Dorrego-Rivas A**, Ezan J, De Neve J, Stanic J, Barranger A, Seynat I, Blanchard C, Dos Santos Carvalho S, Aubailly N, Sans N and Montcouquiol M. *Planar cell polarity proteins in neuronal polarity and axonal function*, Cell Bio ASCB EMBO meeting (December 2020).

- **Dorrego-Rivas A**, Ezan J, De Neve J, Sankar S, Stanic J, Barranger A, Seynat I, Blanchard C, Dos Santos Carvalho S, Aubailly N, Sans N and Montcouquiol M. *A new role for planar cell polarity in neuronal polarity and function*, Forum for the European Neuroscience Societies – FENS (July 2020)

- **Dorrego-Rivas A**, Ezan J, De Neve J, Stanic J, Blanchard C, Barranger A, Dos Santos Carvalho S, Seynat I, Sans N and Montcouquiol M. *The role of planar cell polarity Prickle 2 in neuronal polarity*, Annual Symposium of the Neurocentre Magendie (September 2019)

- **Dorrego-Rivas A**, Ezan J, De Neve J, Stanic J, Blanchard C, Barranger A, Dos Santos Carvalho S, Seynat I, Sans N and Montcouquiol M. *The role of planar cell polarity Prickle 2 in neuronal polarity*, Bordeaux Neurocampus Day (May 2019)

- **Dorrego-Rivas A,** Stanic J, Claverie L, Sans N, Montcouquiol M and Ezan J. *Planar cell polarity: a modulator of neuronal polarity and excitability?* Bordeaux Neurocampus Day (May 2018)

- **Dorrego-Rivas A,** Stanic J, Claverie L, Sans N, Montcouquiol M and Ezan J. *Planar cell polarity: a modulator of neuronal polarity and excitability?* Annual Symposium of the Neurocentre Magendie (April 2018)

List of abbreviations

A/B	Apico-basal
AIS	Axon initial segment
AMPA	α-amino-3-hydroxy-5-methyl-4-isoxazolepropionic acid
AnkB	Ankyrin-B
AnkG	Ankyrin-G
AnkR	Ankyrin-R
Ankr6d	Ankyrin repeat domain 6
AP	Action potential
AP2	Adaptor protein 2
aPKC	Atypical protein kinase C
Arp2/3	Actin-related protein 2/3
ASD	Autism spectrum disorders
BD	Bipolar disorder
ßPIX	ß-PAK interactive exchange factor
C-ter	C-terminus
CA1-CA3	Horns of Ammon 1 and 3
cAMP	Cyclic adenosine monophosphate
CAMSAP2	Calmodulin-regulated spectrin-associated protein 2
Cas9	CRISPR associated protein 9
Ca_v	Calcium voltage-gated channel
Cdc42	Cell division control protein 42
cDNA	Complementary DNA
CE	Convergent extension
Celsr	Cadherin EGF LAG seven-pass G-type receptor
CK2	Casein kinase 2
cKO	Conditional knockout
CRMP-2	Collapsin response mediator protein-2
Crc	Circletail
CRISPR	Clustered regularly interspaced short palindromic repeats
CSF	Cerebrospinal fluid
Cthrc1	Collagen Triple Helix Repeat Containing 1
DEP	Dishevelled, Egl-10 and Pleckstrin domain
DG	Dentate gyrus
Dgo	Diego
Dia	Diaphanous
DIV	Days *in vitro*

DIX	Dishevelled-axin
Dlg	Discs large
DPI	Days post infection
DS	Dravet syndrome
Dsh	Dishevelled
Dvl	Dishevelled-like
E (n)	Embryonic day (n)
ECM	Extracellular matrix
ENU	NN-Ethyl-N-NitrosoUrea
Fmi/Stan	Flamingo/Starry night
Ft/Ds	Fat/Dachsous
Fuzz	Fuzzy
Fuz	Fuzzy homolog
Fz	Frizzled
GABA	Gamma-Aminobutyric Acid
GAT-1	GABA transporter 1
GluN2A/GluN2B	Glutamate receptor subunits 2A and 2B
GSK3ß	Glycogen synthase kinase-3
HC	Hair cell
HF	High frequency
ID	Intellectual disability
Int	Inturned
Int1	Integration 1
Intu	Inturned planar cell polarity protein
JNK	c-Jun NH2-terminal Kinase
KCl	Potassium chloride
kDa	Kilodalton
KIF3	Kinesin-like protein 3
KIF5	Kinesin-like protein 5
KIFC2	Kinesin-like protein KIFC2
KO	Knockout
K_v	Potassium voltage-gated channel
LAP	LRR and PDZ
LF	Low frequency
LGI1	Leucine-rich, glioma inactivated 1
Lgl	Lethal giant larvae

LIM	LIN-11, Isl-1 and MEC-3
LKB1	Liver kinase B1
Lp	Looptail
LRR	Leucine-rich repeat
LTP	Long term potentiation
MAGUK	Membrane-associated guanylate kinase
MAP	Microtubule associated protein
MARK	MAP/microtubule affinity-regulating kinase
mEPSC	Mini excitatory postsynaptic currents
MPS	Membrane periodic skeleton
mRNA	Messenger RNA
MT	Microtubules
MTCL1	Microtubule crosslinking factor 1
MTNB	Medial nucleus of the trapezoid body
mV	Milivolts
Mwh	Multiple wing hairs
N-ter	N-terminus
Na_v	Sodium voltage-gated channel
NEC	Neuroepithelium cells
NF-186	Neurofascin-186
NMDA	N-methyl-D-aspartate receptor
NoR	Node of Ranvier
NR2B	NMDA receptor 2B
NrCAM	Neuronal cell adhesion molecule
NTD	Neural tube disorder
NTR	Neurotrophin receptor
NuMA1	Nuclear mitotic apparatus protein 1
OC	Organ of Corti
P(n)	Postnatal day (n)
Par	Partitioning defective
Pins	Partner of inscuteable
PCP	Planar cell polarity
PDZ	PSD95/ Dlg1/ ZO-1
PET	Prickle-Espinas-Testin
PH	Protein homology
Pk	Prickle

Pk2	Prickle-like 2
PP1/PP2A	Protein phosphatase 1/2A
PSD	Postsynaptic density
PTEN	Phosphatase and tensin homolog
Ptk7	Tyrosine-protein kinase-like 7
PV	Parvalbumin
Qv	Quivering
Rac1	Ras-related C3 botulinum toxin substrate 1
RGC	Retinal ganglion cells or Radial glial cells
RhoA	Ras homolog family member A
Ror2	Receptor Tyrosine Kinase Like Orphan Receptor 2
SAD	Synapses of the amphid defective
Scrib	Scribble
Sec24b	SEC24 Homolog B, COPII Coat Complex Component
sGC	soluble-guanylate-cyclase
shRNA	Short-hairpin RNA
Smurf 1/2	E3 ubiquitin-protein ligase 1 and 2
SNP	Single nucleotide polymorphism
SOP	Sensory organ precursors
Sple	Spiny-legs
STED	Stimulated-emission-depletion
STORM	Stochastic optical reconstruction microscopy
TAG-1	Neural adhesion molecule contactin-2
TEM	Transmission electron microscopy
TGF-ß	Transforming growth factor- ß
TRIM46	Tripartite Motif Containing 46
Vang/Stbm	Vang Gogh/Strabismus
Vangl	Vang Gogh-like
Wdpcp	WD repeat containing planar cell polarity effector
Wnt	Wingless-integration
WT	Wild type
ZO-1	Zonula occludens-1

Abstract / Résumé

Abstract

Planar cell polarity (PCP) classically refers to the coordination of cell polarity within the plane of the epithelium, perpendicularly to the apical-basal axis. A conserved signaling cassette that modulates the cytoskeleton regulates this type of tissue polarity, which in turn controls a wide range of biological processes. PCP signaling has conserved functions in epithelia from drosophila to mammals but its role and function in the central nervous system is still poorly known. However, mutations in some core PCP members result in severe phenotypes for the brain and are incompatible with life.

Neurons are highly polarized cells with two defined compartments that differ in morphology and function: the axonal and the somatodendritic domains. This segregation is crucial for the proper function of neurons. The maintenance of this polarized state throughout life relies in the axon initial segment (AIS). The AIS is a neuronal subdomain that coordinates the axo-dendritic polarity establishment and maintenance and constitutes the site for action potential initiation and tuning. The AIS consists of an organized cytoskeleton meshwork and associated molecules like Ankyrin-G (AnkG) and βIV spectrin. AnkG is the AIS master organizer, since it arrives to the proximal axon first and recruits all the AIS members. Many of the AIS genes are linked to neurodevelopmental pathologies like bipolar disorder, epilepsy or autism, making it a potential target for therapeutical approaches. Despite the critical role of the AIS in neuronal function, the early steps of its assembly are still unknown notably because of few identified direct AnkG partners.

This thesis focuses on the roles of Prickle-like 2 (Pk2) and Scribble (Scrib) in neuronal polarity and axonal function. Pk2 and Scrib accumulate at the AIS in early and late stages of neuronal development, both *in vivo* and *in vitro*. I show a co-localization between these proteins and AnkG and βIV spectrin and confirmed their interactions via specific domains. My data suggest that Pk2 interacts early at the AIS with AnkG to stabilize it at the membrane, while Scrib binds to βIV spectrin to anchor the AIS along the axon.

In vitro downregulation of Pk2 impaired axonal establishment and AIS formation by altering the number of axons per neuron and the levels of AnkG and associated AIS molecules. *In vivo* downregulation of Pk2 via *in utero* electroporation similarly reduced AIS proteins levels in neurons from the developing neocortex. I used a conditional knockout mouse model where both Pk2 and Scrib are deleted in postmitotic excitatory neurons of the hippocampus and cortex. The reduction of PCP proteins was followed by a decrease of the main AIS proteins like AnkG, βIV spectrin and Nav channels.

Altogether, these data unveil an original role of PCP proteins in AIS formation and composition, shedding light on novel PCP function.

Résumé

La polarité cellulaire dans le plan (PCP) désigne classiquement une polarité alignée avec le plan de l'épithélium, et donc perpendiculaire à l'axe apico-basal. Cette polarité est régulée par une cassette de signalisation qui module le cytosquelette, et contrôle un large éventail de processus biologiques. La voie de signalisation de la PCP est conservée dans les épithéliums, de la drosophile aux mammifères, mais son rôle et sa fonction dans le système nerveux central sont encore mal connus. Cependant, des mutations de certains membres cette voie de signalisation conduisent à des phénotypes neuronaux graves et sont incompatibles avec la vie.

Les neurones sont des cellules hautement polarisées comportant deux compartiments définis qui diffèrent par leur morphologie et leur fonction : le domaine axonal et le domaine somatodendritique. Cette ségrégation est cruciale pour le bon fonctionnement des neurones. Le maintien de cet état polarisé tout au long de la vie repose sur le segment initial de l'axone (SIA). Le SIA est un sous-domaine neuronal qui coordonne l'établissement et le maintien de la polarité axo-dendritique et qui constitue le site d'initiation et de modulation du potentiel d'action. Le SIA consiste en un réseau organisé du cytosquelette et de molécules associées comme l'Ankyrin-G (AnkG) et la spectrine βIV. L'AnkG est le maître organisateur du SIA, puisqu'il est recruté le premier à l'axone et qu'il recrute tous les autres membres. Des mutations de nombreux gènes du SIA sont liées à des pathologies neurodéveloppementales comme le trouble bipolaire, l'épilepsie ou l'autisme, ce qui en fait une cible potentielle pour des approches thérapeutiques. Malgré le rôle essentiel dans la fonction neuronale, les premières étapes de l'assemblage du SIA sont peu inconnues, notamment en raison du peu de partenaires directs de l'AnkG identifiés.

Lors de cette thèse, j'ai étudié le rôle de Prickle-like 2 (Pk2) et Scribble (Scrib) dans la polarité neuronale et la fonction axonale. Pk2 et Scrib sont présentes au SIA tout au long de la maturation neuronale, *in vivo* et *in vitro*. J'ai identifié une colocalisation entre ces protéines et AnkG et la spectrine βIV et confirmé leurs interactions via des domaines spécifiques. Mes données suggèrent que Pk2 interagit pour stabiliser AnkG à la membrane, tandis que Scrib se lie à la spectrine βIV pour ancrer au SIA le long de l'axone.

In vitro, la sous-expression de Pk2 perturbe la polarité neuronale et la formation du SIA en diminuant les niveaux d'AnkG et de molécules SIA associées. *In vivo* la sous-expression de Pk2 par électroporation *in utero* conduit également à une diminution des protéines du SIA dans les neurones du néocortex. J'ai utilisé un modèle de souris mutantes conditionnelles où Pk2 et Scrib sont tous deux supprimés dans les neurones excitateurs post-mitotiques de l'hippocampe et du cortex. Dans le cortex de ces mutants, j'observe également une diminution des principales protéines du SIA comme l'AnkG, la spectrine βIV et les canaux Nav.

Au total, ces données révèlent un rôle original de protéines de la PCP dans la mise en place et la composition du SIA, et mettent en lumière de nouvelles fonctions pour les protéines de la PCP.

Chapter I: Introduction

A brief introduction to Wnt signaling pathways

Before going into detail with Planar Cell Polarity (PCP), it is important to briefly revisit the history and definition of Wnt signaling.

When talking about the discovery of Wnt signaling we need to go back to the 90s, when a pioneer study identified a proto-oncogenic gene in mouse called integration 1, abbreviated int1 (Nusse et al., 1984). This gene, which is conserved throughout evolution, has an ortholog in *Drosophila* called Wingless (Wg). Both genes showed similar functions during embryonic development in both flies and mammals. Many int1-related genes were identified later on, with no relationship to int1 initially, but the nomenclature eventually changed to Wnt, which is a mix between Wg and Int and is the current used name (Nusse et al., 1991; Nusse and Varmus, 1992).

Wnts are lipid-modified morphogens that act in a wide range of biological processes, during embryonic development and adulthood, from physiological to pathological contexts, controlling cell proliferation, differentiation, growth and migration among others (reviewed in Nusse, 2005). There is a large number of Wnts, particularly in mammals, with up to 19 Wnt genes identified in mice so far. A pioneer study from 1994 using mammary epithelial cells showed that different Wnts can promote or inhibit cell growth, revealing that they are likely involved in different signaling pathways (Wong et al., 1994).

The three most studied and characterized Wnt pathways are:

1) The canonical Wnt/ß-catenin
2) The non-canonical Wnt/calcium
3) The non-canonical Wnt/PCP

The major difference between the canonical and the non-canonical pathway or PCP pathways is that the canonical one involves a regulation of ß-catenin levels and transcriptional changes (reviewed in Buechling and Boutros, 2011; Komiya and Habas, 2008; Nusse and Clevers, 2017), while the PCP pathways mostly controls cytoskeleton reorganization in absence of transcriptional activity (reviewed in Adler, 2012).

If the outcomes of the three pathways are different, they all involve Frizzled (Fz) receptors. The activation of the most characterized pathway, the Wnt/ß-catenin, starts with the binding of a Wnt to the extracellular domain of Fz and a consecutive cytoplasmic accumulation of ß-catenin, which translocates to the nucleus and activates a series of transcription factors (reviewed in Nusse and Clevers, 2017). The non-canonical Wnt/calcium pathway regulates the calcium release from the endoplasmic reticulum and the non-canonical Wnt/PCP modulates the cytoskeleton via downstream effectors. Even if the three pathways are different in terms of output, they share proteins, like Fz and Dishevelled (**Figure 1**) (reviewed in Komiya and Habas, 2008).

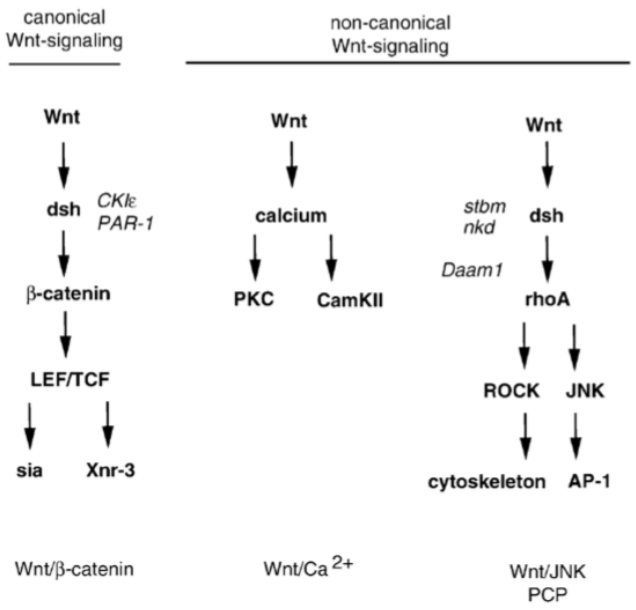

Figure 1: *Schematic showing the canonical and non-canonical Wnt signaling pathways. From Kühl, 2002.*

Although the implication of Wnts in all three pathways has long been under debate (see below), Fz is a common factor to all of them, but some Fz can be specific to the activation of one or another. There are, to date, at least two Fz in *Drosophila* and ten Fz in mammals. A comparison of the amino acid sequences and intron–exon structures determine clusters consisting of Fz1, Fz2, and Fz7 (subfamily 1), Fz5 and Fz8 (subfamily 2), Fz9 and Fz10 (subfamily 3), Fz4 (subfamily 4), and Fz3 and Fz6 (subfamily 5). Because in many tissues there is overlapping expression of multiple Fz, it is complex to assign a specific function to one Fz with corresponding Wnt ligand. But Fz3 and Fz6 appear to be devoted largely to PCP signaling, whereas Fz4 seems to participate in canonical Wnt signaling (reviewed in Wang and Nathans, 2007). Some mammalian Fzs could be involved in more than one pathway, as shown for *Drosophila* Fz, which signals through both the canonical Wnt and PCP pathways (Bhanot et al., 1999; Bhat, 1998; Müller et al., 1999). Others like Fz1, Fz2 and Fz7 can activate the canonical pathway as well (Yu et al., 2012; Hua et al., 2014; for review see Wang and Nathans, 2007).

Following Wnt binding to Fz, Dishevelled is recruited to the cytoplasmic tail of Fz. Dvl is, in fact, a versatile protein whose participation in one or another pathway will be determined by its specific domains. Several studies performed in different species have determined that the DEP domain activates the PCP pathway (Axelrod et al., 1998; Wallingford et al., 2000), the DIX domain is specific to the Wnt/ß-catenin (Moriguchi et al., 1999; Rothbächer et al., 2000) and the PDZ domain can participate in both and is able to distinguish them (reviewed in Moon and Shah, 2002; Boutros and Mlodzik, 1999). In addition, different post-translational modifications of Dishevelled can determine the activation of one pathway or another: for

example, the phosphorylation by Casein Kinase favors the Wnt/ß-catenin and inhibits the PCP pathway (Peters et al., 1999; McKay et al., 2001).

There is a convergence of the three pathways in some contexts. One example is the process of convergent extension during gastrulation in Xenopus. The Wnt/ß-catenin pathway is important for these cell movements (Sokol, 1993), but the non-canonical pathways also participate (reviewed in Kühl, 2002). While activation of the Wnt/ß-catenin favors cell movements during convergent extension (CE) in gastrulation, the injection of Wnt5a, which is known to activate the non-canonical pathway, blocks CE. In fact, this produced a negative interference with the Wnt/ß-catenin pathway, showing that both canonical and non-canonical are interconnected. The role in of PCP singaling in CE is developed later (see *1.2.1 PCP and convergent extension in Xenopus laevis and Zebrafish*).

In summary, while the three Wnt signaling pathways do share common molecular players, their functional diversity and specificity rely on specific combinations of these players, including the implication or not of Wnts, the choice of Fz and their co-receptors, the versatility of Dvl and different downstream effectors (**Figure 1**). In the following part I will explain in detail the non-canonical Wnt/PCP tissue polarity and signaling pathway.

1. Planar Cell Polarity

1.1 Planar Cell Polarity in invertebrates' epithelia

Planar Cell Polarity or PCP classically refers to the alignment of a group of cells within the plane of a tissue, which is perpendicular to the apico-basal axis. PCP proteins were initially identified in *Drosophila* epithelia and are highly conserved between species (Vinson and Adler, 1987; reviewed in Butler and Wallingford, 2017; Peng and Axelrod, 2012; Adler, 2012). More globally, PCP proteins define a signaling pathway that controls the planar axis of a tissue and/or global tissue organization by regulating the cytoskeleton.

Critically, in invertebrates at least, a major difference between the canonical and non-canonical (calcium and PCP) Wnt pathways is the absence of transcriptional regulation in the later. This absence of regulation of ß-catenin severely impairs our ability to study the pathway as there is not clear readout of PCP activation, or tools like luciferase assays. Thus, structural readouts and protein planar asymmetry have been at the roots of PCP signaling deciphering and remain the best tools we have today to study PCP.

Wnts are believed to have a permissive and not an instructive role at least in epithelia, further limiting our access to an extrinsic activator of the PCP pathway. This was demonstrated in recent work in *Drosophila* wing (Yu et al., 2020; Ewen-Campen et al., 2020). Using various technical approaches, the two studies confirm that even in absence of any Wnt, core PCP signaling works and establishes a correct planar polarity within the tissue. This contrasts with several studies that demonstrated that Wnt can orient PCP in different species (Wu et al., 2013; Chu and Sokol, 2016), but the authors postulate that gain of function or Wnt overexpression can hijack the PCP signaling in a non-physiological manner, or that is permissive, but not instructive.

The core PCP signaling cassette is composed by six proteins: the cytosolic proteins Diego (Dgo), Prickle (Pk) and Dishevelled (Dsh) and the transmembrane proteins Vang Gogh/Strabismus (Vang/Stbm), Flamingo/Starry Night (Fmi/Stan) and Frizzled (Fz). Studies in the *Drosophila* wing revealed that these proteins display a planar asymmetric distribution at the apical surface of epithelial cells, at cell-cell junctions, defining a proximal-distal or PCP axis (**Figure 2A, 2B**). In epithelia, Pk and Vang/Stbm colocalize to the proximal side while Dgo, Dsh and Fz are present on the distal part. Fmi/Stan is the only protein that is present on both sides (**Figure 2B**). This specific planar asymmetric distribution defines their function as they are produced at the mRNA level in all the cells of this tissue. An intercellular feedback system, based on interactions between PCP proteins at the cell junctions, is believed to ensure the presence/absence of the proteins at the plasma membrane (Bastock et al., 2003; Das et al., 2004; Jenny et al., 2003, Tree et al., 2002; reviewed in Harrison et al., 2020).

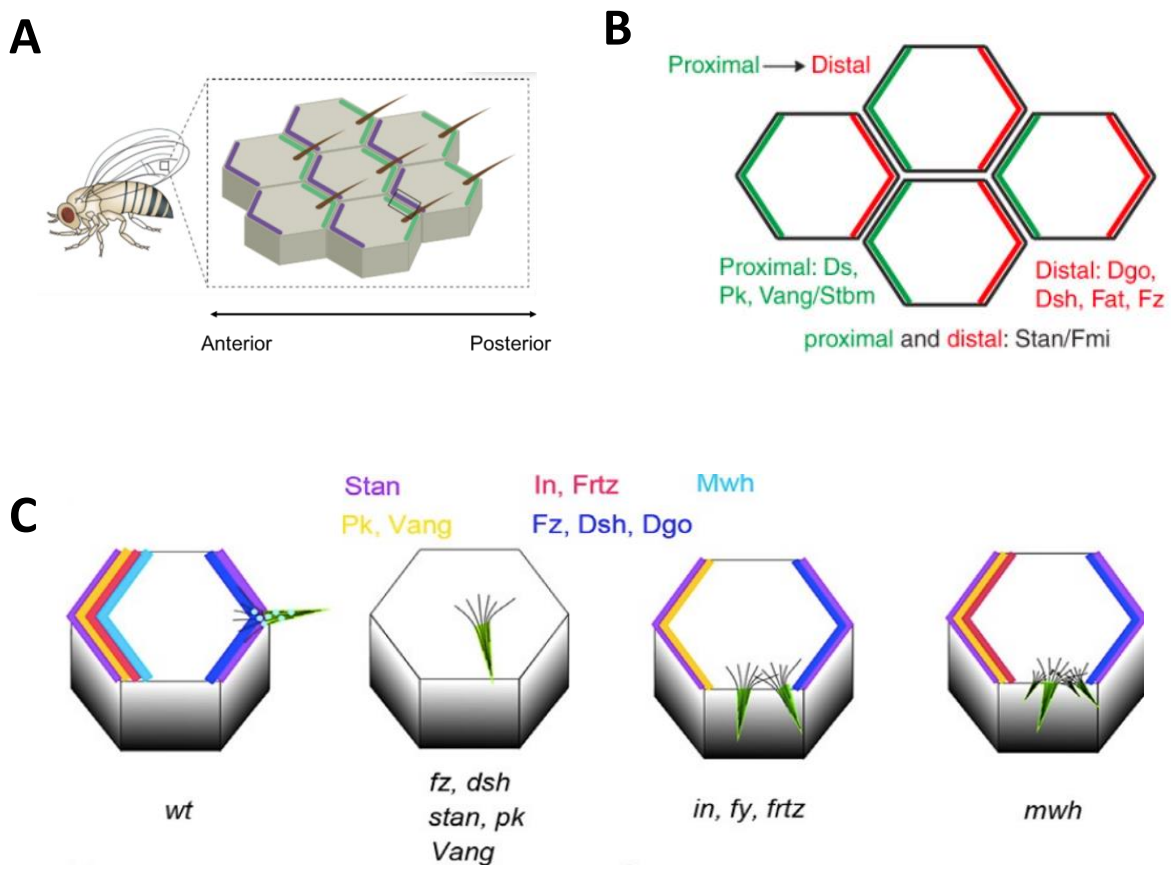

Figure 2: *representation of the distribution of the PCP proteins in the Drosophila wing.* ***(A)*** *Epithelial cells of the wing, with the trichome hair oriented in the distal part.* ***(B)*** *Schematic of the asymmetric distribution of core PCP proteins: in red, Dgo, Dsh, Fz and Fat are restricted to the distal side. Ds, Pk and Vang localize to the proximal part.* ***(C)*** *Trichome localization and orientation disruption in core PCP genes mutants and cytoskeletal effectors (see 1.1.1.1 Intrinsic/cell-autonomous PCP: determination of a specific site for cytoskeleton organization). These mutants are the classical representation of a PCP phenotype. Mwh = Multiple wing hairs; In = Inturned; Frtz = Fritz; fy = fuzzy (gene). Images modified from Butler and Wallingford, 2017; Wang and Nathans, 2007; Adler, 2012.*

Every epithelial cell of the *Drosophila* wing contains a trichome, which is a hair-like structure made of actin and microtubules that is localized at the apical surface of the cell and positioned distally (**Figure 2A**) (Adler, 2002). Trichomes are the result of the polarized assembly of actin and tubulin filaments at the distal part of the cell. The specific planar asymmetry distribution of core PCP proteins defines the localization of the trichome of each epithelial cell, but also the coordination of all trichomes orientation within the tissue. The uniform orientation of all of the trichomes of the wing determines a proximal and distal axis within the plane (perpendicular to the apico-basal polarity) that defines the PCP axis. Of note, the asymmetric distribution of PCP proteins is transient and precedes the manifestation of cell polarity (in this case, the orientation of the trichome). As discussed further in the text, the disruption of core PCP proteins or their cytoskeletal effectors leads to a misorientation of the

hair in the wing cells or the formation of multiple hairs, which constitutes a PCP phenotype (**Figure 2C**)

Besides the epithelial cells in the wing, *Drosophila* shows PCP organization in other structures, including the eye and the mechanosensory bristles of the thorax. *Drosophila* eyes are composed of ommatidia, which are clusters of photoreceptors. PCP proteins are asymmetrically distributed in these structures and determine their sense of rotation in respect to a line called equator (**Figure 3A**) (Singh and Mlodzik, 2012). Similar to the PCP phenotype seen in the *Drosophila* wing, mechanosensory bristles in the thorax/notum of *Drosophila* lose their orientation within the anterior-posterior axis in core PCP mutants (**Figure 3B)** (Singh and Mlodzik, 2012). In addition, PCP signaling controls the asymmetrical division of sensory organ precursor cells (SOP) that will give rise to the sensory bristles in the fly notum. The rotation of the mitotic spindle of these cells during asymmetric cell division defines a PCP axis within the antero-posterior axis of the notum (**Figure 3C**) (Bellaïche et al., 2001; Morin and Bellaïche, 2011; reviewed in Montcouquiol and Kelley, 2020). In this system, the planar asymmetric distribution of core PCP proteins controls the orientation of the mitotic spindle: Vang/Stbm localizes to the anterior cortex and recruits Partner of Inscuteable (Pins) and both control the posterior localization of the apical complex Partitioning defective, Par. This process ensures that the mitotic spindle aligns with the plane of the epithelium (**Figure 3C**).

Considering that the wing is the most studied model regarding PCP in *Drosophila*, I will focus the next sections on this particular structure.

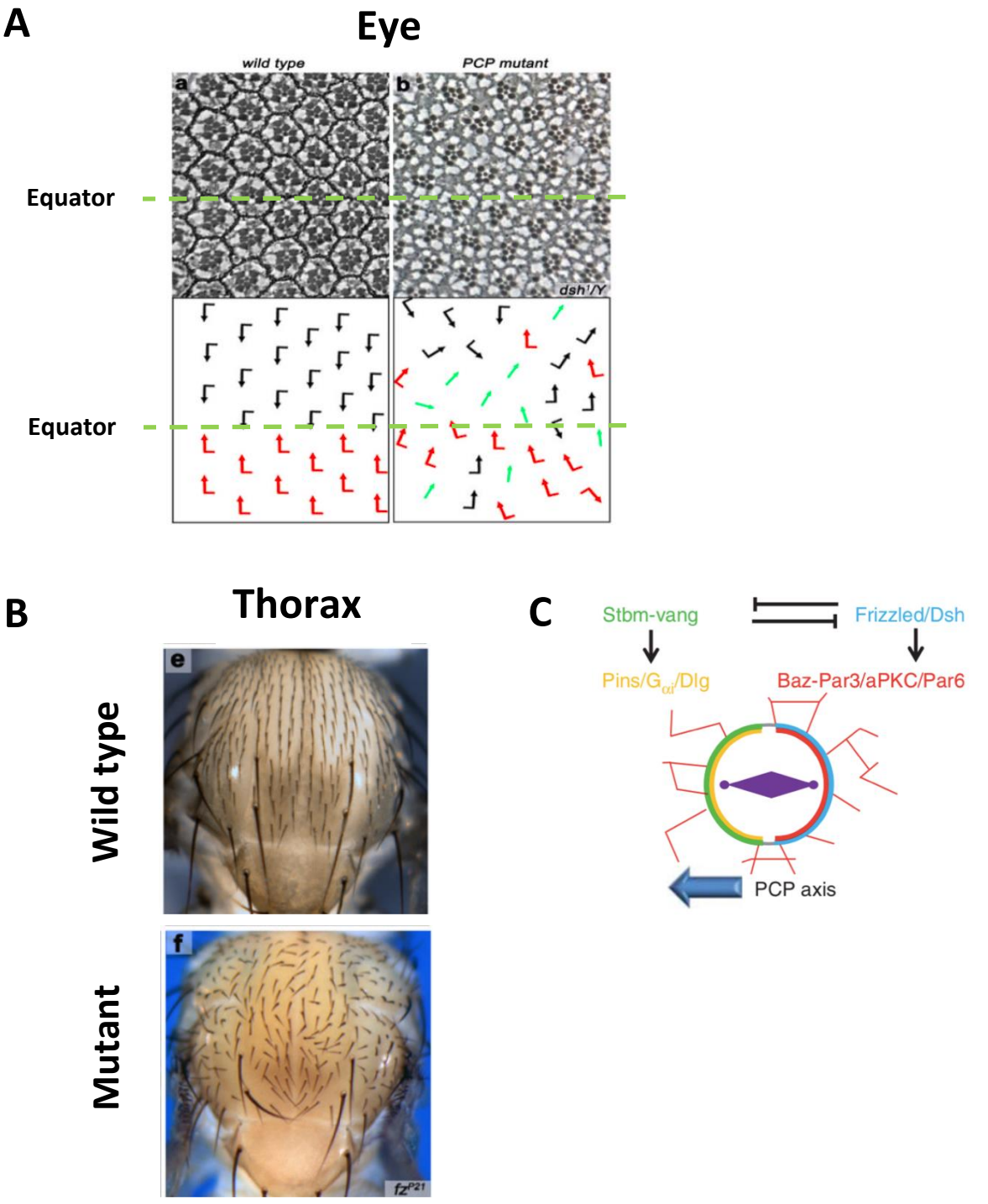

Figure 3: *Examples of PCP in Drosophila.* ***(A)*** *The disruption of core PCP proteins leads to the loss of the rotation angle towards the equator line of the ommatidia (green dotted line) in the Drosophila eye.* ***(B)*** *Hair orientation in the notum/thorax of Drosophila is lost upon depletion of core PCP genes.* ***(C)*** *Surface view of the asymmetric localization of PCP proteins determines the mitotic spindle orientation and asymmetric cell division in sensory organ precursor cells. From Singh and Mlodzik, 2012 and Montcouquiol and Kelley, 2020.*

1.1.1 PCP effectors and cytoskeleton modulation

1.1.1.1 Intrinsic/cell-autonomous PCP: determination of a specific site for cytoskeleton organization

Various studies showed that the specific formation of the trichome at the distal side of the wing cells is regulated by a cell-autonomous coordination and functional organization of all six core PCP proteins. The three transmembrane core PCP proteins are critical in the early recruitment of the proteins, and the cytosolic proteins are believed to participate in the stabilization and amplification of the asymmetry, through various mechanisms.

The planar asymmetric distribution of the six core PCP proteins is believed to restrict the specific recruitment of cytoskeleton protein effectors to the distal side of the cell (**Figure 4**) (Strutt and Warrington, 2008). This results in the specific formation of the trichome only at the distal apex of the epithelial cell. One proposed mechanism behind this process claims that Inturned (Int), Fuzzy (Fuzz) and Fritz (Frtz) are effectors of Vang/Stbm, which recruits them to the proximal side (Adler et al., 2004; Strutt and Warrington, 2008; Adler and Wallingford, 2017). In *Drosophila* wing cells these proteins control Multiple wing hairs (Mwh) recruitment, a homology 3 (FH3)-domain protein member of the formin family, which would block actin polymerization. The proximal localization of Vang/Stbm would therefore lead to the specific recruitment of Int/Fuzz/Fritz, which in turn restrict actin polymerization and hair development to the distal side. Supporting this theory, depletion of Mwh promotes the formation of extra hairs in aberrant positions at the apical surface of wing cells but does not disrupt the asymmetric localization of core PCP proteins (**Figure 2C**) (Wong and Adler, 1993). So, while loss of core polarity protein function (and thus of asymmetric localization) causes formation of a single prehair in the center of the cell, loss of function of these downstream effectors leads to formation of multiple prehairs at cell edges. Genes encoding Inturned, Fuzzy and Fritz have mammalian orthologs (called *Intu*, *Fuz* and *Wdpcp*), all embryonic lethal in knockouts, all leading to early neural tube defects (NTDs) and with more important role for ciliogenesis than for planar polarity (reviewed in Adler and Wallingford, 2017). There are no known *mwh* orthologs in mammals.

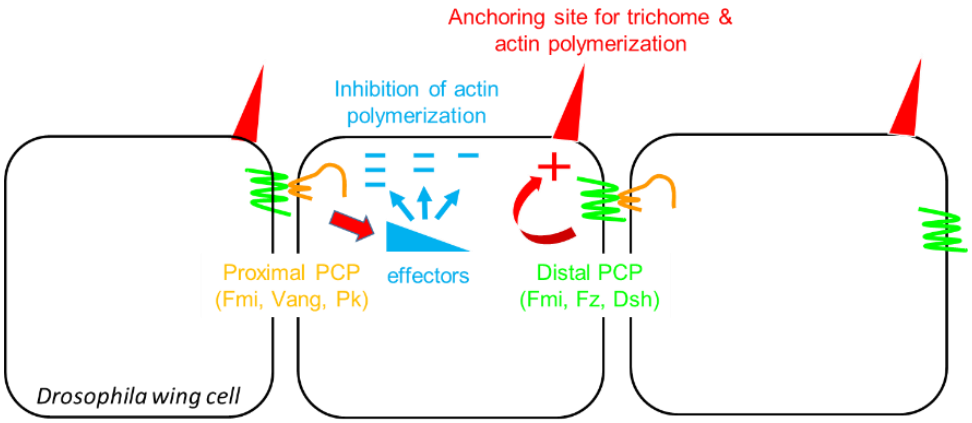

Figure 4: *Schematic of core PCP proteins driving the cytoskeleton modulation behind trichome formation in Drosophila wing cells. Modified from Strutt and Strutt, 2009. Green = Fz, orange = Vang/Stbm.*

Rho kinases also appear to control the number of trichomes formed per cell in the wing (Winter et al., 2001). Mutations in genes encoding actin regulators like RhoA and the formin Diaphanous affect the number of trichomes and their orientation, revealing the important role of actin regulating proteins on hair formation (Winter et al., 2001; Strutt et al., 1997; Yan et al., 2009; Lu and Adler, 2015; Winter et al., 2001; Franke et al., 2010). RhoA tightly regulates the orientation and number of trichomes generated per cell, as RhoA-negative clones display a PCP phenotype that is cell-autonomous. As such, the surrounding cells remain normal (Strutt et al., 1997). RhoA is thought to activate and boost the accumulation of Mwh via a direct interaction, thus driving the specific formation of the hair at the distal side of the cell (Yan et al., 2009).

Diaphanous-related formins, which control actin nucleation and elongation, are activated by Rho kinases. Genetic depletion or expression of a constitutively active Diaphanous affect the orientation and the number of hairs per cell. As this role overlaps with RhoA, it is believed that formins are Rho effectors (Lu and Adler, 2015). In this case, the authors hypothesized that diaphanous gene (*dia*) interacts negatively with *mwh* to restrict the place of actin polymerization and the formation of the hair.

Other putative downstream PCP effectors are JNK proteins. Boutros and colleagues used the *Drosophila* ommatidia as a model to demonstrate that Dsh activates JNK cascades via its DEP domain, which is the region essential for its activity in PCP signaling (Boutros et al., 1998). In fact, disruption of the JNK signaling can induce polarity defects but its activation can reverse the phenotype of Dsh mutants. The relevance of JNK as a PCP effector was described mostly in the context of convergent extension in vertebrates (for review see Roszko et al., 2009), revealing species and tissue specific factors acting as PCP downstream effectors (**Figure 5**).

Altogether, these studies show that the central role of PCP is the regulation of cytoskeleton dynamics, which culminates in a manifestation of polarity: the oriented formation of the trichomes in the wing cells.

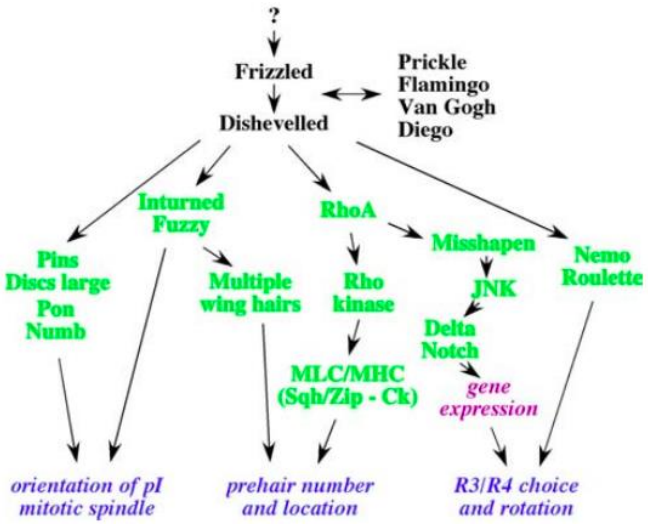

Figure 5: *Schematic of PCP signaling downstream effectors and concrete functions described in Drosophila. From Axelrod and McNeill, 2001.*

1.1.1.2 Tissue level or cell non-autonomous PCP: coordination of PCP within the tissue

Cells need a directional cue across the tissue to coordinate their intrinsic PCP and generate a global, tissue-level PCP. This ensures that every trichome is uniformly oriented within the entire tissue. The three transmembrane core PCP proteins convey this directional signal across every cell.

The cell-non autonomous effect of PCP was first described by Vinson and Adler using mutant clones for *Fz* in chimeras, where *Fz*-lacking cells are surrounded by wild type (WT) cells in the wing (Vinson and Adler, 1987). These chimeras are a fantastic tool to evaluate if a group of mutant cells can affect surrounding WT cells. Strikingly, if the mutant cells exhibited the expected altered PCP phenotype of the trichome, the surrounding WT cells were also affected, but not randomly: when the mutant clone lacked *Fz*, the surrounding WT cells hair pointed towards the mutant clone cells. But when the mutant clone lacked *Vang/Stbm*, the trichomes of the surrounding WT cells were pointing away from the mutant clone cells (Taylor et al., 1998). This was the first observation of a core PCP directional transmission across cells via cell-cell contact signals. It also highlighted the directionality of this signal: from high level Fz-signaling to low-level Fz-signaling. This cell-non autonomy (also called tissue-level PCP) is believed to occur before the cell-autonomous one and defines the axis at tissue level (Wong and Adler, 1993). Importantly, this signal transmission does not require the cytosolic core PCP proteins Pk, Dsh or Dgo, but only the transmembrane ones, Fz, Vang/Stbm and Fmi/Stan.

The Fat/Dachsous (Ft/Ds) pathway acts together with the core PCP pathway to establish tissue-level PCP, although their molecular interplay is still under debate. Ft and Ds cadherins are localized at the cell membrane and bind to each other via heterophilic interactions at the cell junctions (**Figure 6**) (Strutt and Strutt, 2002). This binding is coordinated by the

phosphorylation of their extracellular domains, a process driven by the protein Four-jointed (Fj) (Strutt et al., 2004; Brittle et al., 2010). Ft and Ds are expressed in opposite gradients within the *Drosophila* wing, with Ft showing a distal to proximal gradient and Ds an opposite distribution. This gradient is behind the asymmetric localization of Ft and Ds within a single cell, a distribution that is reminiscent of the asymmetrically distributed core PCP proteins (reviewed in Butler and Wallingford, 2017).

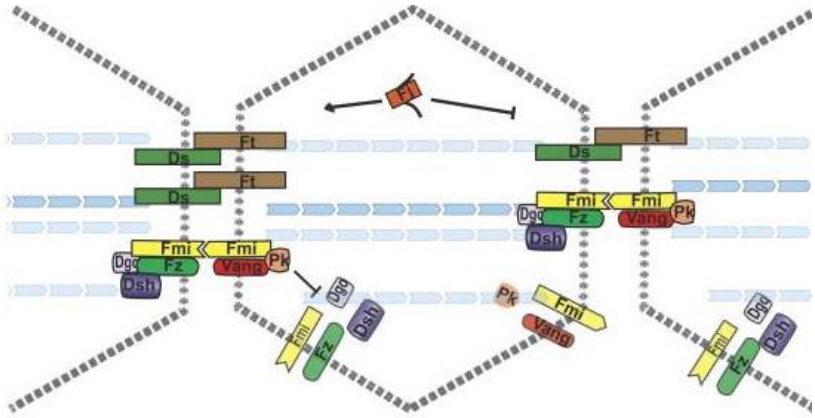

Figure 6: *Schematic of the intercellular distributions of the core PCP and Fat/Dachsous proteins. From Matis and Axelrod, 2013.*

Ft/Ds is believed to act in parallel with PCP core effectors, but this is still under debate. Disruption of Ft/Ds via the absence of Ft, Ds or Fj does not impact asymmetric localization of PCP core proteins but it affects hair polarity in the surrounding cells (Matakatsu and Blair, 2006; Feng and Irvine, 2007; reviewed in Goodrich and Strutt, 2011; Butler and Wallingford, 2017). This reveals an important function for this pathway in tissue polarity establishment (Adler et al., 1998). The alignment of PCP core proteins with Ft/Ds varies depending on the tissue and this could be explained by the interaction of this pathway with the two isoforms of Prickle we find in *Drosophila*: Prickle-Prickle (Pk) and Prickle-Spiny legs (Sple). Cells in the wing with higher levels of Pk show a localization for Fmi/Stan, Vang/Stbm and Pk on the same side of the cell as Ft. On the contrary, cells with a predominant Sple will distribute these proteins to the orientation where Ds is located (Ayukawa et al., 2014; Ambegaonkar et al., 2015). The functional consequence of these differences relies on changes in the microtubule orientation: the plus-ends are usually oriented towards Ds in cells with predominant Pk and towards Ft in cells with Sple (**Figure 7**) (Olofsson et al., 2014). Therefore, Ft/Ds can affect the asymmetric distribution of PCP core proteins by modulating the polarity of the microtubules. The molecular mechanisms behind this process are, however, unknown to this date. For a detailed review on the regulation of the PCP signaling pathway via Ft/Ds, please refer to Matis and Axelrod, 2013.

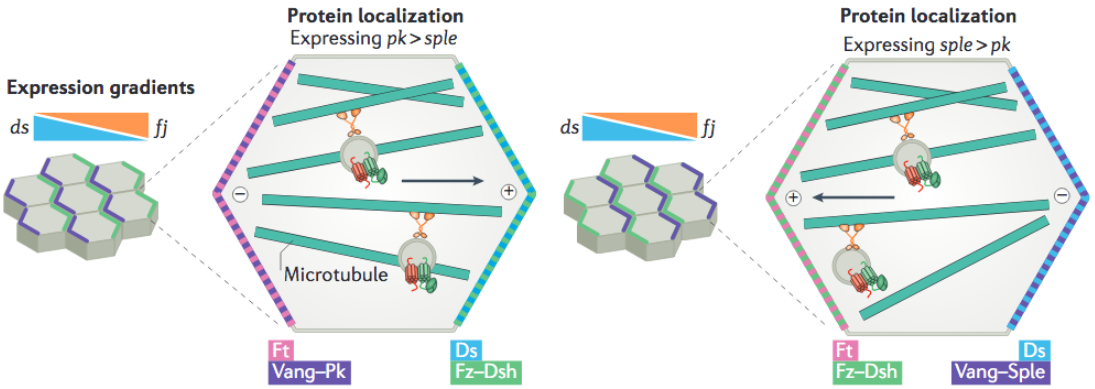

Figure 7: *Regulation of microtubule polarity by the Ft/Ds pathway that results in asymmetric distribution of PCP core proteins. This role is mediated by the two different Pk isoforms in Drosophila, Prickle-Prickle (Pk) and Prickle-Spiny legs (Sple). Image from Butler and Wallingford, 2017.*

PCP pathway controls the organization of the developing fly pupal wing, as it provides an initially disordered tissue with a high organization in terms of cell arrangements and tissue geometry, prior to hair establishment. PCP signaling modulates intercellular junction shrinkage and regrowth, and cadherin recycling through the endocytic pathway (Classen et al., 2005). The large body of work of Thomas Lecuit emphasized this planar polarized remodeling of cell contacts and showed that it is driven by the polarized enrichment of myosin-II at specific junctions and the downregulation of proteins of the apical/adhesion complex (Bertet et al., 2004; for review see Zallen, 2007; Bertet and Lecuit, 2009; Devenport, 2014). His work and that of others show that many tissue morphogenetic events during development have their roots in the spatial and temporal regulation of intercellular tension that is controlled by myosin-II and actin filaments that regulate cell contacts and cell shape. These concepts and the molecules at play are found in all of the tissue whose shape is controlled by PCP.

1.1.2 The core PCP proteins interactome and planar asymmetry

The six core PCP proteins described in *Drosophila* have different structures and domains. As mentioned above, Vang/Stbm, Fz and Fmi/Stan are transmembrane proteins while Dsh, Dgo and Pk are cytosolic (**Figure 8**). These proteins are highly conserved in structure and function from flies to vertebrates. **Table 1** sums up the different features and domains of these proteins and their vertebrate orthologs, and the molecular interactions are discussed in detail further in this section.

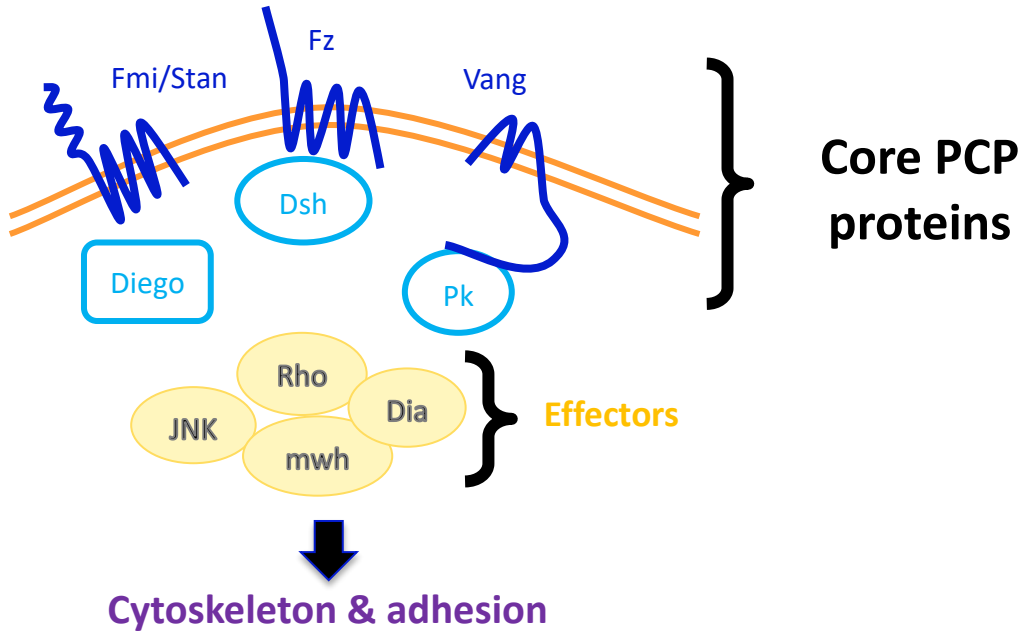

Figure 8: *Schematic of the core PCP proteins in invertebrate epithelial cells, which activate downstream effectors that will modulate the cytoskeleton and cell adhesion. Image from the host lab.*

PCP protein in drosophila	Molecular features	Vertebrate orthologs
Frizzled (Fz)	Seven-pass transmembrane receptor that binds Wnt, Dsh and Dgo. It recruits Dsh and Dgo to the membrane	Several depending on the species, but *Fz3* and *Fz6* high relevant for PCP
Dishevelled (Dsh)	Composed by DIX, DEP and PDZ domains. Cytoplasmic protein that binds to Fz (necessary for Dsh membrane localization), Pk, Vang and Dgo	*Dvl1-3*
Flamingo (Fmi)/Starry night (Stan)	Seven-pass transmembrane cadherin with receptor properties and homophilic cell adhesions. It contributes to the membrane localization of core PCP proteins	*Celsr1-3*
Prickle (Pk)	Made by 3 LIM and one PET domain, cytoplasmic protein recruited to the membrane by Vang. It interacts with Vang, Dsh and Dgo	*Pk1-4*
Vang Gogh (Vang)/Strabismus (Stbm)	4-pass transmembrane protein that interacts with Pk, Dsh and Dgo and binds Pk to the membrane	*Vangl1-2*
Diego (Dgo)	Cytoplasmic protein made by ankyrin repeats. It is recruited to the membrane by Fz and interacts with Vang, Dgo and Dish	*Ankr6d*

Table 1: *List of the core PCP proteins in Drosophila, with their molecular features and their vertebrate orthologs. Adapted from Maung and Jenny, 2011.*

Planar core PCP proteins asymmetry is tightly linked to PCP function, but a detailed molecular level understanding of core PCP asymmetric distribution mechanism is still debated in *Drosophila*. We know that in epithelial cells of invertebrates (and in many species), the interactions between the 6 core PCP proteins are key for their asymmetrical distribution and function. In fact, the precise regulation of the planar asymmetry is tightly linked to their levels of expression since negative or positive manipulation of core PCP gene function often have indistinguishable effects, something that seems to be a general feature of this pathway (Devenport 2014, Butler and Wallingford, 2017, Peng and Axelrod, 2012).

Individual protein-protein interactions have been observed between many of the core pathway proteins *in vitro*: Vang/Stbm, Pk, Dsh, and Dgo can all interact with one another, and Fmi/Stan may interact directly with Fz or Vang/Stbm, while Fz may interact with Vang/Stbm and Dsh (**Figure 9**) (for review, see Harrison et al., 2020). A result of this tight interactome is that the absence of one of them affects the planar distribution of the remaining five, to various degrees, with Fmi/Stan and Fz believed to be at the top of the complex since their absence completely prevents the recruitment of the remaining proteins (Strutt and Strutt, 2008; Struhl et al., 2012).

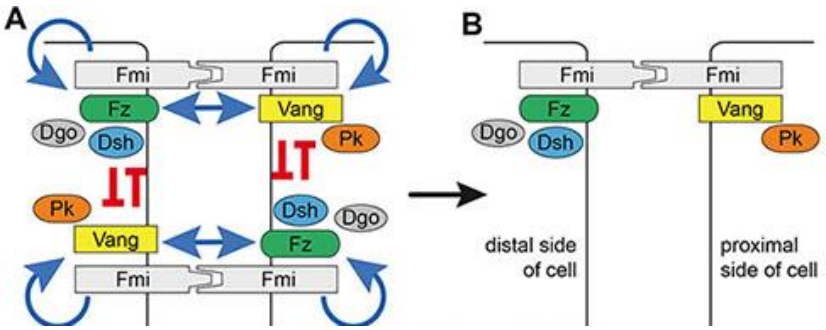

Figure 9: *Representation of the molecular interactions between core PCP proteins in Drosophila, in one cell and between adjacent cells. These are needed for their asymmetric distribution, function and activation of the PCP pathway. Adapted from Axelrod, 2009.*

The stabilization/destabilization of these complexes have been suggested to be driven by feedback mechanisms and cell-cell communication in a way that would amplify any small polarity bias generated by a global cue. A so-called Prickle-dependent intercellular feedback loop was first suggested by the group of Axelrod to explain the asymmetric localization of the proteins (Tree et al., 2002). After an initial recruitment of Fz and Vang/Stbm by Fmi/Stan, Vang/Stbm would recruit Pk (Jenny et al., 2003) and Pk interacts with Dsh to prevent its localization at the membrane. In a feedback loop, Pk-Vang/Stbm could then inhibit Fz accumulation on the proximal part of the neighboring cell (reviewed in Harrison et al., 2020). The complex Pk-Vang/Stbm could then regulate Fz-Dsh activity and initiate symmetry-breaking during polarity signaling. A study led by Das and colleagues showed that Dgo also interacts with Vang/Stbm and Pk (Das et al., 2004).

On the other hand, Dgo and Pk are in competition for binding Dsh: in this model, Dgo promotes Fz activity while Pk inhibits it (Jenny et al., 2005). Cho et al. further showed that the overexpression of Pk promotes an internalization of this protein and that of Vang/Stbm and Fmi/Stan (Cho et al., 2015). Finally, Dsh would regulate Pk localization at the neighboring cells by stabilizing the Fz-Fmi:Fmi-Vang/Stbm complex (**Figure 9**) (Ressurreição et al., 2018). In fact, the depletion of Dsh promotes a Dsh-Fz destabilization and a mislocalized Pk, leading to a disassembly of the core complex proteins.

Like apico-basal polarity, establishment of PCP requires a symmetry breaking step, which is the decision for Fz to accumulate distally and Vang/Stbm proximally. Fmi/Stan is the only core PCP that is symmetrically distributed at junctions in both proximal and distal parts. As such, and by forming trans-homodimers with their large cadherin-rich repeats, Fmi/Stan is the bridge between two cells (**Figure 9**). Mutants for *Fmi/Stan* revealed a reduced presence of Pk and Vang/Stbm at the cell edges and a loss of Dsh, Dgo and Fz, suggesting that it is on top of the asymmetric distribution of the other core PCP proteins (Strutt 2001; Axelrod, 2001; Shimada et al., 2001; reviewed in Harrison et al., 2020). Interestingly, *Fz* mutants exhibit an impaired localization of Fmi/Stan, which is now at the apical domain of the membrane and not at the proximodistal edges (Strutt and Strutt, 2008). Fz and Fmi/Stan are, therefore, acting together as top controllers of PCP signaling. Interestingly, the molecular interaction between Fz-Fmi/Stan was reported only at one side of the cell (**Figure 9**): Fmi/Stan present in the distal and proximal parts of two different cells are interacting. But, in each individual cell, one set of Fmi/Stan is specifically associated with Fz in one side, while the other one does not bind Fz. Thus, these proteins create a bridge Fz-Fmi:Fmi to control PCP signaling and both of them are indispensable for this role (Tree et al., 2002; Bastock et al., 2003; Strutt, 2001; Axelrod, 2001; Shimada et al., 2001; reviewed in Harrison et al., 2020). Besides these mechanisms, the specific transport of core PCP proteins ensuring an asymmetric distribution is still under study. Two studies reported that microtubules have a crucial role on sorting Fz and Dsh towards the distal side (Matis et al., 2014; Shimada et al., 2006). As explained in *1.1.1.2 Tissue level or cell non-autonomous PCP: coordination of PCP within the tissue*, the specific microtubule organization allowing such transport is regulated by the Fat/Dachsous pathway.

The Prickle conundrum

A recent study questioned Pk contribution to the “classical” core PCP signaling (Casal et al., 2018). Casal and colleagues hypothesized that Pk acts in both the core PCP and the Dachsous/Fat (Ds/Ft) pathways. In this study, the core PCP pathway is referred to as Stan/Fz (Stan being the abbreviation for Starry Night, the other name of Flamingo, Fmi). Prickle was proposed to be the link between the initial polarization of the Ds/Ft system and the adaptation of these signals by the Stan/Fz system (Hogan et al., 2011; Ayukawa et al., 2014; Olofsson et al., 2014; Ambegaonkar and Irvine, 2015).

Prickle has two isoforms in *Drosophila*, namely Prickle-Prickle (Pk) and Prickle-Spiny legs (Sple). Out of the two, Sple was thought to be the bridge between the Ds/Ft – Stan/Fz systems. However, several studies contradict this postulate: the Ft/Ds and the core PCP systems can function independently from one another, implying that a link between both is not necessary (Casal et al., 2006). More intriguing, two different studies found that genetic manipulation/depletion of *pk* alone or *pk* and *sple* together increases the domineering non autonomous effect of Fz/Stan in wild type cells mixed with mutant clones (Adler et al., 2000; Lawrence et al., 2004). As some of these studies challenged what was known about the role of Prickle as a core PCP protein, Casal and co-workers aimed to better understand the functions of Pk and Sple. By using the bristles on the *Drosophila* abdomen as a model, the authors confirmed that the Ft/Ds and the Stan/Fz systems are independent (Casal et al., 2018). It is possible that a link between these systems exists, but it would be functionally irrelevant for both pathways. In addition, Pk and Sple were found to function independently from the Stan/Fz system: in cells missing core PCP proteins like Fmi/Stan, the depletion or overexpression of Pk/Sple changed the hair orientation that was already affected in the first place. This means that the aberrant expression of Pk/Sple leads to an additional PCP effect from the one due to Fmi/Stan loss.

How does this fit with the studies showing that Pk is essential for PCP protein localization and signaling establishment? The authors postulated that, even if Fz, Vang/Stbm and Fmi/Stan lose their asymmetrical localization in *pk-sple* negative cells, these cells still respond to the reception from Fz-overexpressing cells. Importantly, sending cells that either have an excess or lack of Ft and/or Ds affect the polarity of wild type and negative *pk-sple* cells. This shows that Prickle isoforms are not necessary for this pathway, but they still modulate it: the changes in polarity of the surrounding cells depend on the levels of Pk and Sple isoforms, showing that Prickle modulates the polarity change outcome initially promoted by a broken Ft/Ds system (**Figure 10**) (Casal et al., 2018).

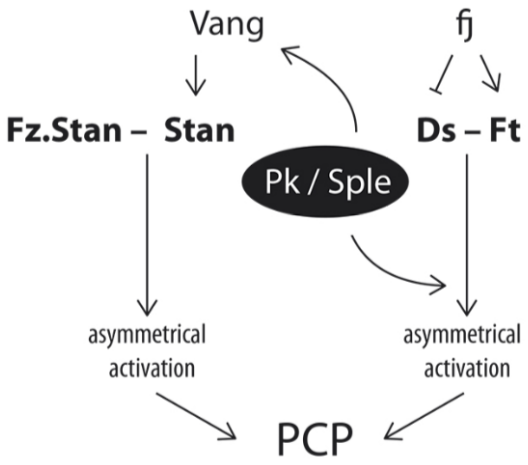

***Figure 10**: schematic of how Pk and Sple contribute to PCP via the modulation of the Fz/Stan and the Ds/Ft systems. From Casal et al., 2018.*

This study is of high relevance, as it demonstrates that Prickle is not essential for the Ft/Ds nor the Stan/Fz pathways, but it contributes to PCP by modulating both. Prickle is, therefore, different from the other described core PCP proteins and this functional divergence must be considered when studying its function in other cell structures and species.

Of note, there is not to our knowledge a mammalian equivalent to the Pk and Sple isoforms.

1.2 Planar Cell Polarity in vertebrates and mammals

Each core PCP gene has several orthologs in mammals, with its corresponding proteins. To date, there are up to four Prickle called Prickle1-4 Planar Cell Polarity Protein or Prickle-like1-4 (Pk1-4), three Dsh (Dvl1-3), two Vang/Stbm (Vangl1-2), three Fmi/Stan (Celsr1-3), several Fz depending on the species, but with Fz3 and Fz6 important for PCP, and one of Diego (Ankr6d/diversin).

PCP proteins and signaling are very conserved in vertebrates epithelia, notably in mammals. But due to the 3D context of many other tissues, it cannot be defined according to a plane axis, and can be described as a mechanism that allows cells and groups of cells to exhibit polarized behaviors that are coordinated with their neighbors and the tissue axes. Such coordination of cell behaviors defines correct tissue morphogenesis and function.

1.2.1 PCP and convergent extension in *Xenopus laevis* and zebrafish

Convergent extension (CE) is a cellular process conserved across different species that is critical to shape many tissues during development. During CE, cells comprising the tissue sense the global, tissue-level planar polarity. As such, a number of core PCP and PCP-associated genes have been shown to be critical for CE (for review, see Gray et al., 2011; Vichas and Zallen, 2011; Roszko et al., 2009).

One of the first and most studied CE process described in vertebrates occurs during notochord formation in *Xenopus laevis* embryo but also zebrafish (*Danio rerio*) (for review see Butler and Wallingford, 2017; Devenport, 2014; Wallingford, 2012). The process extends throughout gastrulation to neurulation during which notochord cells elongate along the mediolateral axis, leading the tissue to become narrower and longer as the cells intercalate with each other in response to many cues, including tissue-level PCP (**Figure 11A**). Typically, a disrupted CE will interrupt the elongation through the anterior-posterior axis and will result in animals with a shorter trunk (reviewed in Wallingford, 2012; Butler and Wallingford, 2017; Devenport, 2016). It is this shorter trunk phenotype that has been used in *Xenopus* and zebrafish mutants as a PCP readout and to identify genes involved in CE (reviewed in Solnica-Krezel, 2006)

Of note, mutations in a number of human core PCP genes, including *CELSR, FZD* and *VANGL*, lead to neural tube defects, comprising spina bifida and the most severe form craniorachischisis. Neural tube closure is a CE-dependent process (see *1.4 PCP mice models and human neurodevelopmental pathologies*).

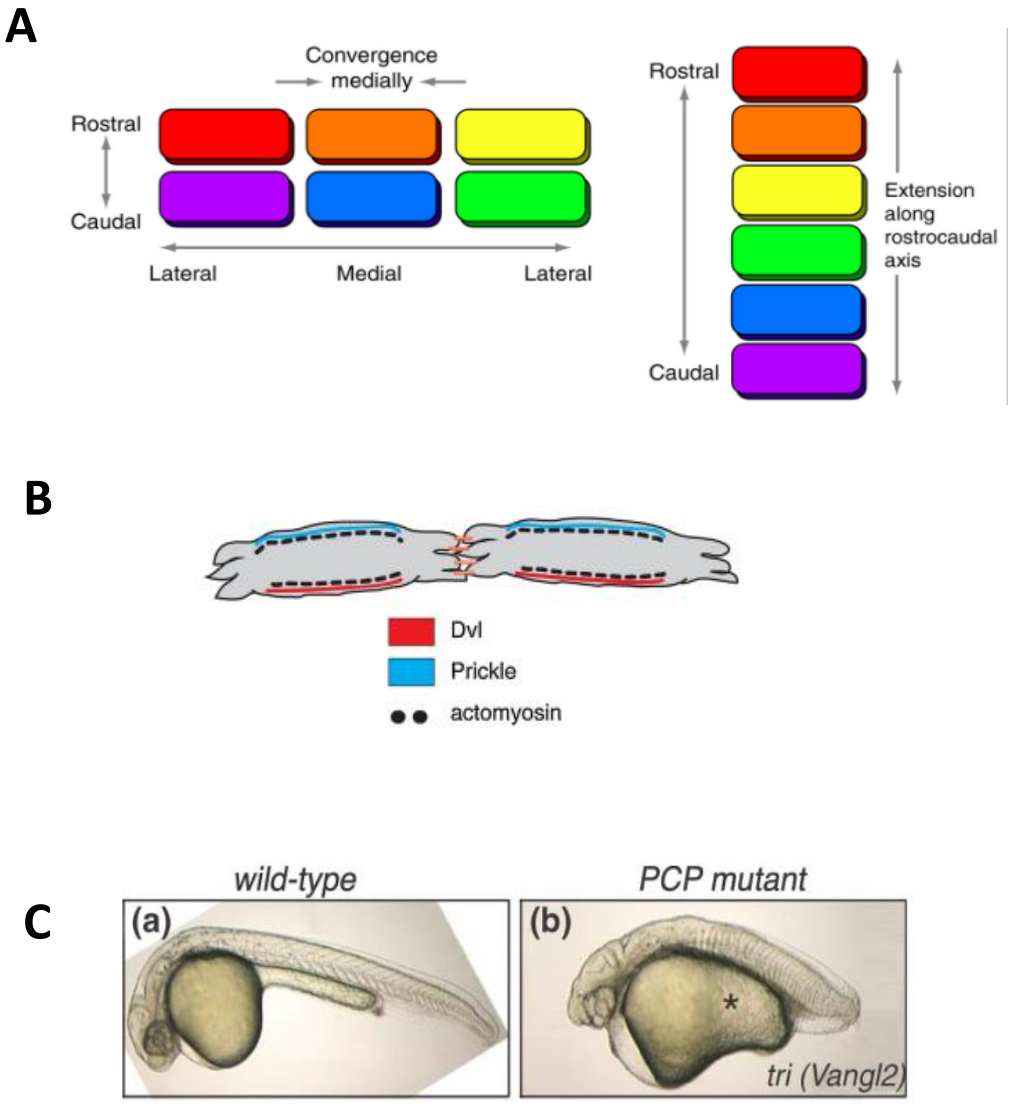

***Figure 11**: Schematic of the convergent extension process. At first, cells are randomly organized within the mediolateral and anterior-posterior axes. **(A)** As CE starts, these cells use their lamellipodia protrusions to gradually intercalate in the mediolateral axis. As the process continues, the cells form an elongated structure all along the anterior-posterior axis. **(B)** PCP proteins are asymmetrically distributed during CE and drive the specific accumulation of actomyosin, which regulates lamellipodia formation. **(C)** The trilobite (tri) mutant for Vangl2 in zebrafish shows a shorter trunk due to defects in convergent extension. Adapted from Montcouquiol et al., 2006; Devenport, 2016 and Singh and Mlodzik, 2012.*

Mechanistically, convergence and organization rely on the capacity of cells to extend lamellipodia protrusions between them. The cells create these protrusions randomly, but they eventually respond to cues in the environment to orient and establish stable connections with the neighboring cells in the medio-lateral axis. The lamellipodia will then exert actomyosin-based tractions, which are key to drive the different cell movements. Asymmetric localization has been reported for Pk and Dvl in these cells in zebrafish, suggesting that they recruit/restrict the actomyosin machinery at both edges (**Figure 11B**) (Yin et al., 2008).

At the end of the 90s, two seminal papers demonstrated that Dsh and Fz8 are key for convergent extension in *Xenopus* (Deardoff et al., 1998; Sokol, 1996). In particular, blocking Dsh function impedes convergent extension resulting in a drastically shortened trunk. Although Dsh has a central role in the conventional Wnt/β-catenin signaling cascade, subsequent work in *Drosophila*, *Xenopus* and zebrafish, making use of mutants, showed that different domains of Dsh could activate either the canonical or the non-canonical pathways (Boutros and Mlodzik, 1999; Heisenberg et al., 2000; Tada and Smith, 2000; Wallingford et al., 2000. See *A brief introduction to Wnt signaling pathways*). Further work confirmed that most of the core PCP proteins are essential regulators of CE, including Vang/Stbm and Pk (**Figure 11C**) (Takeuchi et al., 2003; Veeman et al., 2003; Carreira-Barbosa et al., 2003). Published in the same year, two seminal studies identified the role of Vang/Stbm in CE in *Xenopus* (Goto and Keller, 2002; Darken et al., 2002; Jessen et al., 2002). Excess or defect of Vang/Stbm inhibited CE during gastrulation and neural tube closure processes, resulting in a trunk shortening and open neural tube. Carreira-Barbosa and colleagues showed the importance of Celsr, the ortholog of Fmi/Stan, in CE cell movements during gastrulation in zebrafish (Carreira-Barbosa et al., 2009). The expression of a truncated form of Celsr affects cell cohesion and disrupts CE. For all of these, both the gain and loss of function affect CE mechanisms and result in the same phenotype: animals with a stunted trunk.

However, CE is a complex process, as it occurs in 3D and involve other cell types than epithelial cells (mesenchymal cells), plus additional important players including Wnts, extracellular matrix (ECM) components, integrins, etc. It is in these model systems that much of the molecular links between core PCP molecules and ECM or adhesion molecules have been identified.

Altogether, these studies show that PCP proteins are crucial for the establishment of collective and directional cell movements during convergent extension, often using the same mechanisms and players than *Drosophila* epithelia, with added complexity.

1.2.2 PCP in mammals: the inner ear

The degree of organizational precision of the cochlear epithelium is an exquisite example of tissue complexity requiring PCP signaling and core PCP genes for a correct development. The organ of Corti (OC), the sensory epithelium of the cochlear duct, comprises highly ordered

rows of hair cells (HCs) interdigitated with similarly ordered rows of supporting cells. Each HC is topped with an actin-rich stereociliary bundle that has a V shape. The vertices of all HCs are uniformly aligned along the proximal to distal axis (**Figure 12A, 12B**). The alignment of these bundles is a wonderful example of form and planar polarity following function, as each bundle is directionally sensitive and can only respond to deflections along the neural–abneural or PCP axis (for review, see Montcouquiol and Kelley, 2020).

In 2003, Montcouquiol and colleagues showed that one of the transmembrane core PCP proteins, Vangl2, is needed for the proper orientation of the hair bundles (**Figure 12A, 12B**) (Montcouquiol et al., 2003). Remarkably, the PCP phenotype generated in these cells was highly reminiscent of that of the wing cells in *Drosophila*, validating the conservation of PCP function between species and highlighting this system as one of the best to identify and study core PCP in mammals (**Figure 12C**). The same year, another study revealed that another of the transmembrane core PCP protein, Celsr1 (one of Fmi/Stan orthologs), was also critical in the same system (Curtin et al., 2003). A few years later Fz3/6, orthologs of the last of the three transmembrane core PCP proteins, were identified in the same system to control hair bundle planar polarity (Wang et al., 2006). Later, it was shown that the deletion of the three cytosolic core PCP proteins have only mild or no effects. Dvl1-3 and Diversin/Ankdr6 (Diego) only had a small if any impact (Etheridge et al., 2008; Jones et al., 2014), while Pk1 and Pk2 have no effect in the orientation of the hair bundle in the cochlea (Yang et al., 2017).

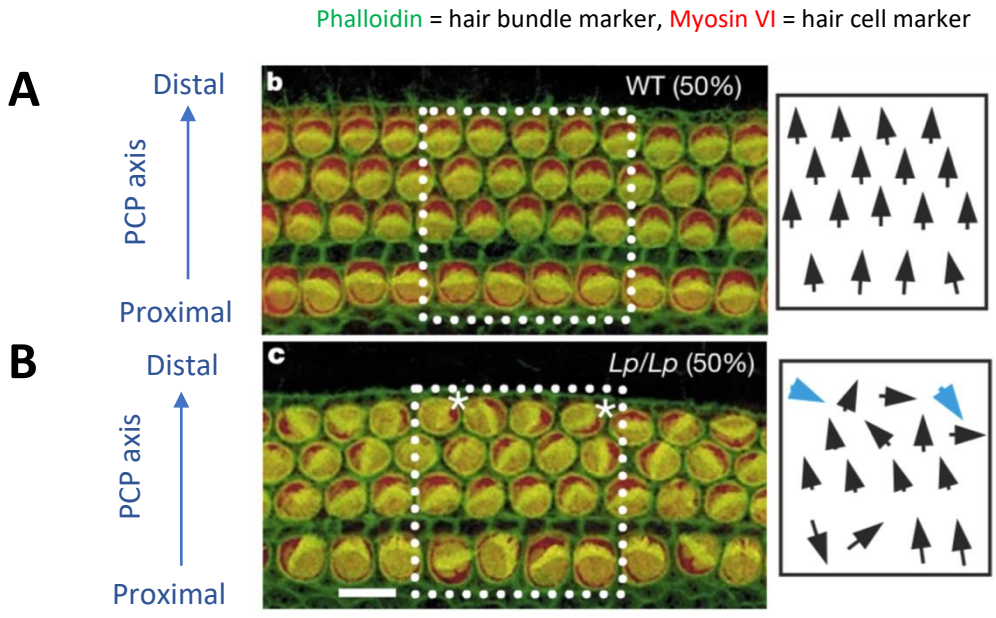

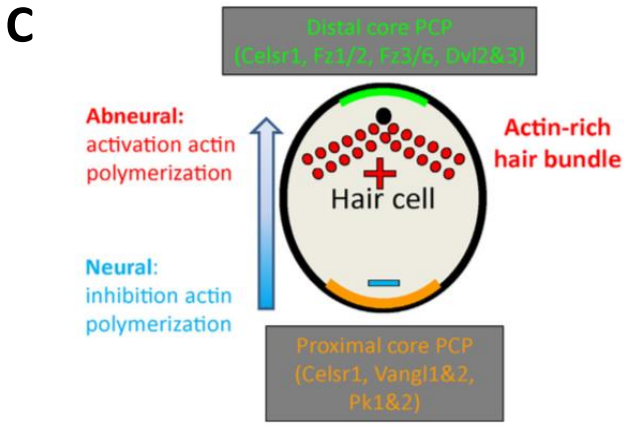

***Figure 12**: Surface view of the OC labeled with myosin VI (red, HC marker) and phalloidin (green, hair bundle marker). From neural to abneural the OC is comprised of 4 rows of HC: the inner hair cells towards the neural edge, and the 3 rows of outer hair cells towards the abneural edge. Phalloidin labels the stereociliary bundles (green) in the apical region of the HC.* ***(A)** In the wild-type (WT) tissue, the hair bundles have a uniform orientation, pointing in the same direction (=PCP axis).* ***(B)** In the mutant for vangl2 (Looptail or Lp) hair bundles are misoriented.* ***(C)** Schematic of the asymmetric distribution of core PCP proteins in the mammalian hair cell. From Montcouquiol et al., 2003 and Ezan and Montcouquiol, 2013.*

Interestingly, Montcouquiol and colleagues also identified *Scribble* (*Scrib*) as a PCP gene, as the orientation of the hair bundle is affected in the *Circletail* mutant. *Circletail (crc)* mice have a frameshift mutation for *Scrib*, a gene that encodes a multi-PDZ (PSD-95, Discs-large and ZO-1) and leucine-rich-repeat scaffolding protein that is part of the conserved machinery regulating apico-basal polarity (Murdoch et al., 2003). In *Drosophila* epithelial cells and neuroblasts cells, Scrib acts with Discs large-1 (Dlg1) and Lethal giant larvae (Lgl) to distinguish the basolateral domain, via reciprocally antagonistic interactions with the atypical Protein Kinase C/Partitioning defective 6 (aPKC/Par6) complex. In fly, Bilder and Perrimon showed that loss of Scrib function results in the misdistribution of apical proteins (Crumbs) and adherens junctions to the basolateral cell surface, while basolateral protein localization remains intact (Bilder and Perrimon, 2000). Besides Scrib, other "PCP associated proteins" were identified in mammals. In 2004, Lu and colleagues found that mutant mice for *Ptk7* (protein tyrosine kinase 7) displayed neural tube closure defects and misoriented stereocilia in the hair cells (Lu et al., 2004). In fact, the authors found that *Ptk7* genetically interacts with *Vangl2*. Some other PCP proteins were identified by screening embryos treated with the mutagenic agent NN-Ethyl-N-NitrosoUrea (ENU). The embryos showing neural tube defects, which are a classic PCP effect, were selected and analyzed. These studies identified several new PCP genes, like *Sec24b*, as well as new mutations on *Scribble* (Wansleeben et al., 2010; Merte et al., 2010). These PCP associated proteins can be differentiated from core PCP proteins because they are not planar polarized, their mutation/deletion does not result in the loss of asymmetry of other core PCP proteins, and their homozygote mutation/deletion often result in mild PCP phenotypes in the cochlea, a phenotype that is worsened by the partial loss of expression of one of the core PCP genes. Many genes fitting that description have been identified using the cochlear phenotype and genetic interactions as described in

Montcouquiol et al., including (but not limited) *Ptk7* (Lu et al., 2004; Paudyal et al., 2010; Lee et al., 2012), *Sec24b* (Merte et al., 2010; Wansleeben et al., 2010) *Smurf1/2* (Narimatsu et al., 2009), *Cthrc1* (Yamamoto et al., 2008) and *Ror2* (Shambony and Wedlich, 2007; Martinez et al., 2015). As expected, proteins involved in apico-basal polarity, protein trafficking, anchoring or stability are the main candidates.

As mentioned before, the planar polarization of all six core PCP protein is a critical aspect of PCP, as it is a clear readout of both cell and tissue PCP. Starting in 2005, the genesis of GFP-reporter mice or the use of specific antibodies showed that Dvl2, Vangl2, Fz3 and Fz6 were also planar polarized in the OC, within the PCP axis defined by hair bundle orientation (Wang et al., 2005; Montcouquiol et al., 2006; Wang et al., 2006). This demonstrated that, in addition to a conservation of function, the planar asymmetric distribution of core PCP proteins was also conserved in mammalian epithelia. Molecularly, Montcouquiol et al. identified a physical and functional interaction between the *Vangl2* and *Scrib* genes by generating a double heterozygote mouse. While single heterozygotes for each gene had only mild effect on cochlear PCP, a double heterozygote *Lp*/+; *Crc*/+ recapitulated the severe phenotype observed in *Lp*/*Lp* mice homozygotes. Because the phenotype of the *Crc*/*Crc* homozygote mutant was mild compared to the *Vangl2* mutant, and since *Scrib* was not a known core PCP gene in *Drosophila*, it was further described as “PCP associated gene”. The idea is that these proteins do not share the characteristics of the core PCP proteins, and are not necessarily effectors, but participate in the establishment of the planar polarity. As such, Scrib is a logical candidate since apico-basal polarity is required for PCP. Much later, Courbard and colleagues confirmed a similar genetic interaction in the *Drosophila* wing cell, although they defined it as an effector in that study (Courbard et al., 2009)

Shortened cochleae have also been reported for mouse lines carrying mutations in *Vangl2*, *Dvl1/Dvl2*, *Wnt5a*, *Dchs1*, and *Fat1/4* (Montcouquiol et al., 2003; Wang et al., 2006; Qian et al., 2007; Mao et al., 2011; Saburi et al., 2012), suggesting also a role for these PCP genes in the convergent extension process. However, other PCP mutants, such as *Fz3/6* and *Celsr1*, which play a role in stereociliary bundle orientation, were not reported to have short cochleae (Curtin et al., 2003; Wang et al., 2006).

Examples of core PCP functions in mammals range from the correct polarization of the cilia in the trachea and brain ventricles (Vladar et al., 2012; Tissir et al., 2010; Guirao et al., 2010), to kidney tubular branching and glomerular maturation (Yates et al., 2010a), lung branching (Yates et al., 2010b), neuronal progenitor regulation (Lake and Sokol, 2009), heart development (Henderson et al., 2001) and alignment of hair follicles (Devenport and Fuchs, 2008). These studies show for PCP a crucial role in most tissue morphogenesis in mammals and suggest a link between the dysfunction of these proteins and the onset of developmental disorders and pathology.

1.3 Planar Cell Polarity in central nervous system development

The brain is made by millions of neurons, whose connections are key for the brain to have a correct function. Neurons receive electrical inputs and transmit them to the neighboring cells through synapses. This information flow process relies on the capacity of these cells to properly establish neuronal polarity. In fact, neurons are highly polarized cells with two compartments that differ in composition and function: the somatodendritic domain and the axon. As neuronal polarity and motility (e.g., neuronal migration) highly rely on cytoskeleton dynamics, a role for PCP signaling in neuron development and function is only logical.

Most PCP genes are present in mammalian cortical progenitors, including *Vangl2*, *Dvl2*, *Dvl3*, *Celsr3* and *Pk2*. However, the higher expression of some of them in postmitotic neurons (like *Dvl3*, *Celsr3* or *Pk2*) suggests an additional role in neuronal maturation rather than proliferation. The work of F. Tissir was key to decipher the expression profile of core PCP components during mouse central nervous system development (Tissir and Goffinet, 2006, Tissir and Goffinet, 2010; 2013).

1.3.1 Ependymal cells

PCP proteins are key for the development and function of ependymal cells, which form the epithelial lining in the ventricles of the brain. These cells have their apical surface covered by cilia, whose beating is key for the circulation of the cerebrospinal fluid (CSF). And like the neuroepithelium of the cochlea (see *1.2.2 PCP in mammals: the inner ear*), they heavily depend on PCP signaling for their function, and retain many of the characteristics identified in *Drosophila* wings. Our group participated in the two seminal studies showing that two of the transmembrane core PCP proteins, Vangl2 and Celsr, organize the uniform beating axis of the motile cilia of the ependymal cells of rodents (Guirao et al., 2010; Tissir et al., 2010). Mutation of *Vangl2* or double deletion of *Celsr2* and *Celsr3* in mice resulted in the disruption of cilia organization of ependymal cells, impairing CSF flow, and lethal hydrocephalus in the case of *Celsr*. Later, Dvl was also reported to have important functions in cilia development (Ohata et al., 2014; reviewed in Ohata and Alvarez-Buylla, 2016). Tissir and colleagues also reported that *Ank6rd* is widely present in the adult brain and particularly enriched in the ventricular, proliferative zones during development (Tissir et al., 2002). Interestingly, the expression profile does not exactly match that of *Celsr1-3*, orthologs of Fmi/Stan in mammals, suggesting that Ankrd6 has a role in nervous system development but not necessarily through interaction with these proteins.

1.3.2 Neural tube closure and CE

Neural tube closure is a critical process during embryo development in which the neural plate narrows and extends to form the neural groove, which subsequently folds and forms the tube. The collective cell movements behind this process are reminiscent of those of convergent extension during gastrulation. A pioneer study in *Xenopus* showed that Dvl was needed for CE in both gastrulation and the formation of the neural tube (Wallingford and Harland, 2001), revealing a role for PCP in this process. As mentioned before, several mutant mice for PCP proteins present an open neural tube phenotype: these include *Looptail* (*Vangl2*), *Circletail* (*Scrib*), *Crash* (*Celsr1*), *Ptk7*, *Dvl1*/*Dvl2* double mutants and *Fz3*/*Fz6* double mutants (Greene et al., 1998; Murdoch et al., 2001; Hamblet et al., 2002; Lu et al., 2004; Wang et al., 2006). Ybot-Gonzalez and colleagues studied in depth the mechanisms of neural tube closure defects in *Looptail* mice and found that *Vangl2* mutation impaired CE in both the mesoderm and in the neural plate (Ybot-Gonzalez et al., 2007). This phenotype was matching the one discovered by Wallingford and Harland with mutated *Dvl* in Xenopus and thus revealed a conserved role for both proteins across species (Wallingford and Harland, 2001). Regarding Scrib, the molecular mechanisms behind the neural tube closure defects in mutants were unclear until recently. In 2017, Kharfallah and colleagues observed that, in the neural plate of *Circletail* mice, the localizations of Vangl2 and partitioning-defective 3 (Par3) were abnormal (Kharfallah et al., 2017). A recent study using *Scrib*^{rumz}, a mutant for Scrib that disrupts its stability and targeting to the membrane, showed that Scrib is necessary for correct cell intercalation and as a consequence the narrowing of the tissue was affected (Lesko et al., 2020, preprinted). In addition, the absence of Scrib resulted in defects in the expression and localization of proteins that are key for apico-basal polarity and junctional remodeling, such as the atypical protein kinase C (aPKC), partitioning-defective 6 and 3 (Par6 and Par3), Zonula Occludin-1 (ZO-1) and N-cadherin.

1.3.3 Axonal guidance and neuronal arborization

PCP has key functions in nervous system development of invertebrates, besides the trichome formation and alignment in the *Drosophila* wing. For example, studies have shown the importance of Fmi/Stan for axonal guidance of neurons in the visual system of flies (Senti et al., 2003; Lee et al., 2003). Fmi/Stan also participates in dendritic development and, interestingly, this function is independent from Fz suggesting different protein complexes (Gao et al., 2000). Further studies showed that PCP regulates axonal guidance and branching in the mushroom neurons of *Drosophila* (Shimizu et al., 2011; Ng, 2012). Mrkusich and colleagues discovered that Pk interacts with Fmi/Stan to drive sensory axon outgrowth during embryo development in flies and they do so at a critical point: the transition from the peripheral to the central nervous system (Mrkusich et al., 2011). In *Caenorhabditis elegans*, VANG-1, PRKL-1 and DSH-1 participate in neuronal polarity establishment by coordinating

neurite development (Sanchez-Alvarez et al., 2011). Defects in PRKL-1 lead to the formation of supernumerary neurites, while its overexpression suppressed neurite formation, showing that a tight balance of PRKL-1 dosage is necessary for the correct polarization of neurons.

In the early 2000's, two papers identified the function of Fz3 and Celsr3 in axonal guidance: mutant mice for *Fz3* (Wang et al., 2002) and *Celsr3* (Tissir et al., 2005) had a similar loss of the major axonal tracts of the brain, including the anterior commissure or the corticospinal tract, suggesting an interaction between both to regulate this process. Additionally, Fenstermaker and colleagues found that Fz3, Celsr3 but also Vangl2 were necessary for axonal guidance of monoaminergic neurons along the anterior-posterior axis of the brainstem (Fenstermaker et al., 2010). A later study showed that Vangl2 could also play a role in axonal growth and guidance by antagonizing Dvl1 and favoring PCP signaling in the growth cone (Shafer et al., 2011). In contrast, the host lab suggested recently that Vangl2 departed from the other two transmembrane core PCP, Fz and Celsr, regarding axonal guidance function. Dos Santos-Carvalho and colleagues demonstrated that Vangl2 is present in the axon and the growth cone of young hippocampal and cortical neurons (DIV3) and modulates their axonal outgrowth in the developing brain (Dos Santos-Carvalho et al., 2020). Early deletion of *Vangl2* in neuronal progenitors of the forebrain leads to the spatially restricted deficit of only two commissural axon bundles, the corpus callosum and hippocampal commissures. Mechanistically, they showed that the absence of Vangl2 leads to an increase in axonal outgrowth due to a reduced turnover of N-cadherin, and a better coupling between the adhesion molecule and the dynamic actin flow in the growth cone. The results support a model in which Vangl2 acts as a cell autonomous regulator of membrane protein endocytosis and junctional remodeling during growth cone exploration, thereby modulating its outgrowth.

Celsr2 is also involved in the maintenance of the complexity and length of the dendritic tree in Purkinje neurons (Shima et al., 2004). In the same line, Sowers et al. showed in 2013 that Prickle-like 2 (Pk2) is needed for dendritic development (Sowers et al., 2013). Using a *Pk2* KO strain, the authors found that neurons in the hippocampus of these mice had a reduced dendritic branching, number of synapses and size of PSDs. These structural defects correlated with problems in synaptic transmission and an autism spectrum disorders (ASD) - like behavior in mutant mice (for more details of Pk2 function in neurons, see *1.5 Prickle (Pk) and Scribble (Scrib)*).

1.3.4 Neuronal migration

In vertebrates, PCP signaling controls neuronal migration in a specific subset of cells in zebrafish and mice: the facial branchiomotor neurons (FBMN). These cells migrate in a tangential way within the plane of the neuroepithelium and extend their axons to innervate the face musculature (**Figure 13A, 13B**). PCP proteins, including Fz3a, Vangl2, Celsr2, and

Prickle1a and b, regulate this type of migration through autonomous and cell non-autonomous mechanisms (Jessen et al., 2002; Wada et al., 2005; Wada et al., 2006; Walsh et al., 2011). In an elegant experiment, the authors showed that wild type (WT) FBMN neurons that are grafted into a neuroepithelium lacking Fz3a, Vangl2 or Celsr2 fail to migrate, demonstrating a cell non-autonomous effect (**Figure 13D**). Prickle1b deficient neurons preserve the migratory "behavior", as they are able to extend directed cell protrusions, however, they get stuck in R4 in wild type neuroepithelium and cannot migrate further (**Figure 13C**) (Mapp et al., 2011).

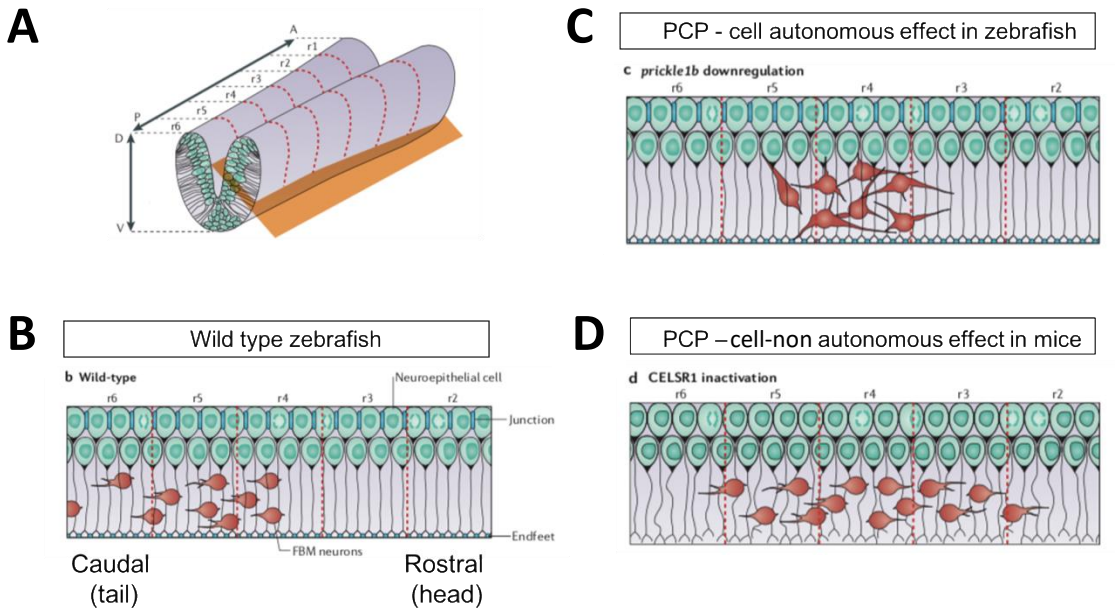

***Figure 13**: PCP controls neuronal migration. **(A)** Schematic of the developing rhombencephalon. **(B)** FBMN neurons, generated at r4, migrate caudally to r6 in control conditions. **(C)** Prickle1a disruption in FBMN neurons impairs their migration and get stuck in r4. It is an example of a cell-autonomous role of PCP on neuronal migration **(D)** Wild type neurons fail to migrate in Celsr1-mutant neuroepithelium, evidencing a cell-non autonomous effect of PCP in this process. Adapted from Tissir and Goffinet, 2013.*

1.3.5 Synaptic function and memory

The team of Yimin Zou attempted to explore the role of PCP signaling in neuronal function. They sugested opposite roles for Celsr3 (promoting) and Vangl2 (inhibiting) excitatory formation (Thakar et al., 2017), while a more recent study suggests that an imbalance in Celsr3 and Vangl2 at the synapses may lead to a synaptic loss in Alzheimer's disease (Feng et al., 2020, preprinted). This study suggests that amyloid ß oligomers, which make aggregates in the brain and are related with the onset of this pathology, bind to Celsr3 and together help Vangl2 on destabilizing the PCP complex Frizzled3-Celsr3, which is crucial for PCP signaling.

The work of Robert and coworkers using mice models with a postmitotic deletion of *Vangl2* suggest a role for the protein in computational processes of the hippocampus (Robert et al., 2020). The authors show that in the absence of Vangl2, granule cells (GCs) of the dentate gyrus stayed in an immature longer, while more mature GCs were unable to elicit long-term potentiation. The resulting defects on the DG-CA3 network promoted an improvement of pattern separation, worsened pattern completion but the spatial learning remained unaltered. This work shows a crucial role for PCP on regulating the hippocampus circuitry.

Altogether, these studies demonstrate the importance of PCP proteins on regulating key processes during central nervous system development and highlights their functional versatility. It is therefore logic that disruption of PCP proteins is associated with a wide range of neurodevelopmental pathologies.

1.4 PCP mice models and human neurodevelopmental pathologies

Given the crucial role of PCP has in the nervous system development, it is not surprising that mutations in core PCP genes are identified in patients, mostly associated with neurodevelopmental disorders, notably neural tube defects (NTD), but also autism spectrum disorders (ASD) and epilepsy. Mice models recapitulate some of these phenotypes and highlight others.

1.4.1 Neural tube defects – NTDs

NTDs are severe defects of the central nervous system that arise from the failure of the neural tube closure during embryonic development (reviewed in Greene and Copp, 2014). There are various types of NTDs, associated with different degrees of severity, depending on which region of the neural tube is affected. For example, spina bifida is the most common NTD and involves the posterior part of the neural tube, which becomes the spinal cord. The most severe form of NTD is craniorachischisis, where both the spinal cord and the brain regions of the neural tube remain open. Embryos with this condition suffer miscarriage during pregnancy or die shortly after birth.

Two first PCP genes identified in mammalian PCP, *Vangl2* and *Scrib*, are both associated with NTDs in mice models, and more precisely craniorachischisis, the most severe form (Montcouquiol et al., 2003). In fact, most mutant mice for core PCP genes develop neural tube defects/craniorachischisis including double mutant *Fz3/Fz6* (Wang et al., 2006), double mutants *Dvl2/Dvl1* (Hamblet et al., 2002) and the *Crash* and *Spin cycle* spontaneous mutants for *Celsr1* (Curtin et al., 2003). Interestingly, mutants for the associated PCP genes such as *Scrib* or *Ptk7* also lead to craniorachischisis (Rachel et al., 2002; Lu et al., 2004) showing a strong association of PCP signaling with this pathology.

Two studies from 2012 and 2013 identified missense mutations for *CELSR1* and *SCRIB* in fetuses suffering from the most severe form of neural tube defects, craniorachischisis (Robinson et al., 2012) and children with spina bifida (Lei et al., 2013). Using constructs with the different point mutations, the authors found that these mutations did not disrupt the interaction of SCRIB with VANGL2 *in vitro*, but it prevented their localization at the membrane. Since a similar craniorachischisis and a lack of membrane localization were reported for the *Looptail* mutation (Montcouquiol et al., 2006), the recruitment of the proteins at the membrane was deemed critical to their NTD function. *PRICKLE1* missense mutations were also found in NTD patients and predicted to be deleterious (Bosoi et al., 2011; Beaumont et al., 2019). In 2012, De Marco and colleagues investigated the role of Dishevelled in neural tube defects and identified missense mutations in the human *DVL2* and *DVL3* genes (De Marco et al., 2012).

1.4.2 Autism spectrum disorders (ASD) and epilepsy

Our team has shown that adult, heterozygous *Circletail* mice, with a truncation mutation for Scrib, displayed sociability defects and improved learning and memory capacities, two behavioral hallmarks of ASD (Moreau et al., 2010; Moreau et al., 2020; preprinted; for more details see *1.5.2 Relation with the cytoskeleton and function in neurons*).

Stam and colleagues reported a deletion or duplication of a specific part of the chromosome 8, 8q24.3, which contains *SCRIB*, in patients with intellectual disabilities, microcephaly and developmental delays (Stam et al., 2009). An inverted duplication of this same region was reported in patients with mental retardation, ASD and epilepsy, among other phenotypes (Battaglia et al., 2013). Besides chromosomic rearrangements involving the *SCRIB* gene, Neale and colleagues found, by using exome sequencing of patients with ASD and their families, a de novo, missense mutation of *SCRIB* (Neale et al., 2012).

But the core PCP gene that is the most convincingly associated to both ASD and epilepsy is *Pk2*, as mice models recapitulate symptoms from both pathologies. In 2011, Tao et al. reported that the overexpression of the wild type zebrafish ortholog *Pk2* or two independent constructs with variants found in epileptic patients disrupted convergent extension movements during gastrulation, resulting in a shorter body axis (Tao et al., 2011). In addition, the overexpression of these mutant constructs in zebrafish embryos reduced calcium release dynamics and shows that human mutations found in epileptic patients alter the activity of Pk2 in zebrafish. Next, the authors showed that mutant mice had a decreased seizure threshold compared to the controls, suggesting a globally increased excitability. Deletion of one allele of *Pk1* or *Pk2* was sufficient for these animals to be more sensitive to developing seizures. Interestingly, the authors observed embryonic lethality for homozygous mice for *Pk1* but not for *Pk2*. The threshold for seizure development was lower in Pk1 than in *Pk2*-/- or *Pk2*+/-, suggesting 1) different contributions of Pk1 and Pk2 to an epileptic phenotype and 2)

a dosage-dependent effect of Pk2 for proper neuronal function. Flies with a recessive point mutation in *Sple* in homozygosis displayed more seizures than the controls. While this study shows a link between Prickle and epilepsy and complements the findings of the point mutations found in human, it does not explain the molecular mechanisms behind this process. A study in *Drosophila* shed some light on this matter, showing that the balance between Pk and Sple is protective against seizure development (Ehaideb et al., 2014). An increase of Sple is associated with a lower threshold for seizures and an enhanced anterograde transport in the axon, showing a possible molecular mechanism behind Prickle and epilepsy.

Mutations in *PRICKLE1* have been identified in different types of epilepsy (Todd and Bassuk, 2018; Mastrangelo et al., 2018; Bassuk et al., 2008). In 2011, Tao and colleagues investigated the role of both *PRICKLE1* and *PRICKLE2* in patients with myoclonic epilepsy (Tao et al., 2011). Two missense mutations of *PRICKLE1* and two of *PRICKLE2* were identified in several patients and a chromosomal deletion comprising *PRICKLE2* was found in one of the subjects. However, a study from 2016 revealed that these mutations may not be causative of epilepsy: Sandford and colleagues performed a genetic screening in the sibling of one of the patients studied in Tao et al. and confirmed the presence of *PRICKLE2* mutations (Sandford et al., 2016). However, the same patient carried three variants of another gene called *POLG*, which is known to be a causative factor for epilepsy in a significant number of patients. Sandford et al. reported that, while the use of mutant mice for Prickle shows a relation between this protein and epilepsy, it does not prove the participation of these particular mutations found in epileptic patients in the disease. As an answer to this comment, Mahajan and Bassuk claimed that the contribution of *PRICKLE2* to epilepsy cannot be ruled out: two different studies reported chromosomic deletions in the region encompassing PRICKLE2 gene in epileptic children (Mahajan and Bassuk, 2016). In conclusion, further work is needed to address, at least, the specific function of *PRICKLE2* variants in epilepsy. This could imply experimental approaches like the evaluation of the localization of these variants in heterologous cells or their overexpression in neurons to assess potential functional defects.

The link of *PRICKLE1* with ASD was first evidenced by Cukier and colleagues, who found single nucleotide variants of this gene in ASD individuals (Cukier et al., 2014). In 2018, another study identified a de novo, missense mutation of *PRICKLE1* in a child suffering from ASD, epilepsy and developmental delay (Todd and Bassuk, 2018). Interestingly, PRICKLE1 was found to interact with SYNAPSIN I, whose gene was classified as an ASD risk gene (Paemka et al., 2013). In addition, the overexpression of a mutated form of *PRICKLE1* in PC12 cells reduced the size of dense-core vesicles containing neurotransmitters, suggesting a similar role in the spines. An extensive transcriptomic study in control and patients of ASD revealed a significant decrease of RNA expression of *PRICKLE1* in the temporal and frontal cortex of ASD patients (Voineagu et al., 2011). Later, Sowers and colleagues identified two variants of *PRICKLE2* in individuals with ASD (Sowers et al., 2013). Chromosomic deletions encompassing the genetic region of *PRICKLE2* were also found in autistic patients (de la Hoz et al., 2015; Schwaibold et al., 2013; Okumura et al., 2014).

Other PCP genes are associated with neurodevelopmental pathologies. Wang and colleagues identified *CELSR3* as a potential epilepsy-related gene, but a more detailed study proving a causative link is still missing (Wang et al., 2017). A recent study using whole exome sequencing has identified a missense mutation of *CELSR3* in ASD patients (Kim et al., 2020). Microdeletions encompassing the genes for *DVL1* and *DVL2* were reported in patients with developmental delay and ID with different degrees of severity (Kaminsky et al., 2011; Zeesman et al., 2012), while Lijam and colleagues showed that mutant mice for Dvl1 displayed abnormal social behavior typical of ASD (Lijam et al., 1997).

The *FZD3* gene is located within the chromosome 8, a region associated with ASD and ID. Different chromosomal rearrangements encompassing the region of *FZD3* have been related with ID, developmental delay, ASD associated features and agenesis of the corpus callosum (Papanikolaou et al., 2006; Sajan et al., 2013).

Finally, the Decipher site, a database for human mutations found in different diseases, shows that some patients suffering from intellectual disabilities (ID), microcephaly and language development impairment presented 1q22 microduplications, a chromosomic region that includes the *VANGL2* gene (reviewed in Sans et al., 2016). Microduplications of 6q15, which includes the *ANK6RD* gene, are described in this database in patients with ID, ASD, delayed speech and language development.

All the studies showing PCP gene mutations in human pathology follow a common pattern: while they elucidate the important role of PCP in nervous system development and function, the molecular mechanisms behind this link are still unknown. Studies at the cellular level, especially in neurons, will be key to fully understand the role of PCP in pathology.

1.5 Prickle and Scribble

The work of this thesis is focused on investigating the specific roles of the core and associated PCP proteins Prickle (particularly Prickle-like 2, or Pk2) and Scribble. In the following points, both of them will be discussed in detail, with a focus on their structural aspect and their function in neurons and in the brain.

1.5.1 Protein structures

As mentioned in previous points, Prickle was first described in *Drosophila* as a core PCP signaling regulator. Gubb and colleagues found in 1999 that the *pk* gene encoded a protein formed by three Linl-1, Isl-1 and Mec-3 (LIM) domains in the C-terminus (C-ter) part of the protein followed by a PET domain located at the N-terminus side (N-ter) (Fig. 14) (Gubb et al., 1999). The PET domain stands for “Prickle-Espinas-Testin” and was named as such after the authors described a highly conserved domain in these three proteins.

What can this specific structure of Prickle tell us about its functions? LIM domains are rich in cysteine and made by a double zinc-finger motif, found in a wide range of proteins with different biological functions (reviewed in Dawid et al., 1998; Kadrmas and Beckerle, 2004). LIM domain-containing proteins have been associated with functions in the actin cytoskeleton and with both nuclear and cytoplasmic localizations. LIM domains are non-catalytic sites driving protein-protein interactions (Kadrmas and Beckerle, 2004). In fact, studies from *Drosophila* have shown that both the LIM and PET domains are involved in the interaction with Dsh, preventing its accumulation at the proximal side of the wing cells (Tree et al., 2002). The PET domain function is less characterized, but Sweede and colleagues suggested that Pk localization to the membrane mainly relies on PET, whose activity is modulated by the three LIM domains (Sweede et al., 2008). The membrane localization of Pk and its role on PCP signaling also depends on a concrete post-translational modification, a farnesylation in the C-ter (Strutt et al., 2013). Of note, the C-ter portion of the protein (which does not include the PET and LIM domains) can also modulate protein-protein interactions: in *Drosophila*, Pk interacts with Dgo via this specific C-ter domain (Das et al., 2004).

Up to 4 *Prickle* genes and proteins have been described in mammals, but it is the 1 and 2 that have been described in detail. Using the sequence of *Prickle* in *Xenopus* as a reference, Katoh and Katoh identified the *PRICKLE1*/*PRICKLE2* and *Prickle1*/*Prickle2* genes in humans and mice (Katoh and Katoh, 2003). The high homology between the resulting proteins was present all along their sequences, including the PET, LIM and the C-ter domains. In addition, the authors characterized the mRNA distribution of *PRICKLE1* and *PRICKLE2* and found them particularly enriched in the brain, eye and testis, suggesting important functions for PRICKLE in these tissues. The comparisons of structure between the *Drosophila* Pk and the mouse Pk1 and Pk2 are shown in **figure 14**.

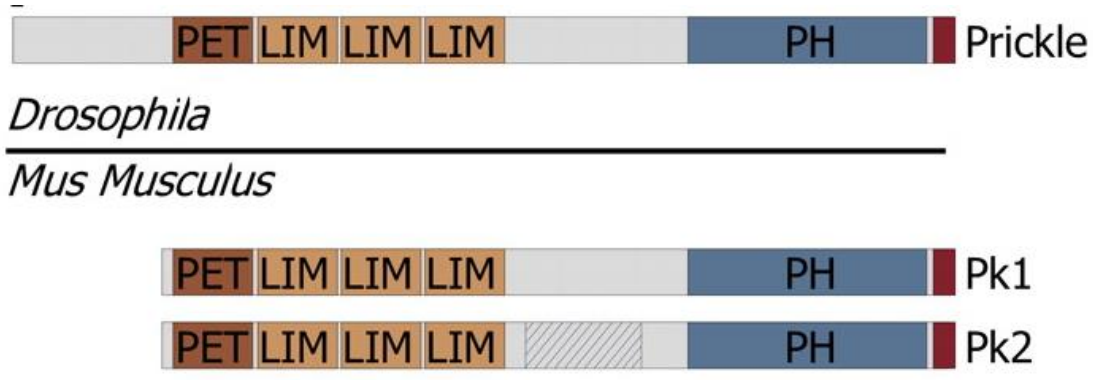

***Figure 14**: protein structures of Prickle in Drosophila and Prickle-1 and Prickle-2 in mice, being the left side the N-ter. PET and LIM domains are highlighted in red and orange, respectively. The PH domain in the C-ter stands for "protein homology" and is the highest conserved part of the protein in this side. Modified from Deans et al., 2007.*

The high homology between the *Drosophila*, mouse and human Prickles suggest a conserved role. However, the literature about the specific functions of Prickle in mammals is limited, particularly in the case of Prickle-2.

The story of Scribble (Scrib) is different, as its role in apico-basal (A/B) polarity in *Drosophila* was described before its functions on PCP (see *1.2.2 PCP in mammals: the inner ear*). A/B polarity divides epithelial cells into two specialized compartments: the apical surface, which is in contact with the lumen, and the basolateral domain that is linked to neighboring cells and the underlying tissue. Scrib is part of one of the three major complexes that are crucial for A/B polarity (Assémat et al., 2008): 1) the apical Par complex, which is localized at the apical side and formed by partitioning-defective 3 and 6 (Par3, Par6) and the atypical Protein Kinase C (aPKC); 2) the apical Crumbs complex formed by Crumbs, the protein-associated with tight junction-1 or PATJ, the multi PDZ domain protein or MUPP1 and Stardust, a MAGUK (Membrane-Associated Guanylate Kinase) protein; and 3) the basolateral Scribble complex, made by Scribble, Lethal giant larvae (Lgl) and Discs large (Dlg). It is in 2000 that Bilder and Perrimon found that mutations in *Scribble* disrupted cell shape in the embryonic mesoderm epithelia via the mislocalization of apical proteins like Crumbs (Bilder and Perrimon, 2000). Years later, Scrib was described as a crucial PCP regulator in mammals (Montcouquiol et al., 2003), revealing a highly versatile protein controlling both types of polarity.

Scrib is member of the leucine-rich repeat and PDZ protein (LAP) family of proteins, which are characterized by having LRR (leucine rich repeats) and PDZ (PSD-95/Dlg/ZO-1) domains and is comprised of Erbin and LANO (Santoni et al., 2002). Scrib structure comprises, from N-ter to C-ter, the following domains (**Figure 15**): a total of sixteen leucine rich repeats (LRR), two LAP-specific domains (LAPSDs) and four PDZ domains (reviewed in Bonello and Peifer, 2019). Scribble is a cytosolic, scaffolding protein that can be targeted to the membrane via its LRR and PDZ domains (Albertson et al., 2004).

Figure 15: *protein structure of Scrib. From left to right (N-ter to C-ter): 16 leucine rich repeats, two LAP domains and four PDZ domains. Image modified from Bonello and Peifer, 2019*

Different studies in LRR-containing proteins showed that this specific domain mediates protein-protein interactions (Enkhbayar et al., 2004). While this holds true for Scrib, it is important to mention that most of the interactions with its partners are driven via the PDZ domains: for example, Kallay and colleagues showed in 2006 that Scrib binds to Lgl2 and

Vangl2 via the LRR and the PDZ 2 and 3 domains, respectively (Kallay et al., 2006). In fact, PDZ domains are well-known for this function and they classically interact with the C-ter of their partners (Ernst et al., 2014). In Scrib, the four PDZ domains interact with different proteins: for example, the PDZ domains 2 and 3 are involved in the interaction between Scrib and NMDA receptors (Piguel et al., 2014) and Vangl2 (Montcouquiol et al., 2003), but the four of them are needed to interact with the exchange factor ß-pix (Audebert et al., 2004). A study performed in 2015 showed that Scrib binds ß spectrins via three spectrin binding motifs found in the C-ter of the protein (Boëda and Etienne-Manneville, 2015). These interactions were shown to be crucial for polarity function. The capacity of Scrib to bind different proteins with its different domains is critical for its functional diversity. Importantly, it was recently demonstrated that other epithelial LAPs could functionally replace mammalian Scrib in apico-basal polarity mechanisms (Choi et al., 2019).

For a more thorough list of Scrib binding partners, please see Bonello and Peifer, 2019; Stephens et al., 2018.

1.5.2 Relation with the cytoskeleton and function in neurons

PCP proteins regulate tissue polarity by recruiting cytoskeleton-modulating proteins to specific cell compartments and sculpting adhesion sites. Several studies have showed the role of Pk and Scrib in neurons.

Molecular links between Pk and the cytoskeleton in neurons are very limited. To this date, only one publication describes a potential link between Prickle and the microtubules in the axon. Ehaideb and colleagues used *Drosophila* mutants for *Prickle* isoforms (*pk* and *sple*) to investigate the molecular mechanisms behind Prickle defects and epileptic seizures development (Ehaideb et al., 2014). The authors found that a tight balance between both isoforms is key for proper neuronal function: if the imbalance leans an excess of Sple creates a mixed microtubule polarity and reduces axonal transport, an excess of Pk has the opposite effect, and the anterograde transport is enhanced and epileptic seizures are developed. The authors speculated that the onset of the seizures was likely due to defects in transport of proteins that are key for neuronal excitability, such as ion voltage-gated channels. However, they did not explore further how Prickle could modulate the polarity of microtubules and the proper axonal transport of molecules. An overexpressed form of Pk was targeted to the axon and colocalized with endogenous kinesin vesicles. During live imaging, these Pk puncta were not moving along with the kinesin and the authors hypothesized this was due to the traffic jam generated by the kinesin vesicles surrounding Pk. One option to decipher Prickle relation with the microtubules would be to investigate the precise localization of the endogenous isoforms in the axon and compare it with identified microtubule-regulating proteins, specifically with those involved in microtubule polarity and orientation (for example, TRIM46 in mammalian axons, van Beuningen et al., 2015. See sections *2. Neuronal polarity* and *3. The axon initial segment* for details). Another study in *Caenorhabditis elegans* showed that Prickle

(PRKL-1), together with Van Gogh (VANG-1) and Dishevelled (DSH-1), three of the core components of PCP signaling, is required in some peripheral motor neurons to restrict neurite emergence to a specific organ axis (Sanchez-Alvarez et al., 2011). The authors suggested a novel role for a PCP-like pathway in maintaining polarized neuronal morphology by inhibiting extraneous neurite formation. But they did not explore the underlying molecular mechanisms, other than demonstrating that the overexpression of PRKL-1was sufficient to override the loss of VANG-1. Carr and colleagues further showed that farnesylation of PRKL-1, which drives its membrane localization, was key for its role on the inhibition of supernumerary neurite formation (Carr et al., 2016).

In 2007, Okuda and colleagues found that the mRNAs of *Prickle 1* and *2* (*Pk1* and *Pk2*) were expressed in the mammalian adult brain, specifically in the hippocampus and cortex, with higher levels of *Pk1* than *Pk2* at that stage (Okuda et al., 2007). During mouse brain development, *Pk1* is highly expressed in comparison with *Pk2*, but reaches constant levels at around E10.5. On the other hand, *Pk2* expression is initially weak and only starts to increase during late brain development, suggesting stage-dependent roles for both genes. During cortical development in mouse, around E14.5, *Pk1* is strongly detected in neurons of the cortical plate but *Pk2* is almost absent. However, at E16.5 both genes are highly expressed in the cortical plate and slightly in the subplate. Therefore, and as neurons have finished their migration and maturation processes, *Pk1* and *Pk2* are expressed in the postmitotic neurons of the cortex. In 2013, Liu and colleagues used a YFP-reporter mouse and confirmed a strong expression of *Pk1* during mid and late corticogenesis as well as in the adult brain, notably the cortex and the hippocampus (Liu et al., 2013). The authors noticed that *Pk1* was present both in pyramidal neurons of the cortex and glia (microglia, oligodendrocytes but not astrocytes) but mostly excluded from the inhibitory calretinin, parvalbumin and calbindin-positive neurons.

Okuda et al. showed that, while depletion of Pk1 and Pk2 had no effects on neuronal differentiation *per se*, it reduced neurite outgrowth in differentiated mouse neuroblastoma Neuro2a cells, suggesting that Pk1 and Pk2 are important for neuritogenesis (Okuda et al., 2007). Similar results were found by Liu and colleagues, showing that Pk1 depletion in hippocampal cultured neurons caused the cells to grow shorter neurites and display an overall immature morphology. Overall, Pk appears to affect the growth and organization of both axon and dendrites, a function conserved from invertebrates to mammals, though the molecular basis of this is unclear.

Hida and colleagues were the first to demonstrate a synaptic function for Pk2 (Hida et al., 2011). They showed that it is enriched in the post-synaptic density fraction of rat brain, it colocalizes with postsynaptic markers (PSD-95, synaptophysin) in cultured hippocampal neurons, and co-immunoprecipitates with NMDA receptors and PSD-95. A work led by Nagaoka et al. suggested that, at the spines, Pk2 interacts with Vangl2 and acts as a competitive inhibitor toward N-cadherin (Nagaoka et al., 2014). As cadherin mediates cell-cell

adhesions at the synapse, the authors postulate that Pk2 may contribute via this interaction to synapse formation and integrity.

Two years later, Sowers and colleagues developed a mouse model for *Pk2*. *In vitro* analysis of neurons from homozygous animals in culture showed a reduction in complexity of neuronal arborization, similar to what Liu et al. observed in Pk1 depleted neurons (Liu et al., 2013). However, the overexpression of a wild type (WT) full-length construct for PK2 revealed the opposite effect, an increase in dendritic complexity, showing for Pk2 a dosage-dependent role on controlling dendritic arborization. The authors further used this *in vitro* system to investigate the possible role of two PK2 variants identified in ASD patients. In contrast with the increased complexity of the dendritic tree and increased frequency and amplitude of synaptic currents observed with WT-PK2 overexpression in a null background, the overexpression of the ASD-PK2 variants had no effect, suggesting a loss of function mutation in these patients. Although they could not conclude about the causality of the PK2 variants, as they were also carried by the parents, their results suggested a synaptic role for Pk2 in ASD. Analysis of the behavior of mutant animals (both heterozygotes and homozygotes) showed behavior relating to ASD (Sowers et al., 2013). These mice were less social than the controls, but also froze more in fear conditioning tests, showing better fear-memory than their control counterparts. Further supporting a synaptopathy, the authors found that neurons in the CA1 and dentate gyrus regions of the hippocampus of *Pk2* mutants had smaller PSDs and abnormal synaptic transmission as revealed by a decrease in frequency (but not amplitude) in excitatory post-synaptic currents. Both the behavioral and the electrophysiological phenotypes observed in the *Pk2* mutants are reminiscent to other models of ASD and converge towards a functional link between Pk2 and this type of neurodevelopmental disorder. But the Pk2-molecular mechanisms driving spine formation and/or function still remain elusive.

The localization and function of Scrib in neurons have been explored in more depth, at least at the synaptic level. Our team has described in detail the specific function of Scrib in spines and its relation with the actin cytoskeleton in this compartment in 2010 (Moreau et al., 2010). The authors described an enrichment of *Scrib* mRNA in pyramidal neurons of the CA1-CA3 regions of the hippocampus, as well as in granule cells and interneurons of the dentate gyrus and astrocytes. Similar to Pk2, Scrib was detected at the spines and in the PSD fraction.

Moreau and colleagues used heterozygous *Circletail* mice, which are compatible with life but have only 50% of the full-length protein, to evaluate Scrib impact on the brain. Like the *Pk2* mutants, these animals developed normally and had no gross body or brain size changes in comparison with the controls. Pyramidal neurons in the CA1 of the mutants had longer basal dendrites and, in contrast to what was found for *Pk2* deficient mice, these cells had an increased complexity of the dendritic arborization. In the same area, the authors observed a reduced number of spines with the remaining ones displaying a larger head. To understand the functional consequences of such a modification, the authors evaluated field responses in the striatum radiatum of the CA1 and identified a decreased synaptic transmission and an

impairment of the glutamatergic transmission. LTP was also decreased in the mutant animals but the ratios of NMDA/AMPA receptors in this area were not changed, despite the fact that, in the CA1, LTP is tightly related to these receptors. Unexpectedly, these animals had an improved learning and spatial memory but decreased social interactions, phenotypes observed by Sowers et al. in *Pk2* mutants.

As PCP proteins are known to be involved in cytoskeleton regulation and LTP depends on actin, the authors explored a possible role for Scrib regulating actin cytoskeleton at the spines. Using heterologous cells, Moreau and colleagues showed that an exogenously expressed tagged construct for Scrib accumulated to the actin stress fibers, and that a truncation in the N-ter of Scrib reduced such accumulation. Actin polymerization assays revealed that the addition of a neuronal activity modulator like KCl promoted a quick change of the G/F actin ratio in the control, but these levels were steady in the mutants. These results reveal a lack of plastic adaptation in neuronal activity changes for the *Circletail* mice. This impaired adaptation could be the result of the reduced levels of Scrib partners that are known to modulate actin organization, like ßPIX. Altogether, this important work shows that Scrib regulates neuronal morphology and function via actin regulation at the dendritic spines.

Another study from our lab further characterized the molecular role of Scrib at the spines (Piguel et al., 2014). The authors found that Scrib expression profile in the brain overlaps with that of the NMDA receptors subunits GluN2A and GluN2B and confirmed an interaction with these two proteins via the PDZ domains 2 and 3. The fact that Scrib did not co-immunoprecipitate with GABA receptors reveals a potential specific function in glutamatergic synapses. Interestingly, the increase of the excitatory activity in cultured neurons promoted a higher enrichment of Scrib in the post-synaptic fraction, which was comparable to that of GluN2A and suggested a functional relation between both proteins. These findings were confirmed *in vivo*, where rats exposed to an enriched environment showed an increase of expression of Scrib and GluN2A in the hippocampus. The authors further found that Scrib modulates the traffic of these receptors by controlling their internalization. An interaction with the adaptor protein AP2, known to participate in the endocytosis of NMDA receptors, is key for this function of Scrib at the spines. Scrib is, therefore, an important player on NMDA receptors trafficking at dendritic spines.

Both of these works revealed important functions for Scrib during development, its link with the cytoskeleton and its functional relevance in neurons. A more recent study from the group demonstrated that Scrib is also required in postnatal stages of maturation and neuronal plasticity (Hilal et al., 2017). The authors developed conditional knockout mice for Scrib that targets postnatal excitatory neurons of the hippocampus using Cre-recombinase under the CaMKIIα promoter. In contrast to the *Circletail* mutant, the authors evaluated here the consequences of the complete absence of Scrib in the CA1. In the CaMK-*Scrib*$^{-/-}$ cKO mutant mice, CA1 neurons had a larger portion of small immature PSDs, similar to *Pk2* KO. While the spine density was similar in both genotypes, mEPSC frequency was reduced in the *Scrib* cKO, suggesting a larger population of CA1 synapses that are nonfunctional or silent synapses

during basal synaptic transmission in the absence of Scrib. This decrease in synaptic transmission resulted in an enhanced LTP –opposite to the *Crc* mutant– but LTD and depotentiation were both abolished at CaMK-*Scrib*$^{-/-}$ CA3-CA1 synapses. The authors showed that Scrib is required for learning and memory consolidation. This study further unveiled a direct molecular interaction between Scrib and PP1/PP2A phosphatases, whose levels were decreased in the postsynaptic density of the cKO. Remarkably, early exposure to enriched environment countered absence of Scrib in memory formation. This work evidences that Scrib is not only essential during early stages of brain development, but also during the postnatal period.

A study performed in *Drosophila* neurons showed that the cell adhesion molecule Neurexin interacts with the complex made by Scrib and ß-PIX at the presynaptic terminal (Rui et al., 2017). This binding is needed for F-actin regulation via Rac1 and synaptic vesicle clustering. Neurexin, at the same time, interacts with neuroligin at the postynapse and is involved in synaptic architecture (reviewed in Bonello and Peifer, 2019).

Altogether, these studies highlight the versatility of Scrib for the structure and synaptic function of the neuron, during embryonic and postnatal stages. While these studies report a global role, Scrib has specific functions in dendrites and axon of neurons.

A recent work has highlighted a role for Scrib in apical dendrite development and sheds light on its contribution to neuronal morphology *in vivo* (Szczurkowska et al., 2020). One known mechanism for the axo-dendritic morphology development is the increased production of cyclic AMP (cAMP) in a single neurite, which becomes the axon, while cyclic guanosine monophosphate (cGMP) levels are increased in the remaining neurites, which will become the dendrites (Shelly et al., 2010). Szczurkowska and colleagues revealed that Scrib was participating in this process at the apical dendrites of CA1 neurons (Szczurkowska et al., 2020). The authors used a *Scrib* cKO where the gene is deleted in pyramidal neurons in the forebrain and *in utero e*lectroporation to sparsely label the pyramidal neurons in the CA1 of these mice. The result was an increase on the population of neurons that had 2 dendrites, but a decrease of neurons with 3 dendrites or more. Scrib depletion in cultured neurons led to an increased number of cells with a ubiquitous localization of cGMP. Scrib was found to be a direct interactor of soluble-guanylate-cyclase (sGC), a cGMP-synthesizing enzyme. This binding is necessary for the increase of cGMP in the neurites and consequent dendrite development. The authors found that the localization of Scrib to the dendrites, and therefore the increase of cGMP in this specific compartment, depends on its association with the kinesin motor KifC2. This work reveals for Scrib an important role on neuronal morphology development, concretely that of apical dendrites.

Links between Scrib and the axon also exist. Notably, Scrib contributes to axonal myelination by modulating the maturation/activity of oligodendrocytes and myelin. Jarjour and colleagues showed in 2015 that Scrib is expressed in oligodendrocytes and in the axo-glial contact areas during axon myelination (Jarjour et al., 2015). In absence of Scrib, the

morphological differentiation of oligodendrocytes is affected and the number of neurons with myelin wraps is consequently reduced. These results were confirmed *in vivo* through the use of conditional knockout mice (cKO) for *Scrib*. In the optic nerve and spinal cord of older animals these defects persisted in only small diameter axons, while the large ones caught up and developed myelin sheets. The authors further found that large axons had thicker myelin sheets due to a hyperactivation of the ERK MAP kinase pathway promoted by the absence of Scrib. Interestingly, Scrib has also an important role on remyelination: after applying a lesion in the corpus callosum, cKO mice displayed a lower number of remyelinated axons than the controls. Altogether, this study shows an indirect neuronal function for Scrib by modulating myelin sheath formation via the oligodendrocytes.

In summary, these works show that both Prickle and Scribble proteins regulate neuronal functions. At the cytoskeleton level, there are many evidences to support a role for Scrib on actin dynamics, but clear links between Pk2 and the cytoskeleton are few, with *Drosophila* Prickle seemingly controlling the polarity of microtubules in the axon.

2. Neuronal polarity

Neurons represent one of the most striking examples of cell polarization. In a similar way to apico-basal polarization in epithelial cells, neurons display an axo-dendritic polarity that is acquired early in development, preserved throughout life and required for function. As a result, neurons have two morphologically and functionally different compartments, the axon and the somatodendritic domain. Neuronal polarity is still a subject under intense research, especially *in vivo*, where its molecular mechanisms remain vastly unknown.

2.1 Neuronal polarity *in vitro*: a cell autonomous process

In 1988, a seminal study led by Dotti, Sullivan and Bankers described with detail the different phases by which hippocampal neurons grow and acquire their polarity *in vitro* (Dotti et al., 1988; reviewed in Banker, 2018). The authors described a series of developmental events and used them to establish a schematic of landmarks of neuronal development (**Figure 16**).

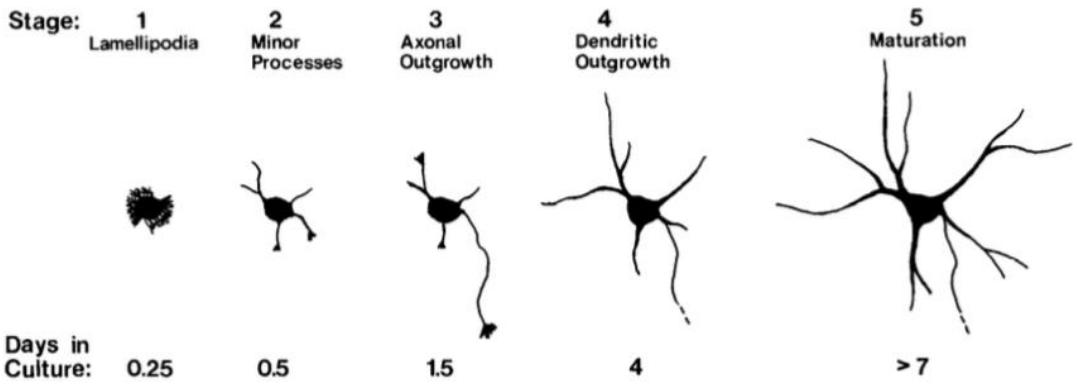

Figure 16: *Schematic representation of the stages of neuronal development in vitro. Each of these stages is associated to a timepoint based on days in culture. The polarized status of the neuron is considered to start at stage 3 with the development of the axon. From Dotti et al., 1988.*

During stage 1, after only a few hours in culture, neurons develop lamellipodia processes. Although the authors postulate that these lamellipodia have no specific function and may be an artefact of the neuron adapting to the dish, they saw that neurites appear to preferentially grow at these protrusion sites. In fact, during stage 2 these lamellipodia turns into the so-called minor processes or immature neurites, all of them showing similar sizes and growth rates. At stage 3, one of these neurites starts to grow faster than the others and becomes the axon. Because of this "break in symmetry", from this stage on the neuron is considered polarized. The authors hypothesize that any immature neurite has the potential to become

an axon, but that when one of them transforms into an axon all the others are prevented from acquiring axonal properties and therefore convert into dendrites.

This hippocampal culture has become the standard for studying neuronal polarity *in vitro*, and notably the specification of the axon, with little changes today (Kaech and Banker, 2006). Of note, the stages of neuronal polarity previously described are not correlated to the days *in vitro* (DIV) or days in culture (**Figure 16**).

Interestingly, a later study reported that the application of mechanical tension to one of the immature neurites can induce axonal formation. This shows that axon establishment is a highly plastic process and can be externally modulated (Lamoureux et al., 2002). Gomis-Rüth et al. argued in 2008 that neuronal polarity mechanisms are still active when the neuron is "mature" (Gomis-Rüth et al., 2008). The authors defined this maturity as DIV10 *in vitro* and showed that the physical section of the axon close to cell body (35 μm of less) promotes the transformation of a dendrite into an axon. The study highlighted the importance of the proximal domain of the axon as a critical region for polarity plasticity/maintenance (See *3. The Axon Initial Segment*).

Although dendrites have an initial lower growth speed than the axon, they keep growing as the neuron develops, suggesting that active mechanisms are pushing dendrites forward once the axon is initiated. It is important to mention that neurons in culture do experience a re-polarization. In the brain, neurons become polarized as soon as they exit the cell cycle, an event that largely undergoes between E16.5 to 18.5 in the rat brain, when most of the hippocampi or cortices used for these cultures are harvested. Therefore, the neurites of the young neurons are sectioned during the dissociation process and grow back once they are on the plate (reviewed in Polleux and Snider, 2010). The fact that neurons can be isolated on a dish and become polarized shows that, at least *in vitro*, neuronal polarity can occur cell-autonomously. A vast number of studies dedicated to this subject have described a series of molecular players in neuronal polarity establishment, most of them pointing to a main actor: the cytoskeleton.

2.1.1 The role of the cytoskeleton

Actin and microtubule dynamics interplay is critical for axonal specification (recently reviewed in Schelski and Bradke, 2017; Muñoz-Lasso et al., 2020; Salinas, 2007). Bradke and Dotti showed that that a highly dynamic pool of actin drives axonal formation (Bradke and Dotti, 1999). In fact, the axonal growth cone is particularly dynamic, as illustrated by the constant extension and retraction of both lamellipodia and filopodia. A long treatment of stage 2 neurons with an actin depolymerization drug, cytochalasin D, promoted the formation of several axons, showing that actin destabilization is a crucial step for axonal establishment. The same effect was triggered with an inhibition of actin-regulating proteins such as Rac, Rho and Cdc42.

Actin and actin binding proteins

But the role of actin modulating proteins in axonal specification is complex. For example, pharmacological and genetic manipulations of the actin-related proteins 2 and 3 (Arp2/3) show different outcomes: inhibition of these proteins prevents axonal formation, while their knockdown results in the overproduction of immature neurites (Tahirovic et al., 2010; Korobova and Svitkina, 2008). These findings were confirmed in granular cells of the cerebellum (Tahirovic et al., 2010) and hippocampal cultured neurons (Korobova and Svitkina, 2008). If the exact role of Arp2/3 in axon establishment is not clear, these studies show that they interfere with neuronal polarity.

Small GTPAses are also key players as regulators of actin dynamics. In 2007, Garvalov et al. demonstrated that the Rho GTPase Cdc42 was key for neuronal polarization, as cultured neurons from Cdc42 knockout mice failed to form an axon (Garvalov et al., 2007). The majority of these cells did not stain for the axonal protein Tau but were MAP2 positive, showing that genetic depletion of Cdc42 exclusively affects axonal establishment but not dendrite formation. In addition, these neurons had defective filopodia extenson/retraction processes of the filopodia, .and decreased cofilin activity, one of the downstream signaling targets of Cdc42. In another study, Tahirovic and colleagues showed that cultured neurons of Rac1 knockout mice failed to properly form an axon (Tahirovic et al., 2010). The absence of Rac1 severely impacted actin dynamics at the axonal growth cone but did not disrupt neurite formation, revealing a specific role of the small GTPase on axonal establishment. Finally, WAVE, one of the targets of Rac1, is disrupted in mutant neurons and impairs actin modulation behind lamellipodia formation.

A seminal study published in 1998 revealed the presence of actin-rich, growth cone- like structures originating close to the neuronal cell body and travelling all along the axon (Ruthel and Banker, 1998). The authors called them “actin waves” because of their shape and hypothesized that they were necessary for the active transport of actin and associated proteins to the growth cone, which was confirmed later for cofilin or Arp2/3 (Flynn et al., 2009; Katsuno et al., 2015). The inhibition of myosin II was reported to promote the formation of multiple axons with neurons showing higher levels of actin waves (Flynn et al., 2009). As this protein controls the F-actin retrograde flow in growth cones, the authors postulated that it contributes to axonal establishment via the control of actin waves. Further studies reported that these waves are initially present in all the neurites but are specifically frequent at the future axon, suggesting an important role in neuronal polarization (Flynn et al., 2009).

Altogether, these studies show the relevance of actin for neuronal polarity establishment via different mechanisms and associated proteins. Further studies reported that a cooperation between actin and microtubules is critical for proper axonal specification.

Microtubules and microtubule binding proteins

A vast number of studies reported the relevance of the microtubule cytoskeleton in neuronal polarity. During the early steps of neuronal development, all the neurites, which are very dynamic and unstable, are rich in tyrosinated microtubules (Witte et al., 2008). Once the neuron is polarized, the axon becomes enriched in acetylated microtubules, which are highly stable. Interestingly, this specific stabilization is observed as early at stage 2, prior to axon specification, in one particular neurite that will develop into the future axon. This shows that microtubule stabilization occurs before axonal establishment and likely modulates this process. It also suggests that molecular polarity occurs before structural polarity.

Reed and colleagues showed that the stabilization of the microtubules drives the binding of kinesin-1: drug-induced microtubule stabilization promotes the presence of this kinesin at the formed axons (Reed et al., 2006). This particular polarized traffic of the kinesin suggests that microtubules participate in specialized cargo distribution during axonal establishment. These studies go in line with pioneer work showing that microtubule dynamics are different all along the axon: more stable at the shaft and more dynamic at the growth cone (Baas et al., 1993). Interestingly, the microtubules in the growth cone of the future axon presented an enrichment of the microtubule end-plus protein EB3, demonstrating constant growth.

Microtubules are polarized in the axon, as they all display a plus-end towards the distal region (the growth cone) while dendrites have a mixed polarity (**Figure 17**). This polarity is key for directed trafficking of axonal proteins and prevention of somatodendritic proteins from entering the axon, contributing to the maintenance of neuronal identity (Baas et al., 1988; recently reviewed in Rao and Baas, 2018; Farías et al., 2015). Baas and colleagues reported in 1989 a sequence of events in cultured neurons regarding this specific orientation of the microtubules (Baas et al., 1989). In stage 2 neurons, microtubules are oriented with the plus-end towards the tips in all the neurites. As this polarity is the same for all of the processes at the beginning, it is not decisive for the fate of a single process as an axon or as a dendrite. This remains unchanged at the onset of axonal specification at stage 3, and only at stage 4 the mixed polarity of microtubules in dendrites starts to appear. A more recent study contradicted these results and showed that dendrites acquire this mixed microtubule polarity before axonal specification (Yau et al., 2016). The authors of the study argued that in the work from Baas and colleagues there was a low sample size, and the selected neurons were not representative enough (Yau et al., 2016). Initially all the neurites have a majority of microtubules with the minus-end oriented towards the tips. The ones of the future axon progressively change the balance towards distal plus-end at stage 3, when axonal establishment starts (**Figure 17**). So, while microtubule polarity does not predict the location of axonal formation, the consequent specialized orientation does contribute to axonal specification and neuronal polarity by selectively regulating if a protein goes to the axon or to the dendrites via different affinities with motor proteins.

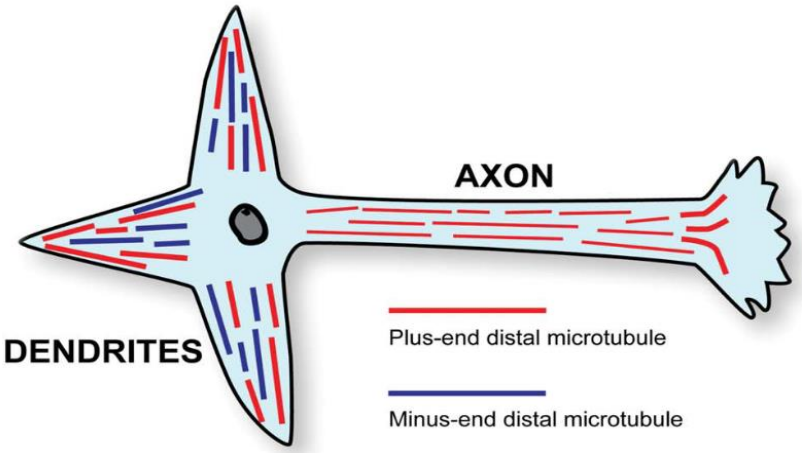

Figure 17: *Microtubule polarities within the neuron. Microtubules in the axon are oriented with their plus end facing the growth cone (plus-end distal). Dendrites have microtubules with mixed polarities, and, unlike the axon, they have a population of microtubules with the minus-end pointing towards the tip (minus-end distal). From Baas and Lin, 2011.*

A series of microtubule-associated proteins have been identified as neuronal polarity players. Inagaki and colleagues showed that collapsing response mediator protein-2 (CRMP-2) accumulates at the growth cone of the developing axon and that its overexpression leads to the formation of supernumerary axons (Inagaki et al., 2001). A recent study showed the crucial role for calmodulin-regulated spectrin-associated protein 2 (CAMSAP2) in controlling microtubule structure and neuronal polarity (Yau et al., 2014). This protein accumulates at the minus-end part of the microtubules, in the proximal axon, and its downregulation in cultured neurons significantly increased the number of cells with multiple axons. Van Beuningen and colleagues showed that TRIM46 controls axonal establishment via regulation of microtubule orientation and fasciculation at the proximal axon, suggesting that both processes are needed for proper axonal establishment (van Beuningen et al., 2015).

Despite having different roles on axonal specification, the crosstalk between actin and microtubules is essential to ensure this activity. Actin is particularly unstable at the growth cones and this allows more space for the pool of highly dynamic microtubules to drive axonal specification (**Figure 18**) (reviewed in Hoogenraad and Bradke, 2009). In addition, actin waves are dependent on microtubule polymerization, showing a link between both structures (Winan et al., 2016). The interplay actin-microtubules is at the root of cell biology processes, especially in the establishment of cell polarity, so it is not surprising to find a similar mechanism for neuronal polarization (reviewed in Dogterom and Koenderink, 2019).

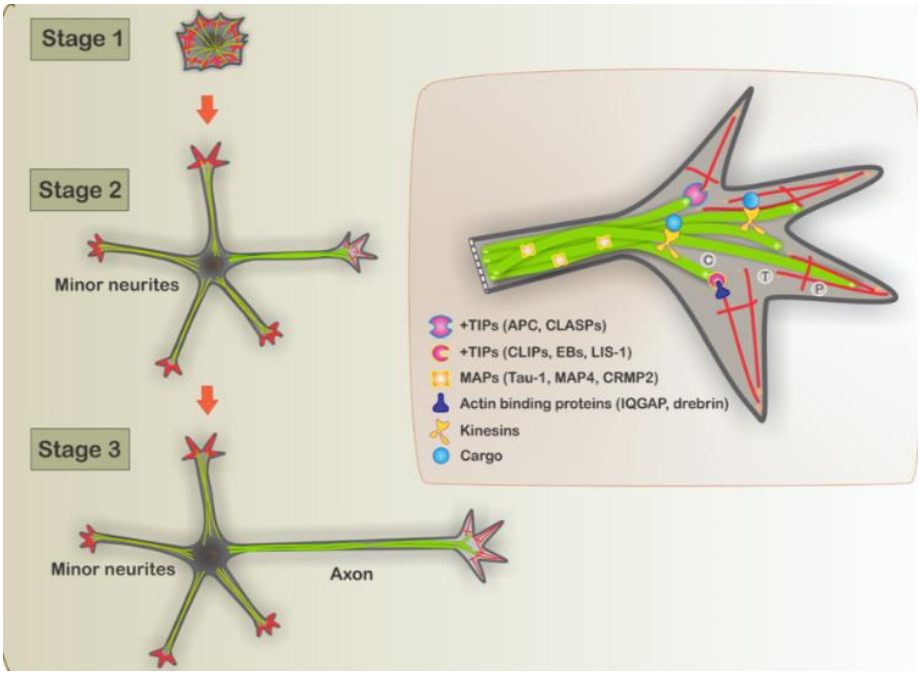

Figure 18: *Schematic of the actin and microtubules cytoskeleton distribution in the developing neuron. The growth cone of the axon is rich on ever-growing microtubules, unstable actin and associated proteins to both cytoskeletons. From Neukirchen and Bradke, 2011.*

2.1.2 Cell polarity proteins and polarity complexes

At the molecular level, neuronal polarity is believed or has been shown to use all of the classical apico-basal complexes described in epithelial cells including the PAR/aPKC, Crumbs and Scrib complex, but also some of the classical downstream and upstream components like the small GTPases and the Wnts (for reviews see Montcouquiol and Kelley, 2020; Bazellières et al., 2020; Margolis, 2018; Rodriguez-Boulan and Macara, 2014).

A seminal work of 2003 showed that partitioning-defective 3 and 6 (Par3 and Par6) are asymmetrically distributed and accumulate at the tip of the growing axon in stage 3 neurons (Shi et al., 2003). Overexpression of Par3 or Par6 and inhibition of the activity of atypical Protein Kinase C (aPKC) resulted in neurons that fail to extend an axon, showing a crucial role for these proteins in neuronal polarity establishment. With this and further studies the authors identified that the PI 3-kinase/Glycogen Synthase Kinase 3ß (GSK3ß) signaling pathway is upstream controlling these events. The inhibition of PI 3-kinase abolishes Par3 localization at the axon and impairs axonal formation (Shi et al., 2003), while an increased activity of PI 3-kinase phosphorylates and deactivates GSK3ß at the tip of the axon, an activity that has been related with the axonal localization of Par3 (Shi et al., 2004). The authors also described a protein complex formed by Par3, the kinesin KIF3 and the adenomatous polyposis coli protein (APC), which moves along microtubules and allows the polarized localization of Par3. In fact, Nishimura and colleagues reported a direct interaction between KIF3 and Par3

that allows also the interaction of aPKC with KIF3 (Nishimura et al., 2004). This interaction is crucial for neuronal polarity, as the disruption of KIF3 abolished the axonal localization of both Par3 and aPKC at the tip of the axon and impaired axonal formation.

The small GTPase Cell division control protein 42 (Cdc42) is considered to be part of the Par3/Par6/aPKC complex (Joberty et al., 2000), and has also a role on axonal establishment: cultured neurons from Cdc42 mutant mice failed to form an axon (Garvalov et al., 2007). The authors showed that this protein controls neuronal polarity via the activation of cofilin which, in turn, regulates actin cytoskeleton.

Members of the Wnt signaling pathway, like Dishevelled-1 (Dvl1), interact with and stabilize the Par3/Par6/aPKC complex (Zhang et al., 2007). In fact, Dvl1 promotes axonal formation *in vitro* via direct regulation of aPKC. Overexpression of the non-canonical Wnt5a activates aPKC and results in a higher number of polarized neurons at stage 2. A previous work led by Ciani and colleagues revealed an important crosstalk between Dvl1 and GSK3ß for microtubule stabilization at the axon (Ciani et al., 2004). Dvl1 localizes to the microtubules and contributes to their stability by inhibiting GSK3ß. Interestingly, the activity of ß -catenin, which is the hallmark of the canonical signaling, is not necessary for this Dvl1 function. A recent study demonstrated that the canonical Wnt signaling pathway effector Wnt3a preferentially accumulates to the nascent axon in cultured neurons and leads to a local activation of this pathway in the compartment (Stanganello et al., 2019). In fact, inhibiting the endogenous secretion of all Wnts led to the loss of axonal localization of Wnt3a, retained at the soma, while all of the other neurites were positively labelled with Tau and MAP2, revealing an important role for Wnt singaling in neuronal polarity establishment via axonal specification. Importantly, overexpression of Wnt3 induced the formation of multiple axons as revealed by the staining of the axon initial segment (AIS) protein Ankyrin-G (AnkG). This effect was similar to that induced by the microtubule stabilizer taxol, suggesting that Wnt canonical signaling regulates microtubules for neuronal polarity establishment. In fact, the authors found that the number of anterograde comets is increased when Wnt3 is overexpressed, suggesting that Wnt3 promotes plus end orientation of microtubules towards the distal axon.

Mammalian homologues and related proteins to Par1 and Par4 have also important roles in neuronal polarity. A study in 2005 showed that cultured neurons from SAD mutant mice displayed neurites of an overall similar length and with mixed stainings for MAP2 and tau (Kishi et al., 2005). SAD kinases possess an evolutionarily conserved kinase domain from the Par1 protein. The Par1 closest homologues in mammals, the MARK kinases, had been initially related with microtubule modulation. Chen and colleagues showed that MARK2 is a downstream target of Par3/Par6/aPKC during neuronal polarity establishment (Chen et al., 2006). Downregulation of MARK2 *in vitro* promoted the formation of multiple axons, phenotype that was rescued by the overexpression of Par3/Par6/aPKC. The authors showed that MARK2 controls microtubule assembly by dephosphorylating microtubule-associated

proteins. A recent study showed that MARK2 activity at the proximal axon is necessary for the transport of TRIM46 to this compartment (Ichinose et al., 2019; van Beuningen et al., 2015).

The mammalian homolog of Par4, LKB1 (Liver Kinase B1), is a serine threonine kinase that forms a complex with the pseudokinase STRAD. Both were found to localize at the tip of the immature neurite that will become the axon (Barnes et al., 2007; Shelly et al., 2007). Barnes and colleagues showed that cultured neurons from LKB1 knockout mice failed to establish an axon while displaying neurites with mixed stainings of Tau and MAP2 (like SAD mutants). Interestingly, LKB1 needs to be activated for axonal formation, like its role in epithelial cell polarity, revealing a conserved mechanism between cell types. LKB1 is an upstream regulator of SAD kinases and MARKs, showing that all those signaling pathways are integrated to ensure proper neuronal polarity establishment (Lizcano et al., 2004; Barnes et al, 2007).

Other kinases, phosphatases and signaling pathways like PTEN, JNK or AKT/Protein kinase B are also involved in axonal establishment, regulating diverse cell processes including cytoskeleton dynamics (reviewed in Polleux and Snider, 2010).

Besides cell polarity proteins and cytoskeleton modulation, other active mechanisms can determine the site of axonal specification and neuronal polarity. Bradke and Dotti reported a cytoplasmic flow in cultured neurons that preceded axonal formation (Bradke and Dotti, 1997). The diverse polarized trafficking of cellular elements to the tip of the future axon, like mitochondria, ribosomes or a higher sorting of trans Golgi network-derived vesicles, reveals an early polarization of cell elements that could drive axonal specification. Extensive literature has explored other molecular players, like local translation/protein degradation in the axon, transcription regulators and centrosome positioning as key processes for axonal establishment (de Anda et al., 2005; reviewed in Polleux and Snider, 2010; Bentley and Banker, 2016; Takano et al., 2019).

These and many other studies have defined the axon as the apical equivalent to the apical surface and tight junctions of epithelial cells because its specification depends on the function and localization of epithelial apical determinants. And, by extension, the somato-dendritic compartment would correspond to the baso-lateral domain of the epithelial cells. It would be interesting to revisit these few studies, in light of KO-validated antibodies and new genetic approaches (CRISPR/Cas9).

2.2 Neuronal polarity *in vivo:* a complex environment with many cues

In vitro, all neurites grow freely and the axon is believed to specialize stochastically. While some of the processes described above are present, the specification of the axon *in vivo* depends on an abundance of environmental factors, adhesion and signaling molecules from cell-cell contact of different cell types, diffusible factors and extracellular matrix components. For example, while neurons in the retina do "inherit" their polarity from the apico-basal polarity of neuronal progenitors, neurons in the neocortex establish their "own" polarity once they are born from the progenitors (for review see Barnes and Polleux, 2009). Just like hippocampal neurons is the classical *in vitro* model of polarity, the neocortex is one of the most studied structures regarding neurogenesis, neuronal migration and polarity, especially in pyramidal neurons, and therefore will be discussed here in detail.

Neurogenesis in the developing cortex starts with the neuronal progenitor cells, which are divided in three main classes: apical progenitors, basal progenitors and subapical progenitors. Apical progenitors are comprised of neuroepithelial cells (NECs) that give rise to almost all the neurons in the cortex (for review see Götz and Huttner, 2005). They are oriented with their apical domain towards the lumen of the neural tube and with their basal domain towards the basal lamina. During the formation of the neocortex, NECs line up in the ventricular zone and can divide symmetrically to produce a reservoir of NECs contributing to the lateral expansion of the tissue. They can also divide asymmetrically and produce radial glial cells (RGC). These cells can either divide symmetrically to keep producing RGC or differentiate into neurons (**Figure 19**). Both neuroepithelial and radial glial cells display an apico-basal polarity and, as such, polarity proteins disruption cause cortical malformations (reviewed in Fietz et al., 2011; Hakanen et al., 2019). Newly generated neurons are multipolar and migrate through the intermediate zone (IZ in **Figure 19**), developing a trailing process that will derive in the axon and a leading process that gives rise to the dendrites (Hatanaka and Yamauchi, 2013). The generation of the trailing process is considered to be the step of symmetry breaking and therefore neuronal polarity establishment of neurons *in vivo.*

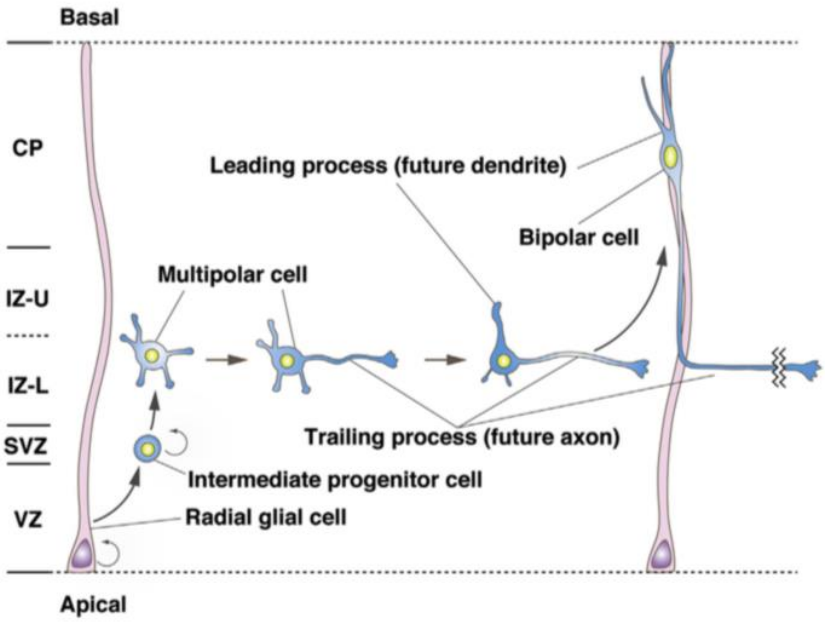

Figure 19: *Neuron development and migration in the cortex. Neurons arise from an asymmetric division of radial glial cells. At first, neurons have many processes and are multipolar. These develop a tangential trailing process that will become the axon, shortly followed by the generation of the leading process, which will generate the dendrites. Trailing process formation is considered to be the symmetry breaking step that leads to neuronal polarity initiation in vivo. From Funahashi et al., 2020.*

But what is determining this trailing process specification? The implementation of techniques like *in utero* electroporation has been key to study this process, however, it is still difficult to distinguish the role for certain proteins on neuronal polarity as their depletion also interferes with migration (for review see Yogev and Shen, 2017). As mentioned, neuronal polarity establishment *in vivo* is driven by a combination of mechanisms. An example is the work of Namba and colleagues, who showed that multipolar neurons in the IZ enter in contact with TAG-1 (an adhesion molecule) expressing axons from neurons that are already polarized and that this contact is essential to trigger axonal formation (Namba et al., 2014). Interestingly, this paper also reports that at least 30% of these neurons develop a leading process first and then a trailing process. This shows that symmetry breaking *in vivo* can start with the formation of a process that will lead to dendrites. In this context, acute deletion of TAG-1 or its downstream effector Lyn via *in utero* electroporation disrupted neuronal polarization, with neurons not able to transition to the bipolar state. Interestingly, mutant mice for TAG-1 did not display such defects and the authors postulated that compensatory mechanisms may be in play to ensure neuronal polarity.

Another important extracellular cue needed for neuronal polarity establishment is TGF-ß (Yi et al., 2010). A gradient of this growth factor generated at the ventricular zone drives neuronal polarization in the developing cortex. In fact, neurons are enriched in TGF-ß

receptors and their disruption impedes axonal establishment via changes in actin dynamics, previously showed as key for axonal formation in cultured neurons (see *2.1.1 The role of the cytoskeleton*). Other secreted extracellular growth factors like neurotrophin are known to participate in neuronal polarity establishment. Zuccaro and colleagues showed that genetic depletion of the neurotrophin receptor $p75^{NTR}$ impaired neuronal polarity development (Zuccaro et al., 2014). Interestingly, the elimination of TGF-ß or neurotrophin receptors impacted axonal formation but not that of the leading edge (Yi et al., 2010; Zuccaro et al., 2014). Additional pathways may then be involved in the formation of that process, which in some neurons is the first step of symmetry breaking from the multipolar state (Namba et al., 2014).

Extracellular factors usually trigger the activation of many downstream effectors that amplify the signal and contribute to different pathways. An example of this is the TGF-ß gradient and subsequent activation of Par6 (Yi et al., 2010). In fact, transforming growth factor-ß (TGF-ß) receptors colocalize with Par6 in the neocortex and both Par6 and Par3 coprecipitate with TGF-ß receptors in brain lysates. The neurotrophic factor BDNF has been reported to activate the PI3-kinase, which is localized at the tip of the developing axon and is essential for neuronal polarity establishment (see Shi et al., 2003 and *2.1.2 Cell polarity proteins and other effectors*). Garvalov et al. showed that knockout animals for *Cdc42* failed to establish an axon *in vivo*, through a mechanism involving the actin modulator protein cofilin (Garvalov et al., 2007). Interestingly, Govek and colleagues demonstrated that Cdc42 is also important for neuronal polarity establishment in the cerebellum, where knockout neurons for this gene stay in a multipolar phase and display migration problems (Govek et al., 2018). The LKB1 kinase, crucial for neuronal polarity establishment *in vitro*, has been shown to act downstream the neurotrophic factor BDNF through direct phosphorylation by PKA (Shelly et al., 2007). LKB1 knockout mice neurons fail to form an axon but their migration is not impaired (Barnes et al., 2007). As reported in cultured neurons, LKB1 controls and targets the SAD kinases A and B, which regulate as well axonal establishment *in vivo* (Kishi et al., 2005).

In comparison with the studies performed in cultured neurons, less is known about how the cytoskeleton modulates neuronal polarity *in vivo*. Some of the microtubule-associated proteins with functions in neuronal polarity *in vitro* contribute to neuronal migration and axonal formation in the developing cortex, like CAMSAP2 (Yau et al., 2014) and MAP6 (Tortosa et al., 2017). Another example is TRIM46, involved in axonal specification *in vitro* and in neuronal migration and axon/dendrites establishment *in vivo* (van Beuningen et al., 2015). Acute deletion of CRMP2 in the developing cortex via *in utero* electroporation severely impacts neuronal migration and multipolar to bipolar transition (Sun et al., 2010). Interestingly, Sakakibara and colleagues showed a particular feature of microtubule organization in neurons of the developing cortex: in the leading process, which gives rise to the dendrites, microtubules are homogeneously oriented with their plus ends towards the tip of the process (Sakakibara et al., 2013). Microtubules at the trailing process, which generates the axon, have mixed polarity. These findings contradict what was reported *in vitro*, where

these orientations are inverted. Finally, it is important to emphasize the ongoing debated role of the centrosome in the determination of the axon. Calderon de Anda and colleagues showed that the centrosome localized to the immature neurite that becomes the axon *in vitro* (de Anda et al., 2005). While the relation of the centrosome position and axonal formation is not clear *in vivo*, it seems to maintain a role in this process as depletion of centrosome related proteins impairs neuronal polarity establishment (Sakakibara et al., 2013; Gärtner et al., 2012; Anda et al., 2010).

All these studies show that neuronal polarity, at least *in vivo*, is a complex process involving different pathways, effectors and extracellular cues. Neuron cultures are a good system to understand cell autonomous processes, but a translation of most of the findings in neuronal polarity to the developing brain is still missing. The fact that some of the proteins involved in axonal establishment *in vivo* interfere as well with neuronal migration is an added difficulty to decipher specific effectors of neuronal polarity. On the other hand, the brain is composed by heterogeneous populations of neurons, including anaxonic cells (Galliano et al., 2018): if the axo-dendritic polarity is essential for neuronal activity, how are those still functional?

In this section I have discussed the past and recent literature about neuronal polarity establishment. But once initiated, this polarized state needs to be maintained throughout the life of the neuron. One of the main actors on ensuring this polarity is the axonal initial segment, which is discussed in depth in the following part.

3. The Axon Initial Segment (AIS)

The axon initial segment is a neuronal subcompartment located within the first 20-60 µm of the axon (**Figure 20**) that has at least 2 important functions: (i) it preserves the polarity of the neuron by acting as a barrier between the somatodendritic and the axonal compartments, and (ii) it is the site for action potential initiation and tuning, thanks to its high concentration of voltage-gated ion channels. The AIS is also a plastic structure that can change in length and/or position to regulate neuronal excitability. Importantly, this crucial domain is also a hub for many pathologies, including epilepsy and autism, where some of the AIS main genes are mutated in patients. Based on these criteria, the relevance of the AIS for neuron and brain function is attracting an ever-increasing interest from neuroscience research.

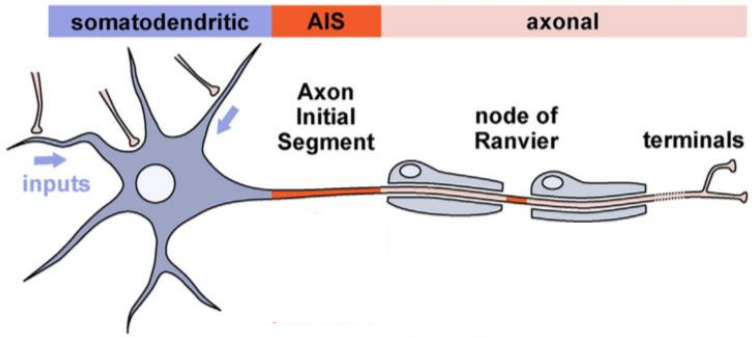

***Figure 20**: Schematic of the different compartments of a neuron. In orange, the AIS. From Leterrier and Dargent, 2014.*

3.1 Composition, assembly and maintenance

3.1.1 Ankyrin-G: the master organizer

Ankyrins are a family of proteins that act as a scaffold between membrane proteins and the cytoskeleton. They are present in many cell types, ranging from erythrocytes to neurons, and are involved in different biological processes. Three ankyrins can be found in vertebrates: Ankyrin-R (AnkR), Ankyrin-B (AnkB) and Ankyrin-G (AnkG). Although all of them are present in the brain, the high presence of AnkG made it the focus of a vast number of studies (reviewed in Smith and Penzes, 2018). In 1990, Kordeli and colleagues showed that AnkR, which had been found in erythrocytes, localizes at the AIS and in the nodes of Ranvier of neurons (Kordeli et al., 1990). However, the same authors hypothesized in 1991 that this ankyrin was the product of a different gene. By studying mutant mice with AnkR (*Ank1*) deficiency in both erythrocytes and the brain, the authors found that this specific ankyrin remained unchanged at the AIS and the nodes of Ranvier (Kordeli and Bennett, 1991). That protein was AnkG, the product of the *Ank3* gene, and was first characterized in the brain by

the same team (Kordeli et al., 1995). By isolating the *ANK3* cDNA from human brain samples, the authors predicted the structure of a protein of 480 kDa in size. Because of its high molecular weight, the protein was named Ankyrin-G, for “giant”.

The model for the protein structure contained the following domains: membrane and spectrin-binding domains at the N-terminus (N-ter), followed by a serine rich domain, an extended tail and a C-terminal (C-ter) sequence (**Figure 21**).

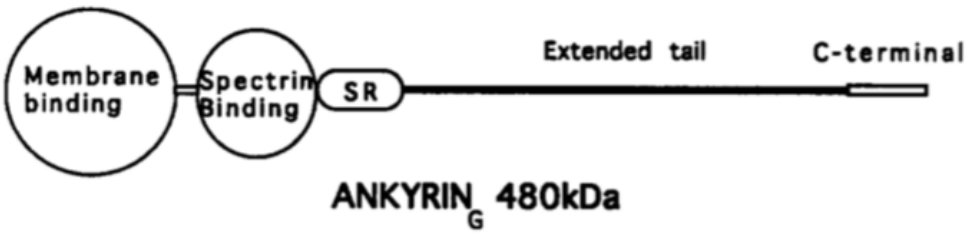

Figure 21*: Predicted model of AnkG-480 in the human brain, with the different domains. From Kordeli et al., 1995.*

Further experiments showed that the *Ank3* gene was subjected to alternative splicing, generating tissue-specific expression of AnkG isoforms. Up to 5 transcripts were identified in rat: two of them were found only in the brain, while a shorter one, which produced a protein of 190 kDa, was identified as well in the kidney (in line with the findings of Peters et al., 1995). The authors confirmed the existence of different AnkG isoforms in blot by using either antibodies against the serine rich or the spectrin binding domains initially predicted on the AnkG-480 kDa. When using the antibody targeting the serine rich domain, two AnkG isoforms with molecular weights of 480 and 270 kDa were detected. Interestingly, these isoforms were found exclusively in the brain and were absent in other tissues. The antibody raised against the spectrin binding domain identified the 190 kDa AnkG. Importantly, when the authors used the antibody targeting the serine-rich domain for immunolabeling, they found an accumulation of AnkG at the AIS and nodes of Ranvier in the hippocampus, cerebellum and cortex in rat. This seminal work identified 3 AnkG isoforms in the brain and showed the specific accumulation of the 480 and 270 kDa proteins to the AIS and nodes of Ranvier (Kordeli et al., 1995).

Subsequent studies characterized the different domains and functions of the three AnkG isoforms, which are generated by the alternative splicing of the exon 37 of the *Ank3* gene (**Figure 22A**). The membrane and spectrin binding domains in the N-ter are preserved in all of the isoforms. Twenty-four ANK repeats ensure the interaction with membrane proteins forming the membrane-binding domain (Bennett and Lorenzo, 2013). Importantly, the palmitoylation of a specific cysteine residue within these ANK repeats is essential for the

membrane targeting of AnkG in different cells, including neurons (He et al., 2012). Ankyrins are known to form complexes with spectrins to coordinate the association of membrane proteins with the cytoskeleton (Bennett and Lorenzo, 2013), and they have a specific domain for such interaction (**Figure 22B**, **in yellow**). The regulatory domain, which is found in all three isoforms (**Figure 22B**, **in blue**), is involved in regulating the interactions of the membrane and the spectrin binding domains (Davis et al., 1992; Hall and Bennett, 1987). The extended tail at the C-ter from the 270 and the 480 kDa isoforms (**Figure 22B**, **in grey**) is the result of the translation of part (AnkG-270) or the full (AnkG-480) exon 37. This tail has been shown to interact with the microtubules at the AIS through EB proteins (see point *3.1.3.2 Microtubules*) and has a serine-rich domain that contributes to the neural specific localization of these isoforms and, concretely, to their presence at the AIS (Zhang and Bennett, 1998). AnkG-190 lacks this specific tail and has what appears to be a ubiquitous localization in the neuron when overexpressed. Proteomic studies have identified the presence of ankyrin proteins in the post-synaptic density (Jordan et al., 2004) and Smith and colleagues confirmed that AnkG-190 is targeted to and has important functions in the spines (Smith et al., 2014). To date, there is no specific antibody to AnkG-190 permitting no conclusion on its absence/presence at the AIS, nor an identified function for AnkG-190 at the AIS, suggesting that it is not enriched at this compartment.

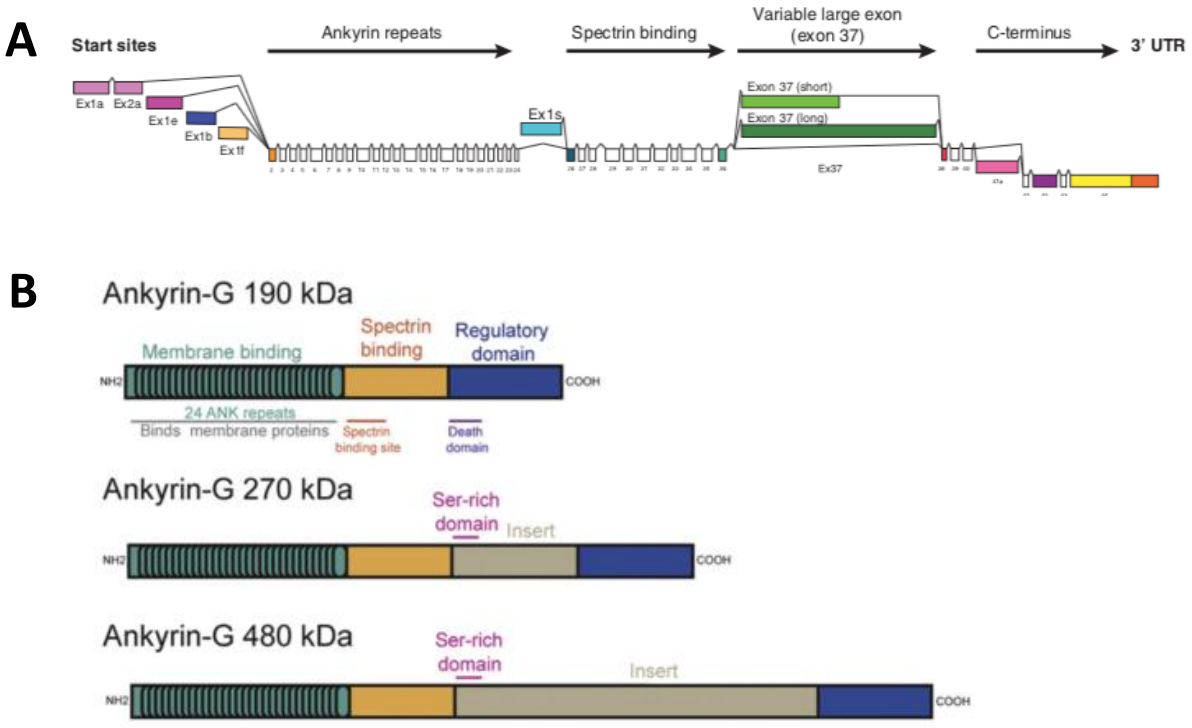

Figure 22**: Structures of the Ank3 gene and the AnkG isoforms in the brain.* ***(A) Schematic of the genetic sequence of *ANK3*. Alternative splicing sites in 5' and 3', leading to the different AnkG isoforms, are indicated. **(B)** The three AnkG isoforms generated by the alternative splicing of exon 37. The membrane and the spectrin binding domains are preserved in all isoforms. AnkG 270/480 kDa isoforms have a tail in C-ter that is absent in the 190 kDa. *Adapted from Rueckert et al., 2013 and Smith and Penzes, 2018.*

As explained in the following lines of this section, AnkG is, so far, commonly considered as the master organizer of the AIS, as it is the first protein that reaches the proximal axon and recruits all the other AIS components. It is widely admitted as the fiducial marker for this structure and it interacts with membrane proteins like voltage-gated ion channels and cell adhesion molecules, anchoring them at the AIS. AnkG is also linked to the actin cytoskeleton through an interaction with ßIV spectrin (see *3.1.3.1 The actin-spectrin network*) and to the microtubules through an interaction with the plus-end microtubule proteins EB3 and EB1. (See *3.1.3.2 Microtubules*).

Jenkins and Bennett detailed a timeline of expression of AIS proteins *in vivo* in Purkinje neurons of the mouse cerebellum: AnkG and ßIV spectrin first accumulate at P2 within the proximal axon, followed later by Na_v channels and the cell adhesion molecules NrCAM and neurofascin-186 (NF-186), which were strongly detected by P9. This study suggests that the first two proteins recruit the others. More importantly, the localization of the three molecules to the AIS is AnkG-dependent (Jenkins and Bennett, 2001). This early accumulation of AnkG in the nascent axon was confirmed during axonal development in the cortex (Galiano et al., 2012). AnkG is first detected in this compartment at P1, with a restriction to the proximal axon by P3. As early as 1988, the association between ankyrin and sodium channels was demonstrated in the brain (Srinivasan et al., 1988), but it was only a decade later that the AnkG relevance as the molecular coordinator of the AIS establishment and function was demonstrated. In 1998, a seminal study by the group of Vann Bennett showed that the genetic ablation of AnkG in Purkinje cells, using an AnkG (*Ank3*)^{exon1b} cKO (see pages 75-76 for details), led to a loss of sodium channels (Na_v) at the AIS, affecting the action potential properties of these neurons and the behavior of the mice (Zhou et al., 1998). In another landmark study, Sobotzik and colleagues showed that loss of AnkG, and therefore the AIS, disrupts neuronal polarity, with Purkinje neurons from AnkG (*Ank3*)$^{-/-}$ mice developing "axonal" spines, which were morphologically, molecularly and functionally identical to the dendritic spines (Sobotzik et al., 2009).

Many *in vitro* studies helped to establish the molecular organization, timing and protein interactions at the AIS. AnkG is essential for AIS formation in cultured hippocampal neurons, as its downregulation impairs the localization of ßIV spectrin, Na_v channels and NF-186 (Hedstrom et al., 2007). While NrCAM is not necessary for AIS establishment (Hedstrom et al., 2007), the depletion of Na_v channels or ßIV-spectrin reduces the number of AnkG-positive neurons, suggesting that AIS formation mainly relies on AnkG but is strengthened by some of its AIS partners (Xu and Shrager, 2005; Leterrier et al., 2017). The role of NF-186 on AIS

establishment seems controversial: Hedstrom and colleagues initially showed that depletion of NF-186 in both hippocampal neurons and *in vivo* (rat cortex) does not impact AnkG levels or AIS formation (Hedstrom et al., 2007). In contrast, Leterrier et al. found that NF-186 knockdown in neurons decreased AnkG levels by about 30% with respect to control using similar strategies: the downregulation of NF-186 is achieved through a short-hairpin RNA (shRNA) that is electroporated in neurons before plating (in Leterrier et al.) or lipofected 3h after plating (in Hedstrom et al.), a difference unlikely to explain the two divergent phenotypes. A more recent study showed that downregulation of NF-186 in cultured hippocampal neurons led to a decrease of around 20% levels of AnkG at the AIS and a shift in the labeling in comparison to other AIS markers, like Na_v channels (Alpizar et al., 2019). In this study, the downregulation strategy was based on CRISPR-Cas9, where the gRNA targeting NF-186 and the Cas9 were transfected (using calcium phosphate) on neurons at DIV5. It is possible that Hedstrom and colleagues did not see a significant decrease of NF-186 as their sample size is lower than the other two papers. A difference in the antibody used could also lead to variability in immnolabeling sensitivity. Finally, while the works of Leterrier and Alpizar do agree on a decrease of AnkG after NF-186 depletion, only the latter shows also a shift away from the soma for the AnkG immunolabeling. This may be due to the severe (more than 90%) downregulation of NF-186, while Leterrier et al. do not mention this data. This would suggest a dosage-dependent role of NF-186 in modulating the AnkG levels and the position of the AIS.

In vitro, AnkG-480 is the major AIS isoform for AIS development and its depletion leads to an overall loss of neuronal polarity as revealed by an axonal invasion of the somatodendritic protein MAP2 (Fréal et al., 2016). The decisive demonstration of the critical role of AnkG-480/270 kDa isoforms on AIS formation over AnkG-190 was provided by Jenkins and colleagues by creating a specific and early (embryonic) conditional knockout (cKO) for the 270 & 480 kDa isoforms (the giant AnkG or gAnkG), hereby referred to as AnkG (*Ank3*)^{exon37} cKO, Nestin-Cre (Jenkins et al., 2015). The neurons from these mice failed to cluster ßIV spectrin, voltage-gated channels and NF-186 to the AIS. Importantly, rescue experiments *in vitro* using the 480, 270 and 190 kDa isoforms demonstrated that only the 480 kDa isoform was able to fully restore the localization of all of the AIS molecules. Also, AnkG-270 was only able to rescue partially Na_v and NF186 recruitment but not ßIV spectrin, while AnkG-190 had no effect. At the functional level, the absence of AnkG-480 led to a loss of neuronal polarity (as observed in Sobotzik et al., 2009), and the network of tight microtubule fascicles, a particular feature of the AIS, was disrupted. One remarkable and unexpected finding was that in absence of AIS, neurons were able to fire action potentials, but with abnormal frequency. AnkG-480 is, therefore, the relevant isoform for AIS assembly and functionality.

Not only AnkG is essential for AIS assembly but also for its maintenance. The knockdown of AnkG in neurons with a mature AIS promotes AIS disassembly, highlighted by the loss of ßIV spectrin, Na_v channels and NF-186, and loss of polarity (Hedstrom et al., 2008). On the other hand, the downregulation at the same stage of other AIS components like Na_v channels, ßIV spectrin or NF-186 did not seem to impact AIS maintenance (i.e., AnkG staining)

(Hedstrom et al., 2008). Using two different quantifications approaches, the authors were "only" able to downregulate NF-186 levels by 30% to 50% and reported similar partial reductions for Na_v channels or ßIV spectrin. They concluded that these AIS components are highly stable proteins with a low turnover ratio once the AIS is in place (Hedstrom et al., 2008). Leterrier and colleagues, using the same shRNA strategy, obtained different results and concluded that the depletion of Na_v channels and NF-186 at DIV8 affects AIS maintenance by decreasing the levels of AnkG, while its size and position remain unaffected. Both studies used the same type of neurons (rat hippocampal neurons), but while Hedstrom et al. used adenoviruses infection to deliver the shRNA to the neurons at DIV10, Leterrier and colleagues use lipofection at DIV8. While this technical divergence could explain differences in the efficiency of the incorporation of the construct, it is unlikely the reason behind such different outcomes. The timings of transfection are similar (DIV10 and DIV8) and the immunocytochemistry is performed at DIV14 for Leterrier et al and different timepoints until DPI 14 (14 days post infection) for Hedstrom and colleagues. But since Leterrier did not report the levels of NF186 reduction using the shRNA it is not possible to extrapolate more on a better downregulation efficiency. Giving these controversial results, further studies are needed to determine the precise role of NF-186 and Na_v channels on AIS maintenance.

Besides the variability in C-ter of the various AnkG isoforms, AnkG has other isoforms derived from the alternative splicing of the exon 1, which results in different N-ter domains, for all three isoforms 480, 270 and 190 kDa (**Figure 22A, 22B**). The spliced mRNA encoding different N-ter peptidic sequences have been called NT1 (for exon 1a), NT2 (for exon 1b) and NT3 (for exon 1e) in a recent study exploring their profile of expression in the brain (Lopez et al., 2017). The expression profile of these isoforms was initially characterized by Zhou and colleagues in 1998: they observed that NT2 mRNAs strongest signal was detected in the cerebellum but poorly in the telencephalon, while NT3 mRNAs were mostly found in the hippocampus and cortex. The authors further created a specific KO for exon 1b (NT2) and validated the maintenance of NT2 in hippocampus and absence in cerebellum (Zhou et al., 1998).

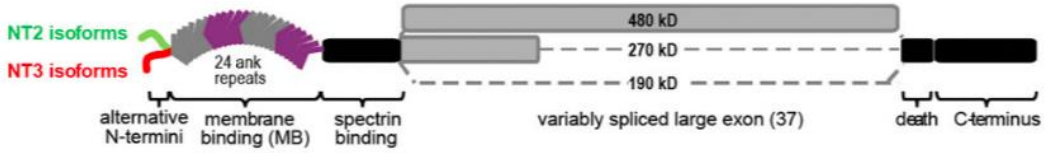

***Figure 23**: Schematic of the different AnkG isoforms differing in N-ter and C-ter. From Lopez et al., 2017*

A later study from 2013 quantified the expression of the transcripts in the adult human brain, concretely in frontal cortex, cingulate cortex and cerebellum (Rueckert et al., 2013). The authors confirmed an enrichment of the exon 1b (NT2) expression in the cerebellum, like in mouse, but also showed high levels in the cortex (frontal and cingulate). For exon 1e (NT3),

the expression was also high in the cortex, but much lower in the cerebellum. Together, these studies drew a picture of a differential profile of expression of AnkG (*Ank3*) splices, with NT2 present in most structures but enriched in the cerebellum while NT3 was mostly present in the telencephalon.

A detailed study from Lopez and colleagues untangled the issue by developing isoforms-specific antibodies to the NT1, NT2 and NT3 proteins. While NT1 had no reactivity in the brain, NT2 and NT3 were both present in the forebrain and the cerebellum with a preference of NT2 for the forebrain and NT3 for the cerebellum, as observed by Zhou et al., 1998. Immunolabeling confirmed that the dentate gyrus of the hippocampus was more strongly reactive to the NT3 antibody than to NT2, but revealed subtle differences globally in the hippocampus. If the AIS of dentate granule cells were reactive to both NT2 and NT3 antibodies, the AIS of hippocampal pyramidal cells were only reactive to NT2. The most interesting detail was that, throughout most regions (cortex, hippocampus, amygdala), the authors identified NT3-positive/NT2-negative cells that were parvalbumin-expressing interneurons. In fact, a specific exon 1b deletion (affecting AnkG NT2) led to a reduction of the main AIS markers and reduced the excitability of the neurons, consecutively leading to an overall reduced inhibition in the mouse. Finally, the authors showed that antibodies against NT2 and NT3 isoforms detect the canonical AnkG 480, 270 and 190 kDa isoforms, in line with the findings at the transcription level. However, it is still unclear if the NT2 and NT3 preferentially express a given C-ter at the protein level. From these studies, it appears that splicing events in exon 37 seem to regulate AnkG subcellular localization in neurons, while splicing events in exon 1 control AnkG cell-type specific expression. However, it is still unclear how the combination of the two is meaningful and this highlights the complexity of AnkG regulation.

AnkG is the master organizer of the AIS and is therefore key for ensuring its functions in the neuron. Among the isoforms generated by the alternative splicing of the exon 37, the giant AnkG 480 kDa is the most relevant for AIS assembly and function, while the 190 kDa isoform is believed to have a role mainly at the spines.

3.1.2 ßIV spectrin

The AIS has a highly organized and robust cytoskeleton network and associated molecules. Apart from AnkG, ßIV spectrin is a core scaffolding protein of the AIS.

Spectrins were initially identified in the inner part of the membrane of erythrocytes and are composed by two subunits, namely alpha (α) and beta (ß), which tightly align to form heterodimers through the association of the N-ter of α with the C-ter of ß. At the same time, these dimers assemble in tetramers in a head-to-head fashion (Clarke, 1971; Shotton et al., 1979). Spectrins are known to bind to actin (Brenner and Korn, 1979) and to have a link with the membrane through an interaction with ankyrin (Bennet and Stenbuck, 1979). In the brain,

spectrin was initially called fodrin, but the high similarities with the erythrocytic spectrin in structure and function revealed that fodrin was another member of the spectrin family of proteins (Levine and Willard, 1981).

Like the erythrocytic one, the brain spectrin was found to bind to the plasma membrane through interaction with ankyrin via the spectrin repeats and to the actin cytoskeleton through a specific domain in the N-ter (Burridge et al., 1982; Bennett et al., 1982; Berghs et al., 2000; Yang et al., 2007). By the end of the 80s, two α (αI and αII) and two ß (ßI and ßII) subunits, encoded by 4 different genes, had been described in the brain (Lazarides and Nelson, 1983; Zimmer et al., 1992). The knowledge about spectrins got broader with the discovery of ßIII (Ohara et al., 1998) and notably of ßIV spectrin. In 2000, Berghs and colleagues cloned the human *SPTBN4* gene (encoding ßIV spectrin) and described up to 4 isoforms generated by alternative splicing named with the letter ε (ε1- ε4) (Berghs et al., 2000). The largest isoform, ε1, was detected at the AIS and nodes of Ranvier in neurons from both the rat central and peripheral nervous systems (protein structure described in **Figure 24**). Importantly, ßIV spectrin colocalizes with AnkG in both structures, suggesting a link between the two proteins.

The group of ßIV spectrin isoforms was completed with the discovery of the human ε5 by Tse and colleagues and the ε6 in mouse, both also generated by alternative splicing (Tse et al., 2001; Komada and Soriano, 2002). In the study led by Komada and Soriano, the authors created a full KO for ßIV spectrin (*Sptbn4*) to further understand its functions in the brain (**Figure 24**).

Figure 24: *Protein structures of the ßIV spectrin isoforms ε1 and ε6. Left side represents the N-ter and the right side the C-ter. The ε6 lacks the actin-binding in N-ter domain and the 1-9 spectrin domains plus half of the 10. The blue arrow indicates the targeted domain in the mutant generated by Komada and Soriano. From Komada and Soriano, 2002.*

This null ßIV spectrin (*Sptbn4*) KO, which affected both ε1 and ε6 isoforms, revealed that AnkG and Na_v channels stainings were either very weak or absent in the AIS of the cerebellum, the hippocampus and nodes of Ranvier of the sciatic nerve (Komada and Soriano, 2002). This was the first evidence demonstrating that ßIV spectrin is necessary for AnkG recruitment

and/or stability and AIS integrity. The authors also found that, in the adult brain, the major isoform seemed to be the ε6 as revealed by western blot experiments. In addition, mutant mice presented a quivering phenotype, based on tremors, contraction of the hindlimbs and gait, signs associated with problems in nerve conductivity. The authors observed that the localization of ßIV spectrin to the AIS and nodes of Ranvier was AnkG-dependent using the same AnkG (*Ank3*) KO as Zhou et al. in 1998 (AnkG (*Ank3*)^{exon1b}) and validated a direct interaction between ßIV spectrin and AnkG. Such interaction was assessed by using a construct for the ε6 isoform and the authors hypothesized that this binding was taking place through the spectrin repeat number 15, as this was the domain reported for the interaction of ankyrin with other spectrins. Years later this postulate was confirmed (Yang et al., 2007).

Lacas-Gervais and colleagues followed with a study of the isoforms ε1 and ε6 and showed that both are present at the AIS and nodes of Ranvier in the cerebellum of adult mice (Lacas-Gervais et al., 2004). While ε1 was highly detected during development suggesting a role at the onset of AIS establishment, ε6 was observed at the time of myelination and suggested a tighter association with the nodes of Ranvier. The use of an ε1-specific KO revealed a residual expression of ε6 at the AIS, but lower compared to the node of Ranvier, showing that ε1 isoform is the most abundant at the AIS. Surprinsingly, while Komada and Soriano had shown a decrease of AnkG and Na_v channels in their mutant, the authors found increased immunolabeling levels for both markers. These mice also presented signs of a quivering phenotype that could arise from the defects observed at the nodes, like an increase in diameter. Mutant mice also had auditory defects, which the authors associated to impaired action potential generation in cochlear spiral ganglion neurons. These particular cells showed a fragmented profile of AnkG and voltage-gated ion channels. Altogether, this study and that of Komada and Soriano shed light on the role of ßIV spectrin isoforms at the AIS and nodes of Ranvier: the deletion of both isoforms leads to a decrease of the AIS main components, while the absence of ε1 shows a stronger detection. Lacas-Gervais and colleagues claimed that the increase of the AIS markers in their mutant is likely due to a higher accessibility of the epitopes of those proteins once the ε1 is absent from the AIS. So, while the specific role of this isoform at the AIS is not clear and its deletion mostly affects the nodes of Ranvier, the absence of both isoforms causes clear defects at the AIS level.

A study in 2016 further characterized the expression profile of the ε1 and ε6 ßIV spectrin isoforms during development (Yoshimura et al., 2016). While the levels of ε1 in the brain seemed relatively stable between birth and 3-month-old mice, those of ε6 started to increase by P12, up to P60. When quantified at the AIS and nodes of Ranvier, the fluorescence intensity levels of the same isoforms showed what the authors called a “switch”, with a decrease (often small) of ε1 over time (between P1 to 5-month-old) concomitant with an increase of ε6. A similar profile was observed in cultured neurons, starting around DIV5. This was consistent with the work of Komada and Soriano, who reported that the ε6 isoform was much highly expressed than the ε1 isoform both at the level of mRNA as well as protein in adult. The authors speculated that the (relative) decay of ε1 expression levels may reflect the

maturation of the AIS and the loss of proteins associated with ε1 that are no longer needed for AIS establishment, but do not explain the need of an increased shorter ßIV spectrin. In contrast, Lacas-Gervais and colleagues reported that the ε1 isoform is the dominant one at the AIS in adult mice while Yoshimura and co-workers showed the ε6 as the major isoform at the AIS in 5-month-old mice. A possible explanation relies on the chosen systems by both studies: Lacas-Gervais and colleagues used cerebellar sections, while Yoshimura et al focused on the cortex. It is possible that the developmental "switch" of these isoforms and their expression profile at nodes and AIS is brain region dependent. An example of a brain-region dependent isoform distribution is the AnkG NT isoforms, with the NT2 being most abundant at the cerebellum and the NT3 absent in that structure and mostly enriched at the cortex (Lopez et al., 2017) (see *3.1.1 Ankyrin-G: the master organizer*).

Yang and colleagues addressed the issue of the reliance of AnkG recruitment on ßIV spectrin (Yang et al., 2007). As mentioned before, they identified that the binding of spectrin repeat (SR) 15 of ßIV spectrin to AnkG was the basis for the localization of βIV spectrin at the AIS. But they further show, by analyzing a *quivering* qv^{3j} mouse model (Parkinson et al., 2001), that the AIS initially forms properly and that the loss of AIS components is gradual (observed in 1.5 months-old animals). In fact, the study from Komada and Soriano also claims the same phenotype by analyzing older mice (3 months old), demonstrating for ßIV spectrin a role on the stability and maintenance of the AIS more than on its formation. These results are supported by the work of Hedstrom et al. showing that the downregulation of ßIV spectrin through a specifi shRNA has no effects on AnkG and AIS formation (Hedstrom et al., 2007).

Overall, these studies highlight the importance of ßIV spectrin for AIS integrity and function, specifically *in vivo* and support its label of an AIS core molecule together with AnkG. The specific link of ßIV spectrin with the AIS actin is discussed in the following part: *3.1.3.1 The actin-spectrin network.*

3.1.3 The AIS cytoskeleton

3.1.3.1 The actin-spectrin network

In 2013, a seminal study described the actin-spectrin cytoskeleton organization at the axon using super-resolution imaging STORM (Stochastic Optical Reconstruction Microscopy, Rust et al., 2006) in 3D, to visualize the protein structures in a x-y-z axes reconstruction (Xu et al., 2013). The authors described an actin ring-like structure, wrapping the inside of the axonal circumference. This pattern was detected in the distal axon and at the AIS and started to form as early as DIV5 but was maintained in older neurons (e.g., DIV28). Later, the work of D'Este et al using STED (Stimulated Emission Depletion) microscopy on live neurons showed that the actin periodic pattern develops as early as DIV2, proving that the assembly of the rings happens shortly after axon specification and is AIS independent, as AIS formation happens after axonal establishment (D'Este et al., 2015; Banker and Goslin, 1988; Hedstrom et al.,

2007). The distance between these rings was highly regular, with a value of 190 nm, and suggested an adjacent structure that keeps such spacing. Interestingly, Xu and colleagues reported that ßII spectrin, which is present at the distal axon (Galiano et al., 2012), also displayed a periodic distribution with a regular spacing of 190 nm, identical to the actin rings. The same study showed that, at the AIS, ßIV spectrin followed the same pattern.

When imaged individually, each protein displayed a periodic distribution. But a co-staining of actin and spectrins revealed alternated periodic patterns: the peaks of intensity of the spectrins (using an antibody against the C-ter, C in **Figure 25**) fall in between two peaks of intensity of actin, and vice versa (**Figure 25**).

In the distal axon, ßII spectrin was detected at the centre of the tetramer, suggesting that there is a spectrin tetramer in between the actin rings connecting one ring to the adjacent one. The interdependence of these structures was shown when latrunculin A, an actin-depolymerizing drug, disrupted the periodic structures of both actin and spectrin. Interestingly, the disassembly of the actin rings only took place after applying a high concentration of latrunculin A, showing the robustness of the structure. In 2017, αII spectrin was identified as a component of this cytoskeleton network. It is enriched at the AIS and, remarkably, shows a similar periodicity than ßIV spectrin, revealing that the tetramer of spectrin present at the AIS is made by ßIV spectrin - αII spectrin (Huang et al., 2017) (**Figure 26A, 26B**). Interestingly, αII spectrin interacts with both isoforms of ßIV spectrin located at the AIS, namely ε1 and ε6, but the interaction is particularly stronger with ε6. Both isoforms have a common binding site with αII spectrin, localized in between the last spectrin repeat and the specific domain. The biggest isoform (ε1) has an extra interaction site localized at the beginning of the 17 spectrin repeats (**Figure 25A**). This study showed the integration of αII spectrin in the spectrin tetramer that is in between the actin rings at the AIS (**Figure 26A, 26B**).

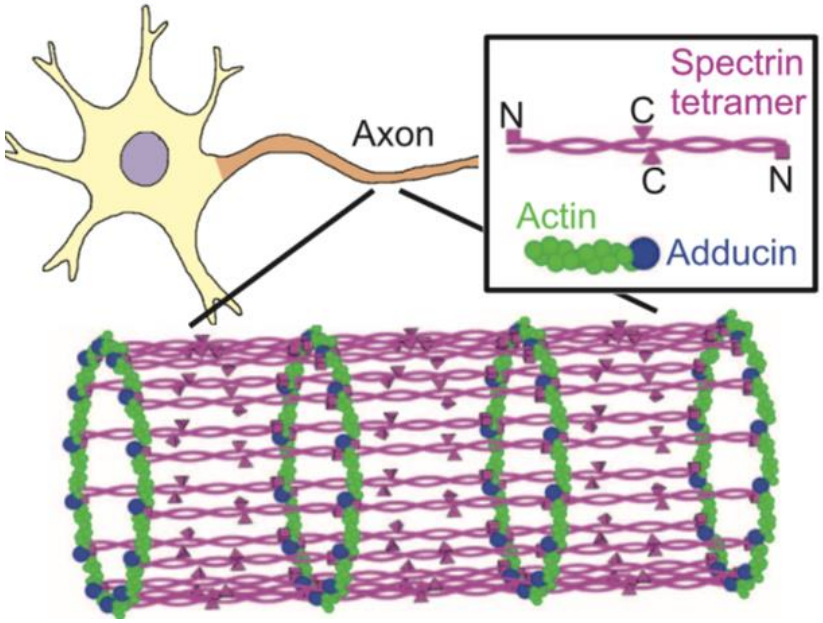

***Figure 25**: Schematic of the actin-spectrin skeleton network in axons. Actin rings (green) are displayed in a periodic pattern and are intercalated by spectrin tetramers (purple). A spectrin tetramer is placed in between the rings: in the schematic, the representation of ß spectrin molecules oriented in a head-to-head fashion. The C-ter, hereby referred as C, is pointing towards the middle of the tetramer while the N-ter, hereby referred as N, is linked to the actin rings. From Xu et al., 2013.*

Besides ßIV spectrin, Na_v channels at the AIS also follow a periodic organization: when ßIV spectrin was detected with an antibody against the N-ter (actin-binding domain, showing the same profile as the actin rings), Na_v was found in the space between two ßIV spectrin peaks, corresponding to the middle of the tetramer (Xu et al., 2013). This reveals that, at the AIS, the distribution of key molecules like Na_v channels is highly organized thanks to the actin-spectrin cytoskeleton, most likely through an interaction with AnkG. D'Este and colleagues also showed that NF-186 displays a periodic pattern at the AIS, intercalating with the actin (D'Este et al., 2015).

In line with these findings, Leterrier and colleagues confirmed that the distributions of ßIV spectrin using antibodies against the C-ter (center of tetramer) and N-ter (actin binding domain) were periodic (Leterrier et al., 2015). However, while the N-ter antibody showed a co-localization with actin, the peaks of intensity using an antibody against the C-ter were intercalated in between the peaks of actin. This suggested that the heterodimers of ßIV spectrin/αII spectrin are connected head-to-head in between the actin rings (**Figure 26A, 26B, 26C**). The authors also confirmed that Na_v and NF-186 distributions at the AIS were periodic and that they were localized between the actin rings (**Figure 27**).

Surprisingly, and contrary to what was observed with ßII spectrin in the distal axon, the periodicity of ßIV spectrin seemed resistant to actin disruption with latrunculin, showing

different robustness of the spectrin network in the AIS and the distal axon. The authors speculated that this was due to the presence of AnkG as a general stabilizer and further explored AnkG orientation in the structure. When using an antibody against the N-ter, concretely recognizing the spectrin-binding and the serine rich domains, the authors found the signal to be in phase with the periodicity of ßIV spectrin detected with an antibody at the C-ter of the protein, close to the center of the tetramer. But when they used an antibody either directed against the tail part or the C-ter of AnkG (**Figure 26D**), the signal was not periodic: interestingly, the AnkG C-ter was radially distributed within the axon and was resistant to actin and microtubule perturbations. This demonstrates that the AIS has a robust and finely organized actin-spectrin network that coordinates the distribution of membrane proteins, like Na_v channels and NF-186, through AnkG.

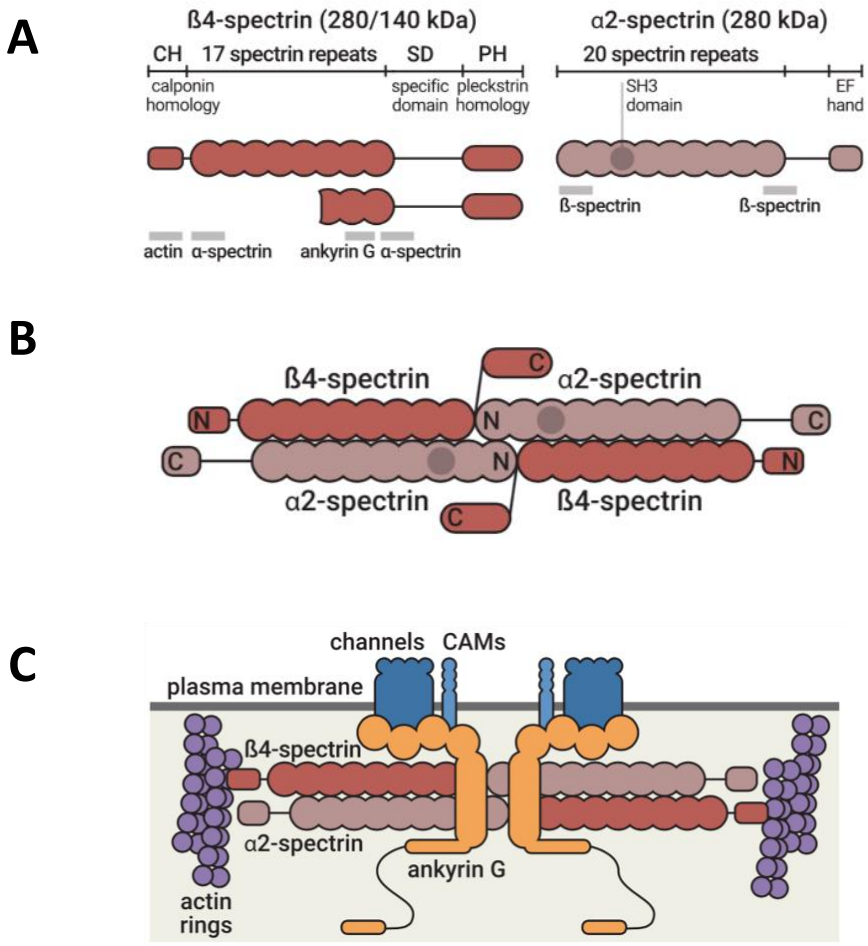

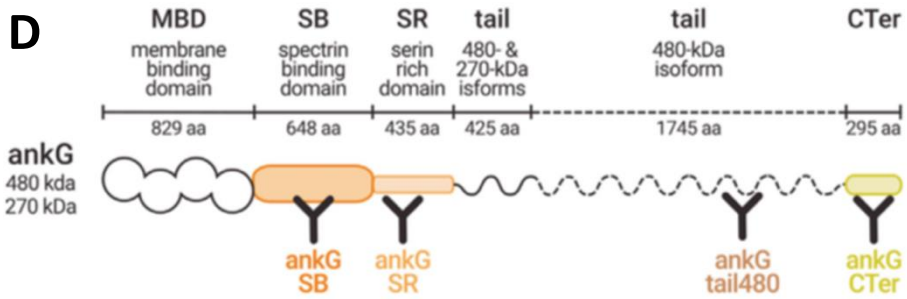

***Figure 26**: Schematic representation of the main AIS molecules distribution in the compartment. **(A)** Structures and domains of the isoforms of ßIV spectrin and αII spectrin. Domains of partner interactions are indicated. **(B)** Spatial organization of the spectrin tetramer at the AIS composed by ßIV and αII spectrin. **(C)** Molecular organization of the AIS, where the spectrin tetramer is located in between the actin rings. **(D)** Schematic of the different antibodies used in the study from Leterrier et al., 2015, to investigate AnkG nanolocalization at the AIS. From Leterrier et al., 2015; 2018.*

How do the AIS periodic proteins adopt this pattern? While the actin rings are detected during the early steps of axon specification, the periodic distribution of the AIS proteins, including AnkG and ßIV spectrin, has been detected only starting from DIV8 and is clearly visible in later stages (Zhong et al., 2014). This suggests that the periodic organization is sequential, and takes place when the AIS is fully developed, suggesting an incorporation into the pre-existing periodic actin structure (for review, see Leite and Sousa, 2016). Interestingly, the same study showed that ßII spectrin is detected all along the axon in form of periodic rings early in axonal formation, but when the AIS is established and ßIV spectrin starts to be periodically distributed, ßII spectrin is restricted to the distal part. Xu et al had shown that disrupting the actin rings did not impact the periodic distribution of ßIV spectrin. Interestingly, a recent study using cultured neurons from *quivering* mice showed that genetic depletion of ßIV spectrin does not impact the periodic distribution of AnkG or Na_v channels (Lazarov et al., 2018). Instead, ßII spectrin was present at the AIS of these mutant mice, showing its classic periodic distribution and likely preserving the pattern of both AnkG and Na_v channels. Altogether, these studies show that the highly organized distribution of AIS molecules is preserved even in actin depolymerization and ßIV spectrin depletion conditions (Xu et al., 2013; Lazarov et al., 2018), showing that the periodic localization of the AIS molecules may be relevant in terms of AIS function.

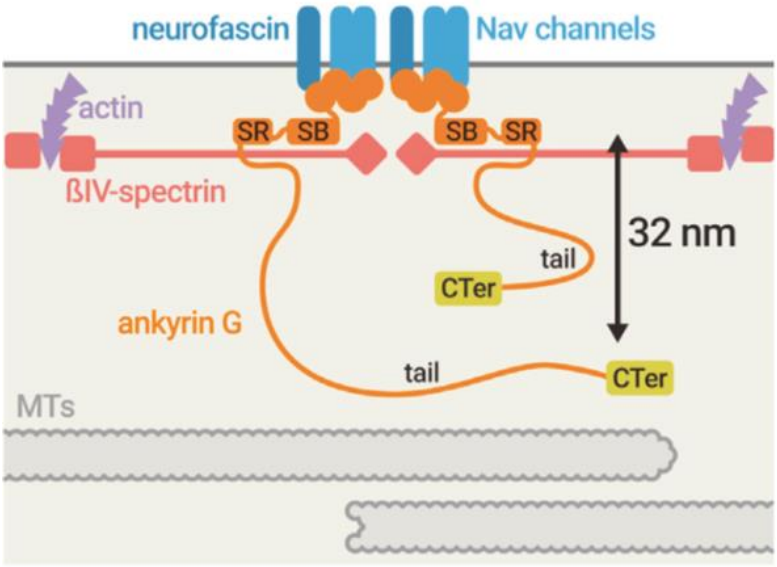

***Figure 27**: Schematic of the distribution of AIS molecules in respect to the membrane and the cytoskeleton. From Leterrier et al., 2015.*

A functional role for the membrane periodic skeleton (MPS, the given name to the periodic skeleton formed by spectrin and actin rings) is still elusive though under intense investigation. One of the proposed functions is to provide flexibility to the axon and protection against mechanical stress (Hammarlund et al., 2007). A recent study showed that the MPS could serve as a platform for ERK signaling activation in neurons: cell adhesion molecules, receptor-tyrosine kinases and G-protein-coupled receptors are recruited to the MPS upon external stimuli and activate signaling cascades (Zhou et al., 2019). Other studies suggest that MPS-associated molecules are also involved in regulating axonal diameter, key for proper conduction of electric signals along the structure (reviewed in Costa et al., 2018; Costa et al., 2020). It is important to mention that the MPS organization was as well found in dendrites, although to a less extent and with a slower development than that of the axon (D'Este et al., 2015; Han et al., 2017). Although the structure is preserved in between dendrites, axon and AIS; specific differences at the molecular level (e.g., the type of spectrin in between the rings) could explain a diversity in functions. For example, a recent study showed a neuronal activity-dependent remodeling of actin rings in the dendrites but not in the axon (Lavoie-Cardinal et al., 2020, preprinted). Further studies are needed to fully understand the functions of the MPS in the axon and dendrites and assess a possible functional specialization of this structure within these neuronal compartments.

Besides the rings, actin at the AIS is also present in other forms. Jones and colleagues showed that the AIS is formed by two populations of actin filaments, one of them being shorter and more stable and another group formed by long, more dynamic filaments (Jones et al., 2014). The specific pool of short filaments is part of the submembranous coat at the AIS and contributes to its stability. A study from 2012 revealed the presence of highly stable,

detergent resistant, actin patches all along the AIS (Watanabe et al., 2012). Filaments at these patches have a specific orientation, with the plus-ends towards the cell body and contribute to the maintenance of neuronal polarity by preventing the axonal entry of somatodendritic proteins (see *3.2.1 The maintenance of neuronal polarity*).

3.1.3.2 Microtubules

In 1968, Palay and colleagues used different sections from the rat brain to observe under transmission electron microscopy (TEM) (Palay et al., 1968). They found that the initial segments of many neuron types, including Purkinje neurons of the cerebellum and pyramidal cells in the cortex, had two particular features: 1) they were enriched on a dense granular material undercoating the plasma membrane and 2) their microtubules were arranged into bundles. Microtubules are tube-like structures made by protofilaments of tubulin units, and each of these cylinders can organize with other microtubules and create the bundles. According to Palay et al, bundles at the AIS can contain different number of microtubules depending on the neuron type, but the average is from 3 to 5. Microtubules in the bundles are linked to each other by electron dense cross-bridges formed by microtubule-associated proteins (**Figure 28**) (Peters et al., 1968). Interestingly, the authors reported that this disposition was not found at any other part of the neuron despite the known presence of microtubules in different neuronal compartments, suggesting that this organization confers them a particular role at the AIS. Jones and colleagues reported that the assembly of the microtubule bundles at the proximal axon starts as early as DIV3 in cultured neurons, period when the AIS starts to form, implying that both processes are coordinated (Jones et al., 2014). A bit later, at around DIV7, a fibrillar-globular coat starts to cover the microtubules. The authors associate the presence of fibrils to the arrival of filamentous proteins during AIS assembly.

Microtubules at the AIS have a series of associated proteins. In 2015, van Beuningen and colleagues identified the tripartite motif containing 46 (TRIM46) as a member of the AIS and an essential regulator of microtubules at this compartment (van Beuningen et al., 2015). The authors showed that TRIM46 localizes to the microtubules and is essential for their parallel organization by acting as a cross-bridge and therefore creating the bundles. TRIM46 also controls the proper polarity of microtubules within the axon: axonal microtubules are oriented with their plus-end distally from the cell body. This orientation ensures the selective trafficking of axonal proteins through the specific binding of motor proteins. An example of this sorting is KIF5, which transports AnkG all along the microtubules to the AIS. This association is essential for AnkG to transport Na_V channels to this compartment (Barry et al., 2014). Axonal cargo transport is severely impaired in the absence of TRIM46. Since TRIM46-deprived neurons fail to form an axon, this reveals for the protein a dual role on contributing first to neuronal polarity establishment and second to the AIS microtubules integrity and function. The authors concluded that, since TRIM46 controls axonal formation and the proper

orientation of microtubules, the latter is likely a requirement for a neuron to be properly polarized (see *2.1 Neuronal polarity in vitro: a cell autonomous process*). The same team published a study in 2019 where they described with detail the role of TRIM46 on creating microtubule bundles, process known as fasciculation, by being part of the electron dense structure acting as a cross-bridge between the microtubules (**Figure 28**) (Harterink et al., 2019). Importantly, this fasciculation process was shown to be dependent also on AnkG, as in AnkG (*Ank3*) $^{-/-}$ neurons the bundles are disorganized (Sobotzik et al., 2009). A recent study showed that TRIM46 participates in a feedback-driven mechanism for AIS formation, in which forms and stabilizes parallel microtubule bundles and contributes to the trafficking of NF-186 to the AIS, where it gets immobilized by AnkG. In turn, NF-186 stabilizes AnkG at the membrane. (Fréal et al., 2019). This molecular loop has been described as essential for AIS formation. Another microtubule protein called MTCL1 was found to partially colocalize with AnkG at the AIS of Purkinje neurons, a similar profile to TRIM46: both proteins are slightly shifted towards the cell body in respect to AnkG (Satake et al., 2017). Depletion of MTCL1 promotes an overall disorganization of the microtubule bundles at the AIS, a mis-localization of AnkG and a loss of neuronal polarity with the formation of axonal spines.

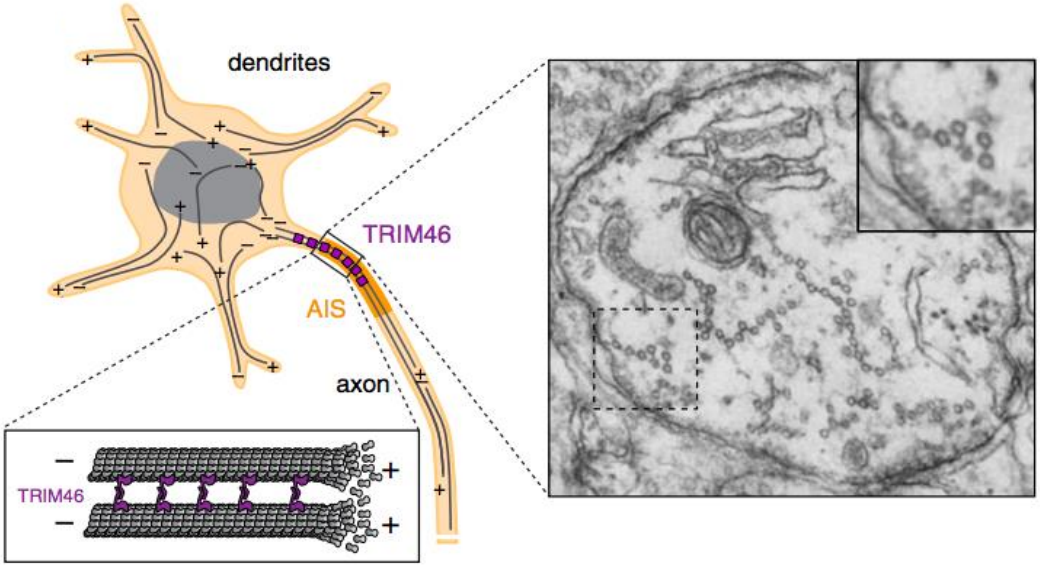

***Figure 28**: TRIM46 controls microtubule polarity and acts as a bridge between microtubules at the proximal axon. Electron microscopy of a cross-section of the proximal axon showing microtubule fascicles. From van Beuningen and Hoogenraad, 2016.*

EB1 and EB3 proteins are critical components of the AIS microtubules. Although they are classically known to bind to the plus-end of microtubules and decorate highly dynamic projections or “comets”, EBs at the AIS represent an immobile fraction all along the fascicles

(Nakata et al., 2003; Leterrier et al., 2011). Initially, Leterrier and colleagues identified EB1 and EB3 accumulating at the AIS and interacting with AnkG (Leterrier et al., 2011). In fact, depletion of these proteins led to an AIS disassembly, while downregulation of AnkG increased the intensity of these markers at the AIS. Interestingly, the increase of EB proteins at the AIS is linked to an altered plasticity (Sohn et al., 2019). The authors claim that an EB accumulation at the microtubules contributes to its stability, as EB-decorated microtubules are more resistant to detergent extraction. Later, Fréal et al. identified that a specific interaction between the tail domain at the C-ter of the AnkG-480 isoform and the EBs was key for driving AIS assembly (Fréal et al., 2016). These studies show an essential crosstalk between AnkG and the microtubules, via EB proteins, for AIS integrity.

It is important to consider that some features of the microtubules that contribute to neuronal polarity are not AIS-exclusive. As discussed above, microtubule filaments are polarized, and one end favors depolymerization (plus-end) while the other one is more stable (minus-end). While in dendrites we find both types of polarities coexisting, axonal microtubules are exclusively oriented with their plus-end towards the axonal tip (Baas et al., 1988). As mentioned in the section *2. Neuronal polarity*, this orientation is key for selective cargo transport to the axon: the different motor proteins have more affinity towards one orientation or the other, therefore determining if a protein ends up in the dendrites or in the axon. For example, the motor proteins kinesins are plus-end directed and go through anterograde transport all along the axon. On the other hand, dyneins have a preference for the minus-end and display a retrograde transport (reviewed in Vale, 2003; Welte, 2004). It is worth mentioning that at the AIS, the presence of a cytoplasmic filter contributes to the sorting of somatodendritic proteins heading to the axon: Song and colleagues reported that the proper exclusion of the somatodendritic protein NR2B and its associated motor protein KIF17 is driven by the affinity of the kinesin by a given microtubule polarity but also by the physical barrier present at the cytoplasm (Song et al., 2009; see *3.2.1 Maintenance of neuronal polarity*). In comparison with axonal proteins, the transport rates of KIF17-NR2B in the proximal axon are slower, which impedes the entry in this compartment. Li and colleagues showed the existence of a retrograde barrier for the axonal protein Tau (Li et al., 2011): once this protein is sorted to the axon during development it cannot go back to the somatodendritic domain. Drug-induced microtubule disassembly promoted a ubiquitous localization of Tau. Therefore, since this function seems to rely on a highly stable pool of microtubules, it is possible that, in this case, the specific stable microtubules at the AIS are contributing to this retrograde barrier.

Altogether, these studies reveal that the AIS microtubule cytoskeleton is a highly organized and robust structure that participates in neuronal polarity via protein sorting and the coordination of AIS assembly and maintenance via AnkG and associated molecules.

3.1.4 Cell adhesion molecules: neurofascin and NrCAM

The AIS is comprised of cell adhesion molecules (CAMs), which are embedded in the membrane and display different functions within the compartment. As early as 1996 the L1 cell adhesion molecules neurofascin (NF) and the neuron glia-related CAM (NrCAM) were found to accumulate at the AIS. The use of AnkG mutants revealed that the localization of these molecules at the AIS is AnkG-dependent (Jenkins and Bennett, 2001). Neurofascin is the most studied CAM at the AIS and has a total of four isoforms, generated by alternative splicing: the 186 kDa (NF-186) isoform specifically accumulates to the AIS, while the 155 kDa (NF-155) is localized in the paranodes and in unmyelinated axons (Davis et al., 1993; Davis and Bennett, 1994; Davis et al., 1996; Hassel et al., 1997).

In 2004 Ango and colleagues showed that the specific localization of NF-186 at the AIS is controlled by AnkG as in the absence of AnkG, NF-186 is distributed widely in soma and axon (Ango et al., 2004). The authors further showed that NF186 was critical for axo-axonic synapses, notably between Purkinje neurons and basket cells (inhibitory/GABAergic), known as pinceau synapses. Upon AnkG depletion, the remaining pool of NF186 at the AIS is not enough for pinceau synapse formation, as revealed by a dramatic decrease of the inhibitory marker GAD65 at the AIS. The AnkG-dependent AIS localization of NF-186 was further confirmed in cultured neurons (Boiko et al., 2007).

However, while Hedstrom and colleagues reported that NF-186 or NrCAM were not necessary for AIS formation (Hedstrom et al., 2007), two recent studies showed that NF-186 knockdown at the onset of AIS formation significantly impairs the levels (Leterrier et al., 2017) and the position (Alpizar et al., 2019) of AnkG (for details on these articles, see *3.1.1 Ankyrin-G: the master organizer*). Recent studies showed that NF-186 contributes to AIS assembly via the stabilization of AnkG at the membrane (Torii et al., 2020; Fréal et al., 2019): Torii and colleagues demonstrated that the nuclear mitotic apparatus protein 1 (NuMA1) inhibits the endocytosis of NF-186 and Fréal et al showed that NF-186 levels at the membrane do stabilize AnkG in the developing AIS.

The role of NF-186 maintenance *in vitro* is still debated (Hedstrom et al., 2007; Leterrier et al., 2017; see *3.1.1 Ankyrin-G: the master organizer*), but the use of *Nfasc* (the gene encoding neurofascin) null mice helped to understand its function *in vivo* (Zonta et al., 2011): cultured organotypic slices from the cerebellum of *Nfasc* null mice have no initial defects in AIS formation besides a loss of NrCAM, but displayed a progressive AIS disassembly after 15 days *in vitro*, revealed by a decrease of AnkG, Na_v channels and ßIV spectrin. The authors confirmed a loss of the pinceau synapses in line with the work of Ango and colleagues (Ango et al., 2004). To investigate the specific role of NF-186 on AIS maintenance *in vivo*, the authors used a mouse carrying one null and one floxed allele for the *Nfasc* gene. The deletion of the floxed allele was performed via a tamoxifen-induced expression of the cre. After 4 weeks of Cre expression, these animals lost AnkG, Na_v channels and ßIV spectrin, confirming a role for

NF-186 on AIS maintenance *in vivo*. Functionally, depletion of NF-186 led to defects in action potential firing of Purkinje neurons, which were overall less excitable.

In respect to the relation of NF-186 with NrCAM, Hedstrom et al showed that downregulation of NF-186 via shRNA *in vitro* reduces the levels of NrCAM (Hedstrom et al., 2007). In the same line, the neurofascin null mutant from Zonta and colleagues revealed an early decrease of this protein. However, the study of Alpizar and colleagues showed no decrease on this marker when they downregulate NF-186 on cultured neurons. The authors attribute these differences in results to the presence of additional factors *in vivo* that may contribute to this decrease of NrCAM (and other AIS molecules). However, this does not explain the difference in results with Hedstrom and colleagues, as both use cultured neurons. Revisiting this study, it is important to notice that the decrease on NrCAM triggered by the downregulation of NF-186 is highly variable in comparison with the other analyzed markers, showing neurons with heterogeneous phenotypes. An increase in sample size could help to determine the exact extent of the effect of NF-186 knockdown on NrCAM levels.

Finally, NF-186 also binds to brevican, an extracellular matrix (ECM) protein whose AIS localization is dependent on NF-186 (Hedstrom et al., 2007). Brevican at the AIS is believed to stabilize NF-186 and therefore support the formation of axo-axonic synapses and promote the stabilization of AnkG at the membrane (Hedstrom et al., 2007; Fréal et al., 2019).

In conclusion, NF-186 has been shown to be a key molecule for AIS maintenance and function, especially *in vivo*. In cultured neurons NF-186 is key for immobilizing AnkG at the proximal axon, therefore participating in AIS establishment.

3.1.5 Voltage-gated ion channels

One of the functions of the AIS is to initiate action potentials, a process that mainly relies on a high concentration of sodium channels (Na_v) (Caterall, 1981; Angelides et al., 1988). Na_v channels are responsible for membrane depolarization and are composed of an α subunit associated with one or several auxiliary ß subunits (reviewed in Caterall, 2020). While the α subunit is enough for the channel to be functional, the ß subunit controls the kinetics and the voltage dependence for the activation and inactivation of the channel. A total of nine Na_v channels, generated by different genes, have been identified in mammals. From these, four are present in the central nervous system: $Na_v1.1$, $Na_v1.2$, $Na_v1.3$, $Na_v1.5$ and $Na_v1.6$ (Goldin et al., 2000; Wang et al., 2017).

Zhou and colleagues showed in 1998 a co-localization of Na_v channels with AnkG at the AIS and a loss of Na_v in absence of AnkG, suggesting an AnkG-dependent mechanism for Na_v channels anchoring at the AIS (Zhou et al., 1998). Further studies determined that $Na_v1.2$ and $Na_v1.6$ channels subtypes are specifically enriched at the AIS, both in cultured neurons and in the brain (Jenkins and Bennett, 2001; Lemaillet et al., 2003; Garrido et al., 2003). Using rat retinal ganglion neurons, Boiko and colleagues highlighted the temporal profile of expression

of the two Na_v channels *in vivo*: while $Na_v1.2$ starts to be present at the onset of AIS formation (P1), $Na_v1.6$ is expressed a few days later when the AIS is more mature (P9) (Boiko et al., 2003). In the adult tissue both are present at the AIS, although $Na_v1.6$ is restricted to the AIS and $Na_v1.2$ is also present all along the unmyelinated axon. In the same type of neurons, $Na_v1.1$ was identified at the very proximal part of the mature AIS (Van Wart et al., 2007) and this exact same localization was found in other parts of the brain, mostly in interneurons (Duflocq et al., 2008). These findings suggest a functional specialization for the Na_v channels. In fact, Hu and colleagues showed that $Na_v1.2$ and $Na_v1.6$ contribute differently to action potential generation and backpropagation in the rat prefrontal cortex (Hu et al., 2009). Importantly, $Na_v1.6$ channels are located at the distal site of the AIS, which is the place where the action potential is initiated. These channels display a lower threshold of activation, which is more suitable for this particular function. On the other hand, $Na_v1.2$ facilitates the backpropagation of the action potential to the somatodendritic compartment, which is compatible with its location closer to the cell body of the neuron (Hu et al., 2009).

Almost published at the same time, two studies identified the AnkG-binding domain of $Na_v1.2$ channels: a highly conserved motif localized within one of the cytoplasmic loops of the α subunit (Garrido et al., 2003; Lemaillet et al., 2003). This motif is also present in $Na_v1.1$ and $Na_v1.6$ and was found to be necessary for $Na_v1.6$ recruitment to the AIS (Gasser et al., 2012). Phosphorylation within this specific domain by the serine/threonine Casein Kinase 2 (CK2) is necessary for the interaction of Na_v channels with AnkG and therefore for their AIS localization (Bréchet et al., 2008).

The role of Na_v channels on AIS formation has been reported by three different studies, where the downregulation of Na_v channels in cultured neurons (hippocampal or spinal motor neurons) leads to a decrease of AnkG levels and therefore impacts AIS establishment (Xu and Shragger, 2005; Hedstrom et al., 2007; Leterrier et al., 2017). However, it is not clear if these channels are involved in AIS maintenance: Hedstrom et al reported no effect on the AIS after Na_v downregulation. In fact, they showed that Na_v channels were quite stable at the AIS and difficult to knockdown once the AIS is established (Hedstrom et al., 2008). It is important to mention that Leterrier and colleagues showed a similar percentage of downregulated Na_v channels in their $shNa_v$ (around 50%) and that this was enough to alter AnkG levels. So, while both studies show that it is difficult to downregulate Na_v channels once the AIS is established, Leterrier and colleagues claim that this is enough to alter AnkG levels and therefore to disrupt AIS maintenance.

The AIS is also rich in voltage-gated potassium channels (K_v) that are comprised of an α core subunit and auxiliary ß subunits. A total of 12 subfamilies have been identified and termed K_v1- K_v 12, with three present at the AIS: K_v1, K_v2 and K_v7 (Gutman et al., 2003; Sanchez-Ponce et al., 2011). Channels from the K_v1 family contribute to action potential (AP) generation and propagation notably by modulating the frequency and duration of single APs by participating in the AP repolarization and transition to the refractory period (Yu and Caterall, 2003; Kole et al., 2007). In the human neocortex $K_v1.2$ was identified at the distal

part of the AIS, but this localization appears to be cell dependent, as in some cell types (like pyramidal neurons from the CA3 of the hippocampus) $K_v1.2$ staining was found all along the AIS (Inda et al., 2006). $K_v1.1$ seems to follow the same profile than that of $K_v1.2$ (Lorincz and Nusser, 2008). Although the AIS localization of these channels is lost upon AnkG depletion *in vitro* (Sanchez-Ponce et al., 2012), the accumulation of K_v1 channels at the AIS is mainly controlled by other mechanisms, including scaffolding proteins (post-synaptic density-93, PSD-93; Ogawa et al., 2008), adhesion molecules (leucine-rich glioma inactivated 1, LGI1; Hivert et al., 2019) and by the association of the channel ß subunits with the microtubule end-binding protein EB1 and kinesin-2 (Vacher et al., 2011). $K_v2.1$ and $K_v2.2$ channels regulate the frequency of action potential firing and depolarization (Sarmiere et al., 2008; Johnston et al., 2008; Malin and Nerbonne, 2002; Guan et al., 2013). Interestingly, the $K_v2.1$ channel defines a unique cluster of AnkG negative spots in the AIS (King et al., 2014) and its localization at the AIS is regulated by specific post-translational phosphorylations (Jensen et al., 2017). $K_v7.2$ and $K_v7.3$ are found in the distal part of the AIS, via interaction with AnkG (Devaux et al., 2004). Interestingly, the AnkG-binding sequence is highly similar to that required for Na_v channels recruitment, showing a highly conserved mechanism of anchoring of ion channels to the AIS (Pan et al., 2006). In addition, the formation of heterodimers between $K_v7.2$ and $K_v7.3$ facilitates their localization at the AIS (Rasmussen et al., 2007). These channels control axon excitability by regulating the availability of Na_v channels and by controlling spontaneous firing. They are therefore important on limiting the dysregulation of neuronal excitability (Battefeld et al., 2014).

Finally, voltage-gated calcium channels (Ca_v) were also identified at the AIS (Callewaert et al., 1996). In this study, the authors found an increase of calcium currents in the proximal axon during action potential generation. Further studies identified $Ca_v3.1$, $Ca_v3.2$ and $Ca_v2.3$ channels at the AIS of the cartwheel cells from the dorsal cochlear nucleus and showed that they modulate membrane depolarization and action potential timing (Bender and Trussell, 2009). The list of calcium channels at the AIS was completed with the article of Yu and colleagues, where they detected $Ca_v2.1$ and $Ca_v2.2$ at the AIS of cortical pyramidal neurons (Yu et al., 2010).

3.1.6 The AIS and the nodes of Ranvier: similar structures, different roles

Most of the axons of the nervous system are myelinated. Glial cells promote the formation of myelin sheaths, which wrap the axons and improve the conduction of the action potential. The domains between these sheaths are called nodes of Ranvier (NoR) whose molecular composition allows fast propagation of the action potential (reviewed in Simons and Trajkovic, 2006; Rasband and Peles, 2021). NoR are surrounded by molecularly different domains called paranodes and those, at the same time, are flanked by the juxtaparanodes. The functions of the AIS and the NoR are different: the AIS is the site for action potential

initiation, modulation and backpropagation while the NoR facilitate fast and efficient conduction of the action potential through the axon (reviewed in Rasband and Peles, 2021).

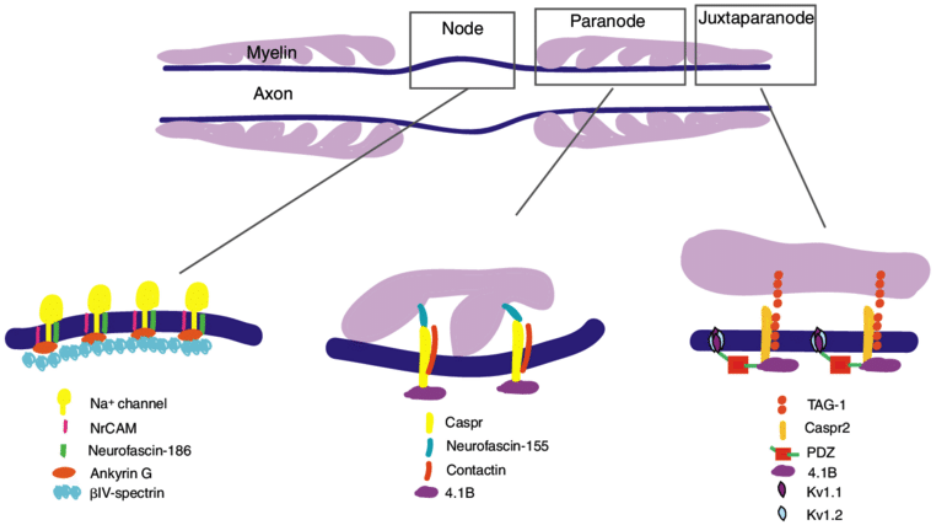

Figure 29: *schematic of the molecular composition of the node of Ranvier, the paranodes and the juxtaparanodes. From Simons and Trajkovic, 2006.*

The molecular composition between AIS and NoR is very similar, as they share main molecules like AnkG 480/270 kDa isoforms, ßIV spectrin, Na_v channels and the cell adhesion molecules NrCAM and NF-186 (**Figure 29**). But the formation mechanisms, including the time of arrival of the proteins to these domains, are very different. The AIS formation is a cell autonomous process and is triggered by the master organizer AnkG, which recruits all the other components, while the assembly of the NoR is believed to be a cell non autonomous mechanism, combining extracellular signals from the glia and intrinsic mechanisms (Kaplan et al., 1997). The first molecules detected at the developing nodes are NF-186 and NrCAM, followed by Na_v channels, AnkG and ßIV spectrin (Lambert et al., 1997; Melendez-Vasquez et al., 2001). Importantly, the glial molecule gliomedin drives NF-186 accumulation at the nodes (Eshed et al., 2005; Koticha et al., 2006). Although the core AIS proteins, like AnkG or ßIV spectrin, are not initial drivers of NoR formation, they are still key for NoR structure: the depletion of these molecules reduces the number of NoR suggesting a stabilization role within the protein network similar to that of the AIS (Jenkins et al., 2015; Lacas-Gervais et al., 2004). Other similarities AIS-NoR include the organization of the respective molecules: like in the AIS, AnkG and ßIV spectrin show a periodic pattern in the NoR (D'Este et al., 2017). Galliano and colleagues showed the relevance of a distal axon skeleton, comprised of AnkB and ßII spectrin, for proper node formation (Galiano et al., 2012). Similar to the AIS, these proteins are excluded from the structure but have an important function on shaping its development.

Interestingly, a recent study showed that the NoR are structurally plastic in the adult mouse brain: two types of neuronal activity modulation (repetitive transcranial stimulation and spatial learning) modify the pre-existent myelin and the length of the NoR (Cullen et al., 2019, preprinted). The AIS also undergoes structural plasticity and shapes the electric activity of the neuron by adapting its length and position (see 3.*3 Structural plasticity and neuronal homeostasis*).

3.2 Functions

3.2.1 The maintenance of neuronal polarity

One of the functions of the AIS is to maintain neuronal polarity throughout the life of a neuron. It defines the boundary between the somatodendritic and the axonal compartments and acts as a barrier by preventing the mis-sorting of proteins and lipids. The first evidence of the existence of such a barrier was the observation of the AIS that Palay and colleagues did in 1968 using electron microscopy: they detected a very dense layer of proteins undercoating the plasma membrane at the AIS, suggesting the existence of a physical obstacle, or barrier, for protein trafficking (Palay et al., 1968). In 1999, Winckler and colleagues observed a restricted mobility of transmembrane proteins at the AIS, which was abolished upon actin depolymerization (Winckler et al., 1999). A study performed by Nakada et al. showed that the lipids inserted in the plasma membrane diffused freely in the neuron but got restricted at the AIS, confirming the barrier theory (Nakada et al., 2003). The maturation of this barrier was seen to happen between DIV7 and DIV10, matching with AIS maturation. Importantly, actin depolymerization led to AIS membrane proteins and lipids drift towards the cell soma and suggested that the basis of this barrier is the crosstalk between the high accumulation of transmembrane proteins in the AIS with a dense mesh of actin, acting together as pickets to physically limit the free diffusion of molecules. These initial studies show that the AIS barrier is happening at many levels, including transmembrane proteins but also the actin cytoskeleton.

A study led by Nishimura and colleagues showed that, besides a general barrier, AIS molecules may control the localization of axonal proteins via direct interactions (Nishimura et al., 2007). ßIV spectrin is essential for the axonal localization of L1CAM, as this protein is transported to the somatodendritic compartment in neurons from ßIV spectrin mutant mice. The authors showed that, since AnkG and L1CAM interact, the mislocalization is likely driven by the disruption of this complex, as AnkG profile is highly disrupted in ßIV spectrin depletion conditions. But as AnkG controls the assembly of the AIS, that including the high density of transmembrane proteins, it is conceivable that both mechanisms are contributing to the axonal restriction of L1CAM. Interestingly, the localization of GluR1 was unaffected in the mutants, suggesting additional mechanisms, besides the AIS, regulating the sorting of this protein.

The work of Song et al demonstrated the existence of a cytoplasmic filter at the AIS (Song et al., 2009). In neurons with an established AIS, small dextrans of 10 kDa freely circulate to the axon, but those of 70 kDa (and beyond) are retained at this compartment and consequently excluded from the axon. This specific sorting appeared as early as DIV5, suggesting that this filter forms at the same time as the AIS. While nocodazole-induced destabilization of microtubules had no effect, actin depolymerization drugs promoted the axonal invasion of the 70 kDa dextran. This reveals a specific role for actin in this cytoplasmic filter. The authors observed that the overexpression of an AnkG construct that lacks the binding to ßIV spectrin impacted actin accumulation at the AIS, suggesting that both may be connected in the establishment of this barrier. In fact, downregulation of AnkG in DIV5 neurons promoted the diffusion of the 70 kDa dextran in the axon, confirming that both actin and AnkG are cooperating in the cytoplasmic filter. The authors further addressed the function of this filter on the active sorting of membrane proteins, besides the passive transport of macromolecules. While the overexpression of the somatodendritic protein NR2B in regular conditions resulted in a correct distribution in this compartment, drug-induced actin depolymerization promoted its axonal localization. Actin, by creating a dense meshwork, may therefore physically impede the entry of somatodendritic vesicles in the axon, while allowing the entry of axonal proteins. The authors suggest that this mechanism, together with the preferential binding of some kinesins to microtubules with a given polarity, contribute to the proper sorting of these proteins.

Altogether, these studies show that there is a barrier at the AIS ensuring the proper distribution of proteins between the somatodendritic and the axonal compartments. This barrier involves the high accumulation of proteins at the membrane, the AIS master organizer AnkG and the participation of the actin and microtubules cytoskeleton. Actin has different roles on this barrier: according to Song and colleagues, it forms a meshwork at the AIS that physically impedes the entry of somatodendritic vesicles in the axon (Song et al., 2009). However, a later study contradicts this hypothesis as no structural data supports the presence of a dense actin network at the AIS (Jones et al., 2014). The experiments from Jones and colleagues reveal that the actin network is not as dense to support a role as a physical barrier. The authors hypothesize that the molecular submembranous coat at the AIS could contribute to this function instead, with short actin filaments preserving its integrity. As commented before, the AIS is rich in actin patches that contribute to neuronal polarity maintenance, as vesicles carrying somatodendritic proteins are retained at this compartment and excluded from the axon (Watanabe et al., 2012). The authors propose that motor proteins, like different types of myosins, do display different affinities for actin filaments polarities and this determines if a protein ends up at the axon or the dendrites (similar to the microtubules). Despite the early formation of actin rings during axon development, coinciding with the assembly of the barrier, these are unlikely contributing to this function as they are present all along the axon. As mentioned in *3.1.3.2 Microtubules,* the proper polarity and stability of these structures at the AIS also contribute to the active sorting of proteins in the axon.

The consequence of the disruption of this barrier is an overall loss of polarity. This is typically what is observed after the depletion of AnkG *in vivo* and in cultured neurons, which results in axonal invasion of somatodendritic proteins like MAP2 and the formation of spines (Jenkins et al., 2015; Fréal et al., 2016; Hedstrom et al., 2007, Sobotzik et al., 2009). Interestingly, Jenkins and colleagues showed that the early deletion of the giant AnkG isoforms (480 and 270 kDa) promoted a partial loss of neuronal polarity, as the distal axon still preserved its molecular identity revealed by the neurofilament staining in this compartment. The maintenance of neuronal polarity may therefore be supported by other mechanisms than the AIS.

3.2.2 Action potential generation and tuning

In the brain, neurons mainly receive input signals via the dendrites and transmit them through the axon, which sends the output signals to other neurons. In basal conditions, the inside of neurons is negatively charged with respect to their extracellular environment: this difference of charge, called resting membrane potential, typically ranges from -70 to -80 millivolts (mV) depending on the neuron type (reviewed in Raghavan et al, 2019, book chapter). This potential mainly relies on the activity of the Na^+ K^+ ATPase enzyme, which pumps out 3 Na^+ ions for every 2 K^+ ions pumped in the cell and thus contributes to the overall negative charge (reviewed in McCormick, 2014, book chapter).

At the synapse, the presynaptic neuron releases a series of neurotransmitters that will increase (excitatory) or decrease (inhibitory) the probability of the postsynaptic neuron to generate an action potential (AP). If the neurotransmitters are excitatory, their interaction with the postsynaptic receptors will trigger the entry of positive ions in the cell via the activation of different channels, including Na_v (reviewed in McCormick, 2014, book chapter). This ion flow will progressively make the membrane potential more positive which, when it goes above a threshold potential, generates the AP (**Figure 30**). The first phase of the AP, called depolarization, happens shortly after crossing the threshold potential and is characterized by very fast and transient opening of Na_v channels that are clustered at the AIS and along the axon at the nodes of Ranvier. This activation of Na_v channels is triggered by the overall increase in voltage inside the cell, promoting a continuous entry of Na^+ ions that keep contributing to make the potential more positive (reviewed in Catterall, 2000) (**Figure 30**). As all the Na_v channels are open, the flow of ions reaches a maximum and so does the voltage membrane. At this point, these channels become quickly inactivated and the potassium channels, whose activation occurs at more positive voltages, start to open, causing a progressive removal of K^+ ions that drives the voltage membrane closer to the threshold potential (repolarization) (Mitterdorfer and Bean, 2002). In fact, the continuous entry of K+ ions sets the membrane voltage to more negative levels than the threshold potential, a process called hyperpolarization (**Figure 30**) Finally, the neuron eventually returns to the resting membrane potential (**Figure 30**).

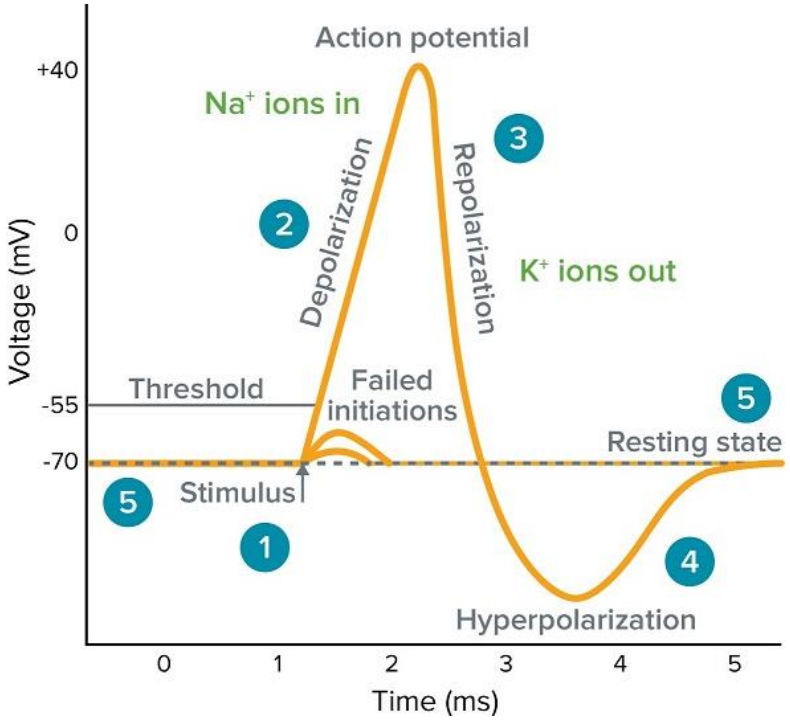

Figure 30: *Schematic of the development of a single action potential, also called spike. The different phases of the action potential are enumerated. Image obtained from the patch clamp section of the Molecular Devices site.*

In most of the neurons the action potential (AP) is initiated at the AIS, where it takes two directions: (i) it backpropagates to the soma and (ii) it is conducted along the axon to reach the next neuron. Why is the AIS a suitable place for AP initiation? Pioneering studies have found the action potential was generated in the proximal axon, suggesting a high accumulation of channels within the AIS (Araki and Otani, 1955; Coombs et al., 1957). Electrophysiological and immunohistochemical approaches confirmed that the levels of Na_v channels with respect to the soma are 30 times higher at the AIS (Kole et al., 2008). Interestingly, measurements of the activity of these channels at the AIS showed that the voltage threshold is lower in the axon than in the soma, facilitating the generation of an AP within this region (Kole and Stuart, 2008). In addition, the position of the AIS close to the soma is a very suitable place to receive the synaptic input from the somatodendritic compartment. (reviewed in Kole and Stuart, 2012). However, some neurons from different brain regions, including the cortex, substantia nigra and the hippocampus, have dendritic-derived AIS whose distance from the soma can go up to 240 µm but still initiate APs (Häusser et al., 1995; Hamada et al., 2016). Finally, the high presence of other channels like potassium (K_v) and calcium (Ca_v) at the AIS contributes to the generation and modulation of the action potential but also to its propagation.

Is it possible to generate action potentials without an AIS? The cerebellum specific AnkG (*Ank3*)$^{exon\ 1b}$ KO used by Zhou and colleagues revealed that neurons had an overall AIS

disassembly and a strong reduction of Na_v channels. Although these neurons were still able to fire action potentials, these were generated at a higher threshold and reached a lower maximum firing rate than the controls, suggesting a reduction in excitability in absence of the AIS. Neurons from the giant AnkG-480 specific cKO (AnkG (*Ank3*) $^{\text{exon 37}}$) used by Jenkins et al. in 2015 were also able to generate action potentials despite the overall loss of neuronal polarity and AIS channels caused by the absence of AnkG-480. These action potentials were, however, abnormal: the AP frequency in the mutant neurons was strongly reduced. These findings were confirmed in *quivering* mice, a spontaneous mutant for ßIV spectrin (*Sptbn4*), which showed a strong decrease of Na_v channels at the AIS (Lazarov et al., 2018). Although neurons from mutant mice were still able to fire action potentials, these had an altered timing and interval as revealed by a stochastic and asynchronous firing. Mutant neurons also displayed a higher threshold for AP firing, suggesting a loss of excitability.

These studies demonstrate that, when present, the AIS is the primary site for AP initiation, but neurons that lack an AIS are still able to elicit APs. The AIS is, therefore, a fine tuner of the spikes, controlling its frequency, timing and precision. Of note, neurons that naturally lack an AIS but still generate action potentials have been identified, like the amacrine cells in the retina or adult-born dopaminergic neurons in the olfactory bulb (Wu et al., 2011; Galliano et al., 2018).

3.2.3 Axo-axonic synapses

The AIS not only contributes to neuronal excitability by initiating and modulating potentials: it is also the site for the formation of axo-axonic GABAergic synapses. The AIS is highly enriched in inhibitory postsynaptic proteins, like α-2 subunit GABA receptors, gephyrin and collybistin (Loup et al., 1998; Panzanelli et al., 2011). Neurons are innervated at their AIS by different interneurons depending on the brain region: stellate and basket cells establish GABAergic synapses —named pinceau— with the AIS of Purkinje neurons in the cerebellum (Blot et al., 2014), while chandelier cells control the excitatory activity of pyramidal neurons in cortex and hippocampus (**Figure 31**) (Szabadics et al., 2006). Defects in these innervations are associated to pathologies where the excitation-inhibition balance is affected, like epilepsy (DeFelipe, 1999) or autism (Rubenstein and Merzenich, 2003).

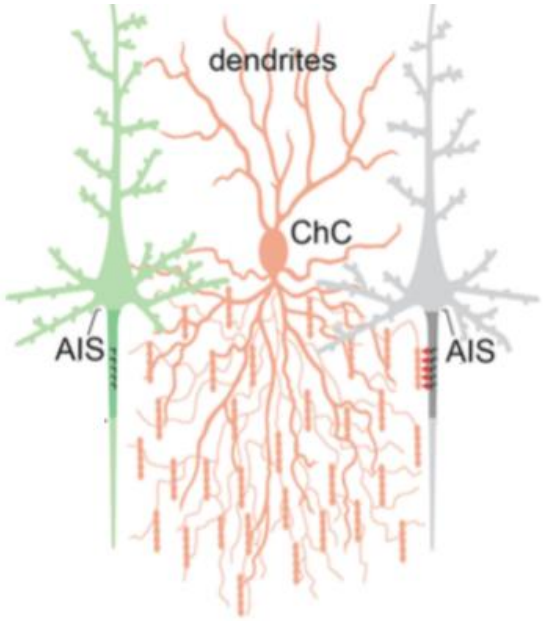

Figure 31: *Schematic representation of a chandelier cell (ChC) innervating a pyramidal neuron through the AIS (cell on the right). Adapted from Tai et al., 2019.*

The team of Juan Burrone has characterized these connections, particularly in chandelier cells that innervate the AIS of pyramidal neurons (Pan-Vazquez et al., 2020). GABAergic neurons are initially excitatory during the early stages of brain development and become inhibitory due to the "GABA switch" (reviewed in Ben-Ari, 2002). Pan-Vazquez and colleagues showed that these chandelier cell-AIS GABAergic contacts follow this switch: indeed, the local application of GABA to the AIS in P12-P28 mice resulted in depolarizing (excitatory) responses, while this same treatment in older animals (P40) promoted a hyperpolarizing response. These synapses are highly plastic: in young adult mice, the increase of activity in the network derived in a boost of inhibitory axo-axonic synapses formation at the AIS, showing that these synapses are ruled by activity dependent plasticity regardless of the excitatory/inhibitory status of the GABAergic neurons.

Molecularly, the formation of axo-axonic GABAergic synapses at the AIS relies on its core molecules. Ango and colleagues found that NF-186 localization at the AIS, which is mediated by AnkG, is necessary for the establishment of these synapses between basket cells and Purkinje neurons (Ango et al., 2004). AnkG (*Ank3*) KO mice exhibited a redistribution of NF-186 and a strong decrease of GAD-67, a GABA synthesis enzyme, in the proximities of the AIS. The use of a dominant negative form of NF-186, which impacts its localization but does not affect AnkG, gave the same results. In the same type of neurons, the deletion of NF-186 in adult mice resulted in a progressive disassembly of the AIS followed by a slow loss of GABAergic synapses. This suggests the presence of other molecules that complement the activity of NF-186 on the maintenance of these synapses (Zonta et al., 2011). The localization

of gephyrin and GABA receptors at the AIS was shown to be dependent on NF-186 in the granule cells of rat hippocampus, confirming a role for neurofascin on preserving GABAergic synapses (Kriebel et al., 2012). Interestingly, the innervation of pyramidal neurons in the cortex is different, as NF-186 is dispensable for their innervation at the AIS by chandelier cells. Instead, these synapses are established and maintained thanks to the axonal protein L1CAM. It is the specific AIS pool of L1CAM, which is linked to and immobilized by AnkG, that establishes and maintains these axo-axonic synapses (Tai et al., 2019).

Although both NF-186 and L1CAM have been linked to the formation and maintenance of these synapses, AnkG is central in this mechanism, as the localization of these CAMs to the AIS ultimately depends on AnkG. The axo-axonic GABAergic synapses at the AIS are the object of active ongoing research: the previously cited studies show the heterogeneity of molecular effectors depending on the brain region and neuron type. Knowledge on how these synapses control the neuron excitability via modulation of the AIS will be key to understand the disorders generated from their dysfunction.

3.3 Structural plasticity and neuronal homeostasis

3.3.1 Activity-dependent plasticity

Despite its strong molecular composition and network, the AIS is a plastic structure that can change both in length and position to regulate neuronal excitability. The plasticity of the AIS occurs in cultured neurons and *in vivo*, but the structural changes are different depending on the neuron type and brain region.

In 2010, Kuba and colleagues found that the AIS of the neurons from the nucleus magnocellularis was longer in auditory deprivation conditions, both during hearing development and in adult animals (Kuba et al., 2010). This increase in length was revealed by AnkG and Na_v channels stainings, which did not show any change in intensity. A higher number of Na_v channels at the AIS was followed by an increased excitability of the neuron, as the action potential thresholds were lower. This change in length of the AIS revealed a role for this subdomain on maintaining neuronal electric homeostasis. In the same year, Grubb and Burrone showed that the AIS is also plastic in cultured neurons: a global depolarization triggered by an experimental increase of extracellular potassium (K^+) promoted a shift of the AIS away from the soma (Grubb and Burrone, 2010). The change in position was reported in all the tested AIS markers, including AnkG, ßIV spectrin and Na_v channels and was correlated with a decrease in neuronal excitability. Interestingly, AIS plasticity is bidirectional, as it goes back to its basal position when neurons were returned to control medium. Another study reported that this shift of the AIS in response to chronic depolarization does not impact the localization of the α2 subunit GABA receptors of the AIS, as they remain in the proximal axon regardless (Muir and Kittler, 2014). Both of these findings were confirmed in hippocampal CA1 neurons in mouse organotypic slices (Wefelmeyer et al., 2015). Chronic activity, achieved

by the induction of an AIS-targeted channelrhodopsin, promoted a shift of the AIS away from the soma and was correlated with a reduction in neuronal excitability. In line with the findings in dissociated neurons, α2-subunit GABA receptors remained in the proximal axon and did not move with the AIS. This is the ideal situation for reducing neuronal excitability, as the AIS is more isolated from the cell body but axo-axonic inhibitory synapses can still be formed. All of these studies have reported plastic changes of the AIS after several days of chronic activity. However, AIS plasticity can also be triggered in a shorter time: 3h of chronic stimulation are enough to promote a shortening of the AIS in cultured neurons and an overall drop in neuronal excitability (Evans et al., 2015).

According to these studies, there is a pattern between AIS changes and electric input: an excess of input seems to be related with a shift or a shortening of the AIS, while the lack of it promotes a lengthening. Further studies have shown that AIS plasticity is more complex and that these structural changes are different depending on neuron type and brain region. In fact, dopaminergic interneurons from the olfactory bulb display an "inverted" type of plasticity: the exposure of these neurons to a chronic activity translated to a shift of the AIS towards the soma and an increase in AIS length (Chand et al., 2015). Although these changes were previously associated with changes in excitability in excitatory neurons, the authors did not detect strong changes in the activity of these cells. They speculated that, in this case, the plasticity is not about controlling excitability but may regulate other AIS functions like the facilitation of molecule transport. Another example of "inverted" plasticity was reported by Galliano and colleagues (Galliano et al., 2021). The authors showed that brief nasal occlusion promoted structural changes in the AIS of axon-bearing dopaminergic neurons in the olfactory bulb: the AIS of these cells was shorter and this correlated with a decrease in intrinsic excitability. Thus, although the shortening of the AIS was followed by a reduced excitability, this change was triggered by stimulus deprivation and not chronic exposure. These different AIS responses may be linked to the neuron type, concretely to the glutamatergic or GABAergic nature of these cells. The AIS may, therefore, regulate intrinsic excitability by displaying cell-specific types of structural plasticity.

Computational studies have predicted the complexity of AIS plasticity by showing differences according to the size and somatodendritic morphology of the neurons: Gulledge and Bravo have reported that, in big and complex neurons, overall excitability is higher when the AIS is longer and/or shifted away from the soma, while smaller neurons achieve higher excitability when the AIS length is intermediate and is located right next to the soma (Gulledge and Bravo, 2016). AIS plasticity triggered by overactivation would, therefore, promote different changes according to the type of neuron and these structural changes will modulate neuronal excitability in a different way. It is important to mention that these results are based on computational simulations and that further studies with additional experimental approaches are needed to confirm these observations at the physiological level.

3.3.2 Plasticity during brain development

The AIS undergoes dynamic structural changes during the development of neurons from different brain structures. These were first shown in the monkey prefrontal cortex, where the AIS shortened during the first six postnatal months and kept the same length afterwards (Cruz et al., 2009). The authors claim that this change may be triggered by other developmental changes, like axonal myelination or an activity-dependent mechanism. In other systems, mainly sensory, AIS plasticity is triggered by developmental-related activity inputs: for example, the AIS of neurons from the visual cortex increases in length during the first postnatal week and progressively gets back to a steady and intermediate size from the fourth postnatal week on (Gutzmann et al., 2014; reviewed in Jamann et al., 2018). This AIS maturation overlaps with the onset of eye opening and vision, which is likely to be the input for these structural changes. In fact, visual deprivation abolished this lengthening and the AIS remained the same size within the different postnatal weeks.

The AIS from neurons in the nucleus laminaris, an auditory brainstem structure, changes in length and position during development: before hearing onset, the AIS is widely located within the proximal axon (Kuba et al., 2014). After hearing onset, the AIS shortened and relocated distally. Ablation of inner ears and the subsequent abolishment of input prevented the shortening of the AIS, which was still located distally, showing that this developmental plasticity is regulated via activity dependent and independent mechanisms. These changes of the AIS have been suggested to be necessary for the spontaneous activity of auditory neurons. The AIS profile within development can also vary within different types of neurons from the same system: high frequency (HF) and low frequency (LF) neurons of the medial nucleus of the trapezoid body (MTNB) from the mouse auditory brainstem are a good example (Kim et al., 2019). Before hearing onset, the AIS of both types of neurons is located close to the soma, but as soon as hearing developed, the AIS of HF neurons got shorter and located distally. No changes in length for AIS of LF neurons were reported, which maintained this size throughout adulthood. After these structural changes, the AIS of HF neurons reached a fixed size in adulthood that was kept throughout life. Interestingly, these plastic changes were altered when sound modifications were applied during early postnatal development, showing an activity dependent developmental mechanism. An adequate degree of plasticity during development is related with correct firing pattern and excitability of these neurons. A recent work has discovered that the AIS of layers II/III and IV of the somatosensory cortex also undergo developmental plasticity triggered by the onset of sensory activity in the whiskers. In the same way than the previous reports on sensory systems, sensory deprivation (based on whisker trimming to reduce the touch input) impacts AIS morphology during development but also once it is established in adulthood, resulting in impaired excitability (Jamann et al., 2021). These studies show that the AIS is plastic during development, particularly within brain sensory regions and that these changes are activity dependent. Disruption of any of these events will lead to an abnormal AIS distribution and defects in neuronal excitability.

Finally, the AIS remains a highly plastic structure even during aging, adapting neuronal excitability upon different triggers. In aged rats and monkeys, the AIS from cortical neurons show a shorter size than those of younger animals. This structural change results in decreased neuronal excitability. Although the causes behind this shortening are not clear yet, it could be a compensatory mechanism to the progressive loss of GABAergic neurons in the aging cortex and a consequent hyperexcitability (Atapour and Rosa, 2017; Ding et al., 2018).

3.4 AIS and pathology

3.4.1 AIS molecules in disease

Genome-wide association studies (GWAS) have identified mutations in genes encoding AIS proteins in patients from different diseases. For example, polymorphisms near the 5' noncoding region of *ANK3*, the human AnkG-encoding gene, were found in patients of bipolar disorder and schizophrenia (Smith et al., 2009; Gella et al., 2011, Guo et al., 2016). Rueckert and colleagues unveiled a possible molecular mechanism behind an *ANK3* SNP found in patients of bipolar disorder and the onset of the disease (Rueckert et al., 2013). First, the authors described the expression profile in the human brain of different AnkG isoforms derived from the alternative splicing of concrete exons. As described previously (see *3.1.1 Ankyrin-G: the master organizer*), transcripts for the exon 1b were mostly expressed in the cerebellum, while the exon 1e was found in the frontal and cingulate cortex. The SNP found in bipolar disorder was predicted to affect the 5' part of the *ANK3* gene, as it overlaps with the exons 1b and 1e. Tissue from patients carrying this SNP revealed a significant decrease of the exon 1b expression in the cerebellum, suggesting a lower activity for the promoter of this specific isoform in this pathology.

Interestingly, one of the *ANK3* variants associated with bipolar disorder was found in patients with altered sustained attention, one of the symptoms of autism spectrum disorders (Hatzimanolis et al., 2012). Iqbal and colleagues identified a frameshift mutation on *ANK3*, predicted to affect specifically the expression of AnkG 480/270, the AIS AnkGs, in patients with severe intellectual disability and epilepsy. This important result suggests that the AIS is contributing to the development of the pathological phenotype (Iqbal et al., 2013). The study further claims that AnkG could be common to several psychiatric disorders that were previously unrelated and/or limited to synaptopathies.

The link between ßIV spectrin and human pathology is more limited. A study from 2017 detected a single patient with several neurological conditions (congenital myopathy, neuropathy and central deafness) who presented a recessive mutation in the *SPTBN4* gene (Knierim et al., 2017). One year later, Wang and colleagues described six individuals with similar neurological conditions and identified seven new ßIV spectrin, which were predicted to affect either the ε1 isoform exclusively or both ε1 and ε6 (Wang et al., 2018). Interestingly, the vast majority of the proteins coded by the ε1-affecting variants failed to cluster at the AIS

when overexpressed in neurons and lost their interaction with AnkG. These variants therefore led to a loss of function phenotype. The authors further analyzed the structure of the nodes of Ranvier by using nerve biopsies from 2 different individuals: one of them carrying two of the variants that were correctly targeted to the AIS and another one who had a loss of function-causing variant. The loss-of-function variant triggered a decrease of nodal markers like NF-186 and sodium/potassium voltage-gated channels. This structural defect could be the basis of a dysfunctional action potential propagation that could explain the neurological symptoms of the patients. Although AIS defects were not directly addressed in these patients, it cannot be excluded that it is affected in light of the results of the variant overexpression in neurons.

Mutations in Na_v channel genes are found in patients suffering from different forms of epilepsy. For example, loss of $Na_v1.1$, which is specifically enriched at the AIS of GABAergic neurons (see *3.1.5 Voltage-gated channels*), is associated with early forms of epilepsy like Dravet syndrome or severe myoclonic epilepsy (Oakley et al., 2011). A point mutation in $Na_v1.2$ was also found in patients of Dravet syndrome (Shi et al., 2009). Interestingly, mutations of Na_v genes are also present in patients with autism spectrum disorder, both inherited and *de novo* (Weiss et al., 2003; O'Roak et al., 2011). In fact, from 5 to 46% of people with ASD do experience seizures, suggesting common molecular roots for both diseases (Jeste, 2011; Amiet et al., 2008; Fassio et al., 2011; Spence and Schneider, 2009). Potassium channels (K_v) at the AIS are also involved in epilepsy: the genetic loci for *KCNQ2* and *KCNQ3* ($K_v7.2$ and $K_v7.3$, respectively) are considered risk regions for the development of neonatal seizures (Leppert et al., 1989). It is important to mention that the expression of some of these voltage-gated channels is not restricted to the AIS, so the pathological phenotype may arise from a combination of a dysfunction of the channels at the AIS and at the rest of the neuron.

These examples illustrate the role of some AIS molecules in pathology. However, these studies are based on a correlation mutation-patient and do not reveal the molecular origins of the protein dysfunction and disease. In addition, most of these proteins are found at other neuronal compartments and it is essential to identify how the AIS is contributing to the pathology. This is why we need animal models based on AIS proteins dysfunction, which I explain in the following point.

3.4.2 Behavioral and pathological features in AIS-related mouse models

The use of animal models is a classical practice to understand the molecular processes behind physiological conditions and disease, and the AIS is no exception. Mouse models lacking the core AIS molecules recapitulate totally or partially the phenotype found in the patients carrying mutations for those genes.

It is not possible to discuss "an" AnkG mutant, as many of them were generated, focusing either on the different AnkG isoforms and a specific location and/or timing for their deletion.

The consequences of these studies are a number of animal models, with varying phenotypes. According to the studies presented in the previous section (*3.4.1 AIS molecules in disease*), AnkG dysfunction may be involved in bipolar disorder. Leussis and colleagues used two different approaches to investigate the relationship between AnkG and bipolar disorder (Leussis et al., 2013): RNA interference of *Ank3* in the dentate gyrus of the mouse hippocampus (a region involved in bipolar disorder) and the analysis of heterozygous KO mice for AnkG (*Ank3*). The two RNA interferences that were used were targeted to the exons 19 (corresponding to the Ankyrin repeats domain) and 28 (corresponding to the spectrin binding domain), respectively. This means that all the possible C-ter isoforms of AnkG (480, 270 and 190 kDa) are downregulated. The AnkG (*Ank3*) KO is the same than Zhou and colleagues used in 1988, which targets the exon 1b (AnkG (*Ank3*)^{exon1b} KO), see *3.1.1 Ankyrin-G: the master organizer*): this means that it affects all the C-ter isoforms of AnkG, but it restricts the effect to the 1b N-ter isoform, which is mostly expressed in the cerebellum but also present in the cortex. The animals injected with AnkG shRNA displayed a reduced anxiety-related behavior and showed a quick entry in aversive environments. Interestingly, the increase of risk taking is one of the features of bipolar disorder patients in manic phase. The treatment of these animals with lithium, a commonly used drug for bipolar disorder, reversed this behavior. The authors only analyzed the AnkG (*Ank3*)$^{exon\ 1b}$ +/- mutants, as the homozygous animals show early-onset ataxia that interferes with their locomotion. The mutant mice had lower levels of AnkG at the AIS in the hippocampus and cortex and followed the same type of behavior than the shRNA-injected animals. They also displayed higher motivation to obtain a reward, also a feature of bipolar disorder mania. This study suggests a protective role for AnkG at the AIS against bipolar disorder. As AnkG is present also in the spines, it would of interest to analyze potential disruptions at this structure after shRNA injection and in the mutants, as it could contribute to the phenotype besides the AIS.

Another animal model, this time based on a deletion of AnkG in the forebrain of adult mice, also displays features of bipolar disorder (Zhu et al., 2017). This AnkG (*Ank3*) cKO targeted the exons 22 and 23 and therefore all the isoforms. The gene was deleted in pyramidal neurons of the cortex starting during adolescence thanks to a CAMKII-driven Cre (AnkG (*Ank3*)$^{22\text{-}23}$ cKO, CAMKII-Cre). Loss of AnkG was reported at the AIS of most of the neurons in the cortex and the 3 isoforms levels were overall decreased in blots, including the 190 kDa that is present at the spines. Like in the previous study, AnkG mutants displayed decreased anxiety, increased exploratory activity and less predisposition to depressive-like behavior, all of them features of manic-like conducts in bipolar disorder patients. These behaviors were reversed by applying classic treatments for the disorder like VTA or lithium. In addition, these animals were hyperactive and a c-fos staining revealed an increase of neuronal activity. The authors hypothesized that this switch in neuronal activity is probably due to changes in the AIS composition, most likely on the formation of axo-axonic inhibitory synapses: the decrease at the AIS of GABA Transporter-1 (GAT-1) reveals a potential loss of inhibitory synapse formation that would explain the hyperactive profile. Interestingly, the decrease of inhibitory connections is seen as well in bipolar disorder (Guidotti et al., 2000).

This hyperactivity could also be related with the deficit of AnkG at the spines, as it is known to regulate AMPA receptors in synapses (Smith et al., 2014).

In 2017, van der Werf and colleagues performed a behavioral-detailed characterization of an AnkG deficient mice (van der Werf et al., 2017). This specific knockout was targeted to the exon 37, meaning that it was deleting only the giant AnkG 480/270 isoforms. The deletion of the gene was achieved using a mouse expressing Cre recombinase under the Nestin promoter, which targets neuronal precursors in all the brain areas except the dentate gyrus, optical nerve and spinal cord. This same strategy was used by Jenkins and colleagues to study AnkG giant defects *in vivo* (AnkG (*Ank3*)^{exon37}, Nestin-Cre cKO, see 3*.1.1 Ankyrin-G: the master organizer*). Contrary to what the previous studies reported, these mice displayed an increased anxiety-like behavior. The authors hypothesized that this striking phenotype may be the result of a fine regulation of anxiety behavior by AnkG 190, which is not abolished in these animals but is absent in the previously described AnkG mutants. Besides, the mutants performed well in the rest of the tests including memory and learning tests and showed mild anatomical alterations in hippocampus and cortex. In conclusion, this study and the previous ones demonstrate that AnkG isoforms are required for a healthy brain and show different roles/balances for the different isoforms on regulating anxiety-related brain circuits. Importantly, these articles reveal different behavioral outcomes depending on which AnkG isoforms are deleted and in which brain region, showing a high functional specialization for this molecule.

Another interesting mouse model for AnkG was developed by Lopez and colleagues in 2017 to study the contribution of the different N-ter isoforms of AnkG to disease (Lopez et al., 2017; see more details at *3.1.1 Ankyrin-G: the master organizer*). The authors used an AnkG (*Ank3*)^{exon1b} KO, as the resulting NT3 isoform is present mostly in parvalbumin (PV) interneurons of the cortex and those have been shown to be affected in bipolar disorder. The AIS of PV neurons displayed an important decrease of sodium channels followed by action potential defects and a reduced excitability, which could explain the seizures phenotype. Seizures are more severe in in the homozygote mutant mice, suggesting a gene-dosage related severity. Heterozygous mice for this isoform were previously reported to display bipolar disorder-related behaviors (Leussis et al., 2013), so this study shows that AnkG NT3 dysfunctions could molecularly connect epilepsy and bipolar disorders.

Regarding ßIV spectrin, the most known mutant is the *quivering* mouse, which carries a spontaneous loss of function mutation of *Sptbn4* (Parkinson et al., 2001). These mice display progressive ataxia, tremors, hindlimb paralysis and deafness, phenotypes that partially match those found in individuals carrying mutations for *SPTBN4* (see *3.4.1 AIS molecules in disease*). At the AIS level, the mutants display a decrease of AnkG and Na_v channels, but those still preserve their periodic localization likely because of the presence of ßII spectrin at the AIS in these animals (Lazarov et al., 2018). Although these neurons are able to generate action potentials, those are asynchronous and their threshold is higher compared to the controls, revealing an altered excitability. This defect at the AIS is likely contributing to the pathological

phenotype of these mice. Although the authors do not explore the possible impact of the nodes of Ranvier in this model, the literature shows that other ßIV spectrin mutants have defects at these structures: the deletion of the ε1 isoform of ßIV spectrin promotes an increase in diameter of the nodes of Ranvier (Lacas-Gervais et al., 2004). As these domains are crucial for axonal conduction, it is conceivable that the observed defects are contributing to the pathological phenotype.

Given the crucial role of voltage-gated ion channels on neuronal excitability, it is not surprising that most of the epileptic mouse models arise from mutations in the genes encoding these proteins (reviewed in Baraban, 2007). For example, a knock-in mouse carrying a *Scn8a* mutation found in epileptic patients displays seizures, ataxia and sudden death (Lopez-Santiago et al., 2017). *Scn8a* is the gene encoding $Na_v1.6$, one of the sodium channels enriched at the AIS (see *3.1.5 Voltage-gated ion channels*). The neurons of this mutant displayed hyperexcitability and revealed $Na_v1.6$ as a molecular link with epilepsy. Mice carrying mutations for *Scn1a* ($Na_v1.1$) recapitulate the clinical features of patients with Dravet syndrome: reduced threshold for heat-induced seizures, cognitive impairment, motor problems and hyperactivity (Ricobaraza et al., 2019). Ogiwara and colleagues reported that both heterozygous KO mice for *Scn2a* ($Na_v1.2$) and knock-in mice *Scn2a* with a mutation found in epileptic patients exhibit lower threshold for induced seizures (Ogiwara et al., 2018). The specific deletion of $Na_v1.2$ in excitatory neurons of the cortex and hippocampus promoted an even more severe phenotype, suggesting that the specific role of $Na_v1.2$ in these neurons is key for their correct function and excitability. Interestingly, different studies reported that mouse models for $Na_v1.2$ recapitulate autistic-like behaviors, showing a potential dual contribution of this channel to pathology (Léna and Mantegazza, 2019; Eaton et al., 2020, preprinted). As commented previously, a number of patients suffering ASD do have more predisposition for seizures, suggesting a common molecular root for both disorders. Finally, mice carrying mutations found in *Kcnq2* and *Kcnq3* genes of epileptic patients (encoding $K_v7.2$ and $K_v7.3$ channels, respectively) displayed both spontaneous seizures and a decreased threshold for induced seizure development (Singh et al., 2008).

Altogether, these studies show the high relevance of the main AIS molecules for normal neuron and brain function, as mutations or genetic depletions in animal models recapitulate the pathological phenotypes found in patients from different disorders. Although some of these studies suggest a link between AIS and pathology, further work is needed to determine how the AIS is specifically contributing to these diseases, as most of these molecules are present in other parts of the neuron, like the nodes of Ranvier or the dendritic spines.

Chapter II: Materials and methods

Rats and transgenic mice

All procedures involving animals were done in accordance with the European Communities Council Directives (2010/63/EU) and the French National Committee (2013-118) recommendations. Animals had free access to food and water and were housed in polypropylene cages under controlled conditions (at 23°C ± 1°C, with lights on from 7:00 a.m. to 7:00 p.m., assuring a 12:12 hr light/dark cycle). Sprague-Dawley rats were purchased from Janvier and used between embryonic day 16 (E16) and 10 weeks old at the time of the experiments. Scrib floxed mice were described before (Hilal et al., 2017), and for Pk2 floxed mice ES cells clones were obtained from EUCOMM/IPMC and the mice generated by CIPHE, Marseille.

Single or double conditional mutants (cKO) were generated by crossing Nex^{Cre} mice with floxed mice: Nex^{Cre} $Pk2^{f/f}$-$Scrib^{f/f}$ (hereby referred to as Pk2-$Scrib^{Nex}$ cKOs). Nex^{Cre} mice were obtained from Klaus-Armin Nave (Max Plank Institute, Germany). $Emx1^{cre}$ mice were purchased from Jax Lab (B6.129S2-Emx1tm1(cre)Krj/J, stock No: 005628) and crossed with *Pk2* and *Scrib* floxed mice to generate the $Pk2^{Emx1}$ and the $Scrib^{Emx1}$ lines.

For the *Pk2* gene trap line, we generated a mouse harboring a *Pk2* tm1a allele in which a LacZ cassette is inserted upstream the critical exon 2 leading to a loss of function. The *Pk2* tm1a allele expresses β-galactosidase under to the endogenous promoter of *Pk2* gene. Subsequent Flp-mediated recombination of the *Pk2* tm1a allele resulted in a *Pk2* tm1c allele that can undergo Cre-mediated deletion of exon 2.

Genotyping and gene excision for all the mice were performed by the genotyping facility of the Neurocentre Magendie.

Antibodies

The following antibodies were used in this study: rabbit polyclonal anti-Pk2 (gift from Doris Wu, NIH, USA; Jiang et al., 2017), rabbit polyclonal anti-Scrib (homemade Ab MM468, Montcouquiol et al., 2006). Mouse monoclonal anti-AnkyrinG, mouse monoclonal anti-βIV spectrin, mouse monoclonal anti-pan Neurofascin mouse (all of them from Neuromab), monoclonal anti-pan Na_v (Sigma), rabbit polyclonal anti-AnkyrinG, guinea pig monoclonal anti-AnkyrinG (Synaptic Systems), mouse monoclonal anti-GAPDH (Millipore), mouse monoclonal anti-Tau (Covance), chicken polyclonal anti-MAP2 (EnCor Biotech), mouse monoclonal anti-βII spectrin (BD Biosciences), chicken polyclonal anti-GFP (Abcam), mouse monoclonal anti-GFP (Roche), mouse monoclonal anti-Flag (Sigma), rabbit polyclonal anti-GFP (Millipore), mouse monoclonal anti-Flag (Sigma), rabbit polyclonal anti-HA (Sigma) and mouse monoclonal anti-myc (Covance). For some of the western blots, custom-made serum rabbit polyclonal anti-Pk2 was used. Rabbit polyclonal anti-AnkG-480 was a gift from Dr. Paul Jenkins

(University of Michigan, USA) and rabbit polyclonal anti-βIV spectrin was kindly provided by Pr. Matthew Rasband (Baylor College of Medicine, Houston, USA).

Alexa fluor secondary antibodies were purchased from Jackson Immunoresearch and Invitrogen. For STORM imaging, actin was detected using phalloidin 647 from Thermo Fisher Scientific. For western blot, secondary antibodies goat anti-mouse or anti-rabbit coupled to the horse radish peroxidase (HRP, from Jackson Immunoresearch), donkey anti-guinea pig HRP (Jackson Immunoresearch) and mouse-anti Rabbit HRP (GE Healthcare UK) were used.

cDNA constructs

The shPk2 (Nagaoka et al., 2014), the shScrib (Moreau et al., 2010) and the shAnkG (Leterrier et al., 2017) were cloned into a pSuper vector (Oligoengine). AnkG-270 kDa and AnkG-190 kDa constructs tagged with GFP were kindly provided by Pr. Vann Bennett (Duke University, USA) (Zhang and Bennett, 1998). AnkG-480-GFP was obtained from Pr. Casper Hoogenraad (Utrecht University, Netherlands) (Fréal et al., 2016). Mouse myc-ßIV spectrin was obtained from Pr. Matthew Rasband (Baylor College of Medicine, USA) (Wang et al., 2008). The HA-Scrib construct was provided by Pr. Jean Paul Borg (Centre de Recherche en Cancérologie, Marseille).

The plasmid for the human Pk2 cDNA tagged with three flag sequences in N-terminal was purchased on Addgene (#24645). GST-Pk2 constructs were obtained by cloning different human Pk2 domains using PCR and inserted into the pGEX-4T-1 (GE) to create in-frame fusions with the GST sequence. GST-tagged hPk2 (1-323) containing PET and LIM domains, GST-hPk2 (323-844) containing the C-ter half of the protein, GST-hPk2 (127-844) containing the LIM domains and the C-ter half of the protein, GST-hPk2 (1-129) containing the PET domain, GST-hPk2 (127-323) containing the LIM domains, GST-hPk2 (323-585) containing the first half of the C-ter half of the protein, GST-hPk2 (585-844) containing the second half of the C-ter half of the protein including the C2 domain (Butler & Wallingford 2015). See Moreau et al., 2010 for information about the GST-Scrib constructs. Briefly, we generated GST-tagged Scrib 4 PDZ containing all PDZ domains and GST-tagged Scrib C-ter containing the C-ter end of Scrib, past the PDZ domains.

Histology

For cresyl violet Nissl staining, mice were perfused transcardially with phosphate buffer (PB) followed by 4% paraformaldehyde (PFA) diluted in PB. Brains were removed and post-fixed in 4% PFA in PB for minimum 48h at 4°C. Coronal vibratome sections (50 µm, VT1000S vibratome from Leica) were mounted on gelatin coated slides and air dried at room temperature for at least 12 hours. Slides were then immersed in 1:1 ethanol-chloroform solution for 12 hours before rehydration in descending series of ethanol solutions. Sections were treated with 1%

cresyl violet solution for 2 minutes followed by differentiation in 95% ethanol for 2 minutes. Sections were dehydrated in 100% ethanol and mounted using Eukitt mounting medium.

For X-gal treatment, mice were perfused as mentioned above. Brains were removed, postfixed in 4% PFA in PB for 6h at 4°C and immersed in PB-4°C for at least 18 more hours. Coronal vibratome sections (40 µm, VT1000S vibratome from Leica) were collected and incubated in X-gal wash buffer (2 mM MgCl 2, 0.01% sodium deoxycholate, 0.02% Nonidet P-40 in 0.1M sodium phosphate buffer) for 15 minutes. X-gal (5- bromo-4-chloro-3-indolyl-/3-D-galactopyranoside, from Sigma) was prepared as a stock solution of 20 mg/ml in dimethyl formamide. Sections were incubated at 37°C for 8-12 h in a final reaction mixture containing 1 mg/ml X-gal, 5 mM potassium ferrocyanide, 5 mM potassium ferricyanide in X-gal wash buffer. After coloration, slices were rinsed in PB, mounted on gelatin coated slides and air dried at RT for at least 12 hours. Sections were mounted using Eukitt mounting medium.

Slices from both experiments were scanned using an Hamatsu NANOZOOMER 2.0 HT at the Bordeaux Imaging Center. For X-gal staining, 3 *Pk2* gene trap mice at P20 were processed. For Nissl cresyl violet staining, 5 cre- and 5 cre+ mice at P21 were used from the Pk2-Scrib^{Nex} line.

Immunohistochemistry

Animals were perfused transcardially with phosphate buffer (PB) followed by 4% paraformaldehyde (PFA) in PB, brains were removed and postfixed in 4% PFA for 2 hr at 4°C. 40-50 µm-coronal vibratome sections (VT1000S vibratome from Leica) were permeabilized with 0.3% Triton X-100 in PBS for 1h at room temperature (RT) and blocked with 5% bovine serum albumin (BSA) 5% normal goat serum (NGS) - PBS for 2h at RT. Primary antibodies were incubated overnight at 4°C. Alexa fluor secondary antibodies (Jackson Immunoresearch) were diluted in PBS or 2% NGS-PBS and incubated for 1h at RT. Slices were mounted using ProLong Gold antifade medium (Life Technologies) or Fluoromont-G (Electron Microscopy Sciences). For pan-Na_v staining in mice, animals were anesthetized with 4% isofluorane and sacrificed quickly via decapitation. The brain was removed and placed in CO_2 saturated, ice cold cutting solution (NaCl 125 mM, $NaHCO_3$ 25 mM, NaH_2PO_4 1.25 mM, KCl 3 mM, Glucose 25 mM, $CaCl_2$ 1 mM, $MgCl_2$ 6 mM) and cut in 300 µm slices using a vibratome VT1200S from Leica. Slices were fixed with 1% PFA for 30 minutes at RT, washed with PBS and permeabilized and blocked with 5% BSA 0.3% Triton X-100 for 1h at RT. Pan-Na_v antibody was incubated in blocking solution for 48h at 4°C. Secondary antibodies were incubated in PBS for 2h at RT. After washes, slices were post-fixed for 10 min with 4% PFA and mounted with ProLong Gold antifade medium (Life Technologies). Rat and mouse brains electroporated *in utero* were dissected at P6 and P3, respectively, and immersed on 4% PFA overnight at 4°C, followed by 24-48h of incubation with 30% sucrose PBS at 4°C. Brains were sliced on coronal 50 µm sections using a vibratome (VT1000S, Leica) and processed for immunohistochemistry.

For mutant mice, a total of 11 cre- and 12 cre+ were used for immunohistochemistry. For *in utero* electroporation, 2 pregnant rats were used for surgery and between 2 and 6 electroporated pups per rat processed for immunostaining. At least 2 mice were used for surgery and between 3 and 5 electroporated pups per mouse processed for immunostaining.

Neuronal cell culture, neuron transfection and immunofluorescence

Sprague-Dawley rats at E18.5 were used for cultures of hippocampal neurons. Hippocampi were harvested together in a Hank's Balanced Salt Solution (HBSS), enzymatically and mechanically dissociated. After 13 min incubation at 37°C in trypsin, hippocampi were rinsed with a Plating Medium (PM) that contains neurobasal medium (Gibco), B27 supplement (50X, Gibco) and 1% of Fetal Bovine Serum (FBS, Gibco). Mechanical dissociation of the hippocampi was achieved through gentle up and down movements with a Pasteur pipette, and then centrifuged at 1 rpm for 8 min at room temperature (RT) after counting. Neurons were further diluted in a suitable volume of PM according to the density and plated on the previously prepared coverslips. Four hours after plating, the PM was replaced by conditioned medium obtained from astrocytes cultures. Neurons were kept in a humidified incubator, at 37°C and with 5% CO_2. All the experiments used either 15mm or 18mm coverslips coated with poly-L-lysine (PLL) and laminin: coverslips were incubated for 2h at 37°C with 30 μg/ml PLL in borax buffer, rinsed with H_2O, then incubated overnight at 4°C with 2μg/ml of laminin diluted in PBS.

Neurons were transfected before plating using Amaxa Rat Neuron Nucleofector kit (Lonza), following the manufacturer's instructions. Calcium phosphate was also used for transfection on late cultures to assess the role of Pk2 in AIS maintenance (Moreau et al., 2010). For immunocytochemistry, neurons were fixed and stained at defined timepoints for 10 min with 4% sucrose 4% PFA at RT. Neurons were then permeabilized and blocked with 5% BSA 0.3% Triton X-100 in PBS for 1h at RT, followed by primary antibodies incubation for 1h at RT. After rinsing, Alexa fluor secondary antibodies (Jackson Immunoresearch) were incubated for 30 min at RT and coverslips were mounted using ProLong Gold antifade medium (Life Technologies). For STORM experiments, neurons were postfixed after rinsing the secondaries with 4% sucrose 4% PFA for 10 min at RT, followed by three quick rinses in PBS.

A minimum of 3 different cultures were used per experiment.

Image acquisition, processing and quantification

Slides were imaged using a Zeiss AxioImager Z1 (63x / 1.40 NA oil objective) equipped with an AxioCam MRm and the Zen software (Zeiss) and a LED light source Colibri 7 from Zeiss (wavelengths: UV 385/30 nm, V 423/44 nm, B 469/38 nm, C 511/44 nm, G 555/30 nm, Y 590/27 nm, R 631/33 nm). For some of the neuron (DIV1-3) and tissue acquisitions, a

confocal/STED microscope (TCS SP8; Leica) with a module STED × 3 was used. For brains from rat *in utero* electroporation, imaging was done using a Z step from 0.25 to 0.35 µm.

For neuron analysis, Z-stacks were collected per cell (5 stacks with a total depth of 1 µm) with sequential wavelength acquisition. Stacks were processed into maximum intensity projections and quantifications of intensity along the AIS were performed using ImageJ (https://imagej.nih.gov/ij/) with a specialized AIS macro designed by Fabrice Cordelières (Bordeaux Imaging Center). Details on each type of quantification are specified in the figure legends. For mutant mice, acquisitions were taken using the Zeiss Axioimager Z1 (63x / 1.40 NA oil objective) plus an Apotome. For AnkG-480, 49 stacks with a total depth of 12.74 µm were taken per region, 40 stacks with a total depth of 10.4 µm were taken per region for pan-AnkG, 49 stacks with a total depth of 12.74 µm were taken per region for ßIV spectrin and 41 stacks with a total depth of 10.66 µm were taken per region for pan-Na_v. Images were processed into maximum intensity projections and quantification of the mean fluorescence intensity per AIS was done using individual measurements in ImageJ. The thickness of the segmented line to measure the AIS intensity was determined following a published protocol (Di Re et al., 2019). Image editing was performed using ImageJ or Photoshop 7.0 (Adobe). Most of the figures were done using the ImageJ plugin "FigureJ" (Mutterer and Zinck, 2013).

In utero electroporations

E16 Sprague-Dawley embryos were injected and electroporated *in utero*. Timed-pregnant E16 females were anesthetized with isoflurane after pre-operative dose of buprenorphine (0.05 mg/kg), 15 min before surgery. The abdomen was cut and the uterine horn exposed. 1 µl of DNA (0.5 µg/µl) prepared in endo-free water mixed with 1% Fast-Green dye (Sigma-Aldrich) was injected through the uterine wall into the lateral ventricle of each embryo using pulled glass capillaries (Harvard Apparatus). Capillaries were prepared using a needle pipette puller (PC-100, Narishige) and injection performed with a Femtojet injector (Eppendorf). For electroporation, five 50 milisecond (ms) pulses at 55 V with 950-ms breaks were delivered through the embryonic brain to target the Cortex using 7-mm electrode paddles connected to a BTX ECM830 electroporator (Harvard Apparatus). After the procedure, the abdomen was filled with a 37°C-warmed PBS solution and the wound was closed using surgical suture. Animals were put back in their home cage in the animal facility. Rats gave birth at E22.5 and the pups were kept with their mother until collection at P6.

For mice, CD1-Swiss embryos were injected and electroporated at E14.5. The surgical procedures were similar to those in rat, adjusting the corresponding dosages of analgesics and anasthetics to the size of the animal. 1 µl of DNA (2 µg/µl) in endo-free water mixed with 1% Fast-Green dye (Sigma-Aldrich) was injected through the uterine wall into the lateral ventricle of each embryo using pulled glass capillaries (Harvard Apparatus). Capillaries were prepared using a needle pipette puller (PC-100, Narishige) and injection performed with a

Femtojet injector (Eppendorf). For electroporation, five 50 milisecond (ms) pulses at 30 V with 950-ms breaks were delivered through the embryonic brain to target the cortex using 5-mm electrode paddles connected to a BTX ECM830 electroporator (Harvard Apparatus). Mice gave birth at E18.5 and the pups were kept with their mother until collection at P3.

STORM imaging

STORM acquisitions were performed at the Bordeaux Imaging Center. 18-mm coverslips were incubated with fluorescent beads (Invitrogen) for 5 min at room temperature, washed thrice with PBS and then placed in a Ludin chamber. STORM media consisted of Tris 50 mM pH 8, NaCl 10 mM, 10% glucose, 100 mM MEA, 3.5 U/mL pyranose oxidase and 40 µg/mL catalase**.** The STORM microscope was a Nikon Ti Eclipse (Nikon France S.A.S., Champigny-sur-Marne, France) equipped with a Perfect Focus System (PFS), a motorized stage TI-S-ER, and an azimuthal Ilas² TIRF arm (Gataca Systems, Massy, France) coupled to a laser bench containing 405 nm (100mW), 491 nm (150mW), 532 nm (1W), 561 nm (200mW) and 642 nm (1W) diodes. Images were acquired using objective Apo TIRF 100 X oil NA 1.49 and a sensitive Evolve EMCCD camera (Photometrics, Tucson, USA). Laser 642 nm at 1000 mW was used for single 647 channel acquisitions, and between 50000 and 100000 frames were taken per neuron. Between 3 and 5 cells were imaged for endogenous Pk2 and Scrib acquisitions and 5 cells for control and 6 cells for shPk2-transfected neurons were imaged for actin. PalmTracer software was used for image treatment and reconstruction (developed by Jean Baptiste Sibarita team at the Interdisciplinary Institute of Neurosciences, Bordeaux).

Western Blot and immunoblot

For mutant mice analysis, cortex from P12 (2 batches of animals: batch 1# having 5 Cre- and 5 Cre+, batch #2 having 4 Cre- and 5 Cre+) and P21 mice (2 batches of animals: batch #1 having 2 Cre- and 2 Cre+, batch #2 having 3 Cre- and 3 Cre+) were dissected, pooled and weighted. A volume of a solution containing 10 mM PB (pH 7.4) 0.32 M sucrose, 1 mM EDTA, 1 mM NaN_3 and protease inhibitors (Roche) was added to the tissues according to their weight. Samples were then homogenized with a polytron (Kinematica PT1200) and sonicated and protein concentration was evaluated twice using BCA analysis (BCA protein Assay Kit from Thermo Scientific). Protein concentration was adjusted for each sample and diluted with 4x SDS loading buffer containing 10% β-mercaptoethanol or 5x SDS loading buffer containing 12.5% β-mercaptoethanol (Zhu et al., 2017). Considering the different molecular weights, proteins were loaded on 10%, 8% or 7% acrylamide gels and ran at 120V between 1h30 and 2h in running buffer (25 mM Tris, 192 mM glycine, pH 8.3 – Biorad). Proteins were then transferred to Immobilion-P polyvinylidene fluoride membranes (Millipore) overnight at 30V or for 2h30 at 60V in transfer buffer (25 mM Tris, 192 mM glycine, pH 8.3 – Biorad) supplemented with

20% methanol or 10% methanol + 0.01% SDS. The membranes were blocked with a 0.05% Tween-TBS (25mM Tris, pH7.5 + 137mM NaCl + KCl 3mM + MilliQ water up to 2L) solution containing 5% non-fat milk for 1h at RT. Primary antibodies were incubated for 1h at RT and extensively washed. Secondary antibodies, coupled to the horse rash peroxidase (HRP), were then incubated for 1h at RT. Membranes were exposed to chemiluminescence kits with different sensitivities (ECL, Thermo Scientific and Bio-Rad) and protein detection was done on Amersham Hyperfilm ECL (GE Healthcare) films with developer and fixer solutions (Carestream Kodak autoradiography GBX). The optic density (OD)*mm^2 was analyzed for each detected band. Quantifications of band intensities were done using the Quantity One software (Bio-Rad).

Cell culture, transfection and COS-7 immunofluorescence

Human embryonic kidney 293 containing the SV40 large T-antigen (HEK293T, from ATCC CRL-11268-G1TM) and COS-7 (ATCC-American Type Culture Collection) were cultured with advanced Dublecco's modified Eagle's medium (DMEM, Gibco) supplemented with 10% fetal bovine serum (FBS, Gibco), 1% L-glutamine 200 mM (Gibco) and 1% penicillin-streptomycin (10000 U/ml, Gibco). Cell cultures were grown in a humidified incubator at 37°C with 5% CO2. Subculture procedure was done following the indications of the distributor. For transfecting HEK293T, cells were plated onto 10 cm dishes in complete DMEM at a suitable dilution to reach 30-40% confluence before transfection. Transfection was performed with polyethylenimine (PEI, linear, Polysciences Inc. 1 mg/ml) with a ratio of 2.5 µl:1 µg cDNA for 16 µg of AnkG cDNA, of 3.5 µl: 1 µg cDNA for 4 µg of Pk2 cDNA, of 3 µl:1 µg cDNA for 5 µg of ßIV spectrin cDNA and 3 µl:1 µg cDNA for 10 µg of GFP-Scrib. Plasmid constructs were mixed with 400 µl of serum free DMEM before addition of PEI; vortexed and incubated 15 min at room temperature. After that, 400 µl of the mix was added dropwise to each dish.

For transfecting COS-7, cells were plated onto 6-well plates with 3 coverslips (15 mm) per well in complete DMEM at a suitable dilution to reach 30-40% confluence before transfection. Cells were transfected using calcium phosphate (Piguel et al., 2014). The different cDNAs were prepared with 12.5 µl of $CaCl_2$ and H_2O until a total volume of 100 µl. For cDNA quantities, 1µg was used for Pk2, 4 µg for AnkG-480, Scrib and βIV spectrin. These values were kept for double transfections. The resulting mix was applied, dropwise, to 100 µl of HBS 2x incubated for 30 min at room temperature in the dark and applied to the cells. The plates were then placed back in the incubator for 5h. After that, 3 abundant washes with serum-free DMEM were performed and the plate cells in the incubator for 10 minutes. Finally, serum-free DMEM was replaced by complete medium. 24h later, cells were fixed and processed for immunocytochemistry.

COS-7 cells were fixed with 4% sucrose 4% PFA for 10 min at RT, permeabilized and blocked with 5% BSA 0.3% triton X-100 in PBS for 1h at RT and incubated with primary

antibodies for 1h at RT. After extensive washes, secondary antibodies were incubated for 30 min at RT and coverslips were mounted using Fluoromount-G antifade medium (Electron Microscopy Sciences).

GST production and purification

Different GST-tagged PK2 constructs were purified from *Escherichia coli* competent strain BL21 (Agilent Technologies) supernatants by standard affinity purification on glutathione-Sepharose 4B beads (GE Healthcare UK). One colony of transformed bacteria per construct was amplified in 200 ml of LB medium (ampicillin resistance) during 4h at 37°C. When optical density (O.D.) at 560 nm reached 1, IPTG at 0.1 mM was added to induce plasmid expression (4h). After centrifugation at 3500g, pellets were flash-frozen in dry ice and re-suspended in TBS supplemented with 200 µg/ml of lysozyme (30 min on ice). After sonication, dithiothreitol (DTT) 15 mM, EDTA 10 mM, sodium fluoride 1mM, sodium orthovanadate 1mM, a protease inhibitor tablet (Roche) and 1.5% sodium lauroyl sarcosinate (Sarkosyl) were added to the samples (15 min on ice). Samples were then centrifuged at 186000g for 40 min before adding 4% Triton X-100 to supernatants to stop action of Sarkosyl. Pre-washed gluthatione sepharose beads were incubated with supernatants (2h at 4°C) to link GST tagged proteins and, after an overnight wash with TBS, beads were resuspended in TBS and kept at 4°C for later use. To evaluate purified GST amounts, samples were loaded on SDS-PAGE, ran at 150V for 1h and acrylamide/bis gel was stained with Coomassie Brilliant Blue (45% methanol, 10% glacial acetic acid, 3g/l of Coomassie Brilliant Blue R250 (Pierce) in distilled water). For details of GST-tagged Scrib constructs production, see Moreau et al., 2010.

Immunoprecipitation and pull-down assays

48h post-transfection, HEK293T cells were collected in cold PBS and centrifuged at 500g for 10 min. (4°C). Pellets were flash-frozen in dry ice and re-suspended in lysis buffer (Tris-HCl 50 mM pH 7.5, NaCl 150 mM, EDTA 2 mM and a protease inhibitor tablet (complete, Pierce)). Cells were then homogenized with a polytron and sonicated. For solubilization, 1% Triton X-100 was added to samples (2h at 4°C) and solubilized material was centrifuged at 112,000g for 40 min. Proteins in supernatant were then immunoprecipitated with 8 µg of rabbit anti-GFP or 8 µg of rabbit IgG (ThermoFisher) for 2h at 4°C. 50 µg of protein A agarose beads (Pierce), pre-rinsed with PBS 0.1% Triton X-100, were incubated with samples O/N at 4°C. After rinsing the beads with increasing amounts of NaCl (50-150 mM), proteins were collected in 2x sample buffer (Tris 125 mM pH 6.8, 20% glycerol, 1% bromophenol blue, 4% sodium dodecyl sulfate (SDS), 10% β-mercapto-ethanol) and bound complexes were analyzed by SDS-PAGE and western blotting.

For endogenous IP, 250-300 mg of cortices from P21 rats were collected in lysis buffer (50 mM Tris, pH 7.5, 150 mM Nacl, 2 mM EDTA and protein inhibitor cocktail (complete™ ULTRA Tablets, Roche) and homogenized with a polytron. Proteins were solubilized with 1% Triton X-100 during 3h at 4°C before centrifugation at 112,000g for 40 min. 8 µg of guinea pig (GP) anti-AnkG or 8 µg of GP IgG were added to supernatant (3h at 4°C) before incubation O/N at 4°C with 50 µL of protein A/G agarose beads (Pierce) pre-rinsed four times with PBS 0.1% Triton X-100. Washing of beads and protein recovery was done in the same manner as for *in vitro* IP.

A pull-down assay was performed with AnkG-270-GFP in HEK293T cells. Cell pellet was re-suspended, homogenized and sonicated in Tris-HCl pH 7.5 containing 5 mM EDTA, 150 mM NaCl, 1 mM sodium fluoride, 1 mM sodium orthovanadate and one tablet of protease inhibitors. Solubilization was achieved with 1% Triton X-100 for 1h30 at 4°C and with 0.5% SDS for 30 min at 4°C. Solubilized material was centrifuged at 150,000g for 40 min and supernatant was incubated O/N with the beads attached to the GST alone or to the GST-Pk2 fusion proteins. After four washes with TBS 0.1% Triton X-100, the beads were suspended in 2x sample buffer and subjected to SDS-PAGE and western blotting. GST amounts per pulldown were evaluated by staining membrane in Ponceau solution (0.2% (w/v) Ponceau S in 3% (v/v) acetic acid). Similar conditions were used for the pulldown of myc-βIV spectrin together with GST-Scrib constructs except solubilization steps that were extended for 5min at 37°C.

Stereotaxic injections

Under sterile conditions, 6 weeks old *Pk2* floxed mice were beforehand anesthetized by inhalation of an air/Isoflurane (4%) mix. Mice were then secured in a digital stereotaxic frame (World Precision Instruments, Inc., Sarasota, FL, USA), maintained on O2/isoflurane inhalation with a mask (2%). Intraperitoneal injections of buprenorphine diluted in PBS were done 15 to 20 min before the first incision (100 µl for a 30 gr mouse, 0.1mg/kg). Before performing the surgical incision, the head of the mouse was shaved, disinfected with Betadine and then rinsed with sterile water. Then 10µl of 50% lidocaine diluted in PBS (5 mg/kg, intradermal) were injected at the incision site for local anesthesia. Holes of the size of the injection needle were drilled into the skull using a microdrill, and injections were distributed using a 30G Nanofil needle attached to a Nanofil syringe (World Precision Instruments, Inc., Sarasota, FL, USA) coupled with a UMP3 UltraMicroPump (WPI). To label neurons in the cortex, 500nl of AAV2/9-CaMKII (0.4)-mCherry-2A-iCre virus (titer of 4.8x10^11 genome copies/ml, diluted in sterile PBS) were injected bilaterally in the cortical zone (coordinates from the bregma: X = +/- 1.2 ; Y = -2 ; Z = -0.75). Mice were then placed back in an individual cage with enrichment and humidified food pellets in a heated compartment (30°C) until its motility is back. The animals were checked twice a day for 48h after the procedure, then placed back in a collective cage. Animals were perfused and the brains processed for immunohistochemistry 4 weeks after the injections.

Electrophysiology recordings

Neuronal cultures (DIV7 and DIV8) were transferred to warmed recording solution composed of (in mM) 125 NaCl, 3 KCl, 25 HEPES, 2, CaCl2, 1 MgSO4, 10 glucose and the pH was set to 7.4 with NaOH. For recordings, neurons were continuously perfused with recording solution and recorded at room temperature. Nucleofected neurons (transfected at the time of plating, DIV0) were identified by their GFP fluorescence on upright microscopes (LN-scope (Luigs-Neumann) or Olympus BX51 (Olympus)) using standard GFP filter sets and LED illumination for transmitted and epifluorescence light. Experimenter was blinded for transfection conditions. Intracellular solution for whole-cell recordings was composed of (in mM) 130 K-gluconate, 10 KCl, 10 HEPES, 4 Mg-ATP, 0.3 Na2-GTP, 10 Na2-phosphocreatine and the pH set to 7.25 with KOH and supplemented with 5 mg/ml biocytin for post-hoc morphological identification. All chemicals used were purchased from Sigma-Aldrich. After recordings, neurons were fixed and processed for immunofluorescence as described in *Neuronal cell culture, neuron transfection and immunofluorescence*.

Whole-cell current and voltage-clamp recordings were performed with Sutter double IPA amplifiers (Sutter Instruments, Novato, CA, USA) and sampled with a minimum rate of 10 kHz and Bessel filtered at 5kHz. Action potential recordings and sodium channel recordings were sampled with 50 kHz. All recordings were analyzed with Sutter-patch software and Igor Pro (Wavemetrics, Lake Oswego, OR, USA) or Axograph X (Axograph.com).

Data and statistical analysis

Data are shown as mean ± SEM unless specified otherwise. All datasets were tested for normality using D'agostino and Pearson normality test (GraphPad Software). Statistical significance was then determined by the corresponding test, considering the normal distribution of the data and the variance (equal or unequal). Sample sizes are indicated in the figure legends and significance was defined as p*<0.05, p**<0.01, p***<0.001, p****<0.0001, n.s. – not significant.

Chapter III: Results

The planar polarity proteins Prickle 2 (Pk2) and Scribble (Scrib) localize with AnkG at the AIS *in vivo*

Using custom-made antibodies, we identified Pk2 and Scrib at the axon initial segment (AIS) in cortical structures (**Figure 1A**) and hippocampus (**Figure 1B**) of P21 rat. Both proteins were enriched in the proximal region of the axon, where they co-localized with Ankyrin-G (AnkG), the AIS master organizer. The two proteins appear to co-localize with AnkG in most neuronal types, including pyramidal neurons of the cortex and the hippocampus and at least in some parvalbumin-positive GABAergic neurons (**Figure 1C**).

We generated a *Pk2* gene trap mutant mouse line that encodes ß-Galactosidase (ß-Gal) under *Pk2* endogenous promoter and enhancer elements. We processed brain tissue sections with X-gal and confirmed the expression pattern of *Pk2* in adult brain tissue, in many regions of the brain, with the highest level in the hippocampus and cortex (**data not shown**).

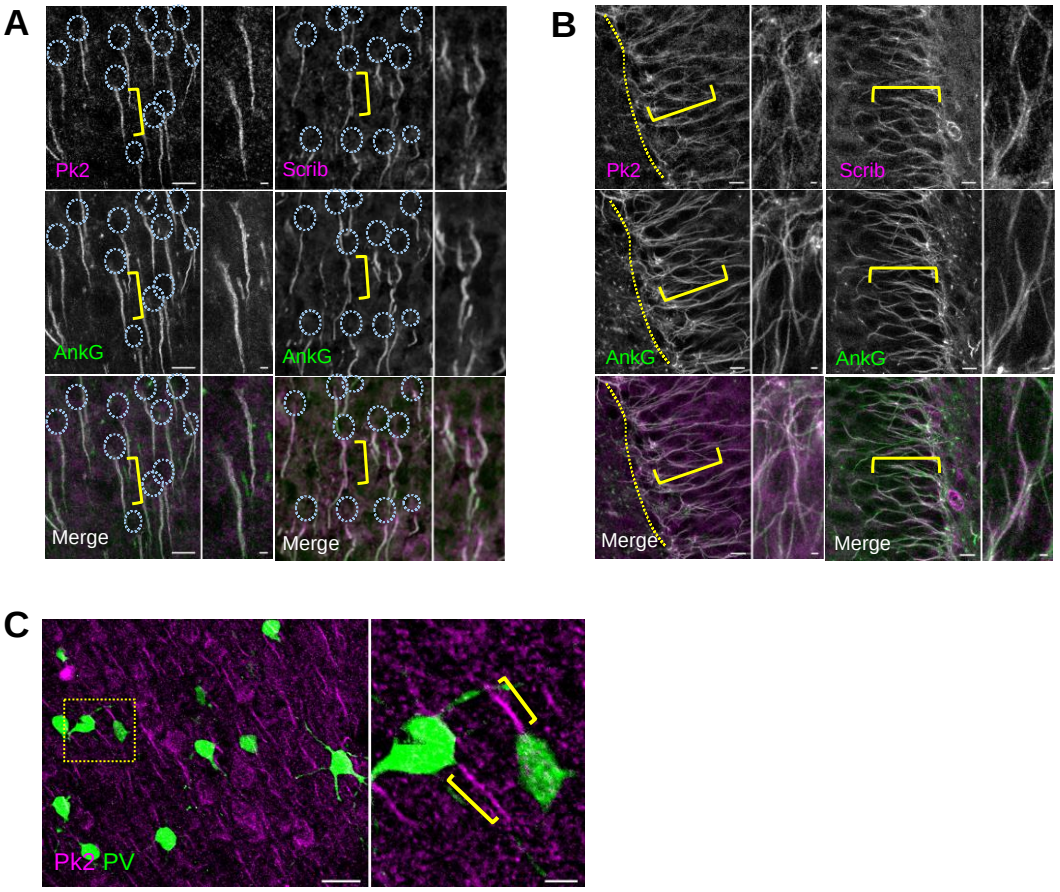

Figure 1. Pk2 and Scrib accumulate at the AIS *in vivo*.

(A) Immunolabeling of Pk2, Scrib and AnkG in the cortex of P21 rat. Dotted circles represent the soma of the neurons. Yellow brackets highlight the co-localization of Pk2 and Scrib with AnkG at the AIS. Scale bars: 10 µm and 2 µm. **(B)** Pk2, Scrib and AnkG detection in the dentate gyrus of the hippocampus from P21 rat. Dotted lines delimit the hilus. High magnification of the AIS shows the co-localization of the PCP proteins with AnkG. Scale bars: 10 µm and 2 µm. **(C)** Staining of GABAergic parvalbumin-positive neurons (green) with Pk2 at the AIS (green) in the cortical layer III of P13 rat. Scale bars: 20 µm and 5 µm.

Pk2 and Scrib are early AIS components *in vitro*

To further analyze the presence of Pk2 and Scrib at the AIS, we performed immunocytochemistry of hippocampal neurons in culture in various states of maturation *in vitro*. We established a spatio-temporal profile for Pk2 and Scrib using average normalized fluorescent intensity profiles in rat hippocampal neurons at 4 days *in vitro* (DIV), in the early phases of AIS formation, and later at DIV7 and DIV10 when the AIS is considered mature structurally. Consistent with the *in vivo* data, the two proteins are enriched at the AIS, identified by AnkG staining, of the cultured neurons at the three stages. At each timepoint Pk2 profile matched with that of AnkG (**Figure 2A-2F, 2I**). However, in the earliest stage, DIV4, we noticed that the peak-to-peak distance for Scrib was shifted by 5 μm from AnkG towards the cell body (**Figure 2A, 2B**). By DIV7, Scrib fully co-localized with Pk2 and AnkG, a profile maintained at DIV10 (**Figure 2C-2F**). These results show that Pk2 and AnkG co-localize at the onset of AIS formation, while the co-localization with Scrib is delayed, suggesting a hierarchy in the requirement of the proteins for AIS formation.

At DIV16, when neurons had a mature AIS, we used direct stochastic optical reconstruction microscopy (dSTORM) imaging using a C-ter antibody to detect eventual periodic patterns, typical of AIS proteins. The antibody against the C-ter of Scrib revealed a periodic pattern of the protein (**Figure 2O, 2P**), reminiscent of that of βIV spectrin, AnkG or actin. Pk2 immunolabeling on the other hand was inconclusive (**Figure 2O, 2P)**. This might be due to the localization of the epitope of our antibody, an internal region spanning amino-acids 345 to 526 (Jiang et al., 2017). These results show that, once the neuron is polarized, at least Scrib is localized in a periodic pattern at the AIS.

To establish a temporal hierarchy in the PCP proteins, we further analyzed their subcellular distribution in the earliest stages of neuronal polarity and AIS assembly. At DIV1, our cultures exhibited a mix between stage 2 and stage 3 neurons (Dotti et al., 1988). In neurons at stages 2/3 with a neurite longer that the others -that we identified as an axon-, Pk2 and AnkG were detected in different vesicles with a mutually exclusive profile (**Figure 2G**, **arrows**), suggesting that they use different machineries to reach the axon. At DIV2 in stage 3 neurons, Pk2 and AnkG profiles switched to a co-localization at the membrane (**Figure 2I**). However, at DIV1, we could not detect Scrib and βIV spectrin while we could already identify proteins such as Tau or βII spectrin in the axon (**Figure 2H**). At DIV2 in stage 3 neurons, when Pk2 and AnkG are at the membrane, we could detect Scrib and ßIV spectrin in vesicles in the axon (**Figure 2J, 2K**). Only between stages 3 and 4 we detected Scrib and βIV spectrin at the membrane in the proximal part of the axon (**Figure 2L, 2M**). Importantly, both Pk2 and Scrib were not affected after detergent Triton X-100 extraction at DIV2, suggesting an early and tight association to the cytoskeleton meshwork (**Figure 2N**).

Altogether, our data show that Pk2 is one of the earliest proteins present at the AIS with AnkG, shortly followed by Scrib and βIV spectrin.

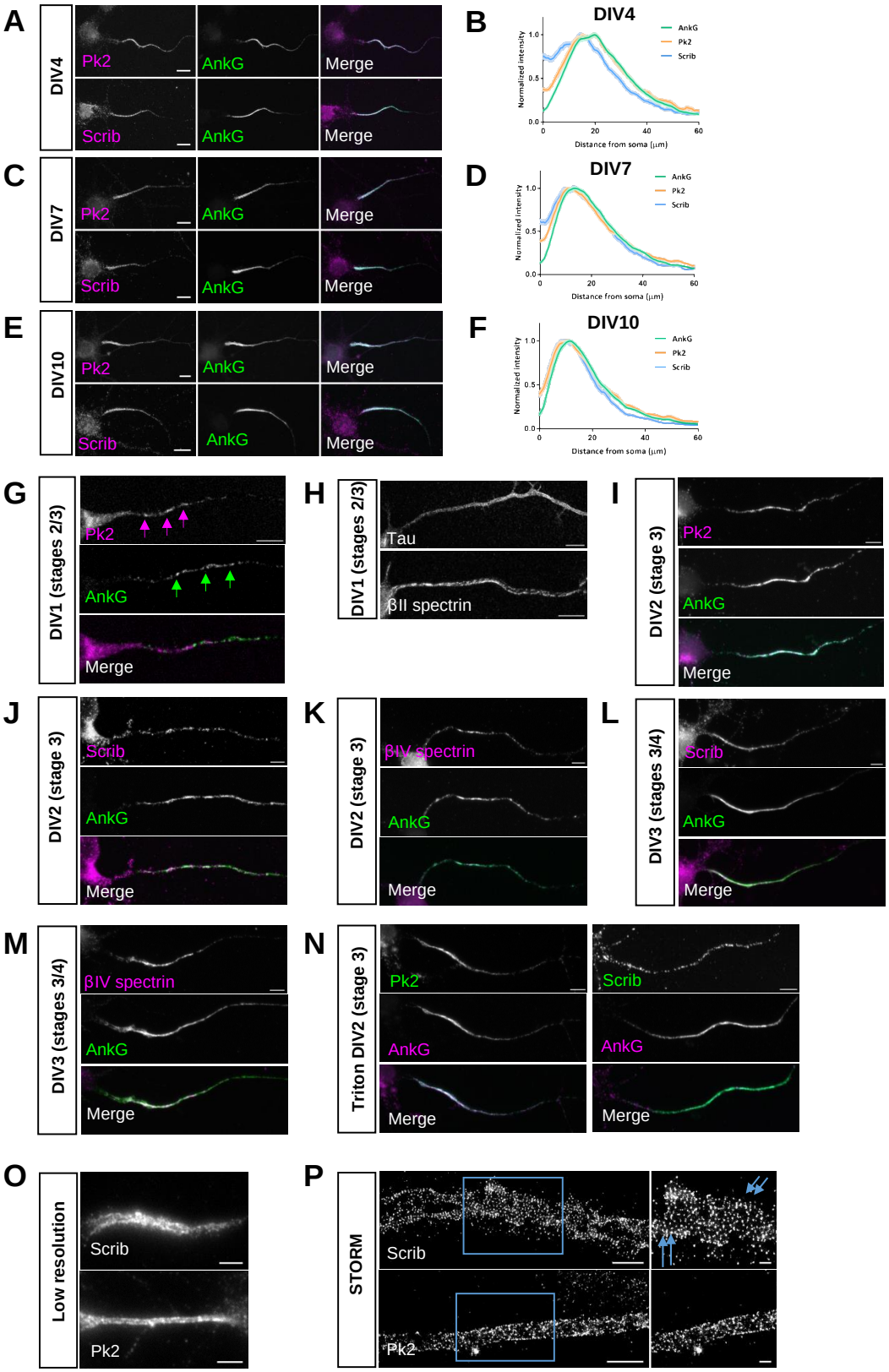
A
DIV4
Pk2
AnkG
Merge
Scrib
AnkG
Merge
B
DIV4
AnkG
Pk2
Scrib
Normalized intensity
Distance from soma (µm)
C
DIV7
Pk2
AnkG
Merge
Scrib
AnkG
Merge
D
DIV7
AnkG
Pk2
Scrib
Normalized intensity
Distance from soma (µm)
E
DIV10
Pk2
AnkG
Merge
Scrib
AnkG
Merge
F
DIV10
AnkG
Pk2
Scrib
Normalized intensity
Distance from soma (µm)
G
DIV1 (stages 2/3)
Pk2
AnkG
Merge
H
DIV1 (stages 2/3)
Tau
βII spectrin
I
DIV2 (stage 3)
Pk2
AnkG
Merge
J
DIV2 (stage 3)
Scrib
AnkG
Merge
K
DIV2 (stage 3)
βIV spectrin
AnkG
Merge
L
DIV3 (stages 3/4)
Scrib
AnkG
Merge
M
DIV3 (stages 3/4)
βIV spectrin
AnkG
Merge
N
Triton DIV2 (stage 3)
Pk2
AnkG
Merge
Scrib
AnkG
Merge
O
Low resolution
Scrib
Pk2
P
STORM
Scrib
Pk2

Figure 2. Pk2 and Scrib are early AIS components and co-localize with AnkG.

(A) Cultured hippocampal neurons at DIV4 immunolabeled with Pk2, Scrib and AnkG antibodies. Scale bars: 10 µm. Mean fluorescence intensity ± SEM at the AIS at DIV4 for Pk2, Scrib and AnkG in **(B)**. Note the 5 µm shift of Scrib with regard to Pk2 and AnkG, which are co-localizing. Total quantified neurons: 77 for Pk2, 70 for Scrib from at least 3 independent experiments. AnkG is represented as the mean of the AnkG co-staining from the total of 147 neurons. **(C)** Staining for Pk2, Scrib and AnkG at DIV7. Scale bars: 10 µm. Mean fluorescence intensity ± SEM at the AIS for Pk2, Scrib and AnkG at DIV7 showing the full co-localization of the three proteins in **(D)**. Total quantified neurons: 87 for Pk2, 57 for Scrib from, at least, 3 independent experiments. AnkG is represented as the mean of the AnkG co-staining from the total of 144 neurons. **(E)** DIV10 neurons stained for Pk2 and AnkG. Scale bars: 10 µm. Mean fluorescence intensity ± SEM at the AIS for Pk2, Scrib and AnkG at DIV10 displaying full co-localization profiles in **(F**). Total quantified neurons: 66 for Pk2, 65 for Scrib. AnkG is represented as the mean of the AnkG co-staining from the total of 131 neurons. **(G)** DIV1 hippocampal neuron, immunolabeled with Pk2 and AnkG antibodies. The arrows point to the vesicles of Pk2 and AnkG with exclusive profiles. Scale bar: 5 µm. **(H)** Staining of Tau and ßII spectrin at DIV1. Scale bars: 10 µm. **(I)** Pk2 and AnkG labelings at DIV2 show a full co-localization at the membrane. Scale bar: 5 µm. **(J)** Detection of Scrib at DIV2 showing a vesicular profile. Scale bar: 5 µm. **(K)** ßIV spectrin staining at DIV2 displaying an axonal profile in vesicles. Scale bar: 5 µm. **(L, M)** DIV3 neurons stained with Scrib and AnkG and ßIV spectrin (L) and AnkG and Scrib (M). Scale bars: 5 µm. **(N)** DIV2 neurons extracted with triton during fixation and stained for Pk2 and Scrib. Scale bars: 5 µm. **(O)** Low resolution images of Scrib and Pk2 at the AIS of DIV16 neurons. Scale bars: 5 µm. **(P)** STORM images of Scrib and Pk2 at the AIS of DIV16 neurons. Scrib displays a periodic pattern at the AIS while the distribution of Pk2 appears aleatory. Scale bars: 2 and 0.5 µm.

AnkG is necessary for Pk2 and Scrib at the AIS

Next, we used a shRNA for AnkG that is known to abolish AIS assembly to evaluate its requirement on Pk2 and Scrib recruitment. As reported, neurons nucleofected with these shRNA loose most of the AnkG staining at the AIS, and as a consequence prevented Pk2 and Scrib accumulation at the proximal axon, with 7.4 ± 3.2 % neurons expressing the shAnkG without AIS-enriched Pk2 versus 97.8 ± 1.8 % for control shRNAs (**Figure 3A, 3B**). These results demonstrate that Pk2 and Scrib localization and stabilization at the AIS depend on AnkG and indicate that Pk2 and Scrib are integral and early components of the AIS.

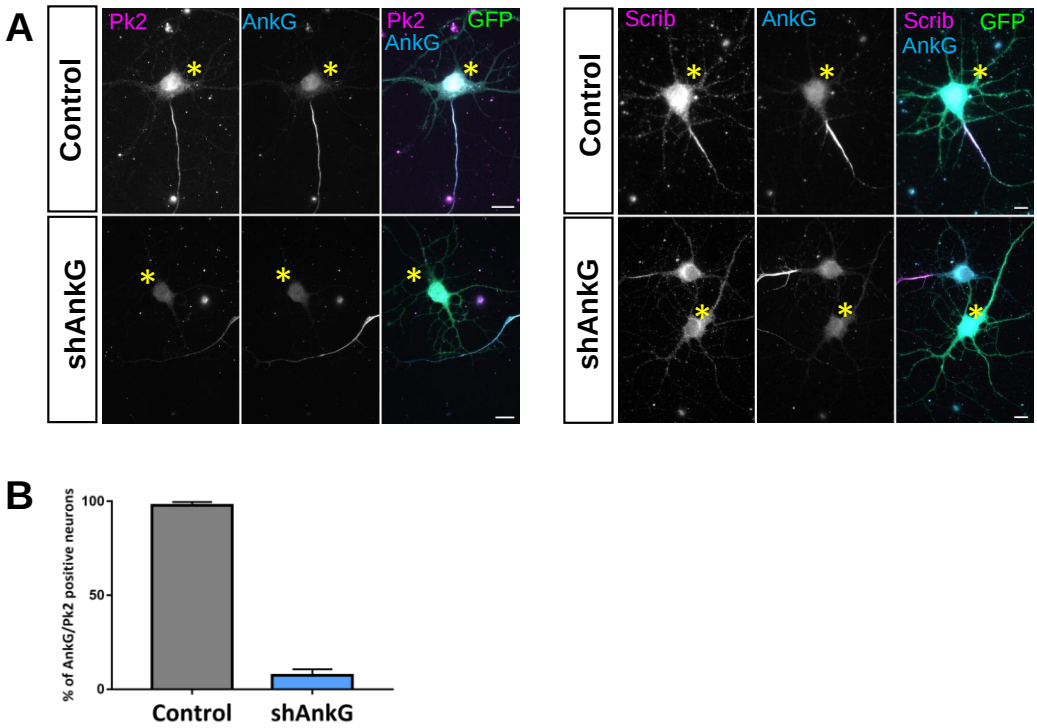

Figure 3. Pk2 and Scrib are AnkG-dependent AIS components

(A) Control and shAnkG neurons stained for GFP, Pk2 and AnkG or GFP, Scrib and AnkG showing the total absence of Pk2 and Scrib when AnkG is downregulated. The yellow asterisk points to the transfected neuron. Scale bars: 10 µm. **(B)** Histogram showing the percentage of AnkG/Pk2 positive neurons in the control versus AnkG-depletion conditions ± SEM. Quantified neurons: 98 for the control and 125 for the shAnkG, from 3 independent experiments.

Pk2 and AnkG interact to form a molecular complex at the AIS

The early accumulation of Pk2 at the proximal axon together with AnkG, closely followed by Scrib and βIV-spectrin, suggests that these PCP proteins could interact by pairs in the earliest phases of AIS assembly. To test this, we first expressed a Flag-tagged Pk2 protein in the presence or absence of GFP-tagged AnkG isoforms 480, 270 and 190 kDa respectively, in heterologous cells (**Figure 4A, 4B**). Cells transfected with Flag-Pk2 had labelling in vesicular and/or aggregated complexes in the cytoplasm and in perinuclear structures (**Figure 4C**), while AnkG-190 and -270 were mostly in smaller cytoplasmic vesicles and AnkG-480 showed a previously described accumulation at the tips of microtubules (**Figure 4D**) (Fréal et al., 2016). These results confirmed the co-localization of Pk2 with the three isoforms of AnkG in cytosolic clusters/aggregates and puncta (**Figure 4E-4G**).

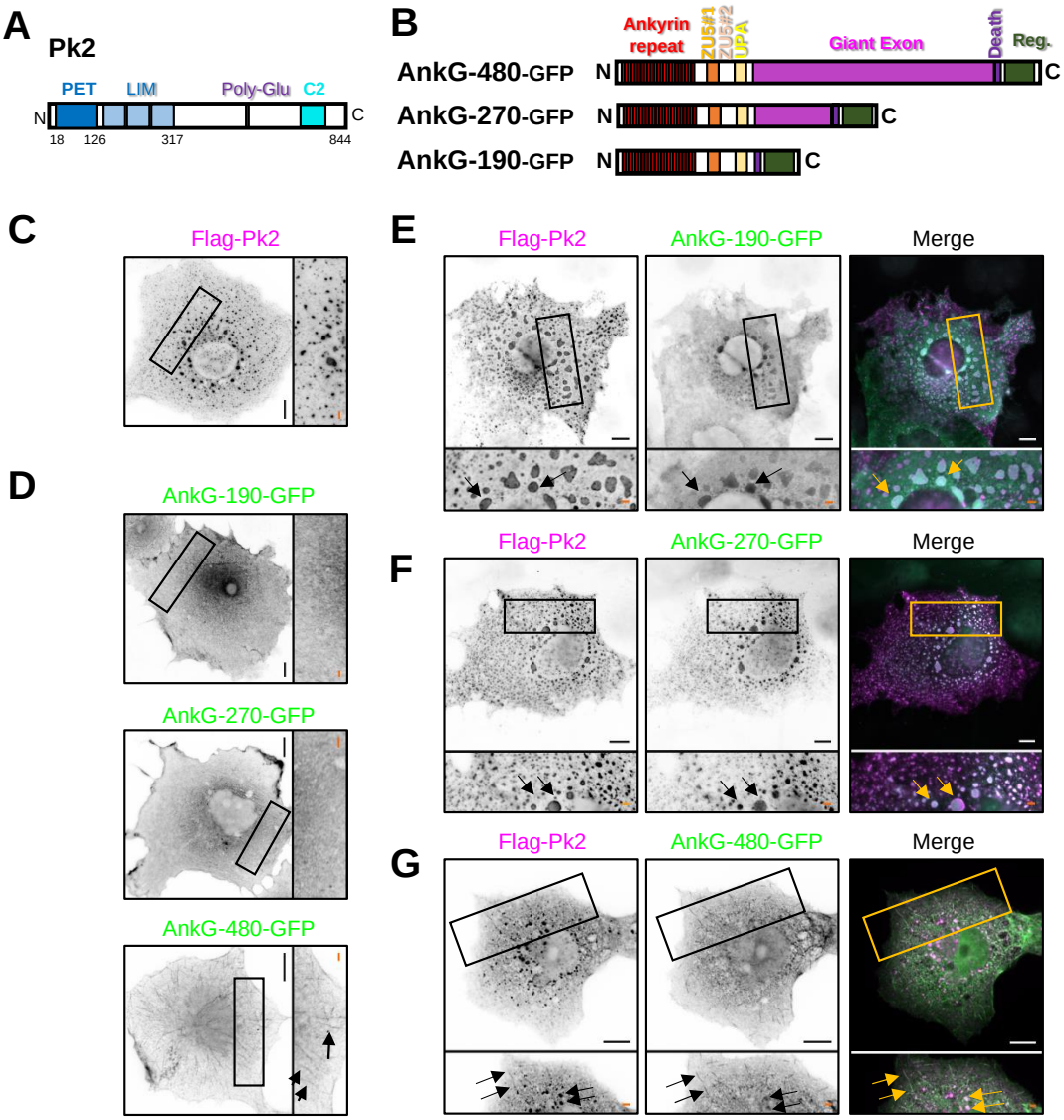

Figure 4. Exogenous Pk2 co-localizes with AnkG isoforms in heterologous cells.

(A, B) Schematic of the protein structures of Pk2 and the AnkG isoforms. One PET and three LIM domains compose the N-ter of Pk2 followed by a C2 domain in the C-ter. In AnkG, the membrane binding domain (formed by ankyrin repeats), the spectrin binding domain (ZU5#1, ZU5#2, UPA) and the regulatory domain at the C-ter are present in all the 3 isoforms. **(C)** Flag-Pk2 distribution in the cytoplasm is mostly in vesicular and/or aggregated structures when transfected alone. Scale bars: 10 and 2 µm. **(D)** AnkG-190-GFP and AnkG-270-GFP show a wide cytoplasmic distribution while AnkG-480-GFP shows comet-like profile at the distal end of the microtubules. Scale bars: 10 and 2 µm. **(E)** When co-transfected, Flag-Pk2 and AnkG-190-GFP co-localize in clusters/aggregates. Scale bars: 10 and 2 µm. **(F)** Flag-Pk2 and AnkG-270-GFP follow the same pattern as in (E). **(G)** Flag-Pk2 and AnkG-480-GFP co-localize in clusters/aggregates but also at the distal end of the microtubules. Scale bars: 10 and 2 µm.

The interaction between Pk2 and AnkG was confirmed using immunoprecipitation (IP) and GST-pulldown assays. Because of the large size of AnkG-480, we restricted our coIP experiments to the -270 and -190 kDa isoforms of AnkG. We were able to co-immunoprecipitate Flag-Pk2 with both anti-GFP-AnkG-190 and AnkG-270 (**Figure 5A, 5B**). These data suggest that the N-terminal part of AnkG, comprising the membrane and spectrin binding domains, and/or the regulatory domain at the C-ter, all of them common to all the isoforms, are critical for the interaction with Pk2.

To further identify the domain of Pk2 required for the binding, we generated glutathione S-transferase (GST) constructs from different regions of Pk2 and performed GST-pulldown assays (**Figure 5C**). We detected two domains of interaction for Pk2: a region corresponding to the LIM domain (aa 127-844), and a region corresponding to the C-ter region of the protein, also called C2 domain (aa 585-844) that appeared to be the strongest binding site (**Figure 5C**). We confirmed this interaction *in vivo* by coIP of Pk2 with AnkG on P21 rat cortex-derived lysates with an expected 100 kDa band for full-length Pk2 and an additional unknown 70 kDa band (**Figure 5D**). Altogether, our results reveal Pk2 as a novel interacting partner of AnkG.

Our data support the hypothesis that Pk2 is one of the earliest interacting partners of AnkG in the nascent axon, at the time of AIS assembly. Since microtubules (MT) are critical in the early phases of AIS establishment, we used a similar assay as in Fréal et al. (2016) that evaluated AnkG interplay with MT. We co-transfected COS-7 cells with tagged cDNA constructs coding for Pk2 and AnkG-480 to evaluate their co-localization. As reported before, in these cells AnkG-480 is enriched in the distal ends of the MT, while Pk2 was mostly vesicular (**Figure 5E, 5F, arrows**). When co-transfected with AnkG-480, Pk2 is recruited to these distal ends, together with AnkG, supporting the interaction with the protein and maybe a link with the MT (**Figure 5G, arrows**).

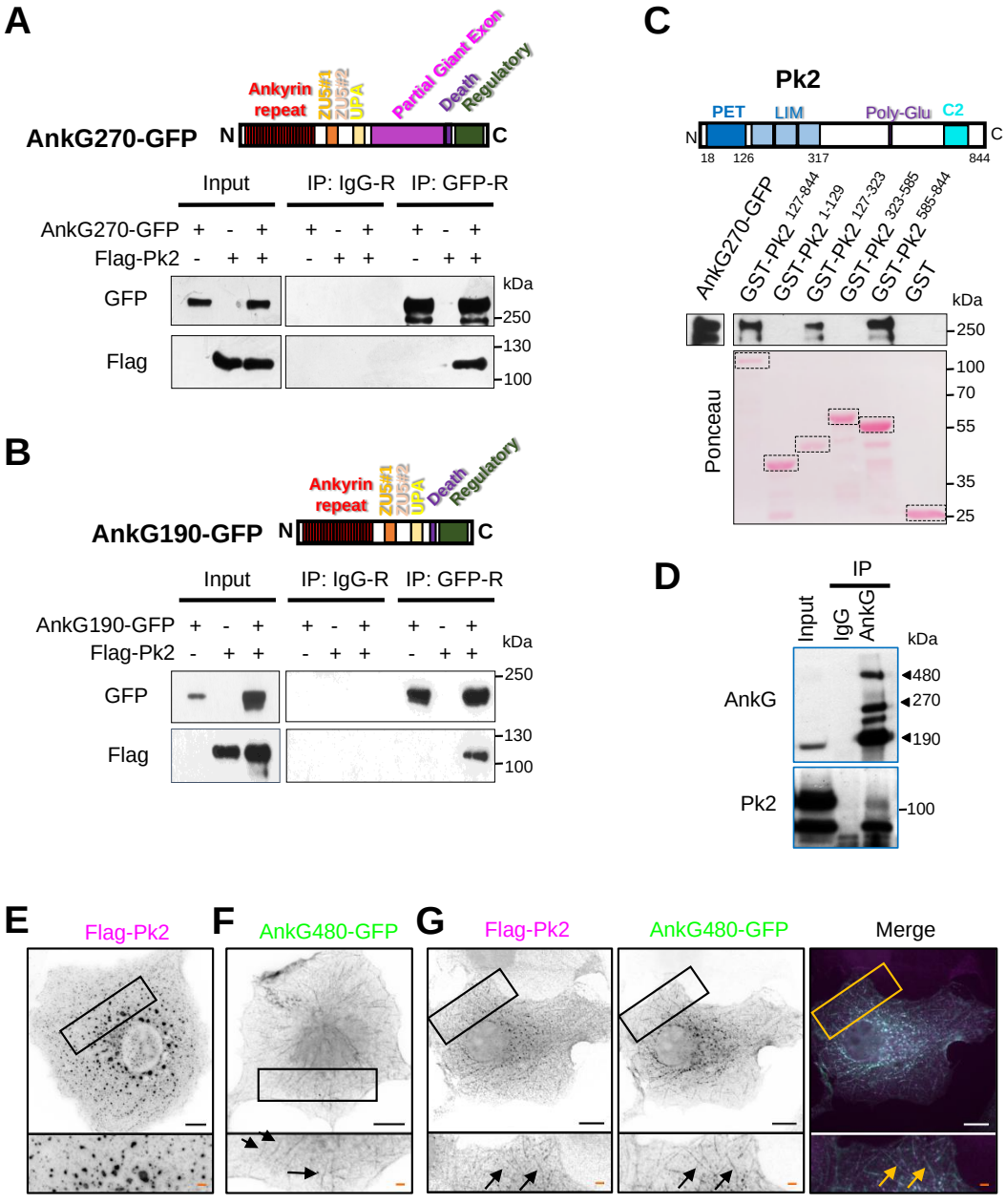
A
Ankyrin repeat
ZU5#1
ZU5#2
UPA
Partial Giant Exon
Death
Regulatory
AnkG270-GFP
N
C
Input
IP: IgG-R
IP: GFP-R
AnkG270-GFP + - + + - + + - +
Flag-Pk2 - + + - + + - + +
GFP
Flag
kDa
250
130
100
B
AnkG190-GFP
AnkG190-GFP + - + + - + + - +
Flag-Pk2 - + + - + + - + +
250
130
100
C
Pk2
PET
LIM
Poly-Glu
C2
18
126
317
844
AnkG270-GFP
GST-Pk2 127-844
GST-Pk2 1-129
GST-Pk2 127-323
GST-Pk2 323-585
GST-Pk2 585-844
GST
Ponceau
250
100
70
55
35
25
D
IP
Input
IgG
AnkG
AnkG
Pk2
480
270
190
100
E
Flag-Pk2
F
AnkG480-GFP
G
Flag-Pk2
AnkG480-GFP
Merge

Figure 5. Pk2 and AnkG form a complex *in vitro* and *in vivo*.

(A, B) Schematic of the AnkG-270 kDa structure. From N-ter to C-ter: membrane binding domain (ankyrin repeats), spectrin binding domain (ZU5#1, ZU5#2, UPA), a partial tail domain deriving from the partial expression of the exon 37 and the regulatory domain at the C-ter. AnkG-190 kDa presents all the domains in the AnkG-270 kDa except the tail at the C-ter derived from the partial exon 37. Flag-Pk2 co-immunoprecipitates with AnkG-270-GFP and AnkG-190-GFP but not with IgG-R control, *in vitro.* **(C)** Schematic of the full-length-Pk2 protein with the different domains and aa number. The detected bands in the blot for the GST constructs used in the pulldown experiments correspond to the LIM domains and to the C-ter of Pk2 interacting with AnkG. GST alone was used as a control for unspecific interactions. On the bottom, ponceau coloration showing the amounts of the different GST constructs (dotted squares). **(D)** Pk2 co-immunoprecipitates with AnkG *in vivo*, but not with IgG control. **(E)** Flag-Pk2 distribution in the cytoplasm of COS7 cells transfected alone. Scale bars: 10 and 2 µm. **(F)** AnkG-480-GFP show comet-like structures that represent the distal end of the microtubules. Scale bars: 10 and 2 µm. **(G)** Flag-Pk2 and AnkG-480-GFP co-localize at the distal end of the microtubules when co-transfected. Scale bars: 10 and 2 µm.

Scrib and ßIV spectrin define an additional stabilization complex

Next, we evaluated the co-localization and interaction between Scrib and βIV spectrin (**Figure 6A**). Cells transfected with HA-Scrib or Myc-βIV spectrin show a labelling in the cytoplasm and in perinuclear structures (**Figure 6B, 6C**). Co-expression of Scrib and βIV spectrin confirmed the co-localizations of the two proteins in cytosolic clusters/aggregates and puncta suggesting strong affinity of the two proteins (**Figure 6D**). We confirmed an interaction between Scrib and βIV spectrin *in vitro* (**Figure 6E**) and we further identified the C-ter of Scrib as the interacting domain by GST-pulldown (**Figure 6F**). Altogether, our results identify Pk2 as a novel interacting partner of AnkG, while βIV spectrin and Scrib can form another protein complex.

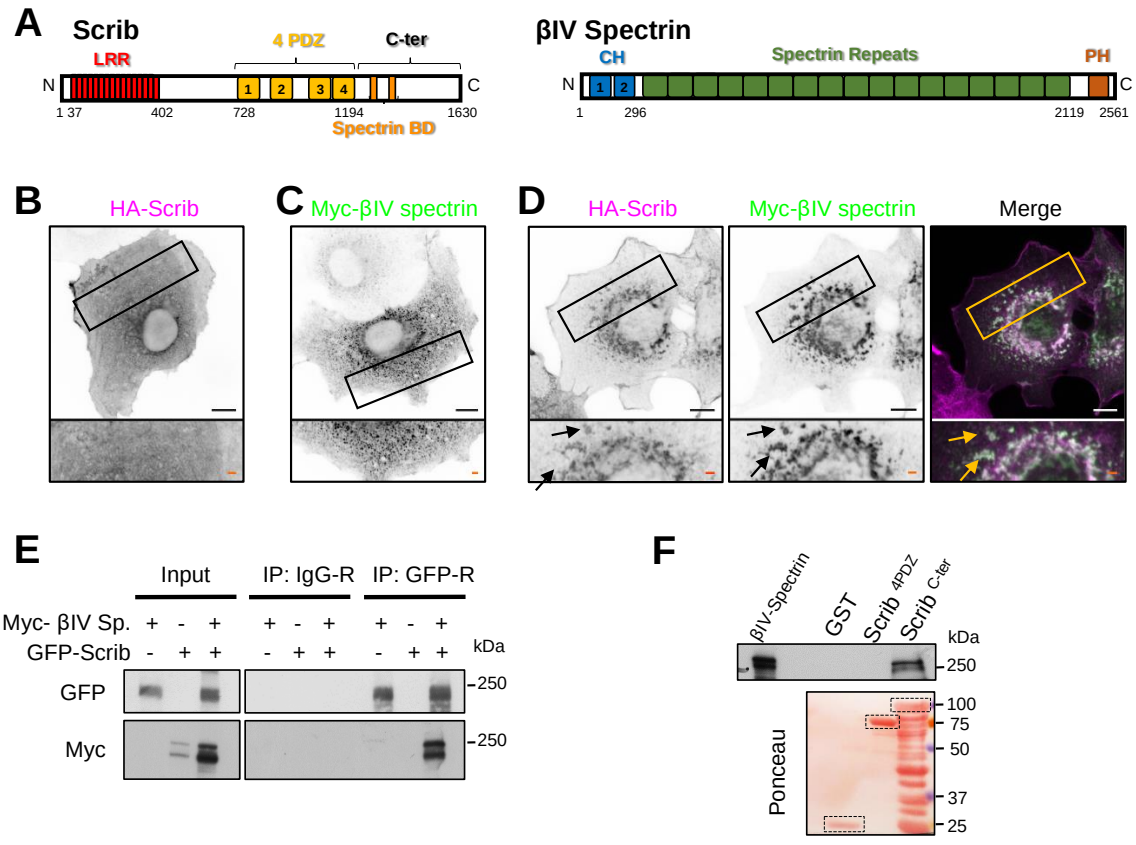

Figure 6. Scrib and ßIV spectrin form a protein complex.

(A) Representation of the structures of Scrib and ßIV spectrin. Scrib has a series of leucine-rich repeats at the N-ter, followed by 4 PDZ domains and the C-ter. Highlighted at the C-ter is the spectrin binding domain. ßIV spectrin is comprised of two calponin homology domains that form the actin-binding domain, followed by a series of spectrin repeats and a pleckstrin homology (PH) domain at the C-ter. **(B)** HA-Scrib shows a wide cytoplasmic profile when overexpressed. Scale bars: 10 and 2 µm. **(C)** Myc-ßIV spectrin accumulates in cytoplasmic inclusions. Scale bars: 10 and 2 µm. **(D)** HA-Scrib profile is re-distributed and co-localizes with myc-ßIV spectrin when co-transfected. Scale bars: 10 and 2 µm. **(E)** Myc-ßIV spectrin co-immunoprecipitates with GFP-Scrib, but not with IgG-R control *in vitro*. **(F)** Immunoblot showing the GST-Scrib fragments corresponding to the C-ter, but not the PDZ domains of Scrib, that pulled down with myc-ßIV spectrin. On the bottom, ponceau coloration showing the amounts of the different GST constructs (dotted squares).

Pk2 is necessary for AIS establishment

Next, we examined the effect of Pk2 knockdown on the localization and levels of several AIS proteins, including AnkG, βIV spectrin, neurofascin (NF-186), and voltage-gated sodium (Na_v) channels. For that, hippocampal neurons were electroporated with shRNA constructs before plating to express either shPk2 or shCtr (shown in the figures as “control”). We used a validated shRNA against Pk2 (Nagaoka et al., 2014), which we further validated for AIS-Pk2

staining (**Figure 7**). Downregulation of Pk2 before AIS formation led to three neuronal phenotypes (**Figure 7A-7D**). Results show that 25 ± 15 % of shPk2-positive neurons had a single AIS/axon with a fragmented or decreased AnkG/Pk2 staining; 62 ± 23 % had a multi AIS/axon profile all with AnkG-positive labeling, and 13 ± 9% had no AnkG/Pk2 staining (**Figure 7E**). In shPk2-positive neurons with 1 AIS/axon and multi AIS/axon, we observed reduced levels of Pk2 fluorescence intensity in comparison with the control (a global 67 ± 1.2 % decrease, **Figure 7F**), and a 63 ± 1.2 % decrease of AnkG fluorescence intensity compared with the control (**Figure 7G**).

A similar preliminary experiment to evaluate the impact of Scrib knockdown, using a previously validated shRNA (Moreau et al., 2010) showed a different and overall weaker phenotype in terms of AIS structure (**Figure 7H**). The AIS was intact, not fragmented, but elongated. Peak-to-peak intensity distance of AnkG shows a difference of 7.6 µm between control and shScrib measurements (peak at control: 8.2 ± 0.03 µm; peak at shScrib: 15.8 ± 0.04 µm), while the average length of the AIS doubled in shScrib-positive neurons, from 21.4 µm in the controls (AIS starts at: 1.7 ± 0.02 µm, AIS ends at: 23.1 ± 0.03 µm) to 42.6 µm in the shScrib-positive neurons (AIS starts at: 1.3 ± 0.02 µm, AIS ends at: 43.9 ± 0.04 µm). Pk2 followed the same profile as AnkG (**Figure 7I**).

Given the strong effect of the shPk2 on AnkG, we further analyzed the levels of AIS proteins in downregulation conditions and saw that the loss of Pk2 also led to a 72 ± 2.3 % decrease of βIV spectrin immunofluorescence (**Figure 8A** and **8B**), a 60 ± 1.8 % for Na_v channels (**Figure 8C** and **8D**), and a 56 ± 1.9 % for NF-186 (**Figure 8E and 8F**). Finally, Scrib was also reduced by 63 ± 2.1 % (**Figure 8G and 8H**).

We next sought to determine if loss of Pk2 affected the highly organized and robust cytoskeleton at the AIS in a multi AIS/axon phenotype by using super-resolution microscopy (dSTORM). We stained control and shPk2 neurons with phalloidin to visualize the actin at the AIS. If neurons transfected with a control construct had a classic periodic actin staining all along the compartment (**Figure 8I**), Pk2 depleted neurons exhibited an overall disorganized actin pattern (**Figure 8J**). Altogether, our findings revealed that Pk2 is involved in the early establishment of the AIS in developing axons and that its loss affects the AIS molecular composition and actin cytoskeleton periodicity, while depletion of Scrib modifies the length but not the cohesion of the AIS.

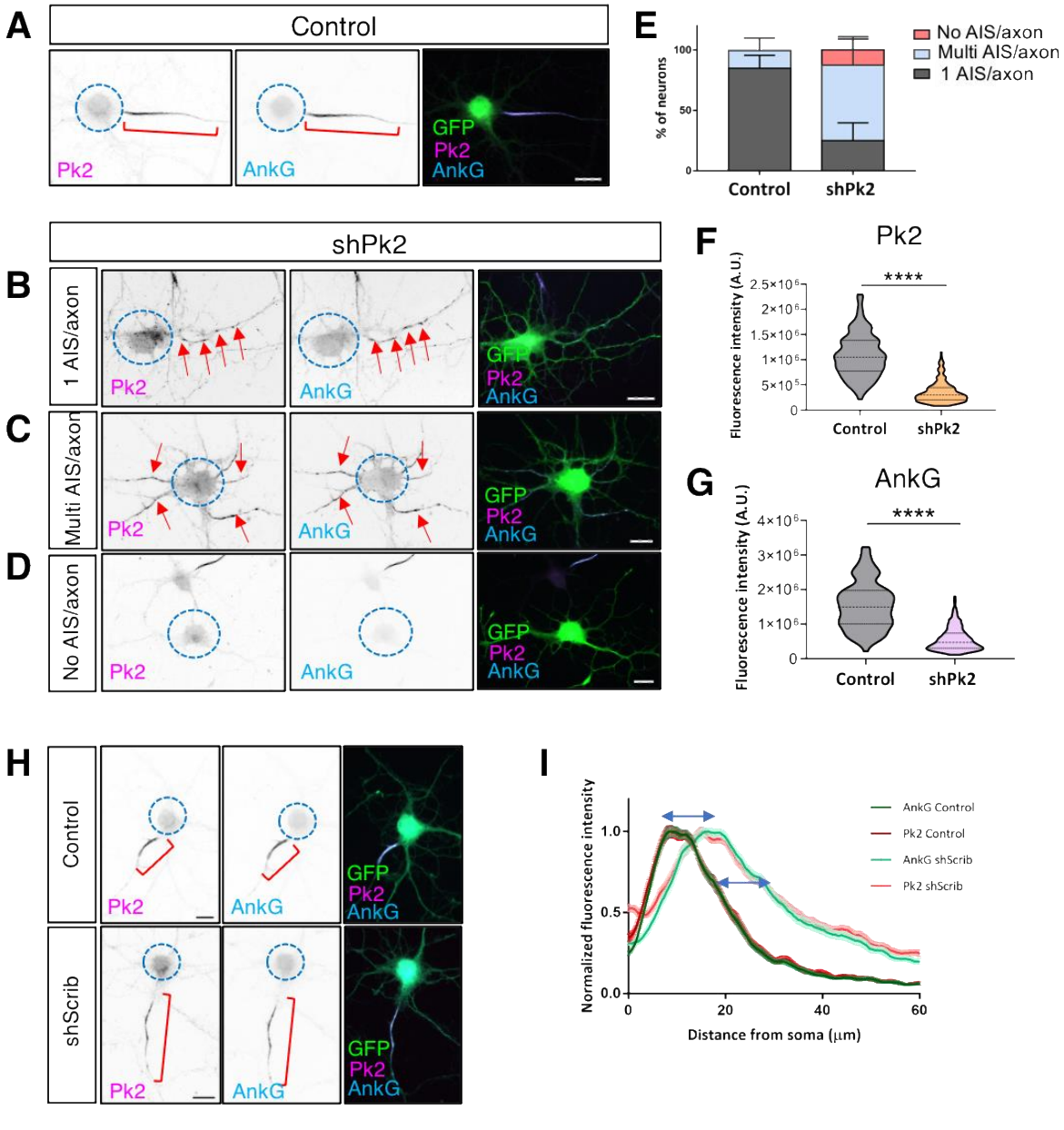
A
Control
Pk2
AnkG
GFP
Pk2
AnkG
shPk2
B
1 AIS/axon
C
Multi AIS/axon
D
No AIS/axon
E
No AIS/axon
Multi AIS/axon
1 AIS/axon
% of neurons
100
50
0
Control
shPk2
F
Pk2
****
Fluorescence intensity (A.U.)
2.5×10⁶
2×10⁶
1.5×10⁶
1×10⁶
5×10⁵
0
Control
shPk2
G
AnkG
****
Fluorescence intensity (A.U.)
4×10⁶
3×10⁶
2×10⁶
1×10⁶
0
Control
shPk2
H
Control
shScrib
I
Normalized fluorescence intensity
1.0
0.5
0.0
0
20
40
60
Distance from soma (μm)
AnkG Control
Pk2 Control
AnkG shScrib
Pk2 shScrib

Figure 7. Loss of Pk2 impacts axon and AIS formation.

(A) DIV7 neuron transfected with a control plasmid. Blue dotted circle shows the cell body. Red bracket shows the AIS. Scale bar: 10 µm. **(B)** shPk2 transfected neuron showing a single AIS/axon with a Pk2/AnkG fragmented profile. The red arrows indicate the Pk2/AnkG fragments and the blue dotted circle shows the cell body. Scale bar: 10 µm. **(C)** Pk2-deprived neuron with a multi AIS/axon profile. The red arrows point to the different AnkG-positive neurites (defined as AIS/axons) and the blue dotted circle shows the cell body. Scale bar: 10 µm. **(D)** shPk2 neuron showing no AIS/axon. The blue dotted circle indicates the cell body. Scale bar: 10 µm. **(E)** Ratios of neurons with the different phenotypes (no AIS/axon, multi AIS/axon and 1 AIS/axon) in control and shPk2 ± SEM. Quantified neurons: 183 for the control and 252 for shPk2, from 3 independent experiments. **(F, G)** Mean fluorescence intensities for Pk2 and AnkG in control and shPk2 neurons. Total intensity per AIS was measured for Pk2 and AnkG. In multi AIS/axon neurons, the resulting intensity is the mean of the total intensity of individual AIS. Dotted, thick middle line indicates the median and the thinner outer lines represent the quartiles. Quantified neurons: 136 for the control and 245 for the shPk2, from 3 independent experiments; ****$p<0.0001$ from Mann Whitney's test. **(H)** DIV7 neurons transfected with control and shScrib plasmids. Dotted circle shows the cell body and the bracket points to the AIS, which is elongated in the shScrib conditions. Scale bar: 10 µm. **(I)** Normalized fluorescence intensity profiles of Pk2 and AnkG in control versus shScrib conditions ± SEM. Blue double arrows show the shifted peak to peak distance profile in Scrib depletion conditions. The start and end positions that were used to determine AIS length correspond, respectively, to the proximal and distal positions where fluorescence intensity of AnkG reached the 35% of the maximum. Quantified neurons: 31 neurons for the control, 33 for the shScrib, from two independent experiments.

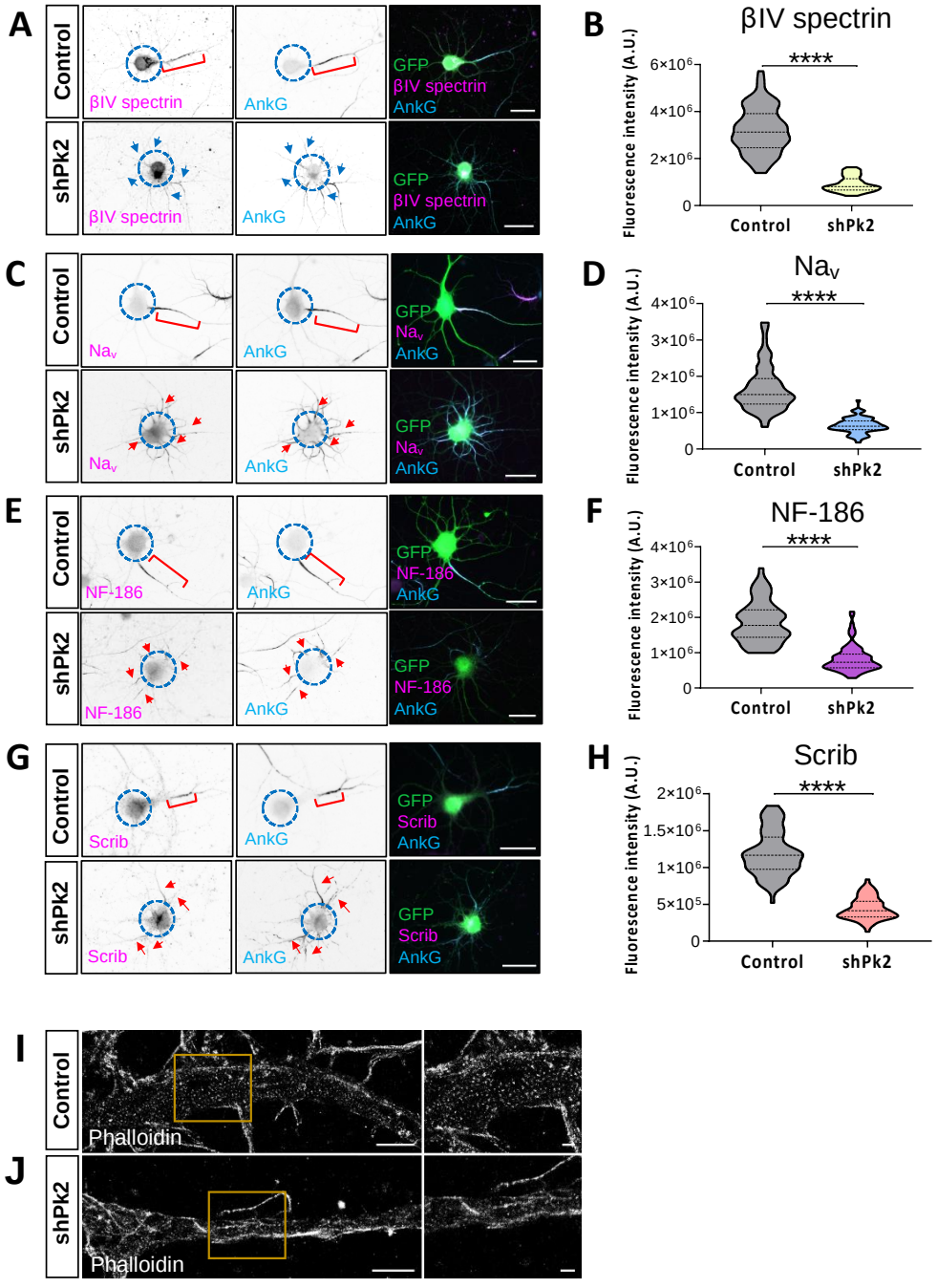
A
Control
shPk2
βIV spectrin
AnkG
GFP
βIV spectrin
AnkG
B
βIV spectrin
Fluorescence intensity (A.U.)
6×10⁶
4×10⁶
2×10⁶
0
****
Control
shPk2
C
Control
shPk2
Nav
AnkG
GFP
Nav
AnkG
D
Nav
Fluorescence intensity (A.U.)
4×10⁶
3×10⁶
2×10⁶
1×10⁶
0
****
Control
shPk2
E
Control
shPk2
NF-186
AnkG
GFP
NF-186
AnkG
F
NF-186
Fluorescence intensity (A.U.)
4×10⁶
3×10⁶
2×10⁶
1×10⁶
0
****
Control
shPk2
G
Control
shPk2
Scrib
AnkG
GFP
Scrib
AnkG
H
Scrib
Fluorescence intensity (A.U.)
2×10⁶
1.5×10⁶
1×10⁶
5×10⁵
0
****
Control
shPk2
I
J
Control
shPk2
Phalloidin
Phalloidin

Figure 8. AIS key molecules are reduced upon Pk2 downregulation.

(A, B) Control and shPk2 neurons showing the redistribution and decrease of ßIV spectrin in downregulation conditions. Blue dotted circle indicates the cell body, the red bracket highlights the intact, single AIS in the control. Red arrows show the presence of multiple AIS/axons in the shPk2 neuron and the blue dotted circle shows the cell body. These bracked/dotted circle/arrows indications are also present in figure 8C-8G. Scale bars: 20 µm. Graph in (B) represents the mean ßIV spectrin fluorescence intensities at the AIS in the control and shPk2 neurons. Total intensity per AIS was measured for ßIV spectrin. In multi AIS/axon neurons, the resulting intensity is the mean of the total intensity of individual AIS. Quantified neurons: 73 for the control and 76 for the shPk2, from three independent experiments; ****p<0.0001 from Mann Whitney's test. **(C, D)** Na_v channels were detected in control and shPk2 neurons using a pan-Na_v antibody. Scale bars: 20 µm. Violin plots in (D) show the mean Na_v intensities in control and shPk2 neurons. Total intensity per AIS was measured for Na_v channels. In multi AIS/axon neurons, the resulting intensity is the mean of the total intensity of individual AIS. Quantified neurons: 67 from the control and 69 from the shPk2, from three independent experiments; ****p<0.0001 from Mann Whitney's test. **(E, F)** NF-186 levels were also affected in the shPk2 as shown by the images and the graph. Graph in (F) shows the mean intensity of NF-186 in control and shPk2 neurons. Total intensity per AIS was measured for NF-186. In multi AIS/axon neurons, the resulting intensity is the mean of the total intensity of individual AIS. Scale bars: 20 µm. Quantified neurons: 60 from the control and 81 from the shPk2, from three independent experiments; ****p<0.0001 from Mann Whitney's test. **(G, H)** Scrib levels are reduced in the absence of Pk2. Violin plot in (H) shows the mean intensities for Scrib in control and shPk2 neurons. Total intensity per AIS was measured for Scrib. In multi AIS/axon neurons, the resulting intensity is the mean of the total intensity of individual AIS. Scale bars: 10 µm. Quantified neurons: 74 from the control and 69 from the shPk2, from three independent experiments; ****p<0.0001 from Mann Whitney's test. **(I, J)** STORM images of DIV7 neurons stained with phalloidin and transfected with the control (I) and shPk2 (J) constructs. The actin periodic pattern at the AIS is disrupted in absence of Pk2. Scale bars: 2 µm and 0.5 µm.

Pk2 is not required for AIS maintenance

To determine the role of Pk2 in AIS maintenance, we examined the impact of Pk2 depletion in hippocampal neurons from DIV10 onwards, when the AIS is assembled. AIS Pk2 immunofluorescence intensity was not reduced in neurons expressing shPk2 at DIV14 as compared to neurons expressing a control plasmid (shCtr, "control" in Figure 9) (**Figure 9A**), and is slightly reduced in neurons expressing the shPk2 at DIV25 as compared to control neurons, with a similar profile that for AnkG (**Figure 9A and 9B**). These data show that Pk2 is a highly stable component of the AIS with a low turnover ratio and its late downregulation does not affect AnkG levels or AIS maintenance.

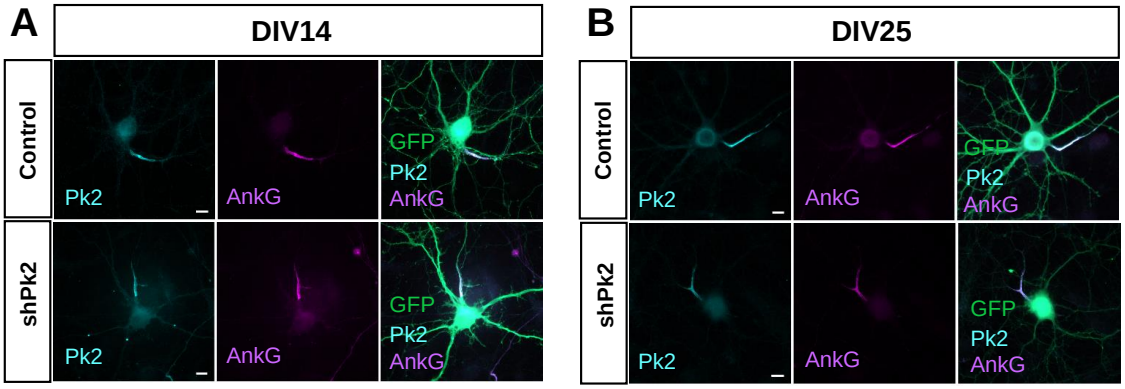

Figure 9. Pk2 is not necessary for AIS maintenance

(A) Neurons transfected at DIV10 with the control and the shPk2 constructs were stained for Pk2 and AnkG 4 days after the transfection. Pk2 levels were intact at this stage. Scale bars: 10 µm. **(B)** At DIV25, 15 days after the transfection, Pk2 is still detected but slightly decreased in respect to the control, similar to AnkG. Scale bars: 10 µm.

Acute downregulation of Pk2 impairs AIS formation in neurons of the developing neocortex

We further evaluated the role of Pk2 in AIS formation *in vivo* by performing *in utero* electroporation of the shPk2 in E16.5 rat embryos. Pk2-depeleted neurons in the neocortex were identified with GFP staining (**Figure 10A**). GFP-shPk2 positive neurons showed low to absent Pk2 immunolabeling versus the non-electroporated surrounding cells, confirming the knockdown efficiency of the construct, while the neuron soma appeared in good shape. This decrease was followed by a strong reduction of AnkG (**Figure 10B**), showing that acute depletion of Pk2 severely impacts AIS formation in the rat developing cortex. When we performed the same experiment in mice, with an shRNA targeting a similar region of Pk2 in this species than the one in rat, we saw that the electroporated neurons presented an altered shape and a series of axonal extensions with a beaded-like shape, typical of dying neurons, and suggestive of a toxicity of the shRNA (**Annexes, Figure 1**).

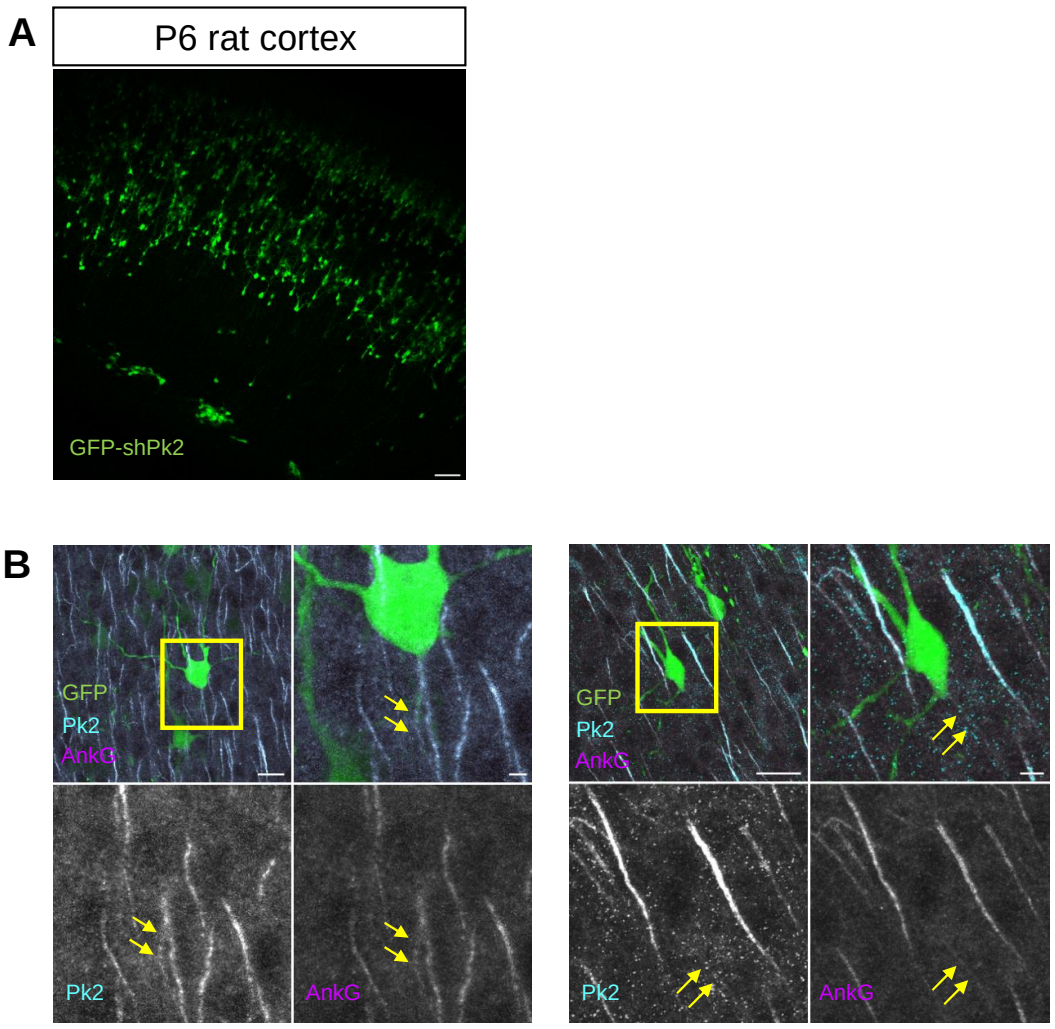

Figure 10. Pk2 drives AIS formation in the developing neocortex.

(A) Immunolabeling with a GFP antibody shows GFP-shPk2 electroporated neurons in P6 rat cortex. Scale bar: 20 µm **(B)** Two shPk2 electroporated neurons with green soma showing reduced levels of Pk2 and AnkG at their AIS. Yellow arrows point the AIS. Scale bars: 20 µm and 4 µm and 5 µm for higher magnifications.

Deletion of Pk2 and Scrib in excitatory postmitotic neurons affects AIS development *in vivo*

We next investigated the functional consequences of *Pk2* and *Scrib* genes deletion at the AIS *in vivo* by generating conditional knockout mice for both *Pk2* and *Scrib*. We crossed a Nex-driven Cre recombinase (Nex^{Cre}) with $Scrib^{f/f}$ mice (Yamben et al. 2013) and $Pk2^{f/f}$ mice (this study) to generate the hereby called Pk2-$Scrib^{Nex}$ cKOs. We used Nex-Cre to specifically delete our genes in postmitotic, glutamatergic neurons of the neocortex and the hippocampus and bypass any embryonic function of both genes (Goebbels et al., 2006). No gross differences in weight and body size were found between the controls and the mutants and Nissl staining revealed no major brain anatomical differences in adult mice (**Figure 11A**).

We validated a strong decrease of Pk2 and Scrib levels in the mutants as early as P12 and at P21 (**Figure 11B**). The reduction of both PCP proteins was followed by a significant decrease of AnkG-480 (41.30 ± 0.05 %) and AnkG-270 (24.90 ± 0.02 %) and a slight reduction of AnkG-190 of 15.7 ± 0.1 % that was not significant (**Figure 11C, 11D**). These numbers were unchanged at P21, with a significant decrease of AnkG-480 (45.4 ± 0.05 %) and overall steady levels of AnkG-190 (+ 0.04 ± 0.03 %) (**Figure 11E, 11F**). At this stage, AnkG-270 was not properly detected and therefore not quantified (**Figure 11E**). Given the importance of AnkG-480 in AIS assembly, we evaluated the levels of other AIS components like βIV spectrin but observed no apparent differences between controls and mutants in both ε1 and ε6 isoforms (**Figure 11G**).

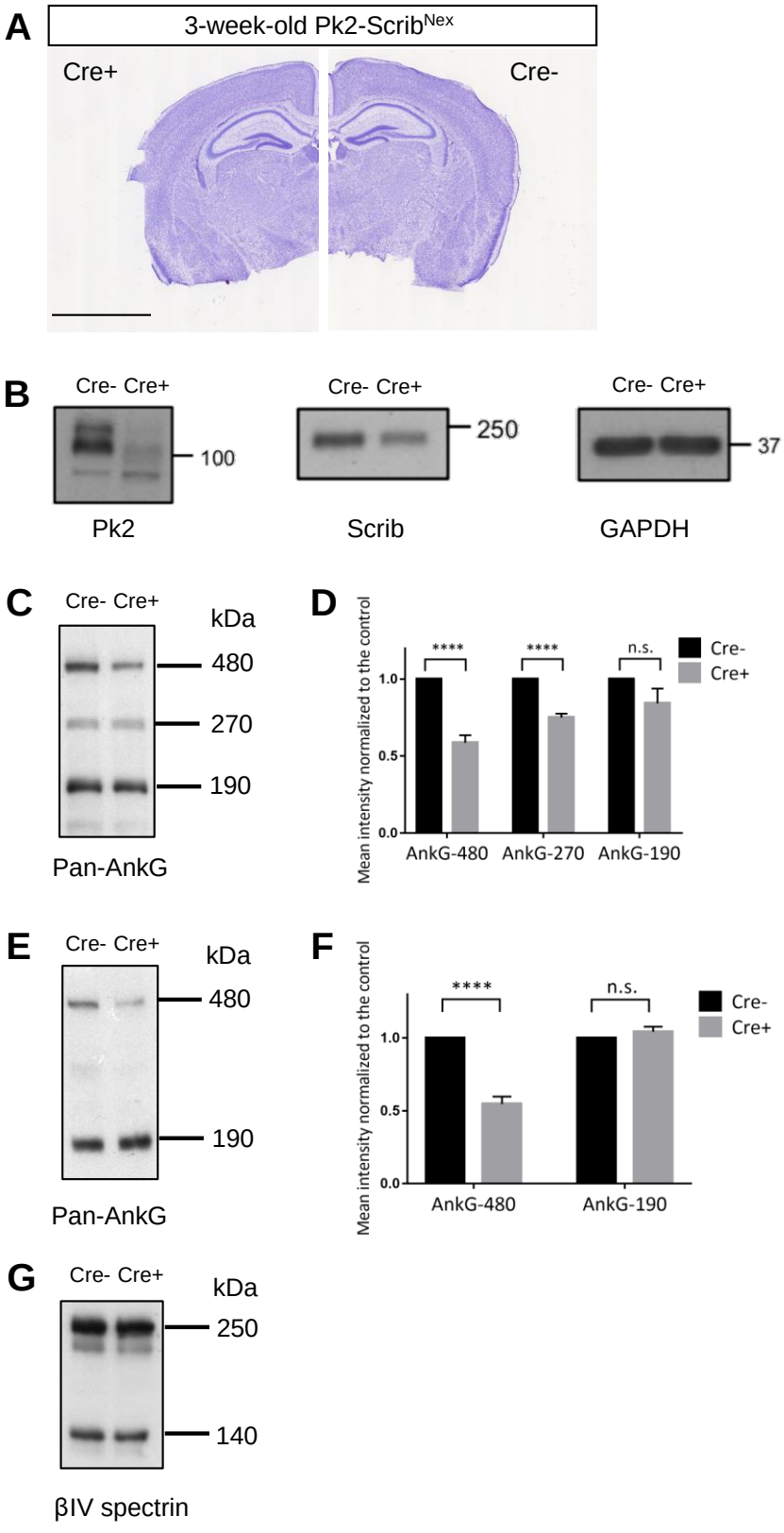
A
3-week-old Pk2-ScribNex
Cre+
Cre-
B
Cre- Cre+
100
Pk2
Cre- Cre+
250
Scrib
Cre- Cre+
37
GAPDH
C
Cre- Cre+
kDa
480
270
190
Pan-AnkG
D
Mean intensity normalized to the control
****
****
n.s.
Cre-
Cre+
1.0
0.5
0.0
AnkG-480
AnkG-270
AnkG-190
E
Cre- Cre+
kDa
480
190
Pan-AnkG
F
Mean intensity normalized to the control
****
n.s.
Cre-
Cre+
1.0
0.5
0.0
AnkG-480
AnkG-190
G
Cre- Cre+
kDa
250
140
βIV spectrin

Figure 11. Deletion of Pk2 and Scrib impact AIS formation *in vivo.*

(A) Brain slices from Cre- and Cre+ mice processed for Nissl staining. No major anatomic brain differences were detected. Scale bar: 2.5 mm. **(B)** Blots showing decreased levels for Pk2 and Scrib in the Cre+ animals (P12), evidencing efficiency of gene deletion. GAPDH showed equal amount of loaded protein. **(C, D)** AnkG detection in blot using a pan-AnkG antibody shows the 480, 270 and 190 kDa isoforms in the Cre- and Cre+ mice at P12. Graph in (D) displays the mean intensity normalized to the control of the AnkG isoforms in Cre- and Cre+ and the SEM. Two batches of samples were analyzed: set #1 had 5 Cre- and 5 Cre+, set #2 had 4 Cre- and 5 Cre+. Each batch was processed for blot twice. The mean intensity in (D) is the result of the mean of all the exposure times per genotype (merging both batches and both blots). For statistical test, each individual exposure time was considered as n=1. ****p<0.0001, from unpaired T-test with Welch's correction. **(E, F)** AnkG detection in blot using a pan-AnkG antibody shows the 480 and the 190 kDa isoforms in Cre- and Cre+ mice at P21. Graph in (F) displays the mean intensity normalized to the control of the AnkG isoforms in Cre- and Cre+ and the SEM. Two batches of samples were analyzed: set #1 had 2 Cre- and 2 Cre+, set #2 had 3 Cre- and 3 Cre+. Each batch was processed for blot twice. The mean intensity in (F) is the result of the mean of all the exposure times per genotype (merging both batches and both blots). For statistical test, each individual exposure time was considered as n=1. ****p<0.0001, from unpaired T-test with Welch's correction. **(E)** Global levels of ßIV spectrin isoforms ε1 and ε6 were unchanged in between control and mutants at P12.

We next examined AnkG immunolabeling in the Pk2-Scrib^{Nex} mutants using an antibody that recognizes all three isoforms (pan-AnkG), and another one specific for the AnkG-480 (Jenkins et al., 2015). In the mutants, AnkG staining was still restricted to the AIS but reduced by 44% ± 0,5 % in pan- AnkG (**Figure 12A, 12B**), and by 51 ± 0,5 % in AnkG-480 (**Figure 12C, 12D**) in neurons of the layers II and III of the cortex from three-week-old mice. Other AIS components were also decreased, including βIV spectrin (reduced by 80 ± 0.6 %) and Na_v (reduced by 36 ± 0.8 %) (**Figure 12E-12F and Figure 12G-12H**, respectively). We observed a similar decrease in the hippocampus but did not quantify them yet because of the difficulty to discriminate individual AIS in that system (**data not shown**). Our results show that the *in vivo* deletion of both Pk2 and Scrib shortly after the cell cycle exit decreases AIS proteins levels.

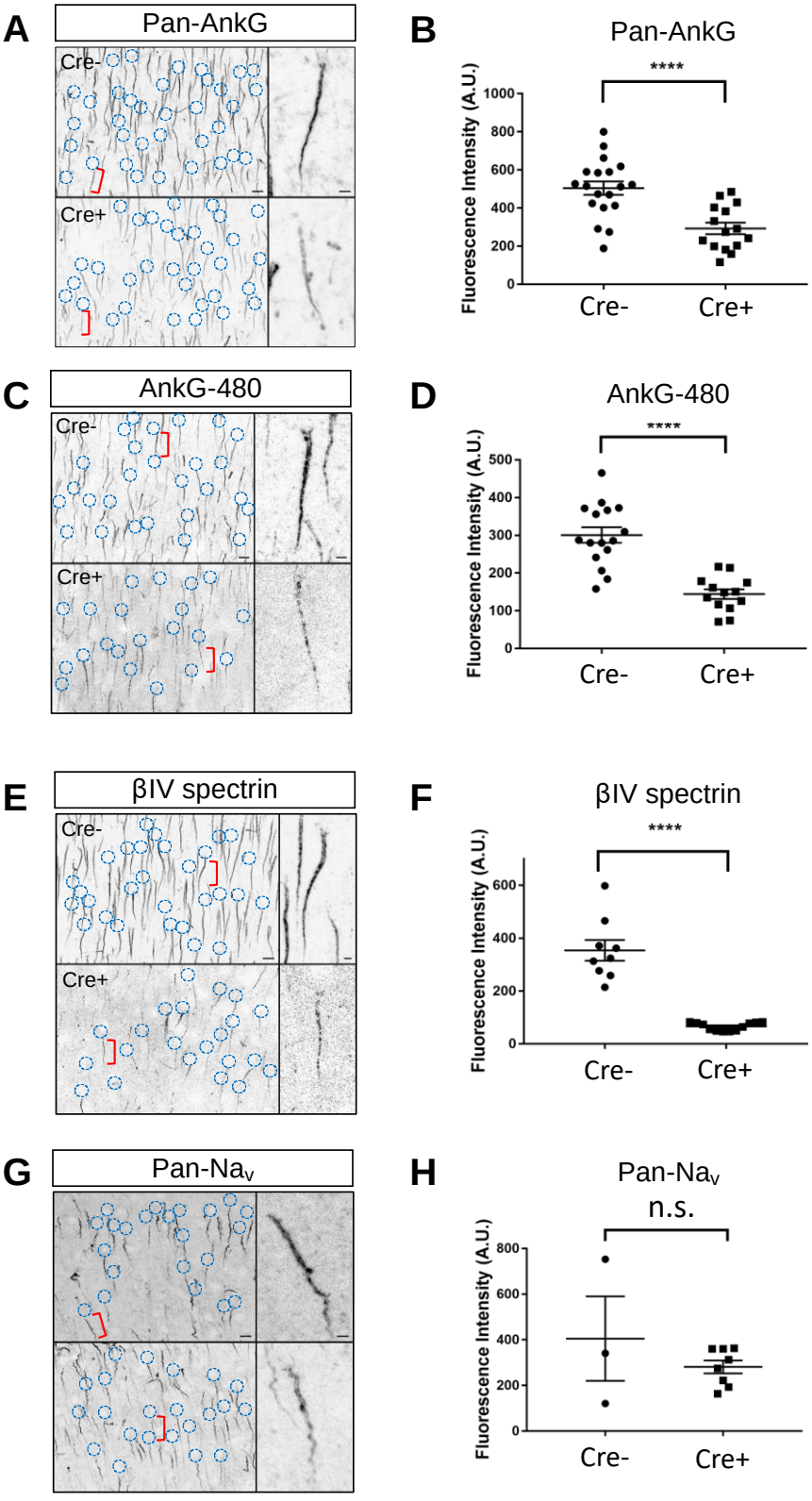
A
Pan-AnkG
Cre-
Cre+
B
Pan-AnkG
****
Fluorescence Intensity (A.U.)
1000
800
600
400
200
0
Cre-
Cre+
C
AnkG-480
Cre-
Cre+
D
AnkG-480
****
Fluorescence Intensity (A.U.)
500
400
300
200
100
0
Cre-
Cre+
E
βIV spectrin
Cre-
Cre+
F
βIV spectrin
****
Fluorescence Intensity (A.U.)
600
400
200
0
Cre-
Cre+
G
Pan-Nav
H
Pan-Nav
n.s.
Fluorescence Intensity (A.U.)
800
600
400
200
0
Cre-
Cre+

Figure 12. Pk2 and Scrib are necessary for AIS formation in cortical post-mitotic neurons

(A, B) Pan AnkG (480 and 270 kDa isoforms) was detected with a pan-AnkG antibody in control and Pk2-Scrib^{Nex} mutants. Scale bars: 10 and 2 µm. Graph in (B) shows the decreased levels of AnkG in the mutants (mean ± SEM). Each point represents the mean intensity of the different AIS from a single acquisition. Between 34 and 72 AIS were measured per acquisition and a minimum of 2 slices were imaged per animal. A total of 884 AIS were quantified for the control and 717 for the mutants. 4 control and 4 mutant mice were analyzed. Statistical tests were performed considering the number of individual acquisitions as the sample size. ****p<0.0001, unpaired T-test with Welch's correction. **(C, D)** AnkG-480, which is the main actor behind AIS assembly and function, was detected with a specific antibody. Scale bars: 10 and 2 µm. Graph in (D) shows the decreased levels of AnkG-480 in the mutants (mean ± SEM). Each point represents the mean intensity of the different AIS from a single acquisition. Between 34 and 73 AIS were measured per acquisition and a minimum of 2 slices were imaged per animal. A total of 806 AIS were quantified for the control and 698 for the mutants. 4 control and 4 mutant mice were analyzed. Statistical tests were performed considering the number of individual acquisitions as the sample size. ****p<0.0001, unpaired T-test with Welch's correction. **(E, F**) ßIV spectrin levels are drastically reduced in the mutants. Scale bars: 10 and 2 µm. Graph in (F) shows the reduced levels of ßIV spectrin in the mutants (mean ± SEM). Each point represents the mean intensity of the different AIS from a single acquisition. Between 12 and 59 AIS were measured per acquisition and a minimum of 2 slices were imaged per animal. A total of 250 AIS were quantified for the control and 441 for the mutants. 2 control and 2 mutant mice were analyzed. Statistical tests were performed considering the number of individual acquisitions as the sample size. ****p<0.0001, Mann Whitney's test. **(G, H)** Na_v channels intensities at the AIS were measured with a pan-Na_v antibody. Scale bars: 10 and 2 µm. Graph in (H) shows the reduced levels of Na_v channels in the mutants (mean ± SEM). Each point represents the mean intensity of the different AIS from a single acquisition. Between 19 and 56 AIS were measured per acquisition and a minimum of 2 slices were imaged per animal. A total of 115 AIS were quantified for the control and 315 for the mutants. 1 control and 2 mutant mice were analyzed. Ns = not significant, statistical tests were not performed due to low sample size.

Acute deletion of Pk2 in adult excitatory neurons does not affect AIS maintenance *in vivo*

To confirm that Pk2 is not involved in AIS maintenance *in vivo* we performed stereotaxic viral injections of an AAV-CAMKII-mCherry-Cre virus in the cortex of 6-weeks-old *Pk2*-floxed mice. After 4 weeks of Cre recombinase expression, we processed brain tissue for immunolabeling with an AnkG antibody and saw no clear changes of AnkG levels in mCherry-positive neurons compared to the surrounding, not infected neurons (**Figure 13**). This result is consistent with our observations on maintenance *in vitro*.

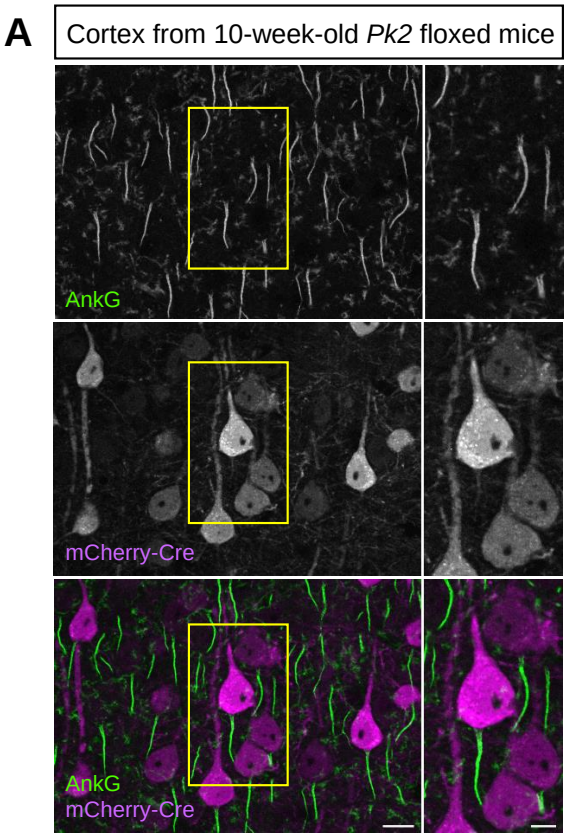

Figure 13. Acute deletion of Pk2 in adult excitatory neurons does not affect AIS maintenance in vivo.

(A) Cre-infected neurons (in magenta) in the cortex of *Pk2* floxed mice show steady levels of AnkG compared to the surrounding neurons. Scale bars: 100 µm and 50 µm.

Chapter IV: General discussion

The objective of this thesis was to decipher the role of the PCP proteins Pk2 and Scrib in neuronal polarity and function. I found that the two proteins participate in the AIS macromolecular complex to regulate the assembly of the AIS, with Pk2 arriving earlier to the AIS and interacting with AnkG and Scrib following later and forming a complex with ßIV spectrin. The PCP-AIS protein complex participates in the assembly, cohesiveness and the length of the AIS most probably by interacting directly or indirectly with the cytoskeleton (Figure 15).

Not only does this study expand the AIS proteome, and extend our understanding of AIS structure and function, but these results are original in the context of the literature on Pk2 and Scrib function in neurons that is currently mostly focused on dendrites and spines. This work suggests that some of the deficits and pathologies associated to the two genes mutations might not be only relevant to synaptopathies, but also to "AISopathies"

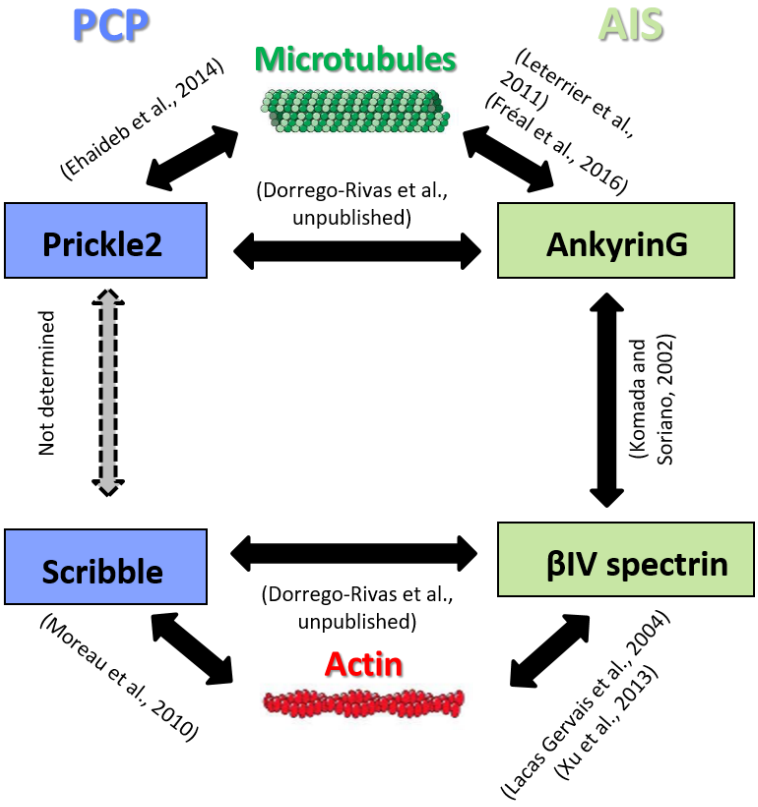

Figure 15. Schematic of the integration of the PCP proteins Pk2 and Scrib in the AIS.

The described and potential relations between both the PCP and AIS proteins with the cytoskeleton are shown.

Pk2 and Scrib are novel and early core members of the AIS

We identified Pk2 as a novel partner of AnkG *in vitro* and *in vivo* (**Figure 14**). *In vitro*, we found that Pk2 interacts with the 270 and 190 kDa isoforms of AnkG. Due to the large size of the AnkG-480, the co-immunoprecipitation (coIP) with this isoform was not performed, but we assume it also binds to Pk2 possibly via the N-ter, which is one of the common domains to all the three AnkG (see below). The pulldown assays with Pk2 reveal that the minimum domain required for this interaction comprises the LIM domain at the N-ter and/or the C-ter portion that includes the C2 domain. *In vivo*, we performed an IP of AnkG in brain lysates and we co-immunoprecipitated Pk2. We attempted to explore if Pk2 has a preferential binding to one or another AnkG isoform by performing a reverse IP in the same system, where we immunoprecipitated Pk2 and discriminated AnkG isoforms in blot, but it has been unconclusive so far. One logical consequence of Pk2 binding to the three isoforms is that Pk2 probably interacts with -and potentially modulates- AnkG-190 at the spines, as both proteins are also present in this compartment. The molecular basis of some of Pk2-related neuronal deficits should therefore be revisited in light of these results (Sowers et al., 2013; Hida et al., 2011; Smith et al., 2014).

Temporally, Pk2 is detected as early as DIV1, together with AnkG, but in separated vesicles suggesting different trafficking cargos. Pk2 could then be recruited to the membrane -at least partially- via its conserved C-terminal farnesylation motif [CAAX motif: KNC(I/T)IS] at the C-terminus (Strutt et al., 2013), just like it is believed that AnkG uses palmitoylation motifs in the N-ter (He et al., 2012). Just one day after, at DIV2, Pk2 and AnkG colocalize at the membrane and maintain this profile in mature neurons. Our results show that AnkG binds to Pk2 through the LIM and the C2 domains in the C-ter (together or not), both reported in the literature to drive protein-protein interactions (Tree et al., 2002; Das et al., 2004). Pk2 is therefore a good candidate to participate in the initial recruitment/stabilization of AnkG at the plasma membrane. The disruption of AIS cohesion and the reduction of AnkG levels observed as a result of Pk2 downregulation fit with this theory (see section *Pk2 is necessary for AIS establishment* in Chapter III: Results). Pk2 is, to date, one of the earliest, if not the earliest, detected partners of AnkG in the nascent axon. Only EB1 was reported as early as DIV2 (Fréal et al., 2016). However, we cannot exclude variability in culture properties affecting the maturation of neurons between laboratories, and the mix of developmental stages of the neurons at DIV1 or DIV2.

Interestingly, the *Drosophila* core PCP protein Diego (Diversin or Ankrd6 in mammals) interacts via its ankyrin repeats with a similar C-ter region (aa 820-908) or C2 domain of the invertebrate ortholog Pk (Das et al., 2004). This strongly suggests that Pk2 might interact with AnkG through its Ankyrin repeats at the N-ter. In *Drosophila* still, Pk and Vang/Stbm also bind to each other via this domain (Jenny et al., 2003). In a more recent study, the group of Wallingford identified the LIM and C2 domains of Pk2 as critical to promote the planar enrichment of Vangl1 in epidermal cells of *Xenopus*, while the C2 domain (but not the PET or

the LIM domains) was required for Pk2 own planar asymmetry (Butler and Wallingford, 2015). We did not find Vangl2 enriched at the AIS of cortical or hippocampal neurons, but we showed recently that it is present in the axon (Dos Santos Carvalho et al., 2020), a result confirmed by a proximity labeling assay of the AIS (Hamdan et al., 2020).

We also identified Scrib as a novel partner of ßIV spectrin *in vitro*, via its C-ter domain (**Figure 14**). The group of S. Etienne-Manneville reported the interaction of the C-ter of Scrib with ß spectrins, but ßIV spectrin was not tested in this study (Boëda and Etienne-Manneville, 2015). Our results complement these findings and show that Scrib also binds to ßIV spectrin. We did not characterize the domain of interaction of ßIV spectrin with Scrib, but we postulate that it is conserved between all members and corresponds to the calponin homology 1, part of the actin binding domain, identified by Boëda and Etienne-Manneville. Temporally, Scrib vesicles reach the axon a day later than Pk2 and AnkG at DIV2, time at which ßIV spectrin vesicles were also detected. Due to antibody species incompatibilities, we were not able to determine if the profiles of Scrib and ßIV spectrin at this stage were matching or exclusive. By DIV3 and DIV4, Scrib is at the membrane where it displays a shift along the axon towards the cell body. Only by DIV10 do all three proteins perfectly colocalize in the AnkG-defined AIS region.

Altogether, our results suggest that Pk2 and Scrib participate in the early assembly and stabilization of the AIS, via direct binding to AnkG and ßIV spectrin, respectively. We propose that an AnkG/Pk2 complex forms in the earliest steps of AIS assembly at the plasma membrane and in the proximal region of the axon, shortly followed by a ßIV spectrin/Scrib complex. The strong affinity of AnkG and ßIV spectrin for each other bridges the two complexes at the membrane and anchors the four-protein complex to the cytoskeleton, stabilizing it at the AIS (**Figure 14**). We do not discuss in detail the downregulation of Scrib *in vitro* as it is part of another project done as a collaboration. However, preliminary data on Scrib knockdown show a weaker phenotypic profile than that of Pk2, with an AIS that is elongated and with a shifted peak-to-peak distance in respect to the control, but is never absent or fragmented (Montersino et al., in preparation; this work). Scrib would therefore participate in the stabilization of the AIS structure and its final shape, but not its integrity. The longer AIS needs further characterization, and notably the evaluation of AnkG and other AIS components levels. Nevertheless, this phenotype would be consistent with the weakening of the intracellular boundary.

The PCP-AIS protein complex we describe is dependent on AnkG, as when we downregulate AnkG using shRNA, Pk2 and Scrib labeling are absent in the vast majority of the analyzed AIS.

Supporting our results, we found that by DIV16, the profile of Scrib at the AIS described a series of periodic stripes, similar to those reported for F-actin and AnkG or ßIV spectrin (Xu et al., 2013; Leterrier et al., 2015). Our antibody is directed against the C-ter of Scrib, the same region that binds to the actin binding domain of ßIV spectrin. Unfortunately, Pk2

nanolocalization at the AIS did not reveal any concrete pattern and rather showed a random distribution. It may be that our antibody is not fit for such a localization. For AnkG or ßIV spectrin (or Scrib), the antibodies used to identify periodicity are directed towards the N-ter or C-ter of the proteins. Our antibody is raised against a 182 amino-acid portion just after the last LIM domain, roughly in the center of the protein, which might not be appropriate for this type of immunolocalization. But it also may well be that Pk2 is not organized in periodicity.

If we cannot identify Pk2 in a periodical pattern like F-actin, Pk2 depletion in cultured neurons resulted in a disruption of the actin cytoskeleton periodicity at the AIS, a phenotype that is not reported or seen upon depletion of the classical core AIS proteins. Similar effects were found by inhibiting actin associated molecules, such as tropomyosin 3.1 (Tpm 3.1, Abouelezz et al., 2019), downregulating ßII spectrin levels (Zhong et al., 2014) or in axonal degeneration contexts (Unsain et al., 2018); although those were less severe than the ones we report here. It is important to mention that the STORM analysis for the actin periodicity was done on the multi-axon phenotype, and that the different axons have different degrees of severity in phenotype with respect to the actin periodicity disruption. In fact, some of them showed residual levels of periodicity. Detailed quantifications of these profiles would be interesting to determine if the phenotype severity correlates with a stronger decrease of the AIS proteins. For the moment, it is unclear how Pk2 could modulate actin rings formation, but it may do so by regulating actin-associated proteins, like Tpm3.1.

There are few hypotheses in the literature regarding possible molecular mechanisms by which AnkG localization is restricted and stabilized to the proximal region of the axon. One hypothesis argues that the distal axon cytoskeleton (comprising ßII spectrin) restricts AnkG to the proximal axon, hence determining the AIS domain (Galiano et al., 2012). A complementary mechanism was recently proposed in two different studies: Fréal and colleagues showed an AIS feedback-driven assembly mechanism, where NF-186 gets endocytosed in all the neuronal compartments except at the AIS, where it stabilizes AnkG (Fréal et al., 2019). The team of Pete Brophy further proposed that a pool of NF-186 is transported from the soma to the AIS, while another one is initially located at the distal axon and gets progressively restricted to the AIS (Ghosh et al., 2020). While the “proximal” NF-186 would stabilize AnkG, the role for the “distal” NF-186 is not clear but the authors suggest it could be used at the nodes of Ranvier. An early role of Pk2 on the stabilization of AnkG would complement either of these hypotheses.

We believe that Pk2 is required in the earliest stages of AIS assembly, but what about maintenance? We addressed this question by depleting Pk2 at DIV10, once the AIS is established, and only observed a slight reduction of Pk2 and AnkG 15 days after transfection, suggesting that Pk2 is stable once incorporated in the AIS macromolecular complex, and/or with a low turnover ratio. Some core AIS components like NF-186 or Na_v channels share the same stability (Hedstrom et al., 2007; Leterrier et al., 2017). We tried a similar experiment *in vivo* in adult Pk2 floxed mice using with a construct coding for Cre recombinase, and we

obtained strong and broad AnkG labeling 2 or 4 weeks later, inconsistent with a disruption of the AIS (see **Figure 13**).

Our results contrast with a recent study showing that Pk2 downregulation in DIV11 neurons (with a formed AIS) leads to "no AnkG" labeling in about 60% of the shPk2-positive neurons, and 30% with a discontinuous/punctate staining the authors associated with a "fragmented AIS" (Chowdhury et al., 2020). These phenotypes partially resemble the ones we describe with an early downregulation of Pk2, although the number of neurons with a "no AnkG" phenotype they report is strikingly high, and the "fragmented phenotype" seems, under close scrutiny, different from what we describe in our work. In the study, the illustration of this fragmented phenotype shows a strong AnkG staining in the proximal region of the axon, and a weaker AnkG labeling that extends much longer than the regular AIS length. The phenotype we report after an early downregulation of Pk2 affects the entirety of the AnkG domain, from the most proximal region, with a fragmentation of AnkG expression and an overall decrease in AnkG labeling intensity (see **Figure 7B**). Chowdhury and colleagues attributed the observed disruption of the AIS to a lack of intra-axonal boundary, and a role for Pk2 in polarized trafficking of some vesicles, although they do not demonstrate or claim that Pk2 is an AIS protein. Their hypothesis is supported by a mostly distal axon labeling of Pk2 in DIV3 neurons that is almost a mirror distribution to what we report in young neurons, where we see Pk2 restricted to the proximal region of the axon from DIV1. Although we do not have a clear explanation for the discrepancy, it seems that by DIV11, when they transfect the shPk2, the developmental intra-axonal boundary mechanism described by Galiano et al. (2012) would have taken place and be completed, and would then refer more to a loss of maintenance. Differences in targeting sequence of shRNAs, the amounts of cDNA used in their protocol, or the type of transfection approach may explain this difference.

We need to emphasize that none of the previous studies on Pk2 reported the current AIS enrichment we show (Sowers et al., 2013; Hida et al., 2011). This, despite the fact that all of the antibodies, including ours, map a similar antigenic region of Pk2, between aminoacids 345 to 526, just after the LIM domains (Deans et al., 2007). The antibody used in this study was raised by Doris Wu, at NIH/NIDCD, and thoroughly characterized in the inner ear (Jiang et al., 2017; Yang et al., 2017; Deans et al., 2007), but also by our team in the brain, by immunoblots and by immunocytochemistry, in control and mutant animals. We detect a band corresponding to the expected size of Pk2 in both mouse and rat brain lysates, and that same band is absent in the conditional mutants, validating its specificity. But while we could detect the protein in both species by immunoblots, we could only observe the AIS staining by immunocytochemistry in rat tissue/neurons. We did confirm the absence of staining for Pk2 in rat neurons after Pk2 downregulation via the shRNA *in vitro* and *in vivo*. We tested the antibodies used in Sowers et al., 2013 and Hida et al. (2011) on mouse brain and both of them recognize the same band as ours in our hands using immunoblotting.

Are other PCP proteins involved in the assembly and/or regulation of the AIS structure and functions? We were able to detect Dishevelled-2 (Dvl2) vesicles in the axon as early as

DIV3, later than Pk2 or Scrib vesicles (data not shown). By DIV10, the profile of expression of Dvl2 is clearly shifted towards the cell body and away from the AnkG/Pk2/Scrib defined domain. A similar shifted profile was reported for microtubule-associated proteins like TRIM46 and MTCL1 (van Beuningen et al., 2015; Satake et al., 2017), suggesting that Dvl2 could participate in microtubules assembly/stabilization in this compartment. This would fit with the large body of publications regarding Dvl members and their modulation/stabilization of microtubules (Ciani et al., 2004; Ciani and Salinas, 2007; reviewed in Salinas, 2007; Gao and Chen, 2010; Sharma et al., 2018). Pk and Dvl are also known to interact (Tree et al., 2002), and there could be a molecular interplay between Pk2 and Dvl2 the AIS. This will be further explored by the host lab in the near future. Finally, transmembrane core PCP proteins like Vangl2 and Fz3 and Fz6 are present in the young and mature axon, consistent with their role in axonal guidance or axonal outgrowth (Dos Santos Carvalho et al., 2020; reviewed in Wang et al., 2016), but not enriched at the AIS.

Pk2 acute downregulation disrupts neuronal polarity/axonal specification

The literature suggests that AIS assembly happens shortly after axonal specification, at least in hippocampal and cortical neurons (reviewed in Yoshimura and Rasband, 2014), and Pk2 seems to participate in both mechanisms, though it is not always straightforward to discriminate them. The early acute depletion of Pk2 *in vitro* via shRNA has three phenotypic consequences in our hands: neurons with no AIS/axon, neurons with multiple AIS/axons, and neurons with one AIS/axon. The two first suggest a loss of polarity or of axonal specification that we also found *in vivo* after Pk2 depletion *(in utero* electroporation). However, even in Pk2 depleted neurons that established one axon, the AnkG staining was either fragmented and/or reduced. On the other hand, we did not observe this loss of polarity phenotypes in the conditional knockout mouse, even if the levels of AnkG and other AIS proteins were strongly decreased. These results highlight the different degrees of severity in response to the timing or efficiency of the genetic deletion or the acute downregulation of Pk2. One of the corollaries of this is that Pk2 participates not only in AIS assembly but also in neuronal polarity, if downregulated strongly and early enough.

A critical role for Pk1 in apico-basal polarity was first identified in 2009 (Tao et al., 2009). The authors showed that the deletion of Pk1 resulted in early embryonic lethality (embryonic day 6) due to a loss of apico-basal polarity and global disorganization of the epiblast tissue, and that part of this function was due to the PET/LIM domains of Pk1. They concluded that Pk is a conserved regulator of apico-basal polarity in vertebrates. In invertebrate's neurons, a study from 2011 reported that the *Caenorhabditis elegans* ortholog Prickle (PRKL-1) was essential for neurite formation in a subset of peripheral motor neurons (Sanchez-Alvarez et al., 2011). In fact, PRKL-1 deletion led to the production of supernumerary neurites, but its

overexpression resulted in a decreased number of these processes. While this is not the same system and the authors do not distinguish the fate of these extra neurites (axons or dendrites), it still suggests that PRKL-1 affects neuronal polarity establishment in this organism that could be conserved in mammals.

Liu and colleagues showed that downregulation of Pk1 via shRNA or overexpression of truncated constructs of *Pk1* (which they deemed as dominant-negative) causes reduced axonal and dendritic extension in mouse hippocampal neurons (Liu et al., 2013). In their study, the authors claim that "generally" normal specification of dendrite and axon occurs, but offer no further labeling or quantification, and our own quantification show that the "no AIS/axon" phenotype is a small, but significant proportion of the shPk2 transfected neurons (see **Figure 7E**). Their description of "neurons extending short, stubby and punctate dendrites and/or axons" would fit with a loss of polarity. The team of Bassuk observed a different outcome after deletion or overexpression of *Pk2* in mouse hippocampal neurons (Sowers et al., 2013). Using Sholl Analysis they showed that *Prickle2*$^{-/-}$ neurons had a significant decrease in dendritic arborization while overexpression of GFP-tagged wild-type human PRICKLE2 greatly increased dendritic complexity, and even rescued arborization deficits present in *Prickle2*$^{-/-}$ neurons, but in their analysis they did not use specific dendritic, axonal or AIS markers. More recently, and as discussed before, Chowdhury and colleagues reported that Pk2 downregulation in DIV11 neurons leads to a large proportion of neurons with no AnkG that could be neurons with no polarity (Chowdhury et al., 2020).

These three studies used different transfection strategies, all three with lipid-based approaches used after plating the neurons and starting the downregulation or the overexpression of the various constructs from DIV3 (Liu et al., 2013), DIV7 (Sowers et al., 2013) or DIV11 (Chowdhury et al., 2020). This contrasts to the nucleofection approach we used, that allows the expression of the shRNA constructs at the time of plating, an approach that we believe will favor the study of the earliest mechanisms of polarity and AIS assembly.

Of note, although we have not yet quantified it, our own results after Pk2 overexpression suggest an overall decrease in neurite arborization length and complexity, and a complex profile for AIS presence or organization, supporting the idea that a proper Pk2 function requires a dosage, with too little or too much being detrimental. This dosage requirement is typical of core PCP protein function, as their discrete distribution in compartments of the cell determine their function (see Montcouquiol and Kelley, 2020). However, if confirmed, this would contrast with the results of Sowers et al., who reported an increase in arborization in Pk2-overexpressing neurons. The different outcomes may be linked to the different developmental points chosen for genetic manipulation (transfection before plating in this study, at DIV7 in Sowers et al.) and a tight regulation of Pk2 needed for proper neurite development and arborization.

Besides the stabilization of AnkG at the membrane, it is possible that Pk2 contributes to maintaining the uniform polarity of microtubules (MT) in the single neurite that will become

the axon (**Figure 14**)**.** A number of studies reported a link between Pk and tubulin. For example, in *Drosophila* wing and abdomen, Pk has been suggested to bias the apical microtubules plus-ends, and thus the movement of some core PCP vesicles, towards a specific side of the cell (Olofsson et al., 2014), although others challenge this vision (Sharp and Axelrod, 2016 Dev). Another study suggested that Pk promotes and/or stabilizes the proper polarity of axonal microtubules in addition to modulating microtubule growth dynamics in *Drosophila* larval motor neurons (Eihadeb et al., 2014). Our preliminary data in heterologous COS7 cells using the same approach as Fréal et al. in 2016 suggest a relocalization of Flag-Pk2 with AnkG-480-GFP at the distal end of the microtubules (see **Figure 5G**), supporting a link between Pk2 and MT organization. Further experiments assessing the retrograde and anterograde rates of vesicle transport should be performed to determine if the orientation of axonal microtubules in the shPk2 neurons is altered.

Pk2 and Scrib deletion consequences *in vivo* and related pathologies

In vitro, the acute depletion of Pk2 or Scrib have different consequences on the morphology of the neuron, its arborization, its polarization and the AIS structure as discussed before. To assess the structural and functional impact of Pk2 and Scrib *in vivo*, we developed two strategies: we generated conditional mice mutants (cKOs) and used mice and rat *in vivo* depletion.

We developed initially a number of single conditional mutants for *Pk2* and *Scrib* (hereby referred to as $Pk2^{Emx1}$, $Scrib^{Emx1}$, $Pk2^{Nex}$, $Scrib^{Nex}$ and Pk2-$Scrib^{Nex}$). We chose the Nex^{Cre} mice line as it expresses the Cre recombinase in postmitotic, excitatory neurons of the cortex and hippocampus, at the onset of AIS assembly (Goebbels et al., 2006), while the $Emx1^{Cre}$ line will generate an early deletion in neuronal and glial progenitors of the telencephalon (Gorski et al., 2002). Because the early analysis of the $Pk2^{Emx1}$ or $Scrib^{Emx1}$ cKOs showed no strong changes in AnkG immunolabeling, we decided to shift entirely to the study of the double cKOs, Pk2-$Scrib^{Nex}$.

The analysis of AnkG levels in these animals (that needs to be completed) shows a solid reduction of the AnkG-480 isoform, a mild decrease for the 270 kDa isoform and no significant changes for the shortest AnkG-190 kDa isoform as early as P12 and confirmed for AnkG-480 and AnkG-190 by P21 in the cortex. The decrease in AnkG was confirmed by immunohistochemistry on brain sections with two different antibodies, one specific for the AnkG-480 and a global one. Given the similar percentages of decrease with both antibodies, it seems that what we are detecting with the global AnkG antibody is mostly the decrease of the AnkG-480, which is consistent with the immunoblots results. These data suggest that, in addition to participating in their recruitment/retention at the AIS, Pk2 and Scrib also affect the overall levels of AnkG.

Contrasting with this, the levels of ßIV spectrin are unchanged, while the immunoreactivity at the AIS of the mutant's cortices was decreased by 80%. This suggests that the early deletion of Pk2/Scrib does not affect the overall levels of ßIV spectrin, but impacts its recruitment/retention at the AIS. Similar results were obtained with the AnkG (*Ank3*) exon 1b mutant mouse and with the giant AnkG (*Ank3)* exon 37 null mice, where the overall levels of known AnkG binding partners, including various Na_v channels, βIV spectrin, or NF-186 were unchanged while the protein were absent from the AIS (Zhou et al., 1998; Jenkins & Van Bennet, 2001; Jenkins et al., 2015). We have to evaluate NF-186 and Na_v levels by immunoblots, but our preliminary data show that Na_v channels immunolabeling is reduced by 36%.

We want to conduct a similar analysis in the single mutants $Pk2^{Nex}$ and $Scrib^{Nex}$ to assess the impact of the individual deletion of each gene affects the overall levels of AIS components and to validate that the strong decrease in AnkG is due to the combined absence of both genes *in vivo*. Given the interaction between Pk2 and AnkG and the strong effect of Pk2 downregulation on AnkG *in vitro*, we wondered if an acute downregulation of Pk2 could be sufficient to affect the AIS assembly. For this, we performed *in utero* electroporation (IUE) of the same shRNA used *in vitro*. Though there was some variability in terms of excision levels of Pk2, we observed numerous rat cortical neurons with reduced Pk2 levels and reduced or no AnkG labeling. In fact, the levels of GFP seemed to correlate with the decrease in Pk2 and AnkG. We reasoned that the contrasting absence of "no AnkG" phenotype in Pk2-$Scrib^{Nex}$ cKOs is most probably due to the acute nature of the downregulation via the shRNA, while gene compensation may take place in the cKO. Such a scenario was reported to happen in several studies focused on the study of neuronal polarity proteins *in vivo*, where the phenotype observed using IUE was not always replicated by animal models (Namba et al., 2014).

Of note, we attempted IUE of a mouse-specific shRNA for Pk2 in mouse, but our results were unconvincing, notably because of the morphological aspect of most of the shPk2-positive neurons, with a misshaped soma and beads-like axons, typical of distressed neurons, many with reduced levels of AnkG at the AIS (**Annexes, Figure 1**). This is one of the reasons why we moved to rat for IUE analysis.

All of the immunoblots quantifications were done with either P12 or P21/P23 mice cortices, to evaluate the early consequences of Pk2/Scrib deletion. But we need to explore later stages, including aging animals, to confirm/infirm the impact of the genes on the long-term maintenance of the AIS/axon function. For example, the literature has showed that the absence of ßIV spectrin only affects the levels of AnkG in older animals (e.g., 3 months old, Komada and Soriano, 2002).

Autism spectrum disorders and social behavior

Given the results on the decrease of the AIS proteins in our mutants, especially AnkG, and that AnkG animal models have a certain type of disrupted behavior, we plan to perform behavioral tests in our animals, focusing on social behavior. Both *Pk2* and *Scrib* mutant animals were reported to show ASD-like behaviors. The analysis of *Pk2* full KO revealed that these animals had a boosted spatial learning while displaying an altered social behavior as shown by reduced interactions with stranger mice (Sowers et al., 2013). The Sfari database scores *Pk2* as a "strong candidate" for ASD, notably due to heterozygous, rare, non-synonymous *PRICKLE2* variants (E8Q and V153I) that were identified in two ASD cases (Sowers et al., 2013; Tao et al., 2013). The V153I variant is notably interesting as it would affect the LIM domain that we identified as a putative interacting domain with AnkG.

A similar phenotype was found in the heterozygote *circletail* mutant mouse for Scrib (Moreau et al., 2010). While the deletion of both genes is ubiquitous and embryonic in these mice models, both studies focus on specific alterations in the hippocampus and describe in detail defects at the spine level, where both Pk2 and Scrib are present. Based on Nex^{cre} profile of expression, our conditional mutants have a deletion in the postmitotic pyramidal neurons and dentate gyrus mossy and granule cells, but not in proliferating neural precursors of the ventricular zone, interneurons, oligodendrocytes, and astrocytes (Goebbels et al., 2006). In fact, Nex-expressing progenitors are committed to become glutamatergic neurons (Wu et al., 2005). We hope that the results of these analyses will extend our comprehension of a disruption of these genes in ASD-like behavior, by restricting their deletion to a late timing and a specific network. We will obviously not be able to assign an AIS-specific function to our proteins in these behavioral tests, and it is a common and ongoing issue in the field. But at least, we could emphasize that some of the behavioral deficits are not entirely due to synapses deficits, but might have an AIS component to them, as it was suggested for some AIS genes found mutated in autistic patients (Hatzimanolis et al., 2012; Weiss et al., 2003).

On the other hand, electrophysiology can directly evaluate the excitability of the axon and the AIS component to an action potential (AP). Preliminary data from our collaborator Dr. Arne Battefeld (IMN, Bordeaux) on DIV7/8 control and shPk2 nucleofected neurons showed that Pk2-depleted cells are able to fire APs, but these are generated at a higher threshold and with a lower frequency, suggesting that these neurons are overall less excitable (**Annexes, Figure 2**). This firing profile fit with the Na_v channels decrease we quantified and is similar to the work from Zhou et al. on AnkG exon 1b mutants (Zhou et al., 1998). Analysis of the more AIS-specific giant AnkG mutant mouse (deletion of AnkG 480 and 270 isoforms) resulted in defective APs generation, with reduced frequency but unaffected threshold (Jenkins et al., 2015). However, in that mutant the AnkG-190 kDa isoform was strongly upregulated, mitigating the results. The strong increase in the synaptic AnkG-190 isoform could explain why the threshold is not affected, as the postsynaptic potentials may remain intact. Our

conditional mutants show a decrease of Na_v channels but unchanged levels of AnkG-190 kDa, so it is possible that our mice will display a firing behavior closer to that mutant.

Epilepsy and seizures

However, this reduced excitability would be in contrast with the lower threshold for developing seizures recorded in the *Pk2* full KO and associated with increased excitability of the neurons (Tao et al., 2011). In their study, the authors showed that *Prickle2*-null mice were viable, but had an increased seizure rate compared to heterozygous mice, indicating a dosage effect. In the same study and an additional one, point mutations where identified on *PK2* in the sister and her brother with severe progressive myoclonic epilepsy (Bird and Shaw, 1978; Tao et al. 2011). Both mutations are projected to result in amino acid changes again in the LIM domain of Pk2 (R148H; V153I) and studies in zebrafish embryos showed that their overexpression resulted in increased Pk2 activity compared to WT when using the planar polarity convergent-extension movements as a functional readout A few years later, Sandford and colleagues (2016) determined that the reported phenotype might be due to a mutation on the *POLG* gene and not from the Pk2 variants, but the original authors maintained their claim (Mahajan and Bassuk, 2016; Tao et al., 2011) (see OMIM 608501). Beyond the controversy, we are curious about the consequences of *Pk2* and *Scrib* single or double deletion on the eventual seizure susceptibility of the mice, or on the axonal excitability after an *in vivo* acute downregulation of Scrib and Pk2 in cortical neurons. While our mutants do not apparently experience spontaneous seizures, an experimental approach based on seizure induction would reveal if these mice have a lower threshold for seizure development than the controls. However, if a reduction of the AIS Na_v channels results in a decrease of neuron excitability, how could this fit with a possible contribution of Pk2 (and potentially Scrib) at the AIS to an epileptic phenotype?

One answer to this conundrum might come from the neuronal type diversity. If we look at the numerous AnkG mutants, only two display epileptic/seizures behavior, which are associated with increased axonal excitability (Lopez et al., 2017). Lopez and colleagues looked into the electrical activity on the cortex of 8-10 weeks old AnkG (*Ank3*)$^{\text{exon 1b}}$ mutant mice. They showed, using electroencephalogram analyses, that AnkG (*Ank3*)$^{\text{exon 1b}}$ +/- and AnkG (*Ank3*)$^{\text{exon 1b}}$ -/- mice had frequent seizures, dependent on AnkG dosage, with AnkG *(Ank3)* $^{\text{exon 1b}}$ -/- suffering further rare convulsions and death, reminiscent of the original observations by Zhou et al. in 1998. The exon 1b of AnkG (*Ank3*) encodes an AnkG splice that is heavily present in the cerebellum, and is the only forms present in PV-positive interneurons (notably in the cortex and hippocampus), while other neuronal types, like granule cells of the hippocampus, can be reactive to a different isoform or a combination of isoforms. This strongly suggests that the seizure phenotype observed in the AnkG (*Ank3*)$^{\text{exon 1b}}$ mutant is mostly due to the PV-positive neuronal disruption. In support for this, in 2017 Zhu and colleagues crossed the AnkG (*Ank3*) exon 22-23 floxed mice (targeting all the AnkG isoforms) with a CAMKIIa-Cre mice

(AnkG (Ank3)$^{22\text{-}23}$ CamKIIa-Cre cKO), and observed mostly bipolar-like disorders, but not seizures or epileptic-like behaviors. When Lopez et al. crossed the same exon 22-23 floxed mouse with a PV-cre mice line, they showed that these mutant mice had seizures, similar to the AnkG (*Ank3*) exon 1b mutants. Since AnkG was only deleted in the inhibitory neurons, this strongly suggested that the epilepsy was due to a decrease of inhibition on glutamatergic neurons, resulting in increased axonal excitability.

Finally, in 2015, Jenkins and Van Bennett showed that a mouse with a floxed exon 37 crossed with a Nestin-Cre line (deleting AnkG-270 and AnkG-480, AnkG (*Ank3*)$^{\text{exon 37}}$ Nestin-Cre cKO) resulted in mice surviving 20 days, with a reduction of AP kinetics and frequency, thereby reducing the synchronization of neurons without impacting the AP generation, in contrast to the increased AP threshold in AnkG (*Ank3*) $^{\text{exon 1b}}$-/- mutant.

These studies show that the phenotypic outcome is different depending on the network or the cell type affected. The deletion of *Pk2* and *Scrib* in our Pk2-Scrib^{Nex} mutants is specific to excitatory neurons. It is therefore key to confirm that both our proteins are present at the AIS of inhibitory cells, which would reveal a crucial role on regulating neuronal excitation/inhibition balance, as its dysfunction is related with epilepsy (Peng et al., 2013). A decrease of excitability in these neurons via the AIS would explain a global effect and a network dysregulation. So far, our preliminary data for Pk2 suggest that the protein is indeed present in PV-positive neurons (see **Figure 1 C**).

Pk2 and Scrib are present at the dendritic spines and mutants for both proteins have abnormal postsynaptic currents. In fact, and in line with the morphological defects observed at the PSD, mini excitatory post synaptic current (mEPSC) frequencies were reduced in Pk2 and Scrib mutants (Sowers et al., 2013; Moreau et al., 2010). This implies that the postsynaptic neuron is going to have less chances of being depolarized, hence of generating an action potential. The possible defects in action potential firing of our mutants could then be a mix of dysfunctional dendritic spines which, altogether, would modulate neuronal excitability.

Is the AIS the neuronal PCP?

The polarized status of a neuron is a superb visual example of cell compartmentalization that results in both a morphological and functional specialization. But while the axon/somatodendritic compartment segregation is accepted as the equivalent to the apical/basolateral domain of the epithelial cells, the definition of planar polarity in neurons is still lacking, for a lack of a plane of reference. If we extrapolate the definition of a PCP axis and PCP proteins from the epithelia, and based on our current data, we could propose that the AIS represents the PCP of the neuron, with similar criteria:

In epithelial cells:

- A/B polarity establishment is needed before PCP.
- PCP proteins are asymmetrically distributed within the plane of the epithelium.
- PCP proteins asymmetry organize the cytoskeleton to define a PCP axis, in the apical domain, and parallel to the plane of the epithelium.

In neuronal cells:

- An axon/somatodendritic polarity establishment is needed before AIS formation.
- (some) PCP proteins are asymmetrically distributed within the neuron.
- PCP proteins asymmetry organize the cytoskeleton, in the axon.

Altogether, this work offers an original vision on the role of some members of the PCP family in neuronal function, and support the idea that PCP signaling is important for brain development and function.

List of references

Abouelezz, A. *et al.* Tropomyosin Tpm3.1 Is Required to Maintain the Structure and Function of the Axon Initial Segment. *iScience* **23**, 101053 (2020).

Abouelezz, A., Micinski, D., Lipponen, A. & Hotulainen, P. Sub-membranous actin rings in the axon initial segment are resistant to the action of latrunculin. *Biol. Chem.* **400**, 1141–1146 (2019).

Adler, P. N. & Wallingford, J. B. From Planar Cell Polarity to Ciliogenesis and Back: The Curious Tale of the PPE and CPLANE proteins. *Trends Cell Biol* **27**, 379–390 (2017).

Adler, P. N. The frizzled/stan pathway and planar cell polarity in the Drosophila wing. *Curr Top Dev Biol* **101**, 1–31 (2012).

Adler, P. N. Planar signaling and morphogenesis in Drosophila. *Dev Cell* **2**, 525–535 (2002).

Adler, P. N., Charlton, J. & Liu, J. Mutations in the cadherin superfamily member gene dachsous cause a tissue polarity phenotype by altering frizzled signaling. *Development* **125**, 959–968 (1998).

Adler, P. N., Taylor, J. & Charlton, J. The domineering non-autonomy of frizzled and Van Gogh clones in the Drosophila wing is a consequence of a disruption in local signaling. *Mechanisms of Development* **96**, 197–207 (2000).

Adler, P. N., Zhu, C. & Stone, D. Inturned localizes to the proximal side of wing cells under the instruction of upstream planar polarity proteins. *Curr Biol* **14**, 2046–2051 (2004).

Albertson, R., Chabu, C., Sheehan, A. & Doe, C. Q. Scribble protein domain mapping reveals a multistep localization mechanism and domains necessary for establishing cortical polarity. *Journal of Cell Science* **117**, 6061–6070 (2004).

Alpizar, S. A., Baker, A. L., Gulledge, A. T. & Hoppa, M. B. Loss of Neurofascin-186 Disrupts Alignment of AnkyrinG Relative to Its Binding Partners in the Axon Initial Segment. *Front Cell Neurosci* **13**, 1 (2019).

Ambegaonkar, A. A. & Irvine, K. D. Coordination of planar cell polarity pathways through Spiny-legs. *Elife* **4**, (2015).

Amiet, C. *et al.* Epilepsy in autism is associated with intellectual disability and gender: evidence from a meta-analysis. *Biol Psychiatry* **64**, 577–582 (2008).

Anda, F. C. de, Meletis, K., Ge, X., Rei, D. & Tsai, L.-H. Centrosome Motility Is Essential for Initial Axon Formation in the Neocortex. *J. Neurosci.* **30**, 10391–10406 (2010).

Angelides, K. J., Elmer, L. W., Loftus, D. & Elson, E. Distribution and lateral mobility of voltage-dependent sodium channels in neurons. *J Cell Biol* **106**, 1911–1925 (1988).

Ango, F. *et al.* Ankyrin-based subcellular gradient of neurofascin, an immunoglobulin family protein, directs GABAergic innervation at purkinje axon initial segment. *Cell* **119**, 257–272 (2004).

Araki, T. & Otani, T. Response of single motoneurons to direct stimulation in toad's spinal cord. *J Neurophysiol* **18**, 472–485 (1955).

Assémat, E., Bazellières, E., Pallesi-Pocachard, E., Le Bivic, A. & Massey-Harroche, D. Polarity complex proteins. *Biochim Biophys Acta* **1778**, 614–630 (2008).

Atapour, N. & Rosa, M. G. P. Age-related plasticity of the axon initial segment of cortical pyramidal cells in marmoset monkeys. *Neurobiol Aging* **57**, 95–103 (2017).

Audebert, S. *et al.* Mammalian Scribble forms a tight complex with the betaPIX exchange factor. *Curr Biol* **14**, 987–995 (2004).

Axelrod, J. D. & McNeill, H. Coupling planar cell polarity signaling to morphogenesis. *ScientificWorldJournal* **2**, 434–454 (2002).

Axelrod, J. D. Progress and challenges in understanding planar cell polarity signaling. *Seminars in Cell & Developmental Biology* **20**, 964–971 (2009).

Axelrod, J. D. Unipolar membrane association of Dishevelled mediates Frizzled planar cell polarity signaling. *Genes Dev* **15**, 1182–1187 (2001).

Axelrod, J. D., Miller, J. R., Shulman, J. M., Moon, R. T. & Perrimon, N. Differential recruitment of Dishevelled provides signaling specificity in the planar cell polarity and Wingless signaling pathways. *Genes Dev* **12**, 2610–2622 (1998).

Ayukawa, T. *et al.* Dachsous-dependent asymmetric localization of spiny-legs determines planar cell polarity orientation in Drosophila. *Cell Rep* **8**, 610–621 (2014).

Baas, P. W. & Lin, S. Hooks and comets: The story of microtubule polarity orientation in the neuron. *Devel Neurobio* **71**, 403–418 (2011).

Baas, P. W., Black, M. M. & Banker, G. A. Changes in microtubule polarity orientation during the development of hippocampal neurons in culture. *J Cell Biol* **109**, 3085–3094 (1989).

Baas, P. W., Deitch, J. S., Black, M. M. & Banker, G. A. Polarity orientation of microtubules in hippocampal neurons: uniformity in the axon and nonuniformity in the dendrite. *Proc Natl Acad Sci U S A* **85**, 8335–8339 (1988).

Baas, P., Ahmad, F., Pienkowski, T., Brown, A. & Black, M. Sites of microtubule stabilization for the axon. *J. Neurosci.* **13**, 2177–2185 (1993).

Banker, G. & Goslin, K. Developments in neuronal cell culture. *Nature* **336**, 185–186 (1988).
Banker, G. The Development of Neuronal Polarity: A Retrospective View. *J. Neurosci.* **38**, 1867–1873 (2018).

Baraban, S. C. Emerging epilepsy models: insights from mice, flies, worms and fish. *Curr Opin Neurol* **20**, 164–168 (2007).

Barnes, A. P. & Polleux, F. Establishment of Axon-Dendrite Polarity in Developing Neurons. *Annu. Rev. Neurosci.* **32**, 347–381 (2009).

Barnes, A. P. *et al.* LKB1 and SAD Kinases Define a Pathway Required for the Polarization of Cortical Neurons. *Cell* **129**, 549–563 (2007).

Barry, J. *et al.* Ankyrin-G Directly Binds to Kinesin-1 to Transport Voltage-Gated Na+ Channels into Axons. *Dev Cell* **28**, 117–131 (2014).

Bassuk, A. G. *et al.* A homozygous mutation in human PRICKLE1 causes an autosomal-recessive progressive myoclonus epilepsy-ataxia syndrome. *Am J Hum Genet* **83**, 572–581 (2008).

Bastock, R., Strutt, H. & Strutt, D. Strabismus is asymmetrically localised and binds to Prickle and Dishevelled during Drosophila planar polarity patterning. *Development* **130**, 3007–3014 (2003).

Battaglia, A. *et al.* Confirmation of chromosomal microarray as a first-tier clinical diagnostic test for individuals with developmental delay, intellectual disability, autism spectrum disorders and dysmorphic features. *Eur J Paediatr Neurol* **17**, 589–599 (2013).

Battefeld, A., Tran, B. T., Gavrilis, J., Cooper, E. C. & Kole, M. H. P. Heteromeric Kv7.2/7.3 channels differentially regulate action potential initiation and conduction in neocortical myelinated axons. *J Neurosci* **34**, 3719–3732 (2014).

Bazellières, E., Aksenova, V., Barthélémy-Requin, M., Massey-Harroche, D. & Le Bivic, A. Role of the Crumbs proteins in ciliogenesis, cell migration and actin organization. *Seminars in Cell & Developmental Biology* **81**, 13–20 (2018).

Beaumont, M. *et al.* Targeted panel sequencing establishes the implication of planar cell polarity pathway and involves new candidate genes in neural tube defect disorders. *Hum Genet* **138**, 363–374 (2019).

Bellaïche, Y., Gho, M., Kaltschmidt, J. A., Brand, A. H. & Schweisguth, F. Frizzled regulates localization of cell-fate determinants and mitotic spindle rotation during asymmetric cell division. *Nat Cell Biol* **3**, 50–57 (2001).

Ben-Ari, Y. Excitatory actions of gaba during development: the nature of the nurture. *Nature Reviews Neuroscience* **3**, 728–739 (2002).

Bender, K. J. & Trussell, L. O. Axon Initial Segment Ca2+ Channels Influence Action Potential Generation and Timing. *Neuron* **61**, 259–271 (2009).

Bennett, V. & Lorenzo, D. N. Spectrin- and ankyrin-based membrane domains and the evolution of vertebrates. *Curr Top Membr* **72**, 1–37 (2013).

Bennett, V. & Stenbuck, P. J. Identification and partial purification of ankyrin, the high affinity membrane attachment site for human erythrocyte spectrin. *J Biol Chem* **254**, 2533–2541 (1979).

Bennett, V., Davis, J. & Fowler, W. E. Brain spectrin, a membrane-associated protein related in structure and function to erythrocyte spectrin. *Nature* **299**, 126–131 (1982).

Bentley, M. & Banker, G. The cellular mechanisms that maintain neuronal polarity. *Nat Rev Neurosci* **17**, 611–622 (2016).

Berger, S. L. *et al.* Localized Myosin II Activity Regulates Assembly and Plasticity of the Axon Initial Segment. *Neuron* **97**, 555-570.e6 (2018).

Berghs, S. *et al.* betaIV spectrin, a new spectrin localized at axon initial segments and nodes of ranvier in the central and peripheral nervous system. *J Cell Biol* **151**, 985–1002 (2000).

Bertet, C. & Lecuit, T. Planar polarity and short-range polarization in Drosophila embryos. *Semin Cell Dev Biol* **20**, 1006–1013 (2009).

Bertet, C., Sulak, L. & Lecuit, T. Myosin-dependent junction remodelling controls planar cell intercalation and axis elongation. *Nature* **429**, 667–671 (2004).

Bhanot, P. *et al.* Frizzled and Dfrizzled-2 function as redundant receptors for Wingless during Drosophila embryonic development. *Development* **126**, 4175–4186 (1999).

Bhat, K. M. frizzled and frizzled 2 play a partially redundant role in wingless signaling and have similar requirements to wingless in neurogenesis. *Cell* **95**, 1027–1036 (1998).

Bilder, D. & Perrimon, N. Localization of apical epithelial determinants by the basolateral PDZ protein Scribble. *Nature* **403**, 676–680 (2000).

Blot, A. & Barbour, B. Ultra-rapid axon-axon ephaptic inhibition of cerebellar Purkinje cells by the pinceau. *Nat Neurosci* **17**, 289–295 (2014).

Boëda, B. & Etienne-Manneville, S. Spectrin binding motifs regulate Scribble cortical dynamics and polarity function. *Elife* **4**, (2015).

Boiko, T. *et al.* Ankyrin-Dependent and -Independent Mechanisms Orchestrate Axonal Compartmentalization of L1 Family Members Neurofascin and L1/Neuron–Glia Cell Adhesion Molecule. *J. Neurosci.* **27**, 590–603 (2007).

Boiko, T. *et al.* Functional specialization of the axon initial segment by isoform-specific sodium channel targeting. *J Neurosci* **23**, 2306–2313 (2003).

Bonello, T. T. & Peifer, M. Scribble: A master scaffold in polarity, adhesion, synaptogenesis, and proliferation. *J Cell Biol* **218**, 742–756 (2019).

Bosoi, C. M. *et al.* Identification and characterization of novel rare mutations in the planar cell polarity gene PRICKLE1 in human neural tube defects. *Hum Mutat* **32**, 1371–1375 (2011).

Boutros, M. & Mlodzik, M. Dishevelled: at the crossroads of divergent intracellular signaling pathways. *Mech Dev* **83**, 27–37 (1999).

Boutros, M., Paricio, N., Strutt, D. I. & Mlodzik, M. Dishevelled activates JNK and discriminates between JNK pathways in planar polarity and wingless signaling. *Cell* **94**, 109–118 (1998).

Bradke, F. & Dotti, C. G. Neuronal polarity: vectorial cytoplasmic flow precedes axon formation. *Neuron* **19**, 1175–1186 (1997).

Bradke, F. & Dotti, C. G. The role of local actin instability in axon formation. *Science* **283**, 1931–1934 (1999).

Bréchet, A. *et al.* Protein kinase CK2 contributes to the organization of sodium channels in axonal membranes by regulating their interactions with ankyrin G. *J Cell Biol* **183**, 1101–1114 (2008).

Brenner, S. L. & Korn, E. D. Spectrin-actin interaction. Phosphorylated and dephosphorylated spectrin tetramer cross-link F-actin. *J Biol Chem* **254**, 8620–8627 (1979).

Brittle, A. L., Repiso, A., Casal, J., Lawrence, P. A. & Strutt, D. Four-jointed modulates growth and planar polarity by reducing the affinity of dachsous for fat. *Curr Biol* **20**, 803–810 (2010).

Buechling, T. & Boutros, M. Wnt signaling signaling at and above the receptor level. *Curr Top Dev Biol* **97**, 21–53 (2011).

Burridge, K., Kelly, T. & Mangeat, P. Nonerythrocyte spectrins: actin-membrane attachment proteins occurring in many cell types. *J Cell Biol* **95**, 478–486 (1982).

Butler, M. T. & Wallingford, J. B. Control of vertebrate core planar cell polarity protein localization and dynamics by Prickle 2. *Development* **142**, 3429–3439 (2015).

Butler, M. T. & Wallingford, J. B. Planar cell polarity in development and disease. *Nat Rev Mol Cell Biol* **18**, 375–388 (2017).

de Anda, F. C., Meletis, K., Ge, X., Rei, D. & Tsai, L.-H. Centrosome motility is essential for initial axon formation in the neocortex. *J Neurosci* **30**, 10391–10406 (2010).

Callewaert, G., Eilers, J. & Konnerth, A. Axonal calcium entry during fast 'sodium' action potentials in rat cerebellar Purkinje neurones. *J Physiol* **495 (Pt 3)**, 641–647 (1996).

Carr, D. *et al.* A Farnesyltransferase Acts to Inhibit Ectopic Neurite Formation in C. elegans. *PLoS One* **11**, e0157537 (2016).

Carreira-Barbosa, F. *et al.* Flamingo regulates epiboly and convergence/extension movements through cell cohesive and signalling functions during zebrafish gastrulation. *Development* **136**, 383–392 (2009).

Carreira-Barbosa, F. *et al.* Prickle 1 regulates cell movements during gastrulation and neuronal migration in zebrafish. *Development* **130**, 4037–4046 (2003).

Casal, J., Ibáñez-Jiménez, B. & Lawrence, P. A. Planar cell polarity: the prickle gene acts independently on both the Ds/Ft and the Stan/Fz systems. *Development* **145**, (2018).

Casal, J., Lawrence, P. A. & Struhl, G. Two separate molecular systems, Dachsous/Fat and Starry night/Frizzled, act independently to confer planar cell polarity. *Development* **133**, 4561–4572 (2006).

Catterall, W. A. From Ionic Currents to Molecular Mechanisms: The Structure and Function of Voltage-Gated Sodium Channels. *Neuron* **26**, 13–25 (2000).

Catterall, W. A. Localization of sodium channels in cultured neural cells. *J Neurosci* **1**, 777–783 (1981).

Catterall, W. A., Lenaeus, M. J. & Gamal El-Din, T. M. Structure and Pharmacology of Voltage-Gated Sodium and Calcium Channels. *Annu Rev Pharmacol Toxicol* **60**, 133–154 (2020).

Chand, A. N., Galliano, E., Chesters, R. A. & Grubb, M. S. A Distinct Subtype of Dopaminergic Interneuron Displays Inverted Structural Plasticity at the Axon Initial Segment. *Journal of Neuroscience* **35**, 1573–1590 (2015).

Chen, Y. M. *et al.* Microtubule affinity-regulating kinase 2 functions downstream of the PAR-3/PAR-6/atypical PKC complex in regulating hippocampal neuronal polarity. *Proc Natl Acad Sci U S A* **103**, 8534–8539 (2006).

Cho, B., Pierre-Louis, G., Sagner, A., Eaton, S. & Axelrod, J. D. Clustering and negative feedback by endocytosis in planar cell polarity signaling is modulated by ubiquitinylation of prickle. *PLoS Genet* **11**, e1005259 (2015).

Choi, J., Troyanovsky, R. B., Indra, I., Mitchell, B. J. & Troyanovsky, S. M. Scribble, Erbin, and Lano redundantly regulate epithelial polarity and apical adhesion complex. Journal of Cell Biology **218**, 2277–2293 (2019).

Chowdhury, M. I. H. *et al.* Prickle2 and Igsf9b Coordinately Regulate the Cytoarchitecture of the Axon Initial Segment. *Cell Struct Funct* **45**, 143–154 (2020).

Chu, C.-W. & Sokol, S. Y. Wnt proteins can direct planar cell polarity in vertebrate ectoderm. *Elife* **5**, (2016).

Ciani, L., Krylova, O., Smalley, M. J., Dale, T. C. & Salinas, P. C. A divergent canonical WNT-signaling pathway regulates microtubule dynamics: dishevelled signals locally to stabilize microtubules. *J Cell Biol* **164**, 243–253 (2004).

Ciani, L. & Salinas, P. C. c-Jun N-terminal kinase (JNK) cooperates with Gsk3beta to regulate Dishevelled-mediated microtubule stability. *BMC Cell Biol* **8**, 27 (2007).

Clarke, M. Isolation and characterization of a water-soluble protein from bovine erythrocyte membranes. *Biochem Biophys Res Commun* **45**, 1063–1070 (1971).

Classen, A.-K., Anderson, K. I., Marois, E. & Eaton, S. Hexagonal packing of Drosophila wing epithelial cells by the planar cell polarity pathway. *Dev Cell* **9**, 805–817 (2005).

Coombs, J. S., Curtis, D. R. & Eccles, J. C. The interpretation of spike potentials of motoneurones. *J Physiol* **139**, 198–231 (1957).

Costa, A. R. *et al.* The membrane periodic skeleton is an actomyosin network that regulates axonal diameter and conduction. *Elife* **9**, (2020).

Costa, A. R., Pinto-Costa, R., Sousa, S. C. & Sousa, M. M. The Regulation of Axon Diameter: From Axonal Circumferential Contractility to Activity-Dependent Axon Swelling. *Front. Mol. Neurosci.* **11**, (2018).

Courbard, J.-R., Djiane, A., Wu, J. & Mlodzik, M. The apical/basal-polarity determinant Scribble cooperates with the PCP core factor Stbm/Vang and functions as one of its effectors. *Dev Biol* **333**, 67–77 (2009).

Cruz, D. A., Lovallo, E. M., Stockton, S., Rasband, M. & Lewis, D. A. Postnatal development of synaptic structure proteins in pyramidal neuron axon initial segments in monkey prefrontal cortex. *J Comp Neurol* **514**, 353–367 (2009).

Cukier, H. N. *et al.* Exome sequencing of extended families with autism reveals genes shared across neurodevelopmental and neuropsychiatric disorders. *Mol Autism* **5**, 1 (2014).

Cullen, C. L. *et al.* Periaxonal and nodal plasticity modulate action potential conduction in the adult mouse brain. *bioRxiv* (2019) doi: 10.1101/726760.

Curtin, J. A. *et al.* Mutation of Celsr1 disrupts planar polarity of inner ear hair cells and causes severe neural tube defects in the mouse. *Curr Biol* **13**, 1129–1133 (2003).

Deardorff, M. A., Tan, C., Conrad, L. J. & Klein, P. S. Frizzled-8 is expressed in the Spemann organizer and plays a role in early morphogenesis. *Development* **125**, 2687–2700 (1998).

D'Este, E., Kamin, D., Balzarotti, F. & Hell, S. W. Ultrastructural anatomy of nodes of Ranvier in the peripheral nervous system as revealed by STED microscopy. *PNAS* **114**, E191–E199 (2017).

D'Este, E., Kamin, D., Göttfert, F., El-Hady, A. & Hell, S. W. STED Nanoscopy Reveals the Ubiquity of Subcortical Cytoskeleton Periodicity in Living Neurons. *Cell Reports* **10**, 1246–1251 (2015).

Darken, R. S. *et al.* The planar polarity gene strabismus regulates convergent extension movements in Xenopus. *EMBO J* **21**, 976–985 (2002).

Das, G., Jenny, A., Klein, T. J., Eaton, S. & Mlodzik, M. Diego interacts with Prickle and Strabismus/Van Gogh to localize planar cell polarity complexes. *Development* **131**, 4467–4476 (2004).

Davis, J. Q. & Bennett, V. Ankyrin binding activity shared by the neurofascin/L1/NrCAM family of nervous system cell adhesion molecules. *J Biol Chem* **269**, 27163–27166 (1994).

Davis, J. Q., Lambert, S. & Bennett, V. Molecular composition of the node of Ranvier: identification of ankyrin-binding cell adhesion molecules neurofascin (mucin+/third FNIII domain-) and NrCAM at nodal axon segments. *J Cell Biol* **135**, 1355–1367 (1996).

Davis, J. Q., McLaughlin, T. & Bennett, V. Ankyrin-binding proteins related to nervous system cell adhesion molecules: candidates to provide transmembrane and intercellular connections in adult brain. *J Cell Biol* **121**, 121–133 (1993).

Davis, L. H., Davis, J. Q. & Bennett, V. Ankyrin regulation: an alternatively spliced segment of the regulatory domain functions as an intramolecular modulator. *Journal of Biological Chemistry* **267**, 18966–18972 (1992).

Dawid, I. B., Breen, J. J. & Toyama, R. LIM domains: multiple roles as adapters and functional modifiers in protein interactions. *Trends Genet* **14**, 156–162 (1998).

de Anda, F. C. *et al.* Centrosome localization determines neuronal polarity. *Nature* **436**, 704–708 (2005).

de la Hoz, A. B. *et al.* 3p14 De Novo Interstitial Microdeletion in a Patient with Intellectual Disability and Autistic Features with Language Impairment: A Comparison with Similar Cases. *Case Rep Genet* **2015**, 876348 (2015).

De Marco, P. *et al.* Genetic analysis of disheveled 2 and disheveled 3 in human neural tube defects. *J Mol Neurosci* **49**, 582–588 (2013).

Deans, M. R. *et al.* Asymmetric distribution of prickle-like 2 reveals an early underlying polarization of vestibular sensory epithelia in the inner ear. *J Neurosci* **27**, 3139–3147 (2007).

Deardorff, M. A., Tan, C., Conrad, L. J. & Klein, P. S. Frizzled-8 is expressed in the Spemann organizer and plays a role in early morphogenesis. *Development* **125**, 2687–2700 (1998).

DeFelipe, J. Chandelier cells and epilepsy. *Brain* **122 (Pt 10)**, 1807–1822 (1999).

Devaux, J. J., Kleopa, K. A., Cooper, E. C. & Scherer, S. S. KCNQ2 is a nodal K+ channel. *J Neurosci* **24**, 1236–1244 (2004).

Devenport, D. & Fuchs, E. Planar polarization in embryonic epidermis orchestrates global asymmetric morphogenesis of hair follicles. *Nat Cell Biol* **10**, 1257–1268 (2008).

Devenport, D. The cell biology of planar cell polarity. *J Cell Biol* **207**, 171–179 (2014).

Devenport, D. Tissue morphodynamics: Translating planar polarity cues into polarized cell behaviors. *Seminars in Cell & Developmental Biology* **55**, 99–110 (2016).

Di Re, J., Kayasandik, C., Botello-Lins, G., Labate, D. & Laezza, F. Imaging of the Axon Initial Segment. *Curr Protoc Neurosci* **89**, e78 (2019).

Ding, Y., Chen, T., Wang, Q., Yuan, Y. & Hua, T. Axon initial segment plasticity accompanies enhanced excitation of visual cortical neurons in aged rats. *Neuroreport* **29**, 1537–1543 (2018).

Dogterom, M. & Koenderink, G. H. Actin-microtubule crosstalk in cell biology. *Nat Rev Mol Cell Biol* **20**, 38–54 (2019).

Dos-Santos Carvalho, S. *et al.* Vangl2 acts at the interface between actin and N-cadherin to modulate mammalian neuronal outgrowth. *Elife* **9**, (2020).

Dotti, C. G., Sullivan, C. A. & Banker, G. A. The establishment of polarity by hippocampal neurons in culture. *J Neurosci* **8**, 1454–1468 (1988).

Duflocq, A., Le Bras, B., Bullier, E., Couraud, F. & Davenne, M. Nav1.1 is predominantly expressed in nodes of Ranvier and axon initial segments. *Mol Cell Neurosci* **39**, 180–192 (2008).

Eaton, M. *et al.* Characterization of a gene-trap knockout mouse model of Scn2a encoding voltage-gated sodium channel Nav1.2. *bioRxiv* (2020) doi: 10.1101/2020.06.23.150367.

Ehaideb, S. N. *et al.* prickle modulates microtubule polarity and axonal transport to ameliorate seizures in flies. *Proceedings of the National Academy of Sciences* **111**, 11187–11192 (2014).

Enkhbayar, P., Kamiya, M., Osaki, M., Matsumoto, T. & Matsushima, N. Structural principles of leucine-rich repeat (LRR) proteins. *Proteins* **54**, 394–403 (2004).

Ernst, A. *et al.* A structural portrait of the PDZ domain family. *J Mol Biol* **426**, 3509–3519 (2014).

Eshed, Y. *et al.* Gliomedin mediates Schwann cell-axon interaction and the molecular assembly of the nodes of Ranvier. *Neuron* **47**, 215–229 (2005).

Etheridge, S. L. *et al.* Murine dishevelled 3 functions in redundant pathways with dishevelled 1 and 2 in normal cardiac outflow tract, cochlea, and neural tube development. *PLoS Genet* **4**, e1000259 (2008).

Etienne-Manneville, S. & Hall, A. Cell polarity: Par6, aPKC and cytoskeletal crosstalk. *Curr Opin Cell Biol* **15**, 67–72 (2003).

Etienne-Manneville, S. & Hall, A. Rho GTPases in cell biology. *Nature* **420**, 629–635 (2002).

Evans, M. D., Dumitrescu, A. S., Kruijssen, D. L. H., Taylor, S. E. & Grubb, M. S. Rapid Modulation of Axon Initial Segment Length Influences Repetitive Spike Firing. *Cell Rep* **13**, 1233–1245 (2015).

Ewen-Campen, B., Comyn, T., Vogt, E. & Perrimon, N. No Evidence that Wnt Ligands Are Required for Planar Cell Polarity in Drosophila. *Cell Reports* **32**, (2020).

Ezan, J. & Montcouquiol, M. Revisiting planar cell polarity in the inner ear. *Semin Cell Dev Biol* **24**, 499–506 (2013).

Farías, G. G., Guardia, C. M., Britt, D. J., Guo, X. & Bonifacino, J. S. Sorting of Dendritic and Axonal Vesicles at the Pre-axonal Exclusion Zone. *Cell Rep* **13**, 1221–1232 (2015).

Fassio, A. *et al.* SYN1 loss-of-function mutations in autism and partial epilepsy cause impaired synaptic function. *Hum Mol Genet* **20**, 2297–2307 (2011).

Feng, B. *et al.* Protecting synapses from amyloid β-associated degeneration by manipulations of Wnt/planar cell polarity signaling. *bioRxiv* (2020) doi:10.1101/2020.09.09.273011.

Feng, Y. & Irvine, K. D. Fat and expanded act in parallel to regulate growth through warts. *Proc Natl Acad Sci U S A* **104**, 20362–20367 (2007).

Fenstermaker, A. G. *et al.* Wnt/planar cell polarity signaling controls the anterior-posterior organization of monoaminergic axons in the brainstem. *J Neurosci* **30**, 16053–16064 (2010).

Fietz, S. A. & Huttner, W. B. Cortical progenitor expansion, self-renewal and neurogenesis-a polarized perspective. *Curr Opin Neurobiol* **21**, 23–35 (2011).

Flynn, K. C., Pak, C. W., Shaw, A. E., Bradke, F. & Bamburg, J. R. Growth cone-like waves transport actin and promote axonogenesis and neurite branching. *Dev Neurobiol* **69**, 761–779 (2009).

Franke, J. D., Montague, R. A. & Kiehart, D. P. Nonmuscle myosin II is required for cell proliferation, cell sheet adhesion and wing hair morphology during wing morphogenesis. *Dev Biol* **345**, 117–132 (2010).

Fréal, A. *et al.* Cooperative Interactions between 480 kDa Ankyrin-G and EB Proteins Assemble the Axon Initial Segment. *J Neurosci* **36**, 4421–4433 (2016).

Fréal, A. *et al.* Feedback-Driven Assembly of the Axon Initial Segment. *Neuron* **104**, 305-321.e8 (2019).

Funahashi, Y., Watanabe, T. & Kaibuchi, K. Advances in defining signaling networks for the establishment of neuronal polarity. *Current Opinion in Cell Biology* **63**, 76–87 (2020).

Galiano, M. R. *et al.* A distal axonal cytoskeleton forms an intra-axonal boundary that controls axon initial segment assembly. *Cell* **149**, 1125–1139 (2012).

Galliano, E. *et al.* Brief sensory deprivation triggers cell type-specific structural and functional plasticity in olfactory bulb neurons. *J Neurosci* (2021) doi:10.1523/JNEUROSCI.1606-20.2020.

Galliano, E. *et al*. Embryonic and postnatal neurogenesis produce functionally distinct subclasses of dopaminergic neuron. *eLife* **7**, e32373 (2018).

Gao, C. & Chen, Y.-G. Dishevelled: The hub of Wnt signaling. *Cellular Signalling* **22**, 717–727 (2010).

Gao, F. B., Kohwi, M., Brenman, J. E., Jan, L. Y. & Jan, Y. N. Control of dendritic field formation in Drosophila: the roles of flamingo and competition between homologous neurons. *Neuron* **28**, 91–101 (2000).

Garrido, J. J. *et al.* A targeting motif involved in sodium channel clustering at the axonal initial segment. *Science* **300**, 2091–2094 (2003).

Gärtner, A. *et al.* N-cadherin specifies first asymmetry in developing neurons. *The EMBO Journal* **31**, 1893–1903 (2012).

Garvalov, B. K. *et al.* Cdc42 regulates cofilin during the establishment of neuronal polarity. *J Neurosci* **27**, 13117–13129 (2007).

Gasser, A. *et al.* An AnkyrinG-Binding Motif Is Necessary and Sufficient for Targeting Nav1.6 Sodium Channels to Axon Initial Segments and Nodes of Ranvier. *J Neurosci* **32**, 7232–7243 (2012).

Gella, A. *et al.* Is Ankyrin a genetic risk factor for psychiatric phenotypes? *BMC Psychiatry* **11**, 103 (2011).

Ghosh, A., Malavasi, E. L., Sherman, D. L. & Brophy, P. J. Neurofascin and Kv7.3 are delivered to somatic and axon terminal surface membranes en route to the axon initial segment. *Elife* **9**, (2020).

Goebbels, S. *et al.* Genetic targeting of principal neurons in neocortex and hippocampus of NEX-Cre mice. *Genesis* **44**, 611–621 (2006).

Goldin, A. L. *et al.* Nomenclature of voltage-gated sodium channels. *Neuron* **28**, 365–368 (2000).

Gomis-Rüth, S., Wierenga, C. J. & Bradke, F. Plasticity of polarization: changing dendrites into axons in neurons integrated in neuronal circuits. *Curr Biol* **18**, 992–1000 (2008).

Goodrich, L. V. & Strutt, D. Principles of planar polarity in animal development. *Development* **138**, 1877–1892 (2011).

Goto, T. & Keller, R. The planar cell polarity gene strabismus regulates convergence and extension and neural fold closure in Xenopus. *Dev Biol* **247**, 165–181 (2002).

Götz, M. & Huttner, W. B. The cell biology of neurogenesis. *Nature Reviews Molecular Cell Biology* **6**, 777–788 (2005).

Govek, E.-E. *et al.* Cdc42 Regulates Neuronal Polarity during Cerebellar Axon Formation and Glial-Guided Migration. *iScience* **1**, 35–48 (2018).

Gray, R. S., Roszko, I. & Solnica-Krezel, L. Planar Cell Polarity: Coordinating Morphogenetic Cell Behaviors with Embryonic Polarity. *Developmental Cell* **21**, 120–133 (2011).

Greene, N. D. E. & Copp, A. J. Neural tube defects. *Annu Rev Neurosci* **37**, 221–242 (2014).

Greene, N. D., Gerrelli, D., Van Straaten, H. W. & Copp, A. J. Abnormalities of floor plate, notochord and somite differentiation in the loop-tail (Lp) mouse: a model of severe neural tube defects. *Mech Dev* **73**, 59–72 (1998).

Grubb, M. S. & Burrone, J. Activity-dependent relocation of the axon initial segment fine-tunes neuronal excitability. *Nature* **465**, 1070–1074 (2010).

Guan, D., Armstrong, W. E. & Foehring, R. C. Kv2 channels regulate firing rate in pyramidal neurons from rat sensorimotor cortex. *J Physiol* **591**, 4807–4825 (2013).

Gubb, D. *et al.* The balance between isoforms of the prickle LIM domain protein is critical for planar polarity in Drosophila imaginal discs. *Genes Dev* **13**, 2315–2327 (1999).

Guidotti, A. *et al.* Decrease in reelin and glutamic acid decarboxylase67 (GAD67) expression in schizophrenia and bipolar disorder: a postmortem brain study. *Arch Gen Psychiatry* **57**, 1061–1069 (2000).

Guirao, B. *et al*. Coupling between hydrodynamic forces and planar cell polarity orients mammalian motile cilia. *Nat Cell Biol* **12**, 341–350 (2010).

Gulledge, A. T. & Bravo, J. J. Neuron Morphology Influences Axon Initial Segment Plasticity. *eNeuro* **3**, (2016).

Guo, X. *et al.* Association analysis of ANK3 gene variants with schizophrenia in a northern Chinese Han population. *Oncotarget* **7**, 85888–85894 (2016).

Gutman, G. A. *et al.* International Union of Pharmacology. XLI. Compendium of Voltage-Gated Ion Channels: Potassium Channels. *Pharmacol Rev* **55**, 583–586 (2003).

Gutzmann, A. *et al.* A period of structural plasticity at the axon initial segment in developing visual cortex. *Front Neuroanat* **8**, 11 (2014).

Hakanen, J., Ruiz-Reig, N. & Tissir, F. Linking Cell Polarity to Cortical Development and Malformations. *Front. Cell. Neurosci.* **13**, (2019).

Hall, T. G. & Bennett, V. Regulatory domains of erythrocyte ankyrin. *J Biol Chem* **262**, 10537–10545 (1987).

Hamada, M. S., Goethals, S., de Vries, S. I., Brette, R. & Kole, M. H. P. Covariation of axon initial segment location and dendritic tree normalizes the somatic action potential. *Proc Natl Acad Sci USA* **113**, 14841–14846 (2016).

Hamblet, N. S. *et al.* Dishevelled 2 is essential for cardiac outflow tract development, somite segmentation and neural tube closure. *Development* **129**, 5827–5838 (2002).

Hamdan, H. *et al*. Mapping axon initial segment structure and function by multiplexed proximity biotinylation. Nat Commun **11**, 100 (2020).

Hammarlund, M., Jorgensen, E. M. & Bastiani, M. J. Axons break in animals lacking beta-spectrin. *J Cell Biol* **176**, 269–275 (2007).

Hammond, J. W. *et al.* Posttranslational modifications of tubulin and the polarized transport of kinesin-1 in neurons. *Mol Biol Cell* **21**, 572–583 (2010).

Han, B., Zhou, R., Xia, C. & Zhuang, X. Structural organization of the actin-spectrin-based membrane skeleton in dendrites and soma of neurons. *Proc Natl Acad Sci U S A* **114**, E6678–E6685 (2017).

Harrison, C., Shao, H., Strutt, H. & Strutt, D. Molecular mechanisms mediating asymmetric subcellular localisation of the core planar polarity pathway proteins. *Biochem Soc Trans* **48**, 1297–1308 (2020).

Harterink, M. *et al.* TRIM46 Organizes Microtubule Fasciculation in the Axon Initial Segment. *J Neurosci* **39**, 4864–4873 (2019).

Hassel, B., Rathjen, F. G. & Volkmer, H. Organization of the neurofascin gene and analysis of developmentally regulated alternative splicing. *J Biol Chem* **272**, 28742–28749 (1997).

Hatanaka, Y. & Yamauchi, K. Excitatory Cortical Neurons with Multipolar Shape Establish Neuronal Polarity by Forming a Tangentially Oriented Axon in the Intermediate Zone. *Cerebral Cortex* **23**, 105–113 (2013).

Hatzimanolis, A. *et al.* Bipolar disorder ANK3 risk variant effect on sustained attention is replicated in a large healthy population. *Psychiatr Genet* **22**, 210–213 (2012).

Häusser, M., Stuart, G., Racca, C. & Sakmann, B. Axonal initiation and active dendritic propagation of action potentials in substantia nigra neurons. *Neuron* **15**, 637–647 (1995).

He, M., Jenkins, P. & Bennett, V. Cysteine 70 of ankyrin-G is S-palmitoylated and is required for function of ankyrin-G in membrane domain assembly. *J Biol Chem* **287**, 43995–44005 (2012).

Hedstrom, K. L. *et al.* Neurofascin assembles a specialized extracellular matrix at the axon initial segment. *J Cell Biol* **178**, 875–886 (2007).

Hedstrom, K. L., Ogawa, Y. & Rasband, M. N. AnkyrinG is required for maintenance of the axon initial segment and neuronal polarity. *Journal of Cell Biology* **183**, 635–640 (2008).

Heffner, C. S. *et al.* Supporting conditional mouse mutagenesis with a comprehensive cre characterization resource. *Nat Commun* **3**, 1218 (2012).

Heisenberg, C. P. *et al.* Silberblick/Wnt11 mediates convergent extension movements during zebrafish gastrulation. *Nature* **405**, 76–81 (2000).

Henderson, D. J. *et al.* Cardiovascular defects associated with abnormalities in midline development in the Loop-tail mouse mutant. *Circ Res* **89**, 6–12 (2001).

Hida, Y. *et al.* Prickle2 is localized in the postsynaptic density and interacts with PSD-95 and NMDA receptors in the brain. *J Biochem* **149**, 693–700 (2011).

Hilal, M. L. *et al.* Activity-Dependent Neuroplasticity Induced by an Enriched Environment Reverses Cognitive Deficits in Scribble Deficient Mouse. *Cereb Cortex* **27**, 5635–5651 (2017).

Hivert, B., Marien, L., Agbam, K. N. & Faivre-Sarrailh, C. ADAM22 and ADAM23 modulate the targeting of the Kv1 channel-associated protein LGI1 to the axon initial segment. *J Cell Sci* **132**, (2019).

Hogan, J., Valentine, M., Cox, C., Doyle, K. & Collier, S. Two frizzled planar cell polarity signals in the Drosophila wing are differentially organized by the Fat/Dachsous pathway. *PLoS Genet* **7**, e1001305 (2011).

Hoogenraad, C. C. & Bradke, F. Control of neuronal polarity and plasticity--a renaissance for microtubules? *Trends Cell Biol* **19**, 669–676 (2009).

Hu, W. *et al.* Distinct contributions of Na(v)1.6 and Na(v)1.2 in action potential initiation and backpropagation. *Nat Neurosci* **12**, 996–1002 (2009).

Hua, Z. L., Chang, H., Wang, Y., Smallwood, P. M. & Nathans, J. Partial interchangeability of Fz3 and Fz6 in tissue polarity signaling for epithelial orientation and axon growth and guidance. *Development* **141**, 3944–3954 (2014).

Hua, Z. L., Jeon, S., Caterina, M. J. & Nathans, J. Frizzled3 is required for the development of multiple axon tracts in the mouse central nervous system. *PNAS* **111**, E3005–E3014 (2014).

Huang, C. Y.-M. *et al.* αII Spectrin Forms a Periodic Cytoskeleton at the Axon Initial Segment and Is Required for Nervous System Function. *J. Neurosci.* **37**, 11311–11322 (2017).

Ichinose, S., Ogawa, T., Jiang, X. & Hirokawa, N. The Spatiotemporal Construction of the Axon Initial Segment via KIF3/KAP3/TRIM46 Transport under MARK2 Signaling. *Cell Reports* **28**, 2413-2426.e7 (2019).

Inagaki, N. *et al.* CRMP-2 induces axons in cultured hippocampal neurons. *Nature Neuroscience* **4**, 781–782 (2001).

Inda, M. C., DeFelipe, J. & Munoz, A. Voltage-gated ion channels in the axon initial segment of human cortical pyramidal cells and their relationship with chandelier cells. *Proceedings of the National Academy of Sciences* **103**, 2920–2925 (2006).

Iqbal, Z. *et al.* Homozygous and heterozygous disruptions of ANK3: at the crossroads of neurodevelopmental and psychiatric disorders. *Hum Mol Genet* **22**, 1960–1970 (2013).

Jamann, N., Jordan, M. & Engelhardt, M. Activity-Dependent Axonal Plasticity in Sensory Systems. Neuroscience **368**, 268–282 (2018).

Jamann, N. *et al.* Sensory input drives rapid homeostatic scaling of the axon initial segment in mouse barrel cortex. *Nature Communications* **12**, 23 (2021).

Jarjour, A. A. *et al.* The polarity protein Scribble regulates myelination and remyelination in the central nervous system. *PLoS Biol* **13**, e1002107 (2015).

Jenkins, P. M. *et al.* Giant ankyrin-G: a critical innovation in vertebrate evolution of fast and integrated neuronal signaling. *Proc Natl Acad Sci U S A* **112**, 957–964 (2015).

Jenkins, S. M. & Bennett, V. Ankyrin-G coordinates assembly of the spectrin-based membrane skeleton, voltage-gated sodium channels, and L1 CAMs at Purkinje neuron initial segments. *J Cell Biol* **155**, 739–746 (2001).

Jenny, A., Darken, R. S., Wilson, P. A. & Mlodzik, M. Prickle and Strabismus form a functional complex to generate a correct axis during planar cell polarity signaling. *EMBO J* **22**, 4409–4420 (2003).

Jenny, A., Reynolds-Kenneally, J., Das, G., Burnett, M. & Mlodzik, M. Diego and Prickle regulate Frizzled planar cell polarity signalling by competing for Dishevelled binding. *Nat Cell Biol* **7**, 691–697 (2005).

Jensen, C. S. *et al.* Trafficking of Kv2.1 Channels to the Axon Initial Segment by a Novel Nonconventional Secretory Pathway. *J Neurosci* **37**, 11523–11536 (2017).

Jessen, J. R. *et al.* Zebrafish trilobite identifies new roles for Strabismus in gastrulation and neuronal movements. *Nat Cell Biol* **4**, 610–615 (2002).

Jeste, S. S. The neurology of autism spectrum disorders. *Curr Opin Neurol* **24**, 132–139 (2011).

Jiang, T., Kindt, K. & Wu, D. K. Transcription factor Emx2 controls stereociliary bundle orientation of sensory hair cells. *Elife* **6**, (2017).

Joberty, G., Petersen, C., Gao, L. & Macara, I. G. The cell-polarity protein Par6 links Par3 and atypical protein kinase C to Cdc42. *Nat Cell Biol* **2**, 531–539 (2000).

Johnston, J. *et al.* Initial segment Kv2.2 channels mediate a slow delayed rectifier and maintain high frequency action potential firing in medial nucleus of the trapezoid body neurons. *J Physiol* **586**, 3493–3509 (2008).

Jones, C. *et al.* Ankrd6 is a mammalian functional homolog of Drosophila planar cell polarity gene diego and regulates coordinated cellular orientation in the mouse inner ear. *Dev Biol* **395**, 62–72 (2014).

Jones, S. L., Korobova, F. & Svitkina, T. Axon initial segment cytoskeleton comprises a multiprotein submembranous coat containing sparse actin filaments. *J Cell Biol* **205**, 67–81 (2014).

Jordan, B. A. *et al.* Identification and verification of novel rodent postsynaptic density proteins. *Mol Cell Proteomics* **3**, 857–871 (2004).

Jossin, Y. & Cooper, J. A. Reelin, Rap1 and N-cadherin orient the migration of multipolar neurons in the developing neocortex. *Nature Neuroscience* **14**, 697–703 (2011).

Kadrmas, J. L. & Beckerle, M. C. The LIM domain: from the cytoskeleton to the nucleus. *Nat Rev Mol Cell Biol* **5**, 920–931 (2004).

Kaech, S. & Banker, G. Culturing hippocampal neurons. *Nat Protoc* **1**, 2406–2415 (2006).

Kallay, L. M., McNickle, A., Brennwald, P. J., Hubbard, A. L. & Braiterman, L. T. Scribble associates with two polarity proteins, Lgl2 and Vangl2, via distinct molecular domains. *J Cell Biochem* **99**, 647–664 (2006).

Kaminsky, E. B. *et al.* An evidence-based approach to establish the functional and clinical significance of copy number variants in intellectual and developmental disabilities. *Genet Med* **13**, 777–784 (2011).

Kaplan, M. R. *et al.* Induction of sodium channel clustering by oligodendrocytes. *Nature* **386**, 724–728 (1997).

Katoh, M. & Katoh, M. Identification and characterization of human PRICKLE1 and PRICKLE2 genes as well as mouse Prickle1 and Prickle2 genes homologous to Drosophila tissue polarity gene prickle. *Int J Mol Med* **11**, 249–256 (2003).

Katsuno, H. *et al.* Actin Migration Driven by Directional Assembly and Disassembly of Membrane-Anchored Actin Filaments. *Cell Rep* **12**, 648–660 (2015).

Kawauchi, T. *et al.* Rab GTPases-dependent endocytic pathways regulate neuronal migration and maturation through N-cadherin trafficking. *Neuron* **67**, 588–602 (2010).

Kharfallah, F. *et al.* Scribble1 plays an important role in the pathogenesis of neural tube defects through its mediating effect of Par-3 and Vangl1/2 localization. *Hum Mol Genet* **26**, 2307–2320 (2017).

Kim, E. J., Feng, C., Santamaria, F. & Kim, J. H. Impact of Auditory Experience on the Structural Plasticity of the AIS in the Mouse Brainstem Throughout the Lifespan. *Front. Cell. Neurosci.* **13**, (2019).

Kim, N. *et al.* Whole Exome Sequencing Identifies Novel De Novo Variants Interacting with Six Gene Networks in Autism Spectrum Disorder. *Genes (Basel)* **12**, (2020).

King, A. N., Manning, C. F. & Trimmer, J. S. A Unique Ion Channel Clustering Domain on the Axon Initial Segment of Mammalian Neurons. *J Comp Neurol* **522**, 2594–2608 (2014).

Kishi, M., Pan, Y. A., Crump, J. G. & Sanes, J. R. Mammalian SAD Kinases Are Required for Neuronal Polarization. *Science* **307**, 929–932 (2005).

Knierim, E. *et al.* A recessive mutation in beta-IV-spectrin (SPTBN4) associates with congenital myopathy, neuropathy, and central deafness. *Hum Genet* **136**, 903–910 (2017).

Kole, M. H. P. & Stuart, G. J. Is action potential threshold lowest in the axon? *Nat Neurosci* **11**, 1253–1255 (2008).

Kole, M. H. P. & Stuart, G. J. Signal Processing in the Axon Initial Segment. *Neuron* **73**, 235–247 (2012).

Kole, M. H. P. *et al.* Action potential generation requires a high sodium channel density in the axon initial segment. *Nat Neurosci* **11**, 178–186 (2008).

Kole, M. H. P., Letzkus, J. J. & Stuart, G. J. Axon initial segment Kv1 channels control axonal action potential waveform and synaptic efficacy. *Neuron* **55**, 633–647 (2007).

Komada, M. & Soriano, P. [Beta]IV-spectrin regulates sodium channel clustering through ankyrin-G at axon initial segments and nodes of Ranvier. *J Cell Biol* **156**, 337–348 (2002).

Komiya, Y. & Habas, R. Wnt signal transduction pathways. *Organogenesis* **4**, 68–75 (2008).

Konishi, Y. & Setou, M. Tubulin tyrosination navigates the kinesin-1 motor domain to axons. *Nat Neurosci* **12**, 559–567 (2009).

Kordeli, E. & Bennett, V. Distinct ankyrin isoforms at neuron cell bodies and nodes of Ranvier resolved using erythrocyte ankyrin-deficient mice. *J Cell Biol* **114**, 1243–1259 (1991).

Kordeli, E., Davis, J., Trapp, B. & Bennett, V. An isoform of ankyrin is localized at nodes of Ranvier in myelinated axons of central and peripheral nerves. *J Cell Biol* **110**, 1341–1352 (1990).

Kordeli, E., Lambert, S. & Bennett, V. AnkyrinG. A new ankyrin gene with neural-specific isoforms localized at the axonal initial segment and node of Ranvier. *J Biol Chem* **270**, 2352–2359 (1995).

Korobova, F. & Svitkina, T. Arp2/3 complex is important for filopodia formation, growth cone motility, and neuritogenesis in neuronal cells. *Mol Biol Cell* **19**, 1561–1574 (2008).

Koticha, D. *et al.* Neurofascin interactions play a critical role in clustering sodium channels, ankyrin G and beta IV spectrin at peripheral nodes of Ranvier. *Dev Biol* **293**, 1–12 (2006).

Kriebel, M., Wuchter, J., Trinks, S. & Volkmer, H. Neurofascin: A switch between neuronal plasticity and stability. *The International Journal of Biochemistry & Cell Biology* **44**, 694–697 (2012).

Kuba, H., Adachi, R. & Ohmori, H. Activity-Dependent and Activity-Independent Development of the Axon Initial Segment. *J Neurosci* **34**, 3443–3453 (2014).

Kuba, H., Oichi, Y. & Ohmori, H. Presynaptic activity regulates Na(+) channel distribution at the axon initial segment. *Nature* **465**, 1075–1078 (2010).

Kühl, M. Non-canonical Wnt signaling in Xenopus: regulation of axis formation and gastrulation. *Semin Cell Dev Biol* **13**, 243–249 (2002).

Lacas-Gervais, S. *et al.* BetaIVSigma1 spectrin stabilizes the nodes of Ranvier and axon initial segments. *J Cell Biol* **166**, 983–990 (2004).

Lake, B. B. & Sokol, S. Y. Strabismus regulates asymmetric cell divisions and cell fate determination in the mouse brain. *J Cell Biol* **185**, 59–66 (2009).

Lambert, S., Davis, J. Q. & Bennett, V. Morphogenesis of the Node of Ranvier: Co-Clusters of Ankyrin and Ankyrin-Binding Integral Proteins Define Early Developmental Intermediates. *J Neurosci* **17**, 7025–7036 (1997).

Lamoureux, P., Ruthel, G., Buxbaum, R. E. & Heidemann, S. R. Mechanical tension can specify axonal fate in hippocampal neurons. *J Cell Biol* **159**, 499–508 (2002).

Lavoie-Cardinal, F. *et al.* Neuronal activity remodels the F-actin based submembrane lattice in dendrites but not axons of hippocampal neurons. *bioRxiv* (2020) doi: 10.1101/2020.05.27.119453.

Lawrence, P. A., Casal, J. & Struhl, G. Cell interactions and planar polarity in the abdominal epidermis of Drosophila. *Development* **131**, 4651–4664 (2004).

Lazarides, E. & Nelson, W. J. Erythrocyte and brain forms of spectrin in cerebellum: distinct membrane-cytoskeletal domains in neurons. *Science* **220**, 1295–1296 (1983).

Lazarov, E. *et al.* An axon initial segment is required for temporal precision in action potential encoding by neuronal populations. *Sci. Adv.* **4**, eaau8621 (2018).

Lee, J. *et al.* PTK7 regulates myosin II activity to orient planar polarity in the mammalian auditory epithelium. *Curr Biol* **22**, 956–966 (2012).

Lee, R. C. *et al.* The protocadherin Flamingo is required for axon target selection in the Drosophila visual system. *Nature Neuroscience* **6**, 557–563 (2003).

Lei, Y. *et al.* Identification of Novel CELSR1 Mutations in Spina Bifida. *PLOS ONE* **9**, e92207 (2014).

Leite, S. C. & Sousa, M. M. The neuronal and actin commitment: Why do neurons need rings? *Cytoskeleton (Hoboken)* **73**, 424–434 (2016).

Lemaillet, G., Walker, B. & Lambert, S. Identification of a conserved ankyrin-binding motif in the family of sodium channel alpha subunits. *J Biol Chem* **278**, 27333–27339 (2003).

Léna, I. & Mantegazza, M. NaV1.2 haploinsufficiency in Scn2a knock-out mice causes an autistic-like phenotype attenuated with age. *Sci Rep* **9**, 12886 (2019).

Leppert, M. *et al.* Benign familial neonatal convulsions linked to genetic markers on chromosome 20. *Nature* **337**, 647–648 (1989).

Lesko, A. C., Keller, R., Chen, P. & Sutherland, A. Scribble mutation disrupts convergent extension and apical constriction during mammalian neural tube closure. *bioRxiv* (2020) doi:10.1101/2020.09.18.303446.

Leterrier, C. & Dargent, B. No Pasaran! Role of the axon initial segment in the regulation of protein transport and the maintenance of axonal identity. *Semin Cell Dev Biol* **27**, 44–51 (2014).

Leterrier, C. *et al.* Ankyrin G Membrane Partners Drive the Establishment and Maintenance of the Axon Initial Segment. *Front Cell Neurosci* **11**, 6 (2017).

Leterrier, C. *et al.* End-binding proteins EB3 and EB1 link microtubules to ankyrin G in the axon initial segment. *Proc Natl Acad Sci U S A* **108**, 8826–8831 (2011).

Leterrier, C. *et al.* Nanoscale Architecture of the Axon Initial Segment Reveals an Organized and Robust Scaffold. *Cell Rep* **13**, 2781–2793 (2015).

Leterrier, C. The Axon Initial Segment: An Updated Viewpoint. *J Neurosci* **38**, 2135–2145 (2018).

Leung, V. *et al.* The planar cell polarity protein Vangl2 is required for retinal axon guidance. *Dev Neurobiol* **76**, 150–165 (2016).

Leussis, M. P. *et al.* The ANK3 bipolar disorder gene regulates psychiatric-related behaviors that are modulated by lithium and stress. *Biol Psychiatry* **73**, 683–690 (2013).

Levine, J. & Willard, M. Fodrin: axonally transported polypeptides associated with the internal periphery of many cells. *J Cell Biol* **90**, 631–642 (1981).

Li, X. *et al.* Novel diffusion barrier for axonal retention of Tau in neurons and its failure in neurodegeneration. *EMBO J* **30**, 4825–4837 (2011).

Lijam, N. *et al.* Social interaction and sensorimotor gating abnormalities in mice lacking Dvl1. *Cell* **90**, 895–905 (1997).

Liu, C. *et al.* Prickle1 is expressed in distinct cell populations of the central nervous system and contributes to neuronal morphogenesis. *Hum Mol Genet* **22**, 2234–2246 (2013).

Lizcano, J. M. *et al*. LKB1 is a master kinase that activates 13 kinases of the AMPK subfamily, including MARK/PAR-1. *EMBO J* **23**, 833–843 (2004).

Lopez-Santiago, L. F. *et al.* Neuronal hyperexcitability in a mouse model of SCN8A epileptic encephalopathy. *Proc Natl Acad Sci U S A* **114**, 2383–2388 (2017).

Lopez, A. Y. *et al.* Ankyrin-G isoform imbalance and interneuronopathy link epilepsy and bipolar disorder. *Mol Psychiatry* **22**, 1464–1472 (2017).

Lorincz, A. & Nusser, Z. Cell-type-dependent molecular composition of the axon initial segment. *J Neurosci* **28**, 14329–14340 (2008).

Loup, F. *et al.* A highly sensitive immunofluorescence procedure for analyzing the subcellular distribution of GABAA receptor subunits in the human brain. *J Histochem Cytochem* **46**, 1129–1139 (1998).

Lu, Q. & Adler, P. N. The diaphanous gene of Drosophila interacts antagonistically with multiple wing hairs and plays a key role in wing hair morphogenesis. *PLoS One* **10**, e0115623 (2015).

Lu, X. *et al.* PTK7/CCK-4 is a novel regulator of planar cell polarity in vertebrates. *Nature* **430**, 93–98 (2004).

Mahajan, V. B. & Bassuk, A. G. Response to Sandford *et al*.: PRICKLE2 Variants in Epilepsy: A Call for Precision Medicine. *Am J Hum Genet* **98**, 590–591 (2016).

Malin, S. A. & Nerbonne, J. M. Delayed Rectifier K+ Currents,IK, Are Encoded by Kv2 α-Subunits and Regulate Tonic Firing in Mammalian Sympathetic Neurons. *J Neurosci* **22**, 10094–10105 (2002).

Mao, Y. *et al.* Characterization of a Dchs1 mutant mouse reveals requirements for Dchs1-Fat4 signaling during mammalian development. *Development* **138**, 947–957 (2011).

Mapp, O. M., Walsh, G. S., Moens, C. B., Tada, M. & Prince, V. E. Zebrafish Prickle1b mediates facial branchiomotor neuron migration via a farnesylation-dependent nuclear activity. *Development* **138**, 2121–2132 (2011).

Margolis, B. The Crumbs3 Polarity Protein. *Cold Spring Harb Perspect Biol* **10**, a027961 (2018).

Martinez, S. *et al.* The PTK7 and ROR2 Protein Receptors Interact in the Vertebrate WNT/Planar Cell Polarity (PCP) Pathway. *J Biol Chem* **290**, 30562–30572 (2015).

Mastrangelo, M. *et al.* PRICKLE1-related early onset epileptic encephalopathy. *Am J Med Genet A* **176**, 2841–2845 (2018).

Matakatsu, H. & Blair, S. S. Separating the adhesive and signaling functions of the Fat and Dachsous protocadherins. *Development* **133**, 2315–2324 (2006).

Matis, M. & Axelrod, J. D. Regulation of PCP by the Fat signaling pathway. *Genes Dev* **27**, 2207–2220 (2013).

Matis, M., Russler-Germain, D. A., Hu, Q., Tomlin, C. J. & Axelrod, J. D. Microtubules provide directional information for core PCP function. *Elife* **3**, e02893 (2014).

Maung, S. M. T. W. & Jenny, A. Planar cell polarity in Drosophila. *Organogenesis* **7**, 165–179 (2011).

McKay, R. M., Peters, J. M. & Graff, J. M. The casein kinase I family in Wnt signaling. *Dev Biol* **235**, 388–396 (2001).

McCormick, D. A. Chapter 12 - Membrane Potential and Action Potential. in *From Molecules to Networks (Third Edition)* (eds. Byrne, J. H., Heidelberger, R. & Waxham, M. N.) 351–376 (Academic Press, 2014). doi:10.1016/B978-0-12-397179-1.00012-9.

Melendez-Vasquez, C. V. *et al.* Nodes of Ranvier form in association with ezrin-radixin-moesin (ERM)-positive Schwann cell processes. *Proc Natl Acad Sci U S A* **98**, 1235–1240 (2001).

Merte, J. *et al.* Sec24b selectively sorts Vangl2 to regulate planar cell polarity during neural tube closure. *Nat Cell Biol* **12**, 41–46; sup pp 1-8 (2010).

Mitterdorfer, J. & Bean, B. P. Potassium Currents during the Action Potential of Hippocampal CA3 Neurons. *J. Neurosci.* **22**, 10106–10115 (2002).

Montcouquiol, M. & Kelley, M. W. Development and Patterning of the Cochlea: From Convergent Extension to Planar Polarity. *Cold Spring Harb Perspect Med* **10**, (2020).

Montcouquiol, M. *et al.* Asymmetric localization of Vangl2 and Fz3 indicate novel mechanisms for planar cell polarity in mammals. *J Neurosci* **26**, 5265–5275 (2006).

Montcouquiol, M. *et al.* Identification of Vangl2 and Scrb1 as planar polarity genes in mammals. *Nature* **423**, 173–177 (2003).

Montcouquiol, M., Crenshaw, E. B. & Kelley, M. W. Noncanonical Wnt signaling and neural polarity. *Annu Rev Neurosci* **29**, 363–386 (2006).

Moon, R. T. & Shah, K. Developmental biology: signalling polarity. *Nature* **417**, 239–240 (2002).

Moreau, M. M. *et al.* Scribble controls social behaviors through the regulation of the ERK/Mnk1 pathway. *bioRxiv* (2020) doi:10.1101/2020.09.10.289397.

Moreau, M. M. *et al.* The Planar Polarity Protein Scribble1 Is Essential for Neuronal Plasticity and Brain Function. *J. Neurosci.* **30**, 9738–9752 (2010).

Moriguchi, T. *et al.* Distinct domains of mouse dishevelled are responsible for the c-Jun N-terminal kinase/stress-activated protein kinase activation and the axis formation in vertebrates. *J Biol Chem* **274**, 30957–30962 (1999).

Morin, X. & Bellaïche, Y. Mitotic spindle orientation in asymmetric and symmetric cell divisions during animal development. *Dev Cell* **21**, 102–119 (2011).

Mrkusich, E. M., Flanagan, D. J. & Whitington, P. M. The core planar cell polarity gene prickle interacts with flamingo to promote sensory axon advance in the Drosophila embryo. *Dev Biol* **358**, 224–230 (2011).

Muir, J. & Kittler, J. T. Plasticity of GABAA receptor diffusion dynamics at the axon initial segment. *Front Cell Neurosci* **8**, 151 (2014).

Müller, H. A., Samanta, R. & Wieschaus, E. Wingless signaling in the Drosophila embryo: zygotic requirements and the role of the frizzled genes. *Development* **126**, 577–586 (1999).

Muñoz-Lasso, D. C., Romá-Mateo, C., Pallardó, F. V. & Gonzalez-Cabo, P. Much More Than a Scaffold: Cytoskeletal Proteins in Neurological Disorders. *Cells* **9**, 358 (2020).

Murdoch, J. N. Disruption of scribble (Scrb1) causes severe neural tube defects in the circletail mouse. *Human Molecular Genetics* **12**, 87–98 (2003).

Murdoch, J. N. *et al.* Circletail, a new mouse mutant with severe neural tube defects: chromosomal localization and interaction with the loop-tail mutation. *Genomics* **78**, 55–63 (2001).

Mutterer, J. & Zinck, E. Quick-and-clean article figures with FigureJ. *J Microsc* **252**, 89–91 (2013).

Nagaoka, T. *et al.* The Wnt/planar cell polarity pathway component Vangl2 induces synapse formation through direct control of N-cadherin. *Cell Rep* **6**, 916–927 (2014).

Nakada, C. *et al.* Accumulation of anchored proteins forms membrane diffusion barriers during neuronal polarization. *Nat Cell Biol* **5**, 626–632 (2003).

Nakata, T. & Hirokawa, N. Microtubules provide directional cues for polarized axonal transport through interaction with kinesin motor head. *J Cell Biol* **162**, 1045–1055 (2003).

Namba, T. *et al.* Pioneering Axons Regulate Neuronal Polarization in the Developing Cerebral Cortex. *Neuron* **81**, 814–829 (2014).

Narimatsu, M. *et al.* Regulation of planar cell polarity by Smurf ubiquitin ligases. *Cell* **137**, 295–307 (2009).

Neale, B. M. *et al.* Patterns and rates of exonic *de novo* mutations in autism spectrum disorders. *Nature* **485**, 242–245 (2012).

Neukirchen, D. & Bradke, F. Neuronal polarization and the cytoskeleton. *Seminars in Cell & Developmental Biology* **22**, 825–833 (2011).

Ng, J. Wnt/PCP proteins regulate stereotyped axon branch extension in Drosophila. *Development* **139**, 165–177 (2012).

Nishimura, K., Akiyama, H., Komada, M. & Kamiguchi, H. βIV-spectrin forms a diffusion barrier against L1CAM at the axon initial segment. *Molecular and Cellular Neuroscience* **34**, 422–430 (2007).

Nishimura, T. *et al.* PAR-6–PAR-3 mediates Cdc42-induced Rac activation through the Rac GEFs STEF/Tiam1. *Nature Cell Biology* **7**, 270–277 (2005).

Nishimura, T. *et al.* Role of the PAR-3–KIF3 complex in the establishment of neuronal polarity. *Nature Cell Biology* **6**, 328–334 (2004).

Nusse, R. & Clevers, H. Wnt/β-Catenin Signaling, Disease, and Emerging Therapeutic Modalities. *Cell* **169**, 985–999 (2017).

Nusse, R. & Varmus, H. E. Wnt genes. *Cell* **69**, 1073–1087 (1992).

Nusse, R. *et al.* A new nomenclature for int-1 and related genes: The Wnt gene family. *Cell* **64**, 231 (1991).

Nusse, R. Wnt signaling in disease and in development. *Cell Res* **15**, 28–32 (2005).

Nusse, R., van Ooyen, A., Cox, D., Fung, Y. K. T. & Varmus, H. Mode of proviral activation of a putative mammary oncogene (int -1) on mouse chromosome 15. *Nature* **307**, 131–136 (1984).

O'Roak, B. J. *et al.* Exome sequencing in sporadic autism spectrum disorders identifies severe de novo mutations. *Nat Genet* **43**, 585–589 (2011).

Oakley, J. C., Kalume, F. & Catterall, W. A. Insights into pathophysiology and therapy from a mouse model of Dravet syndrome. *Epilepsia* **52 Suppl 2**, 59–61 (2011).

Ogawa, Y. *et al.* Postsynaptic density-93 clusters Kv1 channels at axon initial segments independently of Caspr2. *J Neurosci* **28**, 5731–5739 (2008).

Ogiwara, I. *et al.* Nav1.2 haplodeficiency in excitatory neurons causes absence-like seizures in mice. *Commun Biol* **1**, 96 (2018).

Ohara, O., Ohara, R., Yamakawa, H., Nakajima, D. & Nakayama, M. Characterization of a new beta-spectrin gene which is predominantly expressed in brain. *Brain Res Mol Brain Res* **57**, 181–192 (1998).

Ohata, S. & Alvarez-Buylla, A. Planar Organization of Multiciliated Ependymal (E1) Cells in the Brain Ventricular Epithelium. *Trends in Neurosciences* **39**, 543–551 (2016).

Ohata, S. *et al.* Loss of Dishevelleds disrupts planar polarity in ependymal motile cilia and results in hydrocephalus. *Neuron* **83**, 558–571 (2014).

Okuda, H., Miyata, S., Mori, Y. & Tohyama, M. Mouse Prickle1 and Prickle2 are expressed in postmitotic neurons and promote neurite outgrowth. *FEBS Lett* **581**, 4754–4760 (2007).

Okumura, A. *et al.* 3p interstitial deletion including PRICKLE2 in identical twins with autistic features. *Pediatr Neurol* **51**, 730–733 (2014).

Olofsson, J., Sharp, K. A., Matis, M., Cho, B. & Axelrod, J. D. Prickle/spiny-legs isoforms control the polarity of the apical microtubule network in planar cell polarity. *Development* **141**, 2866–2874 (2014).

Paemka, L. *et al.* PRICKLE1 interaction with SYNAPSIN I reveals a role in autism spectrum disorders. *PLoS One* **8**, e80737 (2013).

Palay, S. L., Sotelo, C., Peters, A. & Orkand, P. M. The axon hillock and the initial segment. *J Cell Biol* **38**, 193–201 (1968).

Pan-Vazquez, A., Wefelmeyer, W., Sabater, V. G., Neves, G. & Burrone, J. Activity-Dependent Plasticity of Axo-axonic Synapses at the Axon Initial Segment. *Neuron* **106**, 265-276.e6 (2020).

Pan, Z. *et al.* A common ankyrin-G-based mechanism retains KCNQ and NaV channels at electrically active domains of the axon. *J Neurosci* **26**, 2599–2613 (2006).

Panzanelli, P. *et al.* Distinct mechanisms regulate GABAA receptor and gephyrin clustering at perisomatic and axo-axonic synapses on CA1 pyramidal cells. *J Physiol* **589**, 4959–4980 (2011).

Papanikolaou, K. *et al.* A case of partial trisomy of chromosome 8p associated with autism. *J Autism Dev Disord* **36**, 705–709 (2006).

Parkinson, N. J. *et al.* Mutant beta-spectrin 4 causes auditory and motor neuropathies in quivering mice. *Nat Genet* **29**, 61–65 (2001).

Paudyal, A. *et al.* The novel mouse mutant, chuzhoi, has disruption of Ptk7 protein and exhibits defects in neural tube, heart and lung development and abnormal planar cell polarity in the ear. *BMC Dev Biol* **10**, 87 (2010).

Peng, Y. & Axelrod, J. D. Asymmetric protein localization in planar cell polarity: mechanisms, puzzles, and challenges. *Curr Top Dev Biol* **101**, 33–53 (2012).

Peng, Z. *et al.* A reorganized GABAergic circuit in a model of epilepsy: evidence from optogenetic labeling and stimulation of somatostatin interneurons. *J Neurosci* **33**, 14392–14405 (2013).

Peters, A., Proskauer, C. C. & Kaiserman-Abramof, I. R. The small pyramidal neuron of the rat cerebral cortex. The axon hillock and initial segment. *J Cell Biol* **39**, 604–619 (1968).

Peters, J. M., McKay, R. M., McKay, J. P. & Graff, J. M. Casein kinase I transduces Wnt signals. *Nature* **401**, 345–350 (1999).

Peters, L. L. *et al.* Ank3 (epithelial ankyrin), a widely distributed new member of the ankyrin gene family and the major ankyrin in kidney, is expressed in alternatively spliced forms, including forms that lack the repeat domain. *J Cell Biol* **130**, 313–330 (1995).

Piguel, N. H. *et al.* Scribble1/AP2 complex coordinates NMDA receptor endocytic recycling. *Cell Rep* **9**, 712–727 (2014).

Polleux, F. & Snider, W. Initiating and Growing an Axon. *Cold Spring Harbor Perspectives in Biology* **2**, a001925–a001925 (2010).

Qian, D. *et al.* Wnt5a functions in planar cell polarity regulation in mice. *Dev Biol* **306**, 121–133 (2007).

Rachel, R. A., Wellington, S. J., Warburton, D., Mason, C. A. & Beermann, F. A new allele of Gli3 and a new mutation, circletail (Crc), resulting from a single transgenic experiment. *Genesis* **33**, 55–61 (2002).

Raghavan, M., Fee, D. & Barkhaus, P. E. Generation and propagation of the action potential. *Handb Clin Neurol* **160**, 3–22 (2019).

Rao, A. N. & Baas, P. W. Polarity Sorting of Microtubules in the Axon. *Trends Neurosci* **41**, 77–88 (2018).

Rasband, M. N. & Peles, E. Mechanisms of node of Ranvier assembly. *Nat Rev Neurosci* **22**, 7–20 (2021).

Rasband, M. N. The axon initial segment and the maintenance of neuronal polarity. *Nature Reviews Neuroscience* **11**, 552–562 (2010).

Rasmussen, H. B. *et al.* Requirement of subunit co-assembly and ankyrin-G for M-channel localization at the axon initial segment. *J Cell Sci* **120**, 953–963 (2007).

Reed, N. A. *et al.* Microtubule acetylation promotes kinesin-1 binding and transport. *Curr Biol* **16**, 2166–2172 (2006).

Ressurreição, M., Warrington, S. & Strutt, D. Rapid Disruption of Dishevelled Activity Uncovers an Intercellular Role in Maintenance of Prickle in Core Planar Polarity Protein Complexes. *Cell Rep* **25**, 1415-1424.e6 (2018).

Ricobaraza, A. *et al.* Epilepsy and neuropsychiatric comorbidities in mice carrying a recurrent Dravet syndrome SCN1A missense mutation. *Sci Rep* **9**, 14172 (2019).

Robert, B. J. A. *et al.* Vangl2 in the Dentate Network Modulates Pattern Separation and Pattern Completion. *Cell Rep* **31**, 107743 (2020).

Robinson, A. *et al.* Mutations in the planar cell polarity genes CELSR1 and SCRIB are associated with the severe neural tube defect craniorachischisis. *Human Mutation* **33**, 440–447 (2012).

Rodriguez-Boulan, E. & Macara, I. G. Organization and execution of the epithelial polarity programme. *Nature Reviews Molecular Cell Biology* **15**, 225–242 (2014).

Roszko, I., Sawada, A. & Solnica-Krezel, L. Regulation of convergence and extension movements during vertebrate gastrulation by the Wnt/PCP pathway. *Semin Cell Dev Biol* **20**, 986–997 (2009).

Rothbächer, U. *et al.* Dishevelled phosphorylation, subcellular localization and multimerization regulate its role in early embryogenesis. *EMBO J* **19**, 1010–1022 (2000).

Rubenstein, J. L. R. & Merzenich, M. M. Model of autism: increased ratio of excitation/inhibition in key neural systems. *Genes Brain Behav* **2**, 255–267 (2003).

Rueckert, E. H. *et al.* Cis-acting regulation of brain-specific ANK3 gene expression by a genetic variant associated with bipolar disorder. *Mol Psychiatry* **18**, 922–929 (2013).

Rui, M. *et al.* The neuronal protein Neurexin directly interacts with the Scribble-Pix complex to stimulate F-actin assembly for synaptic vesicle clustering. *J Biol Chem* **292**, 14334–14348 (2017).

Rust, M. J., Bates, M. & Zhuang, X. Sub-diffraction-limit imaging by stochastic optical reconstruction microscopy (STORM). *Nat Methods* **3**, 793–795 (2006).

Ruthel, G. & Banker, G. Actin-dependent anterograde movement of growth-cone-like structures along growing hippocampal axons: a novel form of axonal transport? *Cell Motil Cytoskeleton* **40**, 160–173 (1998).

Saburi, S., Hester, I., Goodrich, L. & McNeill, H. Functional interactions between Fat family cadherins in tissue morphogenesis and planar polarity. *Development* **139**, 1806–1820 (2012).

Sajan, S. A. *et al.* Both rare and de novo copy number variants are prevalent in agenesis of the corpus callosum but not in cerebellar hypoplasia or polymicrogyria. *PLoS Genet* **9**, e1003823 (2013).

Sakakibara, A. *et al.* Dynamics of Centrosome Translocation and Microtubule Organization in Neocortical Neurons during Distinct Modes of Polarization. *Cerebral Cortex* **24**, 1301–1310 (2014).

Salinas, P. C. Modulation of the microtubule cytoskeleton: a role for a divergent canonical Wnt pathway. *Trends Cell Biol* **17**, 333–342 (2007).

Sanchez-Alvarez, L. *et al.* VANG-1 and PRKL-1 cooperate to negatively regulate neurite formation in Caenorhabditis elegans. *PLoS Genet* **7**, e1002257 (2011).

Sánchez-Ponce, D., DeFelipe, J., Garrido, J. J. & Muñoz, A. Developmental Expression of Kv Potassium Channels at the Axon Initial Segment of Cultured Hippocampal Neurons. *PLOS ONE* **7**, e48557 (2012).

Sanchez-Ponce, D., Muñoz, A. & Garrido, J. J. Casein kinase 2 and microtubules control axon initial segment formation. *Molecular and Cellular Neuroscience* **46**, 222–234 (2011).

Sandford, E., Bird, T. D., Li, J. Z. & Burmeister, M. PRICKLE2 Mutations Might Not Be Involved in Epilepsy. *Am J Hum Genet* **98**, 588–589 (2016).

Sans, N., Ezan, J., Moreau, M. M. & Montcouquiol, M. Chapter 13 - Planar Cell Polarity Gene Mutations in Autism Spectrum Disorder, Intellectual Disabilities, and Related Deletion/Duplication Syndromes. in *Neuronal and Synaptic Dysfunction in Autism Spectrum Disorder and Intellectual Disability* (eds. Sala, C. & Verpelli, C.) 189–219 (Academic Press, 2016). doi:10.1016/B978-0-12-800109-7.00013-3.

Santoni, M.-J., Pontarotti, P., Birnbaum, D. & Borg, J.-P. The LAP family: a phylogenetic point of view. Trends Genet **18**, 494–497 (2002).

Sarmiere, P. D., Weigle, C. M. & Tamkun, M. M. The Kv2.1 K+ channel targets to the axon initial segment of hippocampal and cortical neurons in culture and in situ. *BMC Neurosci* **9**, 112 (2008).

Satake, T. *et al.* MTCL1 plays an essential role in maintaining Purkinje neuron axon initial segment. *EMBO J* **36**, 1227–1242 (2017).

Schambony, A. & Wedlich, D. Wnt-5A/Ror2 regulate expression of XPAPC through an alternative noncanonical signaling pathway. *Dev Cell* **12**, 779–792 (2007).

Schelski, M. & Bradke, F. Neuronal polarization: From spatiotemporal signaling to cytoskeletal dynamics. *Mol Cell Neurosci* **84**, 11–28 (2017).

Schwaibold, E. M. C. *et al.* A 3p interstitial deletion in two monozygotic twin brothers and an 18-year-old man: further characterization and review. *Am J Med Genet A* **161A**, 2634–2640 (2013).

Senti, K.-A. *et al.* Flamingo regulates R8 axon-axon and axon-target interactions in the Drosophila visual system. *Curr Biol* **13**, 828–832 (2003).

Shafer, B., Onishi, K., Lo, C., Colakoglu, G. & Zou, Y. Vangl2 promotes Wnt/planar cell polarity-like signaling by antagonizing Dvl1-mediated feedback inhibition in growth cone guidance. *Dev Cell* **20**, 177–191 (2011).

Sharma, M., Castro-Piedras, I., Simmons, G. E. & Pruitt, K. Dishevelled: A masterful conductor of complex Wnt signals. *Cell Signal* **47**, 52–64 (2018).

Shelly, M., Cancedda, L., Heilshorn, S., Sumbre, G. & Poo, M.-M. LKB1/STRAD promotes axon initiation during neuronal polarization. *Cell* **129**, 565–577 (2007).

Shi, S.-H., Cheng, T., Jan, L. Y. & Jan, Y.-N. APC and GSK-3β Are Involved in mPar3 Targeting to the Nascent Axon and Establishment of Neuronal Polarity. *Current Biology* **14**, 2025–2032 (2004).

Shi, S.-H., Jan, L. Y. & Jan, Y.-N. Hippocampal Neuronal Polarity Specified by Spatially Localized mPar3/mPar6 and PI 3-Kinase Activity. *Cell* **112**, 63–75 (2003).

Shi, X. *et al.* Missense mutation of the sodium channel gene SCN2A causes Dravet syndrome. *Brain Dev* **31**, 758–762 (2009).

Shima, Y., Kengaku, M., Hirano, T., Takeichi, M. & Uemura, T. Regulation of dendritic maintenance and growth by a mammalian 7-pass transmembrane cadherin. *Dev Cell* **7**, 205–216 (2004).

Shimada, Y., Usui, T., Yanagawa, S., Takeichi, M. & Uemura, T. Asymmetric colocalization of Flamingo, a seven-pass transmembrane cadherin, and Dishevelled in planar cell polarization. *Curr Biol* **11**, 859–863 (2001).

Shimada, Y., Yonemura, S., Ohkura, H., Strutt, D. & Uemura, T. Polarized transport of Frizzled along the planar microtubule arrays in Drosophila wing epithelium. *Dev Cell* **10**, 209–222 (2006).

Shimizu, K., Sato, M. & Tabata, T. The Wnt5/planar cell polarity pathway regulates axonal development of the Drosophila mushroom body neuron. *J Neurosci* **31**, 4944–4954 (2011).

Shotton, D. M., Burke, B. E. & Branton, D. The molecular structure of human erythrocyte spectrin. Biophysical and electron microscopic studies. *J Mol Biol* **131**, 303–329 (1979).

Simons, M. & Trajkovic, K. Neuron-glia communication in the control of oligodendrocyte function and myelin biogenesis. *Journal of Cell Science* **119**, 4381–4389 (2006).

Singh, J. & Mlodzik, M. Planar cell polarity signaling: coordination of cellular orientation across tissues. *Wiley Interdiscip Rev Dev Biol* **1**, 479–499 (2012).

Singh, N. A. *et al.* Mouse models of human KCNQ2 and KCNQ3 mutations for benign familial neonatal convulsions show seizures and neuronal plasticity without synaptic reorganization. *The Journal of Physiology* **586**, 3405–3423 (2008).

Smith, E. N. *et al.* Genome-wide association study of bipolar disorder in European American and African American individuals. *Mol Psychiatry* **14**, 755–763 (2009).

Smith, K. R. & Penzes, P. Ankyrins: Roles in synaptic biology and pathology. *Mol Cell Neurosci* **91**, 131–139 (2018).

Smith, K. R. *et al.* Psychiatric risk factor ANK3/ankyrin-G nanodomains regulate the structure and function of glutamatergic synapses. *Neuron* **84**, 399–415 (2014).

Sobotzik, J.-M. *et al.* AnkyrinG is required to maintain axo-dendritic polarity in vivo. *Proc Natl Acad Sci U S A* **106**, 17564–17569 (2009).

Sohn, P. D. *et al.* Pathogenic Tau Impairs Axon Initial Segment Plasticity and Excitability Homeostasis. *Neuron* **104**, 458-470.e5 (2019).

Sokol, S. Y. Analysis of Dishevelled signalling pathways during Xenopus development. *Curr Biol* **6**, 1456–1467 (1996).

Sokol, S. Y. Mesoderm formation in Xenopus ectodermal explants overexpressing Xwnt8: evidence for a cooperating signal reaching the animal pole by gastrulation. *Development* **118**, 1335–1342 (1993).

Solnica-Krezel, L. Gastrulation in zebrafish -- all just about adhesion? *Curr Opin Genet Dev* **16**, 433–441 (2006).

Song, A. *et al.* A Selective Filter for Cytoplasmic Transport at the Axon Initial Segment. *Cell* **136**, 1148–1160 (2009).

Sowers, L. P. *et al.* Disruption of the non-canonical Wnt gene PRICKLE2 leads to autism-like behaviors with evidence for hippocampal synaptic dysfunction. *Mol Psychiatry* **18**, 1077–1089 (2013).

Spence, S. J. & Schneider, M. T. The role of epilepsy and epileptiform EEGs in autism spectrum disorders. *Pediatr Res* **65**, 599–606 (2009).

Srinivasan, Y., Elmer, L., Davis, J., Bennett, V. & Angelides, K. Ankyrin and spectrin associate with voltage-dependent sodium channels in brain. *Nature* **333**, 177–180 (1988).

Stam, A. J., Schothorst, P. F., Vorstman, J. A. & Staal, W. G. The genetic overlap of attention deficit hyperactivity disorder and autistic spectrum disorder. *Appl Clin Genet* **2**, 7–13 (2009).

Stanganello, E. *et al.* Wnt Signaling Directs Neuronal Polarity and Axonal Growth. *iScience* **13**, 318–327 (2019).

Stephens, R. *et al.* The Scribble Cell Polarity Module in the Regulation of Cell Signaling in Tissue Development and Tumorigenesis. *J Mol Biol* **430**, 3585–3612 (2018).

Struhl, G., Casal, J. & Lawrence, P. A. Dissecting the molecular bridges that mediate the function of Frizzled in planar cell polarity. *Development* **139**, 3665–3674 (2012).

Strutt, D. & Warrington, S. J. Planar polarity genes in the Drosophila wing regulate the localisation of the FH3-domain protein Multiple Wing Hairs to control the site of hair production. *Development* **135**, 3103–3111 (2008).

Strutt, D. I. Asymmetric localization of frizzled and the establishment of cell polarity in the Drosophila wing. *Mol Cell* **7**, 367–375 (2001).

Strutt, D. I., Weber, U. & Mlodzik, M. The role of RhoA in tissue polarity and Frizzled signalling. *Nature* **387**, 292–295 (1997).

Strutt, H. & Strutt, D. Asymmetric localisation of planar polarity proteins: Mechanisms and consequences. *Semin Cell Dev Biol* **20**, 957–963 (2009).

Strutt, H. & Strutt, D. Differential stability of flamingo protein complexes underlies the establishment of planar polarity. *Curr Biol* **18**, 1555–1564 (2008).

Strutt, H. & Strutt, D. Nonautonomous planar polarity patterning in Drosophila: dishevelled-independent functions of frizzled. *Dev Cell* **3**, 851–863 (2002).

Strutt, H., Mundy, J., Hofstra, K. & Strutt, D. Cleavage and secretion is not required for Four-jointed function in Drosophila patterning. *Development* **131**, 881–890 (2004).

Strutt, H., Thomas-MacArthur, V. & Strutt, D. Strabismus promotes recruitment and degradation of farnesylated prickle in Drosophila melanogaster planar polarity specification. *PLoS Genet* **9**, e1003654 (2013).

Sun, S. D., Purdy, A. M. & Walsh, G. S. Planar cell polarity genes Frizzled3a, Vangl2, and Scribble are required for spinal commissural axon guidance. *BMC Neuroscience* **17**, 83 (2016).

Sun, Y. *et al.* The Suppression of CRMP2 Expression by Bone Morphogenetic Protein (BMP)-SMAD Gradient Signaling Controls Multiple Stages of Neuronal Development. *J. Biol. Chem.* **285**, 39039–39050 (2010).

Swartz, M. E. *et al.* A screen of zebrafish mutants identifies ethanol-sensitive genetic loci. *Alcohol Clin Exp Res* **38**, 694–703 (2014).

Sweede, M. *et al.* Structural and membrane binding properties of the prickle PET domain. *Biochemistry* **47**, 13524–13536 (2008).

Szabadics, J. *et al.* Excitatory effect of GABAergic axo-axonic cells in cortical microcircuits. *Science* **311**, 233–235 (2006).

Szczurkowska, J. *et al.* A Localized Scaffold for cGMP Increase Is Required for Apical Dendrite Development. *Cell Reports* **31**, (2020).

Tada, M. & Smith, J. C. Xwnt11 is a target of Xenopus Brachyury: regulation of gastrulation movements via Dishevelled, but not through the canonical Wnt pathway. *Development* **127**, 2227–2238 (2000).

Tahirovic, S. *et al.* Rac1 regulates neuronal polarization through the WAVE complex. *J Neurosci* **30**, 6930–6943 (2010).

Tai, Y., Gallo, N. B., Wang, M., Yu, J.-R. & Van Aelst, L. Axo-axonic Innervation of Neocortical Pyramidal Neurons by GABAergic Chandelier Cells Requires AnkyrinG-Associated L1CAM. *Neuron* **102**, 358-372.e9 (2019).

Takano, T., Funahashi, Y. & Kaibuchi, K. Neuronal Polarity: Positive and Negative Feedback Signals. *Front Cell Dev Biol* **7**, 69 (2019).

Takeuchi, M. *et al.* The prickle-related gene in vertebrates is essential for gastrulation cell movements. *Curr Biol* **13**, 674–679 (2003).

Tao, H. *et al*. Mouse prickle1, the homolog of a PCP gene, is essential for epiblast apical-basal polarity. Proc Natl Acad Sci U S A **106**, 14426–14431 (2009).

Tao, H. *et al.* Mutations in Prickle Orthologs Cause Seizures in Flies, Mice, and Humans. *Am J Hum Genet* **88**, 138–149 (2011).

Tao, H. *et al.* Nuclear localization of Prickle2 is required to establish cell polarity during early mouse embryogenesis. *Dev Biol* **364**, 138–148 (2012).

Taylor, J., Abramova, N., Charlton, J. & Adler, P. N. Van Gogh: a new Drosophila tissue polarity gene. *Genetics* **150**, 199–210 (1998).

Thakar, S. *et al.* Evidence for opposing roles of Celsr3 and Vangl2 in glutamatergic synapse formation. *PNAS* **114**, E610–E618 (2017).

Tissir, F. & Goffinet, A. M. Expression of planar cell polarity genes during development of the mouse CNS. *Eur J Neurosci* **23**, 597–607 (2006).

Tissir, F. & Goffinet, A. M. Planar cell polarity signaling in neural development. *Curr Opin Neurobiol* **20**, 572–577 (2010).

Tissir, F. & Goffinet, A. M. Shaping the nervous system: role of the core planar cell polarity genes. *Nat Rev Neurosci* **14**, 525–535 (2013).

Tissir, F. *et al.* Lack of cadherins Celsr2 and Celsr3 impairs ependymal ciliogenesis, leading to fatal hydrocephalus. *Nat Neurosci* **13**, 700–707 (2010).

Tissir, F., Bar, I., Goffinet, A. M. & Lambert De Rouvroit, C. Expression of the ankyrin repeat domain 6 gene (Ankrd6) during mouse brain development. *Dev Dyn* **224**, 465–469 (2002).

Tissir, F., Bar, I., Jossin, Y., De Backer, O. & Goffinet, A. M. Protocadherin Celsr3 is crucial in axonal tract development. *Nat Neurosci* **8**, 451–457 (2005).

Todd, B. P. & Bassuk, A. G. A de novo mutation in PRICKLE1 associated with myoclonic epilepsy and autism spectrum disorder. *J Neurogenet* **32**, 313–315 (2018).

Torii, T. *et al.* NuMA1 promotes axon initial segment assembly through inhibition of endocytosis. *J Cell Biol* **219**, (2020).

Tortosa, E. *et al.* Dynamic Palmitoylation Targets MAP6 to the Axon to Promote Microtubule Stabilization during Neuronal Polarization. *Neuron* **94**, 809-825.e7 (2017).

Tree, D. R. P. *et al.* Prickle mediates feedback amplification to generate asymmetric planar cell polarity signaling. *Cell* **109**, 371–381 (2002).

Tse, W. T. *et al.* A new spectrin, beta IV, has a major truncated isoform that associates with promyelocytic leukemia protein nuclear bodies and the nuclear matrix. *J Biol Chem* **276**, 23974–23985 (2001).

Unsain, N. *et al.* Remodeling of the Actin/Spectrin Membrane-associated Periodic Skeleton, Growth Cone Collapse and F-Actin Decrease during Axonal Degeneration. *Scientific Reports* **8**, 3007 (2018).

Vacher, H. *et al.* Cdk-mediated phosphorylation of the Kvβ2 auxiliary subunit regulates Kv1 channel axonal targeting. *Journal of Cell Biology* **192**, 813–824 (2011).

Vale, R. D. The molecular motor toolbox for intracellular transport. *Cell* **112**, 467–480 (2003).

van Beuningen, S. F. & Hoogenraad, C. C. Neuronal polarity: remodeling microtubule organization. *Curr Opin Neurobiol* **39**, 1–7 (2016).

van Beuningen, S. F. B. *et al.* TRIM46 Controls Neuronal Polarity and Axon Specification by Driving the Formation of Parallel Microtubule Arrays. *Neuron* **88**, 1208–1226 (2015).

van der Werf, I. M. *et al.* Behavioural characterization of AnkyrinG deficient mice, a model for ANK3 related disorders. *Behav Brain Res* **328**, 218–226 (2017).

Van Wart, A., Trimmer, J. S. & Matthews, G. Polarized distribution of ion channels within microdomains of the axon initial segment. *J Comp Neurol* **500**, 339–352 (2007).

Veeman, M. T., Slusarski, D. C., Kaykas, A., Louie, S. H. & Moon, R. T. Zebrafish prickle, a modulator of noncanonical Wnt/Fz signaling, regulates gastrulation movements. *Curr Biol* **13**, 680–685 (2003).

Vichas, A. & Zallen, J. A. Translating cell polarity into tissue elongation. *Semin Cell Dev Biol* **22**, 858–864 (2011).

Vinson, C. R. & Adler, P. N. Directional non-cell autonomy and the transmission of polarity information by the frizzled gene of Drosophila. *Nature* **329**, 549–551 (1987).

Vladar, E. K., Bayly, R. D., Sangoram, A. M., Scott, M. P. & Axelrod, J. D. Microtubules enable the planar cell polarity of airway cilia. *Curr Biol* **22**, 2203–2212 (2012).

Voineagu, I. *et al.* Transcriptomic analysis of autistic brain reveals convergent molecular pathology. *Nature* **474**, 380–384 (2011).

Wada, H. *et al.* Dual roles of zygotic and maternal Scribble1 in neural migration and convergent extension movements in zebrafish embryos. *Development* **132**, 2273–2285 (2005).

Wada, H., Tanaka, H., Nakayama, S., Iwasaki, M. & Okamoto, H. Frizzled3a and Celsr2 function in the neuroepithelium to regulate migration of facial motor neurons in the developing zebrafish hindbrain. *Development* **133**, 4749–4759 (2006).

Wallingford, J. B. & Harland, R. M. Xenopus Dishevelled signaling regulates both neural and mesodermal convergent extension: parallel forces elongating the body axis. *Development* **128**, 2581–2592 (2001).

Wallingford, J. B. *et al.* Dishevelled controls cell polarity during Xenopus gastrulation. *Nature* **405**, 81–85 (2000).

Wallingford, J. B. Planar cell polarity and the developmental control of cell behavior in vertebrate embryos. *Annu Rev Cell Dev Biol* **28**, 627–653 (2012).

Wallingford, J. B., Fraser, S. E. & Harland, R. M. Convergent extension: the molecular control of polarized cell movement during embryonic development. *Dev Cell* **2**, 695–706 (2002).

Walsh, G. S., Grant, P. K., Morgan, J. A. & Moens, C. B. Planar polarity pathway and Nance-Horan syndrome-like 1b have essential cell-autonomous functions in neuronal migration. *Development* **138**, 3033–3042 (2011).

Wang, C.-C. *et al.* βIV Spectrinopathies Cause Profound Intellectual Disability, Congenital Hypotonia, and Motor Axonal Neuropathy. *The American Journal of Human Genetics* **102**, 1158–1168 (2018).

Wang, J. *et al.* Dishevelled genes mediate a conserved mammalian PCP pathway to regulate convergent extension during neurulation. *Development* **133**, 1767–1778 (2006).

Wang, J. *et al.* Epilepsy-associated genes. *Seizure* **44**, 11–20 (2017).Wang, J. *et al.* Regulation of polarized extension and planar cell polarity in the cochlea by the vertebrate PCP pathway. *Nat Genet* **37**, 980–985 (2005).

Wang, J., Ou, S.-W. & Wang, Y.-J. Distribution and function of voltage-gated sodium channels in the nervous system. Channels **11**, 534–554 (2017).

Wang, Y. & Nathans, J. Tissue/planar cell polarity in vertebrates: new insights and new questions. *Development* **134**, 647–658 (2007).

Wang, Y., Guo, N. & Nathans, J. The Role of Frizzled3 and Frizzled6 in Neural Tube Closure and in the Planar Polarity of Inner-Ear Sensory Hair Cells. *J. Neurosci.* **26**, 2147–2156 (2006).

Wang, Y., Thekdi, N., Smallwood, P. M., Macke, J. P. & Nathans, J. Frizzled-3 Is Required for the Development of Major Fiber Tracts in the Rostral CNS. *J Neurosci* **22**, 8563–8573 (2002).

Wang, Y., Chang, H., Rattner, A. & Nathans, J. Chapter Seven - Frizzled Receptors in Development and Disease. in *Current Topics in Developmental Biology* (ed. Wassarman, P. M.) vol. **117** 113–139 (Academic Press, 2016).

Wansleeben, C. *et al.* Planar cell polarity defects and defective Vangl2 trafficking in mutants for the COPII gene Sec24b. *Development* **137**, 1067–1073 (2010).

Watanabe, K. *et al.* Networks of polarized actin filaments in the axon initial segment provide a mechanism for sorting axonal and dendritic proteins. *Cell Rep* **2**, 1546–1553 (2012).

Wefelmeyer, W., Cattaert, D. & Burrone, J. Activity-dependent mismatch between axo-axonic synapses and the axon initial segment controls neuronal output. *Proc Natl Acad Sci U S A* **112**, 9757–9762 (2015).

Weiser, D. C., Row, R. H. & Kimelman, D. Rho-regulated Myosin phosphatase establishes the level of protrusive activity required for cell movements during zebrafish gastrulation. 10.

Weiss, L. A. *et al.* Sodium channels SCN1A, SCN2A and SCN3A in familial autism. *Mol Psychiatry* **8**, 186–194 (2003).

Welte, M. A. Bidirectional Transport along Microtubules. *Current Biology* **14**, R525–R537 (2004).

Winans, A. M., Collins, S. R. & Meyer, T. Waves of actin and microtubule polymerization drive microtubule-based transport and neurite growth before single axon formation. *Elife* **5**, e12387 (2016).

Winckler, B., Forscher, P. & Mellman, I. A diffusion barrier maintains distribution of membrane proteins in polarized neurons. *Nature* **397**, 698–701 (1999).

Winkelman, J. D., Anderson, C. A., Suarez, C., Kovar, D. R. & Gardel, M. L. Evolutionarily diverse LIM domain-containing proteins bind stressed actin filaments through a conserved mechanism. *Proc Natl Acad Sci* U S A **117**, 25532–25542 (2020).

Winter, C. G. *et al.* Drosophila Rho-associated kinase (Drok) links Frizzled-mediated planar cell polarity signaling to the actin cytoskeleton. *Cell* **105**, 81–91 (2001).

Witte, H., Neukirchen, D. & Bradke, F. Microtubule stabilization specifies initial neuronal polarization. *J Cell Biol* **180**, 619–632 (2008).

Wong, G. T., Gavin, B. J. & McMahon, A. P. Differential transformation of mammary epithelial cells by Wnt genes. *Mol Cell Biol* **14**, 6278–6286 (1994).

Wong, L. L. & Adler, P. N. Tissue polarity genes of Drosophila regulate the subcellular location for prehair initiation in pupal wing cells. *J Cell Biol* **123**, 209–221 (1993).

Wu, C., Ivanova, E., Cui, J., Lu, Q. & Pan, Z.-H. Action Potential Generation at an Axon Initial Segment-Like Process in the Axonless Retinal AII Amacrine Cell. *J Neurosci* **31**, 14654–14659 (2011).

Wu, J., Roman, A.-C., Carvajal-Gonzalez, J. M. & Mlodzik, M. Wg and Wnt4 provide long-range directional input to planar cell polarity orientation in Drosophila. *Nat Cell Biol* **15**, 1045–1055 (2013).

Wu, S.-X. *et al*. Pyramidal neurons of upper cortical layers generated by NEX-positive progenitor cells in the subventricular zone. *Proc Natl Acad Sci U S A* **102**, 17172–17177 (2005).

Xu, K., Zhong, G. & Zhuang, X. Actin, Spectrin, and Associated Proteins Form a Periodic Cytoskeletal Structure in Axons. *Science* **339**, 452–456 (2013).

Xu, X. & Shrager, P. Dependence of axon initial segment formation on Na+ channel expression. *Journal of Neuroscience Research* **79**, 428–441 (2005).

Yamamoto, S. *et al.* Cthrc1 selectively activates the planar cell polarity pathway of Wnt signaling by stabilizing the Wnt-receptor complex. *Dev Cell* **15**, 23–36 (2008).

Yamben, I. F. *et al.* Scrib is required for epithelial cell identity and prevents epithelial to mesenchymal transition in the mouse. *Dev Biol* **384**, 41–52 (2013).

Yan, J., Lu, Q., Fang, X. & Adler, P. N. Rho1 has multiple functions in Drosophila wing planar polarity. *Dev Biol* **333**, 186–199 (2009).

Yang, T., Kersigo, J., Wu, S., Fritzsch, B. & Bassuk, A. G. Prickle1 regulates neurite outgrowth of apical spiral ganglion neurons but not hair cell polarity in the murine cochlea. *PLOS ONE* **12**, e0183773 (2017).

Yang, X. *et al*. Establishment of planar cell polarity is coupled to regional cell cycle exit and cell differentiation in the mouse utricle. *Sci Rep* **7**, 43021 (2017).

Yang, Y., Ogawa, Y., Hedstrom, K. L. & Rasband, M. N. betaIV spectrin is recruited to axon initial segments and nodes of Ranvier by ankyrinG. *J Cell Biol* **176**, 509–519 (2007).

Yates, L. L. *et al.* The PCP genes Celsr1 and Vangl2 are required for normal lung branching morphogenesis. *Hum Mol Genet* **19**, 2251–2267 (2010).

Yates, L. L. *et al.* The planar cell polarity gene Vangl2 is required for mammalian kidney-branching morphogenesis and glomerular maturation. *Hum Mol Genet* **19**, 4663–4676 (2010).

Yau, K. W. *et al.* Dendrites In Vitro and In Vivo Contain Microtubules of Opposite Polarity and Axon Formation Correlates with Uniform Plus-End-Out Microtubule Orientation. *J. Neurosci.* **36**, 1071–1085 (2016).

Yau, K. W. *et al.* Microtubule Minus-End Binding Protein CAMSAP2 Controls Axon Specification and Dendrite Development. *Neuron* **82**, 1058–1073 (2014).

Ybot-Gonzalez, P. *et al.* Convergent extension, planar-cell-polarity signalling and initiation of mouse neural tube closure. *Development* **134**, 789–799 (2007).

Yi, J. J., Barnes, A. P., Hand, R., Polleux, F. & Ehlers, M. D. TGF-β Signaling Specifies Axons during Brain Development. *Cell* **142**, 144–157 (2010).

Yin, C., Kiskowski, M., Pouille, P.-A., Farge, E. & Solnica-Krezel, L. Cooperation of polarized cell intercalations drives convergence and extension of presomitic mesoderm during zebrafish gastrulation. *J Cell Biol* **180**, 221–232 (2008).

Yin, H., Copley, C. O., Goodrich, L. V. & Deans, M. R. Comparison of phenotypes between different vangl2 mutants demonstrates dominant effects of the Looptail mutation during hair cell development. *PLoS One* **7**, e31988 (2012).

Yogev, S. & Shen, K. Establishing Neuronal Polarity with Environmental and Intrinsic Mechanisms. *Neuron* **96**, 638–650 (2017).

Yoshimura, T. & Rasband, M. N. Axon initial segments: diverse and dynamic neuronal compartments. *Current Opinion in Neurobiology* **27**, 96–102 (2014).

Yoshimura, T., Stevens, S. R., Leterrier, C., Stankewich, M. C. & Rasband, M. N. Developmental Changes in Expression of βIV Spectrin Splice Variants at Axon Initial Segments and Nodes of Ranvier. *Front Cell Neurosci* **10**, 304 (2016).

Yoshioka, T., Hagiwara, A., Hida, Y. & Ohtsuka, T. Vangl2, the planner cell polarity protein, is complexed with postsynaptic density protein PSD-95. *FEBS Letters* **587**, 1453–1459 (2013).

Yu, F. H. & Catterall, W. A. Overview of the voltage-gated sodium channel family. *Genome Biol* **4**, 207 (2003).

Yu, H., Ye, X., Guo, N. & Nathans, J. Frizzled 2 and frizzled 7 function redundantly in convergent extension and closure of the ventricular septum and palate: evidence for a network of interacting genes. *Development* **139**, 4383–4394 (2012).

Yu, J. J. S. *et al.* Frizzled-Dependent Planar Cell Polarity without Secreted Wnt Ligands. *Dev Cell* **54**, 583-592.e5 (2020).

Yu, Y., Maureira, C., Liu, X. & McCormick, D. P/Q and N Channels Control Baseline and Spike-Triggered Calcium Levels in Neocortical Axons and Synaptic Boutons. *J Neurosci* **30**, 11858–11869 (2010).

Zallen, J. A. Planar polarity and tissue morphogenesis. *Cell* **129**, 1051–1063 (2007).

Zeesman, S. *et al.* Microdeletion in distal 17p13.1: a recognizable phenotype with microcephaly, distinctive facial features, and intellectual disability. *Am J Med Genet A* **158A**, 1832–1836 (2012).

Zhang, X. & Bennett, V. Restriction of 480/270-kD ankyrin G to axon proximal segments requires multiple ankyrin G-specific domains. *J Cell Biol* **142**, 1571–1581 (1998).

Zhang, X. *et al.* Dishevelled promotes axon differentiation by regulating atypical protein kinase C. *Nature Cell Biology* **9**, 743–754 (2007).

Zhong, G. *et al.* Developmental mechanism of the periodic membrane skeleton in axons. *Elife* **3**, (2014).

Zhou, D. *et al.* AnkyrinG is required for clustering of voltage-gated Na channels at axon initial segments and for normal action potential firing. *J Cell Biol* **143**, 1295–1304 (1998).

Zhou, R., Han, B., Xia, C. & Zhuang, X. Membrane-associated periodic skeleton is a signaling platform for RTK transactivation in neurons. *Science* **365**, 929–934 (2019).

Zhu, S. *et al.* Genetic disruption of ankyrin-G in adult mouse forebrain causes cortical synapse alteration and behavior reminiscent of bipolar disorder. *Proc Natl Acad Sci U S A* **114**, 10479–10484 (2017).

Zimmer, W. E., Ma, Y., Zagon, I. S. & Goodman, S. R. Developmental expression of brain beta-spectrin isoform messenger RNAs. *Brain Res* **594**, 75–83 (1992).

Zonta, B. *et al.* A critical role for Neurofascin in regulating action potential initiation through maintenance of the axon initial segment. *Neuron* **69**, 945–956 (2011).

Zuccaro, E. *et al.* Polarized Expression of p75NTR Specifies Axons during Development and Adult Neurogenesis. *Cell Reports* **7**, 138–152 (2014).

Annexes

1

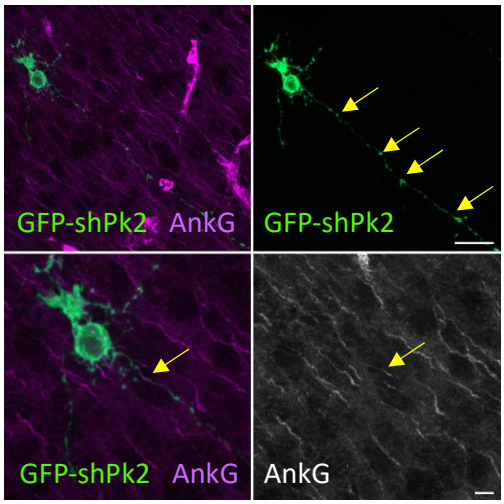
GFP-shPk2 AnkG
GFP-shPk2
GFP-shPk2 AnkG
AnkG

2

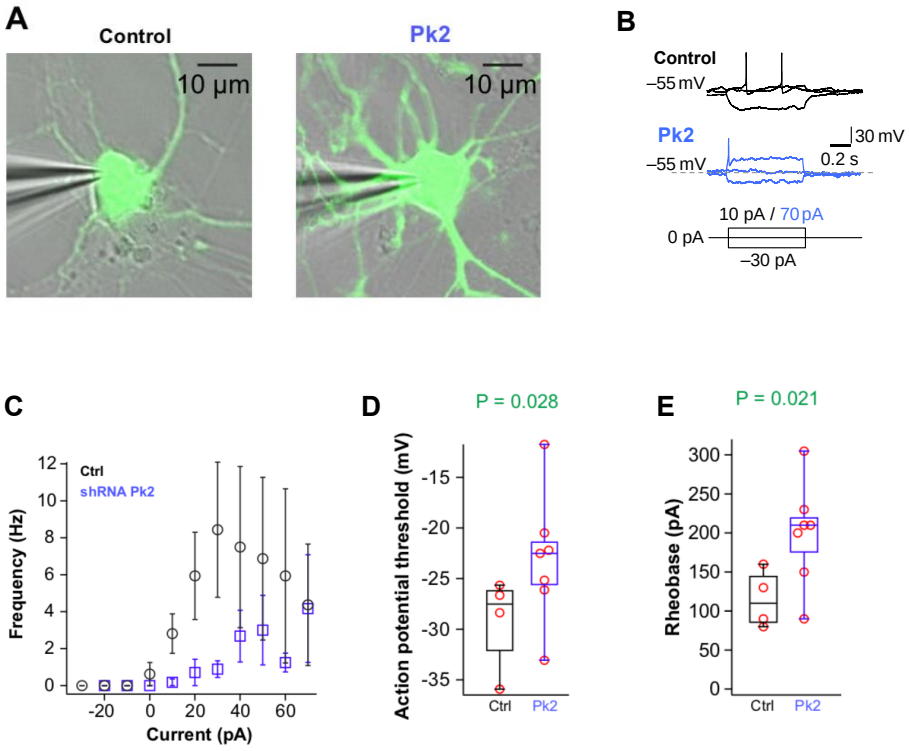
A
Control
Pk2
10 µm
10 µm
B
Control
–55 mV
Pk2
–55 mV
30 mV
0.2 s
10 pA / 70 pA
0 pA
–30 pA
C
Ctrl
shRNA Pk2
Frequency (Hz)
Current (pA)
D
P = 0.028
Action potential threshold (mV)
Ctrl
Pk2
E
P = 0.021
Rheobase (pA)
Ctrl
Pk2

Figures annexes. (1) GFP-shPk2 electroporated neurons in the mouse cortex at P3. The arrows point at axonal protrusions in the GFP indicating potential toxicity. The pointed decrease of AnkG observed at the electroporated neuron may be product of this toxicity. Scale bars: 20 µm and 5 µm. **(2) (A)** Oblique contrast images overlaid with GFP fluorescence to identify neurons transfected with control shRNA or Pk2 shRNA at DIV8. Pk2 shRNA expressing neurons display a more complex morphology. Somatic recording pipettes are visible. **(B)** Voltage responses (top, middle) to 800 ms long current injections (bottom) from the two cells shown in A. The Pk2 shRNA expressing neuron requires higher current injection to fire a single action potential. Shown are the action potentials at threshold potential. **(C)** F-I (Firing frequency-current) curve for control and PK2 shRNA neurons at DIV8 determined from 800 ms long current injections. Experiments were averaged for the two groups (control: n = 4; Pk2 shRNA: n = 7), mean ± SEM. Neurons expressing shRNA against Pk2 fire later and with a lower frequency. **(D)** The action potential threshold is more depolarized in Pk2 shRNA expressing neurons. Wilcoxon Rank test. **(E)** The rheobase current (threshold current) for a single action potential is increased in Pk2 shRNA expressing neurons. Wilcoxon Rank test.

Planar cell polarity (PCP) classically refers to the coordination of cell polarity within the plane of the epithelium, perpendicularly to the apical-basal axis. A conserved signaling cassette that modulates the cytoskeleton regulates this type of tissue polarity, which in turn controls a wide range of biological processes. PCP signaling has conserved functions in epithelia from drosophila to mammals but its role and function in the central nervous system is still poorly known. However, mutations in some core PCP members result in severe phenotypes for the brain and are incompatible with life.

Neurons are highly polarized cells with two defined compartments that differ in morphology and function: the axonal and the somatodendritic domains. This segregation is crucial for the proper function of neurons. The maintenance of this polarized state throughout life relies in the axon initial segment (AIS). The AIS is a neuronal subdomain that coordinates the axo-dendritic polarity establishment and maintenance and constitutes the site for action potential initiation and tuning. The AIS consists of an organized cytoskeleton meshwork and associated molecules like Ankyrin-G (AnkG) and βIV spectrin. AnkG is the AIS master organizer, since it arrives to the proximal axon first and recruits all the AIS members. Many of the AIS genes are linked to neurodevelopmental pathologies like bipolar disorder, epilepsy or autism, making it a potential target for therapeutical approaches. Despite the critical role of the AIS in neuronal function, the early steps of its assembly are still unknown notably because of few identified direct AnkG partners.

This thesis focuses on the roles of Prickle-like 2 (Pk2) and Scribble (Scrib) in neuronal polarity and axonal function. Pk2 and Scrib accumulate at the AIS in early and late stages of neuronal development, both in vivo and *in vitro*. I show a colocalization between these proteins and AnkG and βIV spectrin and confirmed their interactions via specific domains. My data suggest that Pk2 interacts early at the AIS with AnkG to stabilize it at the membrane, while Scrib binds to βIV spectrin to anchor the AIS along the axon.

In vitro downregulation of Pk2 impaired axonal establishment and AIS formation by altering the number of axons per neuron and the levels of AnkG and associated AIS molecules. *In vivo* downregulation of Pk2 via *in utero* electroporation similarly reduced AIS proteins levels in neurons from the developing neocortex. I used a conditional knockout mouse model where both Pk2 and Scrib are deleted in postmitotic excitatory neurons of the hippocampus and cortex. The reduction of PCP proteins was followed by a decrease of the main AIS proteins like AnkG, βIV spectrin and Nav channels.

Altogether, these data unveil an original role of PCP proteins in AIS formation and composition, shedding light on novel PCP function.

Planar cell polarity (PCP) classically refers to the coordination of cell polarity within the plane of the epithelium, perpendicularly to the apical-basal axis. A conserved signaling cassette that modulates the cytoskeleton regulates this type of tissue polarity, which in turn controls a wide range of biological processes. PCP signaling has conserved functions in epithelia from drosophila to mammals but its role and function in the central nervous system is still poorly known. However, mutations in some core PCP members result in severe phenotypes for the brain and are incompatible with life.

Neurons are highly polarized cells with two defined compartments that differ in morphology and function: the axonal and the somatodendritic domains. This segregation is crucial for the proper function of neurons. The maintenance of this polarized state throughout life relies in the axon initial segment (AIS). The AIS is a neuronal subdomain that coordinates the axo-dendritic polarity establishment and maintenance and constitutes the site for action potential initiation and tuning. The AIS consists of an organized cytoskeleton meshwork and associated molecules like Ankyrin-G (AnkG) and βIV spectrin. AnkG is the AIS master organizer, since it arrives to the proximal axon first and recruits all the AIS members. Many of the AIS genes are linked to neurodevelopmental pathologies like bipolar disorder, epilepsy or autism, making it a potential target for therapeutical approaches. Despite the critical role of the AIS in neuronal function, the early steps of its assembly are still unknown notably because of few identified direct AnkG partners.

This thesis focuses on the roles of Prickle-like 2 (Pk2) and Scribble (Scrib) in neuronal polarity and axonal function. Pk2 and Scrib accumulate at the AIS in early and late stages of neuronal development, both in vivo and *in vitro*. I show a colocalization between these proteins and AnkG and βIV spectrin and confirmed their interactions via specific domains. My data suggest that Pk2 interacts early at the AIS with AnkG to stabilize it at the membrane, while Scrib binds to βIV spectrin to anchor the AIS along the axon.

In vitro downregulation of Pk2 impaired axonal establishment and AIS formation by altering the number of axons per neuron and the levels of AnkG and associated AIS molecules. *In vivo* downregulation of Pk2 via *in utero* electroporation similarly reduced AIS proteins levels in neurons from the developing neocortex. I used a conditional knockout mouse model where both Pk2 and Scrib are deleted in postmitotic excitatory neurons of the hippocampus and cortex. The reduction of PCP proteins was followed by a decrease of the main AIS proteins like AnkG, βIV spectrin and Nav channels.

Altogether, these data unveil an original role of PCP proteins in AIS formation and composition, shedding light on novel PCP function.